NASA CONTRACTOR
REPORT

NASA CR-124075
REVISION A

ISOGRID DESIGN HANDBOOK

McDonnell Douglas Astronautics Company
5301 Bolsa Avenue
Huntington Beach, Ca 92647

February 1973

(NASA-CR-124075) ISOGRID DESIGN HANDBOOK (McDonnell-Douglas Astronautics Co.) 222 p HC $13.25 CSCL 13M

N73-19911

Unclas
G3/32 17333

Prepared For

NASA-GEORGE C. MARSHALL SPACE FLIGHT CENTER
Marshall Space Flight Center, Alabama 35812

MCDONNELL DOUGLAS

ISOGRID DESIGN HANDBOOK

FEBRUARY 1973

MDC G4295A

PREPARED BY:

MCDONNELL DOUGLAS ASTRONAUTICS COMPANY

FOR:

NASA MARSHALL SPACE FLIGHT CENTER
CONTRACT NAS 8 28619

MCDONNELL DOUGLAS ASTRONAUTICS COMPANY-WEST

5301 Bolsa Avenue, Huntington Beach, CA 92647

FOREWORD

This program, the development of the isogrid design handbook, was conducted by the McDonnell Douglas Astronautics Company at Huntington Beach, California under NASA Contract NAS 8-28619. The contract was administered under the direction of John Key, Marshall Space Flight Center, NASA.

The McDonnell Douglas program was conducted under the direction of Dr. George Moe, Director, Research and Development, with M. B. Harmon acting as principal investigator. Dr. Robert R. Meyer was the principal contributor to this document, being responsible for Sections 2 and 4, basic theory and analytical techniques. Other major contributors include Mr. O. P. Harwood and Mr. J. I. Orlando.

The information in the document was obtained from: (1) the results of analysis, test, and advanced manufacturing studies of Independent Research and Development programs, (2) a phase B space shuttle booster study funded by the NASA Marshall Space Flight Center, (3) an isogrid tank test program funded by the NASA Marshall Space Flight Center, and (4) the Delta program isogrid structural tests funded by the NASA Goddard Space Flight Center.

Appreciation is expressed to Mr. Jack Furman of the NASA Marshall Space Flight Center for his continued interest in the development and application of isogrid to aerospace structures.

CONTENTS

FIGURES

TABLES

ISOGRID DEFINITIONS

t = thickness of skin

b = width of rib web

d = depth of web

c = depth of flange

w = width of flange

$s = t+d$ = plate thickness of unflanged isogrid

h = height of triangle

a = leg of triangle, i.e., distance center to center of nodes

$\delta = \frac{d}{t}$, $\lambda = \frac{c}{t}$, $\alpha = \frac{bd}{th}$, $\mu = \frac{wc}{th}$

non-dimensional parameters

$$\beta^2 = (1 + \alpha + \mu)\left[3(1+\delta)^2 + 3\mu(1+\lambda)^2 + 1 + \alpha\delta^2 + \mu\lambda^2\right] - 3\left[(1+\delta) - \mu(1+\lambda)\right]^2$$

bending stiffness parameter. (For unflanged isogrid, $\lambda = \mu = 0$,

$$\beta^2 = \left[3\alpha(1+\delta)^2 + (1+\alpha)(1+\alpha\delta^2)\right].)$$

$K = \frac{Et}{1-\nu^2}(1 + \alpha + \mu)$ = extensional stiffness ($\mu = 0$ for unflanged isogrid)

$D = \left(\frac{Et^3}{12(1-\nu^2)}\right)\left(\frac{\beta^2}{1 + \alpha + \mu}\right)$ bending stiffness ($\mu = 0$ for unflanged isogrid)

$t_{eff} = t(1 + \alpha + \mu)$ = equivalent thickness for membrane stresses ($\mu = 0$ for unflanged isogrid)

$\bar{t} = t(1 + 3\alpha + 3\mu)$ = equivalent weight thickness ($\mu = 0$ for unflanged isogrid)

$$t^* = t\,\frac{\beta}{1+\alpha+\mu}$$

$$E^* = E\,\frac{(1+\alpha+\mu)^2}{\beta}$$

} = Equivalent thickness and Young's modulus to obtain correct K and D ($\mu = 0$ for unflanged isogrid)

Use of E* and t* in monocoque equations gives correct stress resultants, couples, strains, curvature changes and displacements.

Section 1
INTRODUCTION

1.1 BACKGROUND

The establishment of new, lightweight, economical, and efficient structural concepts for aerospace structures has long been an objective of NASA and the industry.

Lightweight, compression-load-carrying structures form part of all aircraft, booster, and space vehicle structures. Aircraft such as the DC-6 or DC-7 used mechanically attached stringer, frame, and skin construction, which are of course 90-degree stiffened structures. Boosters, however, were designed as integrally stiffened structures because of leakage considerations. In the Saturn vehicle, the S-II second stage duplicated aircraft 0- to 90-degree patterns with an integral, constant-height machined pattern. The S-IVB stage, as well as the Thor, used square patterns rotated through 45 degrees.

The 0- to 90-degree and 45-degree stiffening patterns used in the stages of the Saturn vehicle are extremely efficient in certain load regimes. However, they are inherently four bar links prevented from collapsing by the integral skin and as a result have little in-plane torsional resistance capability.

In 1964, Dr. Robert R. Meyer under a NASA-MSFC contract, Reference 1-1, set out to find the optimum stiffening pattern for compressively loaded domes. A goal was to find a structural arrangement that negated the shortcomings of the 0- to 90-degree and 45-degree patterns without introducing other penalties such as increased weight. The concept that was found to be the most promising was triangulation of the stiffening members. This pattern took advantage of the simple fact that triangular trusses are very efficient structure. This work showed significant promise and was extended to cylinders as an Independent Research and Development program. After

many years of development, this stiffening concept is now being used as structure for Delta vehicle tanks and interstages (Reference 1-2), Delta shrouds, orbital shrouds, and Orbital Workshop interiors.

The new structure is called "Isogrid" since it acts like an isotropic material.

In a recent phase B design study funded by NASA for a recoverable space shuttle booster, isogrid (triangular integral stiffening) was used in the fuselage design. The vehicle requirements included (1) the capability of carrying high torques from the wings, (2) supplying multiple attach points for an external thermal protection system, and (3) the need to resist very high point loads from the attached piggyback orbiter. The isogrid construction had (1) high torsional resistance, (2) many nodal points, which could be used as attach points for the thermal protection system standoff structures, and (3) the capability of resisting the orbiter attach loads with local stiffening of the isogrid pattern and a few added internal compression members. Full-scale and model testing was conducted to supplement test results previously obtained for the Delta vehicle. These tests served to verify the structural concept.

It is important to note that studies have shown that the lowest structural cost is associated with structure having the fewest parts. Relative costs of major subassemblies of the Saturn S-IVB stage, Figure 1-1, are indicative of this cost pattern. The tank cylinder was designed with integrally machined 45-degree waffle panels to assure leak tightness, not to save money. The cost difference between the aft skirt and interstage, both built in the same structural style, must be attributed mainly to the installation of equipment in non-standard fashion in the former compartment (see Figure 1-2). Evidently, these secondary functions cannot be ignored in the selection of a concept for primary structure. The evidence suggests that a waffle type of structure, such as isogrid, with a pattern of rib intersections usable for equipment attachment is an economical way to design structure if its efficiency is to be fully realized.

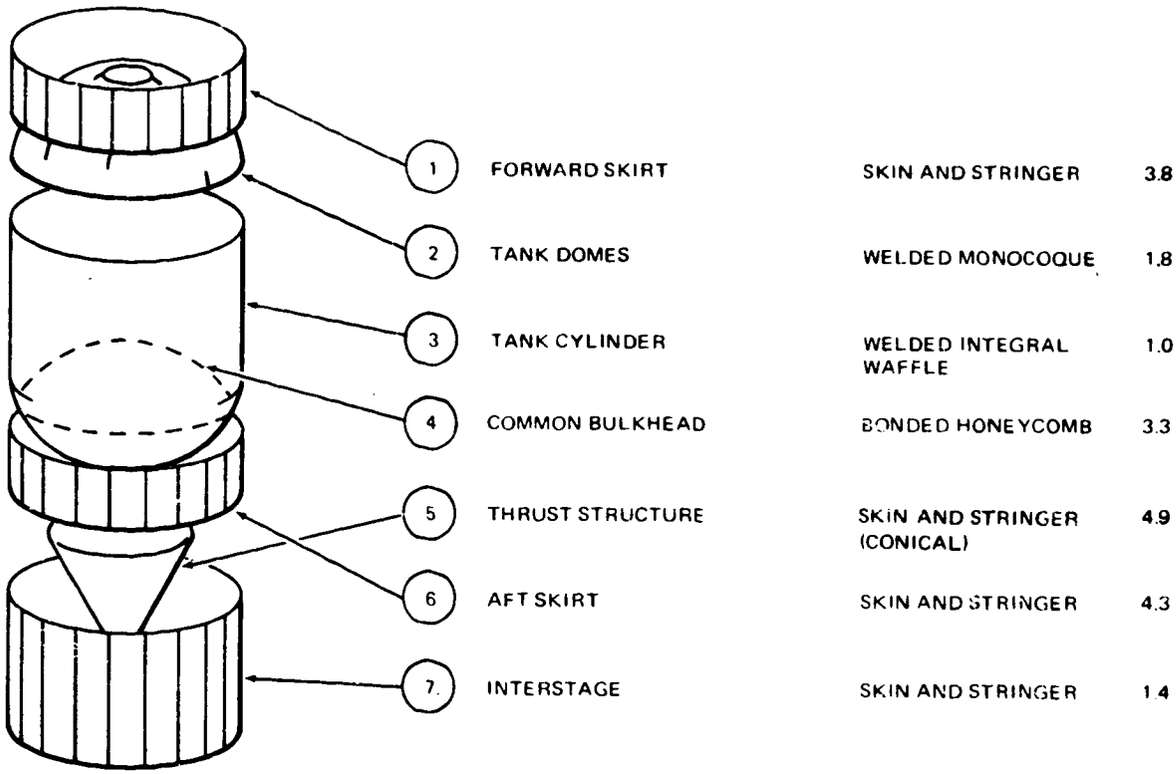

Figure 1-1. S-IVB Relative Costs

1.2 USE OF THE HANDBOOK

This handbook presents information needed to design isogrid, triangular integral stiffened structures. Some key points about isogrid are shown in Table 1-1.

The handbook covers both unflanged and flanged isogrid with the information on flanged isogrid being so designated. All other information applies to unflanged isogrid.

The basic theory for the analysis of isogrid is presented in Section 2. The user should acquaint himself with this analysis and its assumptions before using the handbook. Both unflanged and flanged isogrid are covered by this section. The basic theory is summarized at the end of the section to serve as a ready reference.

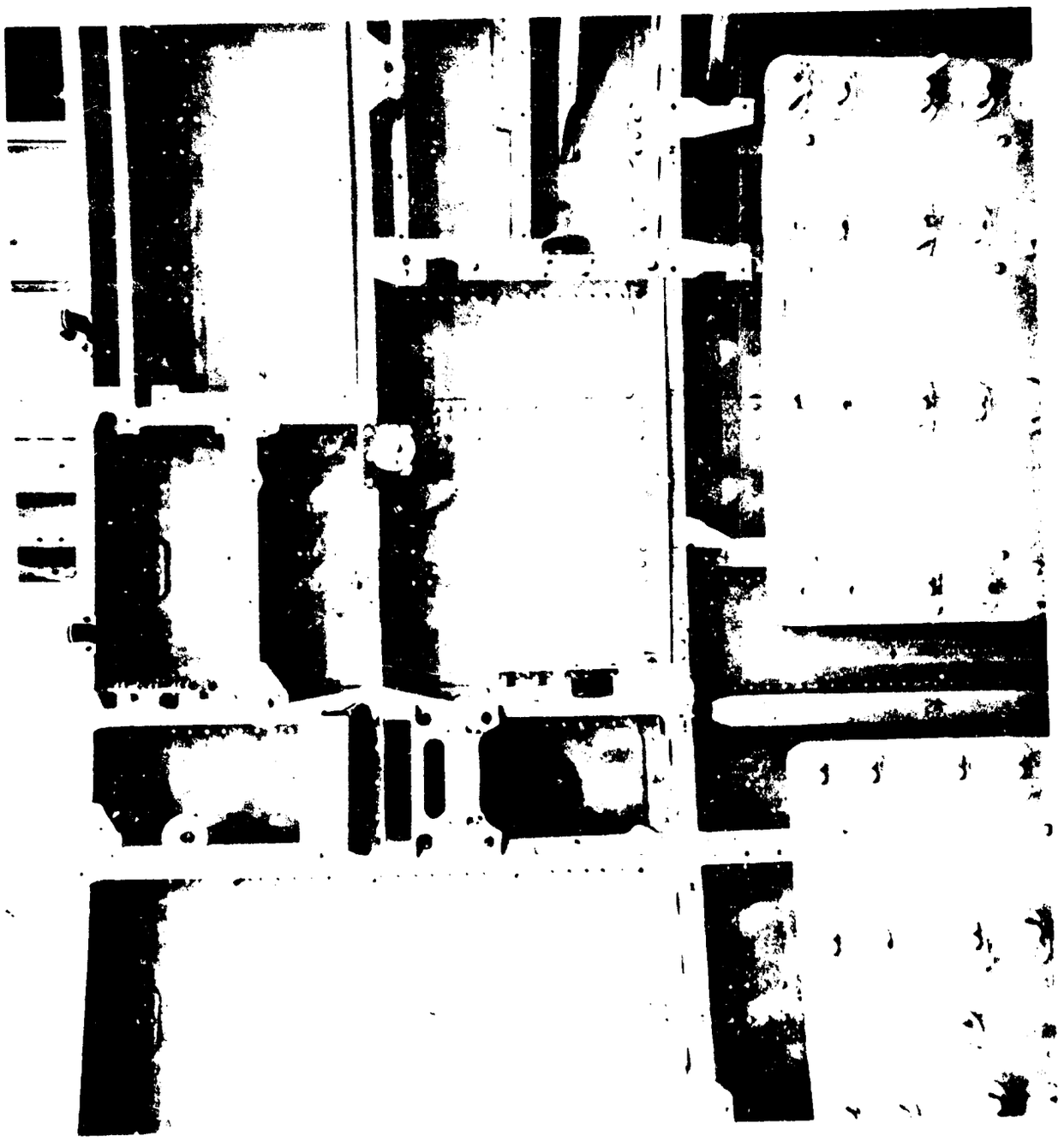

Figure 1.2 Non-Standard Installation of Equipment

Table 1-1

ISOGRID

- A lattice of intersecting ribs forming an array of equilateral triangles
- Characteristics:
  - Isotropic (no directions of instability or weakness)
  - Poisson's ratio 1/3
  - Efficient in compression and bending
- Advantages:
  - Easily analyzed
  - Can be optimized for wide range of loading intensities
  - Standard pattern for attachment (nodes accommodate equipment mounting without change)
  - Readily reinforced for concentrated loads and cutouts
  - Redundant load paths
  - Less structural depth
- In use on two major space programs, Thor-Delta and Skylab, and extensively investigated and tested on space shuttle study effort

Section 3 describes the characteristics and advantages of isogrid, including some current and future applications for vehicle structure.

Section 4 presents the analysis methods for typical structure found in aerospace vehicles. Typical design situations are described for each type of structure, and methods of optimizing the structure for minimum weight are given where such methods exist. The method of analysis is followed by worked examples, which are given to guide the user in the application of the equations and of the graphs. The graphs enable the user to quickly and accurately size isogrid structure. The structural types presented are:

- Spherical cap with reverse pressure
- Cylinders in compression, bending
- Cylinders under torsional shear

- Cylinders under uniform external pressure
- In-plane concentrated load in an infinite sheet
- In-plane concentrated load at the edge of a sheet
- Cutout reinforcement
- Open isogrid shear webs
- Open isogrid cylinders in compression, bending
- Open and skinned isogrid plates

Other structural types such as cones have not been analyzed to date and are not included.

To complete the sections, information is given on: (1) the minimum overall weight for cylinders subjected to axial compression and bending, and (2) off-optimum isogrid. Section 4.12 is a very important note on the use of the x, y, α, and δ curves to ensure accuracy.

Section 5 describes the effect of node flexibility on the local stress distributions in isogrid and recommends methods of analysis. Section 6 presents information on model, sub-scale, and full-scale testing. Finally, Section 7 presents information on manufacturing techniques developed on production hardware and in advanced manufacturing research programs to date. The topics covered are:

- Machining
- Power brake forming
- Creep and age forming
- Compound curvatures

References used in the text are listed.

This handbook is set up to allow the user to insert new pages of data or entire new sections by using the decimal page numbers. Care should be taken to remove obsolete material immediately and to add test information as it becomes available to the user from research or development in his company or NASA agency.

Section 2
BASIC THEORY

The isogrid rib-grids are analyzed by "smearing out", averaging, or taking mean values of the grid properties so that the gridwork is considered as a solid continuous sheet of material with appropriate elastic properties.

It is shown that if one assumes a uniaxial state of stress in the bars, the smeared-out elastic constants are identical to those of an isotropic material in plane stress.

When ribs and skin are combined, the composite construction is treated as an isotropic layered material, with appropriate elastic constants for each layer, viz., rib-grid and skin.

The key to the analysis is strain in the construction. The internal strains in the composite construction are determined by the stress resultants and couples in the composite construction. These relations are shown to be isotropic in character. From the composite strains, the stresses in the elements of the individual layers may be determined. For the bars, these depend upon the bar orientation. For the skin, they are dependent upon the orientation of the normal of the plane upon which the stresses are assumed to act.

2.1 HOOKE'S LAW FOR ISOGRID RIB-GRID

The isogrid rib pattern consists of a network of equilateral (60 degree) triangles. The Hooke's law relations are developed by isolating an element of the gridwork and assuming that the individual bars are in a state of uniaxial stress.

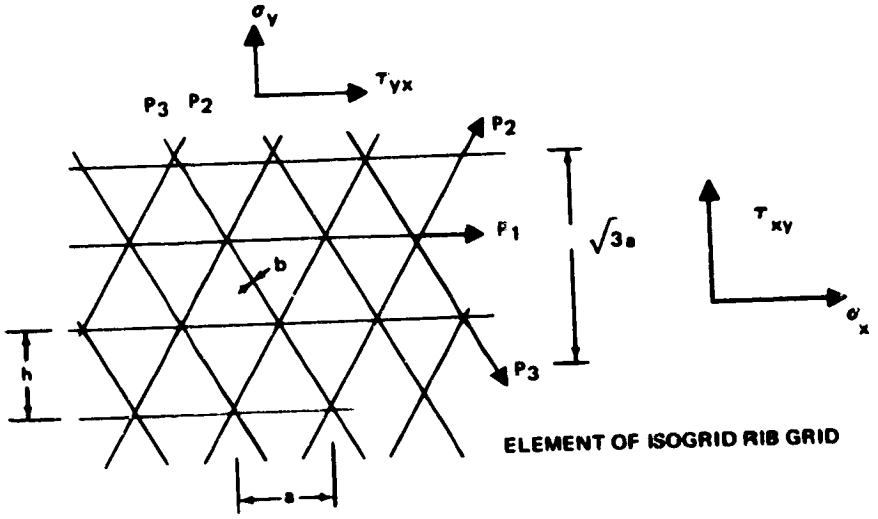

Element of Isogrid Rib Grid

By means of the strain transformation law,

$$e_i = e_x \cos^2 \theta_i + \gamma_{xy} \sin \theta_i \cos \theta_i + e_y \sin^2 \theta_i \qquad (2.1.1)$$

one obtains the relation between the uniaxial bar strains, e_i, and the x, y grid coordinate strains, e_x, e_y and γ_{xy}.

$$\begin{Bmatrix} e_1 \\ e_2 \\ e_3 \end{Bmatrix} = \frac{1}{4} \begin{bmatrix} 4 & 0 & 0 \\ 1 & \sqrt{3} & 3 \\ 1 & -\sqrt{3} & 3 \end{bmatrix} \begin{Bmatrix} e_x \\ \gamma_{xy} \\ e_y \end{Bmatrix} \qquad (2.1.2)$$

Note that the strain transformation is invertable, so that if (e_1, e_2, e_3) are known (for example from strain gage readings) then (e_x, γ_{xy}, e_y) may be determined. In fact,

$$\begin{Bmatrix} e_x \\ \gamma_{xy} \\ e_y \end{Bmatrix} = \frac{1}{3} \begin{bmatrix} 3 & 0 & 0 \\ 0 & 2\sqrt{3} & -2\sqrt{3} \\ -1 & 2 & 2 \end{bmatrix} \begin{Bmatrix} e_1 \\ e_2 \\ e_3 \end{Bmatrix} \qquad (2.1.3)$$

The uniaxial bar loads are:

$$P_i = bEe_i \qquad i = 1, 2, 3 \tag{2.1.4}$$

Resolutes of the bar loads in the x and y directions divided by the periodic lengths, a and $\sqrt{3}$ a give the "smeared-out" or mean value stresses in the grid element.

$$\sigma_x = \frac{2P_1 + (P_2 + P_3)\cos 60^\circ}{\sqrt{3}a} = \frac{4P_1 + P_2 + P_3}{2\sqrt{3}a} \tag{2.1.5}$$

$$\sigma_y = \frac{(P_2 + P_3)\sin 60^\circ}{a} = \frac{\sqrt{3}\,(P_2 + P_3)}{2a} \tag{2.1.6}$$

$$\tau_{xy} = \tau_{yx} = \frac{(P_2 - P_3)\sin 60^\circ}{\sqrt{3}a} = \frac{P_2 - P_3}{2a} \tag{2.1.7}$$

Using eq. (2.1.4) and (2.1.2), these become,

$$\begin{Bmatrix}\sigma_x \\ \sigma_y\end{Bmatrix} \quad \frac{9}{8}\frac{bE}{h}\begin{bmatrix}1 & 1 & 3 \\ 1/3 & 1 & \end{bmatrix}\begin{Bmatrix}e_x \\ e_y\end{Bmatrix} \tag{2.1.8}$$

$$\tau_{xy} \quad \tau_{yx} = \frac{3}{8}\frac{bE}{h}\gamma_{xy} \tag{2.1.9}$$

where

$h = \frac{\sqrt{3}}{2}a$, the triangle height.

By comparing eq. (2.1.8) and (2.1.9) with the Hooke's law relation for isotropic materials in plane stress,

$$\begin{Bmatrix} \sigma_x \\ \sigma_y \end{Bmatrix} = \frac{E}{1-\nu^2} \begin{bmatrix} 1 & \nu \\ \nu & 1 \end{bmatrix} \begin{Bmatrix} e_x \\ e_y \end{Bmatrix} \tag{2.1.10}$$

$$\tau_{xy} = \tau_{yx} = \frac{E}{2(1+\nu)} \gamma_{xy} \tag{2.1.11}$$

it is evident that eq. (2.1.8), (2.1.9) are a special case of (2.1.10), (2.1.11) where

$$\bar{\nu} = \frac{1}{3}$$

$$\bar{E} = \frac{b}{h} E \tag{2.1.12}$$

and the barred quantities indicate the equivalent Poisson's ratio and Young's modulus of the gridwork.

2.2 EXTENSIONAL AND BENDING STIFFNESS FOR COMPOSITE RIB-GRID AND SKIN CONSTRUCTIONS

Many constructions may be idealized as elastic plates and shells. This concept is a two-dimensional approximation of three-dimensional elasticity, which replaces the three-dimensional body by a two-dimensional surface. The loading on the surface is considered to be resisted by stress resultants and stress couples obtained by integrating the stresses and moments in the thickness direction,

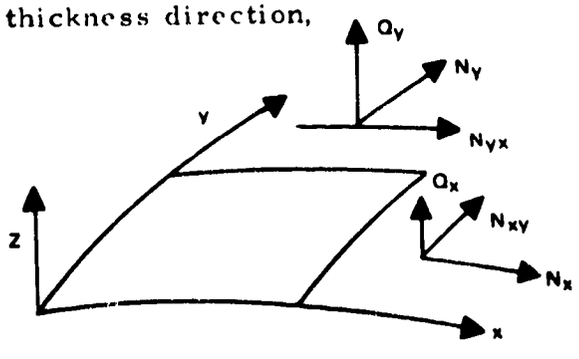

STRESS RESULTANTS ON REFERENCE SURFACE ELEMENT

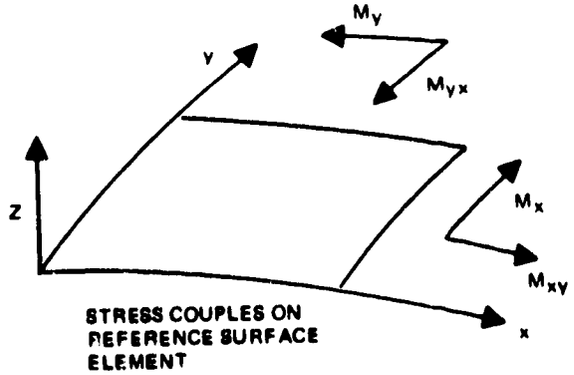

STRESS COUPLES ON REFERENCE SURFACE ELEMENT

These are computed per unit length of the reference surface coordinates, x and y. If the small differences in length of a surface parallel to the reference surface at a distance Z from the reference surface is neglected, these stress resultants and couples may be written as follows.

$$\begin{Bmatrix} N_x \\ N_{xy} \\ N_y \\ Q_x \\ Q_y \end{Bmatrix} = \int_Z \begin{Bmatrix} \sigma_x \\ \tau_{xy} \\ \sigma_y \\ \tau_{zx} \\ \tau_{zy} \end{Bmatrix} dz \qquad (2.2.1)$$

$$\begin{Bmatrix} M_x \\ -M_{xy} \\ M_y \end{Bmatrix} = \int_Z \begin{Bmatrix} \sigma_x \\ \tau_{xy} \\ \sigma_y \end{Bmatrix} ZdZ \qquad (2.2.2)$$

where

$$N_{xy} = N_{yx} \text{ and } M_{xy} = M_{yx}$$

By use of the Kirchhoff-Love assumption of linear strain,

$$\begin{Bmatrix} \hat{\epsilon}_x(z) \\ \hat{\gamma}_{xy}(z) \\ \hat{\epsilon}_y(z) \end{Bmatrix} = \begin{Bmatrix} \epsilon_x \\ \gamma_{xy} \\ \epsilon_y \end{Bmatrix} - Z \begin{Bmatrix} \chi_x \\ 2\chi_{xy} \\ \chi_y \end{Bmatrix} \qquad (2.2.3)$$

where $(\epsilon_x, \gamma_{xy}, \epsilon_y)$ are reference surface strains and $(\chi_x, 2\chi_{xy}, \chi_y)$ are reference surface changes of curvature, together with the appropriate Hooke's law relation for each layer. The relations between stress results and couples and reference surface strains and changes of curvature may be expressed in the following form.

$$\begin{Bmatrix} N_x \\ N_y \\ -M_x \\ -M_y \end{Bmatrix} = \begin{bmatrix} K & \nu K & 0 & 0 \\ \nu K & K & 0 & 0 \\ 0 & 0 & D & \nu D \\ 0 & 0 & \nu D & D \end{bmatrix} \begin{Bmatrix} \epsilon_x \\ \epsilon_y \\ \chi_x \\ \chi_y \end{Bmatrix} \qquad (2.2.4)$$

$$\begin{Bmatrix} N_{xy} \\ M_{xy} \end{Bmatrix} = \begin{Bmatrix} N_{yx} \\ M_{yx} \end{Bmatrix} = \frac{1-\nu}{2} \begin{bmatrix} K & 0 \\ 0 & D \end{bmatrix} \begin{Bmatrix} \gamma_{xy} \\ 2\chi_{xy} \end{Bmatrix} \qquad (2.2.5)$$

K is the extensional stiffness,

$$K = \frac{1}{1-\nu^2} \int_z E(z)\, dz \qquad (2.2.6)$$

D is the bending stiffness

$$D = \frac{1}{1-\nu^2} \int_z E(z)\, z^2 dz \qquad (2.2.7)$$

and the reference surface has been chosen so that

$$\int_z E(z)\, z dz = 0 \qquad (2.2.8)$$

E(z) of course is the appropriate Young's modulus of ribs or skin as a function of the thickness coordinate, z.

The integrals (2.2.6) - (2.2.8) may be evaluated geometrically by a device known as the method of the "transformed section."

Let E_o be a constant reference modulus.

$$K = \frac{E_o}{1-\nu^2} \int_z \frac{E(z)}{E_o}\, dz \qquad (2.2.9)$$

$$D = \frac{E_o}{1 - \nu^2} \int_z \frac{E(z)}{E_o} z dz \qquad (2.2.10)$$

$$0 = \int \frac{E(z)}{E_o} z^2 dz, \qquad (2.2.11)$$

The quantity $E(z)/E_o$ may now be thought of as a "transformed width" of the unit section. It is convenient to take E_o as the modulus of the skin. The skin width will then be 1.00. Only the rib will be transformed.

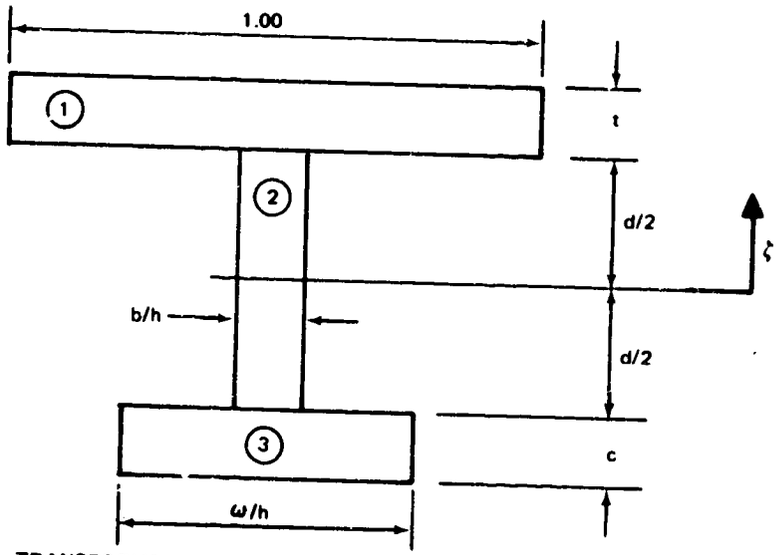

TRANSFORMED SECTION OF ISOGRID WITH FLANGE

Let

t = skin thickness

b, d = rib web thickness and depth

w, c = flange width and depth

h = triangle height

The transformed rib width is b/h. The transformed flange width is w/h. Choose an initial normal coordinate, ξ, from the midpoint of the rib web. The final normal coordinate, z, will be chosen to satisfy the condition,

$$\int_z \frac{E(z)}{E_o} \, z dz = 0$$

This is equivalent to saying that $z = 0$ is the centroid of the transformed section.

Define the following non-dimensional parameters.

$$d = \delta t$$

$$c = \lambda t$$

$$\alpha = \frac{bd}{th}$$

$$\mu = \frac{wc}{th}$$

Using the parallel axis theorem, a tabular analysis of the geometric properties of the transformed section appears as follows:

Part	A_i	ξ_i	$A_i \xi_i$	$A_i \xi_i^2$	$I_o = \frac{A_i d_i^2}{12}$
(1)	t	$\frac{t}{2}(1+\delta)$	$\frac{t^2}{2}(1+\delta)$	$\frac{t^3}{4}(1+\delta)^2$	$\frac{t}{12}(t^2)$
(2)	$t\alpha$	0	0	0	$\frac{t\alpha}{12}(\delta t)^2$
(3)	$t\mu$	$-\frac{t}{2}(1+\lambda)$	$-\frac{t^2}{2}\mu(1+\lambda)$	$\frac{t^3}{4}\mu(1+\lambda)^2$	$\frac{t\mu}{12}(\lambda t)^2$
Σ	$t(1+\alpha+\mu)$		$\frac{t^2}{2}\left[(1+\delta) - \mu(1+\lambda)\right]$	$\frac{t^3}{4}\left[(1+\delta)^2 + \mu(1+\lambda)^2\right]$	$\frac{t^3}{12}\left[1+\alpha\delta^2+\mu\lambda^2\right]$

Then

$$A = \sum_i A_i$$

$$\bar{\xi} = \frac{\Sigma_i A_i \xi_i}{A}$$

$$I = \sum_i A_i \xi_i^2 + \sum_i I_{oi} - A\bar{\xi}^2$$

A and I are respectively the area and moment of inertia of the transformed sectio .

$$A = t(1 + \alpha + \mu)$$

$$\bar{\xi} = \frac{t}{2} \frac{\left[(1+\delta) - \mu(1+\lambda)\right]}{1 + \alpha + \mu}$$

$$I = \frac{t^3}{12} \left\{ 3(1+\delta)^2 + 3\mu(1+\lambda)^2 + 1 + \alpha\delta^2 + \mu\lambda^2 - \frac{3\left[(1+\delta) - \mu(1+\lambda)\right]^2}{1 + \alpha + \mu} \right\}$$

or

$$I = \frac{t^3 \beta^2}{12(1 + \alpha + \mu)},$$

where

$$\beta^2 = (1 + \alpha + \mu)\left[3(1+\delta)^2 + 3\mu(1+\lambda)^2 + 1 + \alpha\delta^2 + \mu\lambda^2\right] - 3\left[(1+\delta) - \mu(1+\lambda)\right]^2$$

The number of independent non-dimensional parameters is four: α, δ, λ, and μ.

From eq. (2.2.9) and (2.2.10) one obtains

$$D = \frac{9}{8} E_o I$$

$$K = \frac{9}{8} E_o A \qquad (2.2.12)$$

since

$$\nu = 1/3.$$

The foregoing analysis assumes that the Poisson's ratio of the skin material is also 1/3. If this condition is not satisfied, it will not be possible to express eq. (2.2.4) and (2.2.5) in the simple form shown, Reference 2-1. For aluminum materials $\nu = 1/3$.

Certain small terms not obtainable from the foregoing integration process and arising from the twisting rigidities of the bars may be added to eq. (2.2.4) and (2.2.5). For thin rib, these terms are negligible, Reference 2-1.

2.3 NON-DIMENSIONAL STIFFNESSES FOR UNFLANGED ISOGRID

For unflanged isogrid, $\lambda = \mu = 0$ in the equations developed for flanged isogrid on the preceding pages.

$$\beta = \beta(\alpha, \delta) = \left[3\alpha(1+\delta)^2 + (1+\alpha)(1+\alpha\delta^2)\right]^{1/2} \qquad (2.3.1)$$

For construction consisting of skin alone (monocoque),

$$\alpha = \delta = o,$$

$$\beta = 1 \qquad (2.3.2)$$

In terms of α and β,

$$K = \frac{E_o t}{1-\nu^2} (1+\alpha) \qquad (2.3.3)$$

$$D = \frac{E_o t^3}{12(1-\nu^2)} \frac{\beta^2}{1+\alpha} \qquad (2.3.4)$$

It will be noted that $E_o t/1-\nu^2$ and $E_o t^3/12(1-\nu^2)$ are the extensional and bending stiffnesses of the skin alone, while the non-dimensional factors $(1+\alpha)$ and $\beta^2/(1+\alpha)$ represent the relative increases in extensional and bending stiffnesses due to the ribs.

A plot of $\beta(\alpha, \delta)$ is shown in Figure 2-1. This graph is useful when β is known and it is required to determine α and δ.

Suppose, for example, the required D and t are known. Then,

$$\frac{\beta^2}{1+\alpha} = C$$

where C is some constant value. Solving for β,

$$\beta = \sqrt{C(1+\alpha)}$$

If this relation is plotted on transparent paper to the same β, α scale as the $\beta(\alpha, \delta)$ graph and superimposed on the $\beta(\alpha, \delta)$ graph, acceptable values of α and δ may be read off.

The $\beta(\alpha, \delta)$ graph will also be found very useful for off-optimum perturbation from optimum construction.

2.4 MEMBRANE STRESSES

For many conditions the changes of curvature and associated bending stresses are negligible. The membrane stresses may be determined by simple

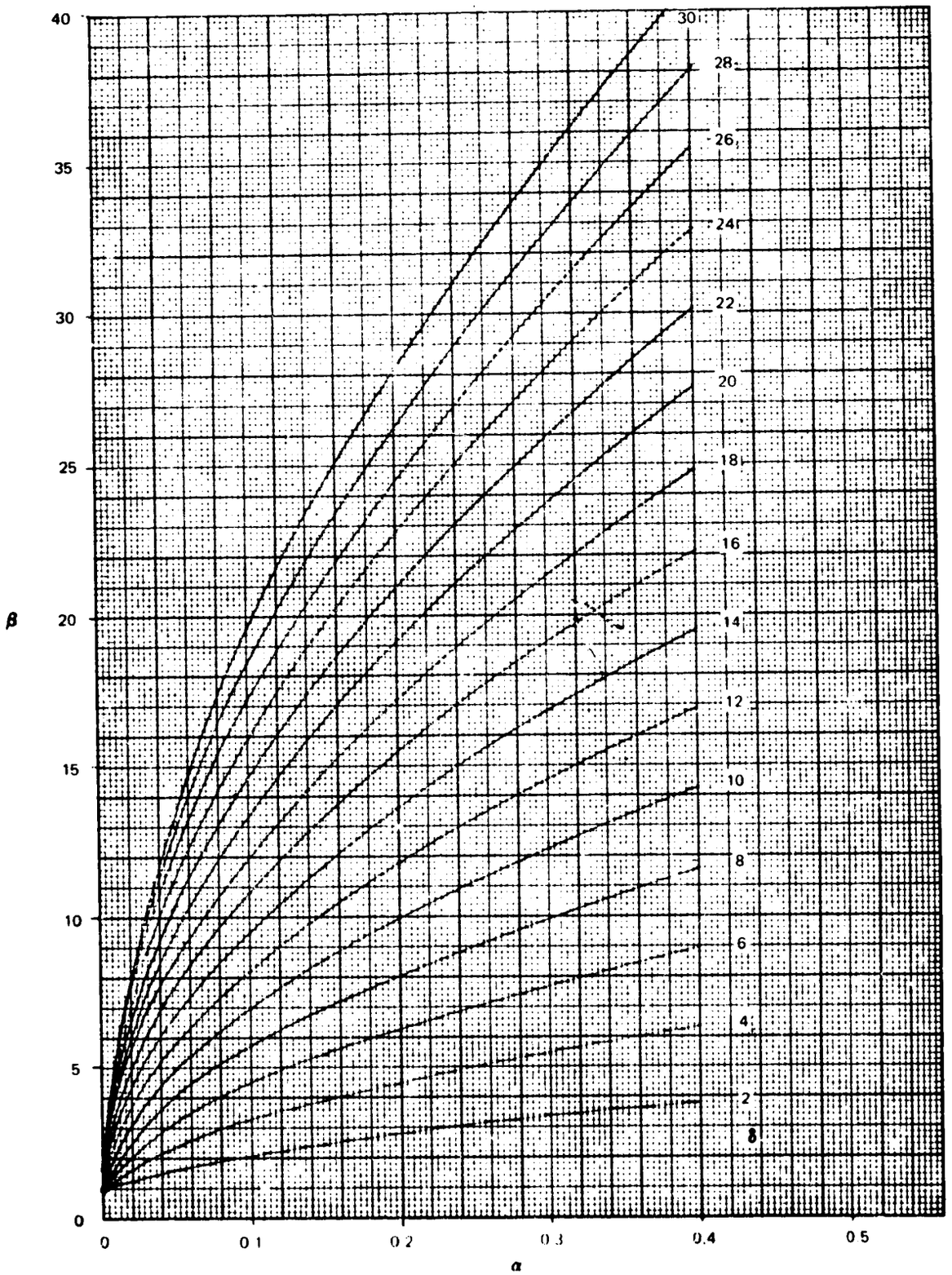

Figure 2-1. Plot of β (α , δ) Curves

equilibrium conditions or may be known from plane stress solutions in classical elasticity, Reference 2-2. Thus N_x, N_{xy}, and N_y may be regarded as given. The problem now is to solve for the skin and rib stresses. Eq. (2.2.4) reduces to,

$$\begin{Bmatrix} N_x \\ N_y \end{Bmatrix} = K \begin{bmatrix} 1 & 1/3 \\ 1/3 & 1 \end{bmatrix} \begin{Bmatrix} e_x \\ e_y \end{Bmatrix} \tag{2.4.1}$$

while

$$N_{xy} = \frac{1}{3} K \gamma_{xy} \tag{2.4.2}$$

and

$$K = \frac{9}{8} Et(1+\alpha) \tag{2.4.3}$$

solving for the strains,

$$\begin{Bmatrix} e_x \\ e_y \end{Bmatrix} = \frac{1}{Et(1+\alpha)} \begin{bmatrix} 1 & -1/3 \\ -1/3 & 1 \end{bmatrix} \begin{Bmatrix} N_x \\ N_y \end{Bmatrix} \tag{2.4.4}$$

$$\gamma_{xy} = \frac{8}{3} \frac{N_{xy}}{Et(1+\alpha)} \tag{2.4.5}$$

2.4.1 Skin Stresses

These are given by this Hooke's law relation for the skin.

$$\begin{Bmatrix} \sigma_x \\ \sigma_y \end{Bmatrix} = \frac{E}{1-\nu^2} \begin{bmatrix} 1 & 1/3 \\ 1/3 & 1 \end{bmatrix} \begin{Bmatrix} e_x \\ e_y \end{Bmatrix} \tag{2.4.6}$$

$$\tau_{xy} = \frac{E}{2(1+\nu)} \gamma_{xy} \tag{2.4.7}$$

By use of (2.4.4) and (2.4.5) one obtains the skin stresses, σ_x, σ_y, τ_{xy}.

$$\begin{Bmatrix} \sigma_x \\ \sigma_y \end{Bmatrix} = \frac{1}{t(1+\alpha)} \begin{Bmatrix} N_x \\ N_y \end{Bmatrix} \tag{2.4.8}$$

$$\tau_{xy} = \frac{1}{t(1+\alpha)} N_{xy} \tag{2.4.9}$$

If the quantity $t_{eff} = t(1+\alpha)$ is defined, then, (2.4.10)

$$\boxed{\sigma_x = \frac{N_x}{t_{eff}}, \quad \sigma_y = \frac{N_y}{t_{eff}}, \quad \tau_{xy} = \frac{N_{xy}}{t_{eff}}} \tag{2.4.11}$$

These stresses must be equal to or less than the allowable stresses in the construction. If the stresses are tensile, they may be compared with yield or ultimate allowable stress. If the stresses are compressive, one may consider constructions with buckled or unbuckled skin. In the case of buckled skin, the problem is to determine the effective stiffness of the panel. One may use effective width concepts in this case where the effective skin material is treated as a portion of this rib. In the case of unbuckled skin, the problem is to determine the buckling allowable in the skin panel. This depends upon the size of the triangle, the skin thickness, the stress field in the skin, Young's modulus and the edge fixity of the triangle. The edge fixity, in turn, depends upon the geometry of the ribs and the stress field in the ribs. Some tests have been conducted to determine conservative estimates of edge fixity and more are under development.

Triangle sizes will vary considerably depending upon buckled or unbuckled skin requirements and edge fixity values.

2.4.3 Rib Stresses

The rib stresses are a little more complicated than the skin stresses. This is due to the fact that the bars are not all oriented in the coordinate directions x and y.

From eq. (2.1.3) and (2.1.4),

$$\sigma_1 = \frac{P_1}{b} = E\, e_x$$

$$\sigma_2 = \frac{P_2}{b} = \frac{E}{4}\,(e_x + \sqrt{3}\,\gamma_{xy} + 3\,e_y)$$

$$\sigma_3 = \frac{P_3}{b} = \frac{E}{4}\,(e_x - \sqrt{3}\,\gamma_{xy} + 3\,e_y)$$

Using eq. (2.4.1) and (2.4.2) these become,

$$\boxed{\begin{aligned} \sigma_1 &= \frac{1}{3t\,(1+\alpha)}\,(3N_x - N_y) \\ \sigma_2 &= \frac{2}{3t\,(1+\alpha)}\,(N_y + \sqrt{3}\,N_{xy}) \\ \sigma_3 &= \frac{2}{3t\,(1+\alpha)}\,(N_y - \sqrt{3}\,N_{xy}) \end{aligned}} \qquad (2.4.12)$$

One notes that if N_x and N_y are principal stress resultants, $N_{xy} = 0$

$$\sigma_1 = \frac{1}{t(1+\alpha)}\left(N_x - \frac{1}{3}\,N_y\right) \qquad (2.4.13)$$

$$\sigma_2 = \sigma_3 = \frac{2}{3t(1+\alpha)}\,N_y$$

If, in addition, $N_y = 0$, then $\sigma_2 = \sigma_3 = 0$

and

$$\sigma_1 = \frac{N_x}{t_{eff}} \qquad (2.4.14)$$

Note in the application of eq. (2.4.12) that the 1 bar is oriented in the direction of the x axis and that the 2 and 3 bars are at ±60 degrees to the x axis, see sketch on Page 2.0.019.

For example, consider a cylinder with internal pressure with one set of ribs in the circumferential direction. In this case, x is the hoop coordinate and y is the longitudinal coordinate.

$$N_x = pR,$$

$$N_y = \frac{pR}{2},$$

$$N_{xy} = 0$$

and,

$$\sigma_x = \frac{pR}{t_{eff}},$$

$$\sigma_y = \frac{pR}{2t_{eff}},$$

$$\sigma_1 = \frac{5}{6}\frac{pR}{t_{eff}},$$

$$\sigma_2 = \sigma_3 = \frac{pR}{3t_{eff}}$$

2.5 EQUIVALENT MONOCOQUE E* AND t*

Because of the isotropic properties of the construction, it is possible to use all the established isotropic solutions from extensively developed theory for plates and shells, References 2-2 to 2-8.

In many cases, these are expressed in terms of the bending and extensional stiffness. In other cases, however, the solutions have been reduced to more primitive parameters. For such cases, it is possible to determine an equivalent monocoque thickness, t* and Young's modulus, E*, which will give the same bending and extensional stiffnesses as (2.2.7) and (2.2.6).

Thus,

$$K = \frac{E^* t^*}{1-\nu^2} = \frac{E_o A}{1-\nu^2} = \frac{E_o t}{1-\nu^2}(1+\alpha) \qquad (2.5.1)$$

$$D = \frac{E^* t^{*3}}{12(1-\nu^2)} = \frac{E_o I}{1-\nu^2} = \frac{E_o t^3}{12(1-\nu^2)} \frac{\beta^2}{1+\alpha} \qquad (2.5.2)$$

where A and I are the transformed area and moment of inertia and where the expressions in α and β are valid for unflanged isogrid.

Solving (2.5.1) and (2.5.2) for t* and E*,

$$t^* = \sqrt{\frac{12I}{A}} = t\frac{\beta}{1+\alpha} \qquad (2.5.3)$$

$$E^* = E\frac{A}{t^*} = E\frac{(1+\alpha)^2}{\beta} \qquad (2.5.4)$$

Note that once again, the first factor pertains to the skin property and that the second non-dimensional factor represents the influence of the rib grid. Thus for no ribs,

$$t^* = t$$

$$E^* = E$$

Since $\alpha = 0$ and $\beta = 1$ for no ribs.

In using eq. (2.5.3) and (2.5.4) a word of caution is required. Since t* and E* reproduce the required bending and extensional stiffnesses, D and K, it is important to note that these are related to stress resultants and stress couples only and not to stresses. Thus, the equations into which t* and E* are to be substituted must be expressed in terms of stress resultants and couples.

Use of t* and E* for deflections is also permissible since deflections are geometrically related to strains.

To obtain a quantitative idea of the magnitude of t* and E*, it is found by experience that for many optimum constructions, one has approximately,

$$\alpha = 1/3,$$

$$\beta = 16$$

Since the equivalent weight thickness, $\bar{t}$, is given by

$$\bar{t} = t(1+3\alpha) \tag{2.5.6}$$

this implies an equal distribution of rib and skin material.

Thus,

$$\begin{cases} t^*_{opt} = 16\left(\frac{3}{4}\,t\right) = 12t & (2.5.7) \\ E^*_{opt} = \left(\frac{16}{9}\right)\left(\frac{1}{16}\,E\right) = \frac{1}{9}E_o & (2.5.8) \end{cases}$$

$$\begin{cases} K_{opt} = \dfrac{E_o t}{1-\nu^2}\left(\dfrac{4}{3}\right) & (2.5.9) \\ D_{opt} = \dfrac{E_o t^3}{12(1-\nu^2)}\left[\dfrac{(16)^2}{1+\frac{1}{3}}\right] & \\ D_{opt} = \dfrac{E_o t^3}{12(1-\nu^2)}\,192 & (2.5.10) \end{cases}$$

Thus the extensional stiffness for many optimized constructions is increased by a factor of 4/3, and the bending stiffness is increased by a factor of 192 by the addition of an equal weight of material in ribs to the original skin material.

2.6 SUMMARY OF BASIC THEORY

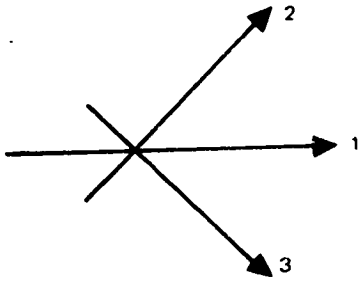

RIB ORIENTATIONS

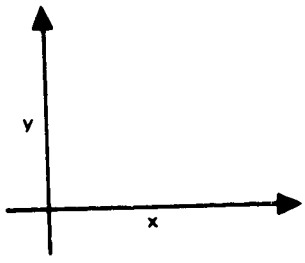

COORDINATES

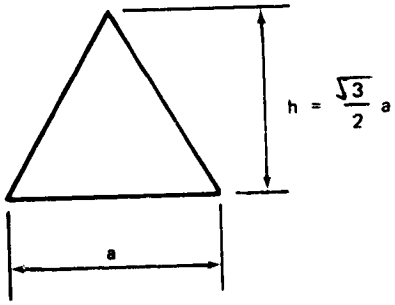

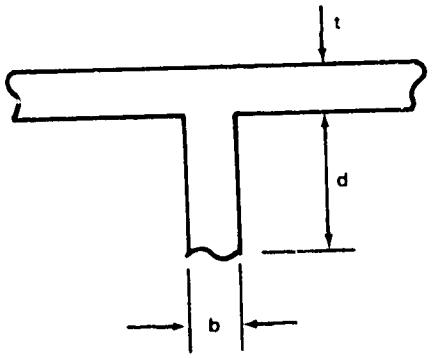

GRID GEOMETRY

2.6.1 Non-dimensional Parameters

$$\alpha = \frac{bd}{th},$$

$$\delta = \frac{d}{t},$$

$$\beta = \left[3\alpha(1+\delta)^2 + (1+\alpha)(1+\alpha\delta^2)\right]^{1/2}$$

2.6.2 Grid Moduli

$$\bar{E} = \frac{b}{h} E ,$$

$$\bar{\nu} = 1/3$$

2.6.3 Rigidities

Extensional, K

$$K = \frac{9}{8} \int_z E(z)\, dz = \frac{9}{8} E_o A = \frac{9}{8} E_o t(1+\alpha)$$

Bending, D

$$D = \frac{9}{8} \int_z E(z)\, z^2 dz = \frac{9}{8} E_o I = \frac{9}{8} \frac{E_o t^3}{12} \left(\frac{\beta^2}{1+\alpha} \right)$$

Neutral Axis

$$\int_z E(z)\, z dz = 0 = \text{centroid of transformed area, A.}$$

2.6.4 Equivalent t* and E*

$$t^* = \sqrt{\frac{12I}{A}} = t \frac{\beta}{1+\alpha}$$

$$E^* = E_o \frac{A}{t^*} = E_o \frac{(1+\alpha)^2}{\beta}$$

2.6.5 Composite Stress-Strain Relations

$$\begin{Bmatrix} N_x \\ N_y \end{Bmatrix} = K \begin{bmatrix} 1 & 1/3 \\ 1/3 & 1 \end{bmatrix} \begin{Bmatrix} e_x \\ e_y \end{Bmatrix}$$

$$\begin{Bmatrix} M_x \\ M_y \end{Bmatrix} = -D \begin{bmatrix} 1 & 1/3 \\ 1/3 & 1 \end{bmatrix} \begin{Bmatrix} \chi_x \\ \chi_y \end{Bmatrix}$$

$$N_{xy} = \frac{K}{3} \gamma_{xy},$$

$$M_{xy} = \frac{D}{3} (2\chi_{xy})$$

2.6.6 Membrane Skin Stresses

$$\sigma_x = \frac{N_x}{t_{eff}},$$

$$\sigma_y = \frac{N_y}{t_{eff}},$$

$$\tau_{xy} = \frac{N_{xy}}{t_{eff}}$$

$t_{eff} = t(1+\alpha)$ = A = Transformed area

2.6.7 Membrane Rib Stresses

$$\sigma_1 = \frac{1}{t_{eff}} (N_x - \tfrac{1}{3} N_y)$$

$$\sigma_2 = \frac{2}{3t_{eff}} (N_y + \sqrt{3}\, N_{xy})$$

$$\sigma_3 = \frac{2}{3t_{eff}} (N_y - \sqrt{3}\, N_{xy})$$

2.6.8 Equivalent Weight Thickness

$$E = t(1+3\alpha)$$

Section 3
ISOGRID CHARACTERISTICS AND ADVANTAGES

Isogrid is a lattice of stiffening ribs forming an array of contiguous equilateral triangles. This is the simplest arrangement of bar elements that exhibits isotropic properties, hence the name "isogrid". Intersecting ribs so arranged make a complete structure whether attached to a skin as stiffening or used as an open lattice.

Because of the isotropic property and an effective Poisson's ratio of 1/3, like most homogeneous structural metals, isogrid can be mathematically transformed to an equivalent homogeneous material layer (see Figure 3-1). The transformed expression can be substituted into the shell equations in available literature to analyze the gross behavior of isogrid structures. More detailed finite element analysis is needed to examine local stresses in the critical areas of nodal intersections and the bars.

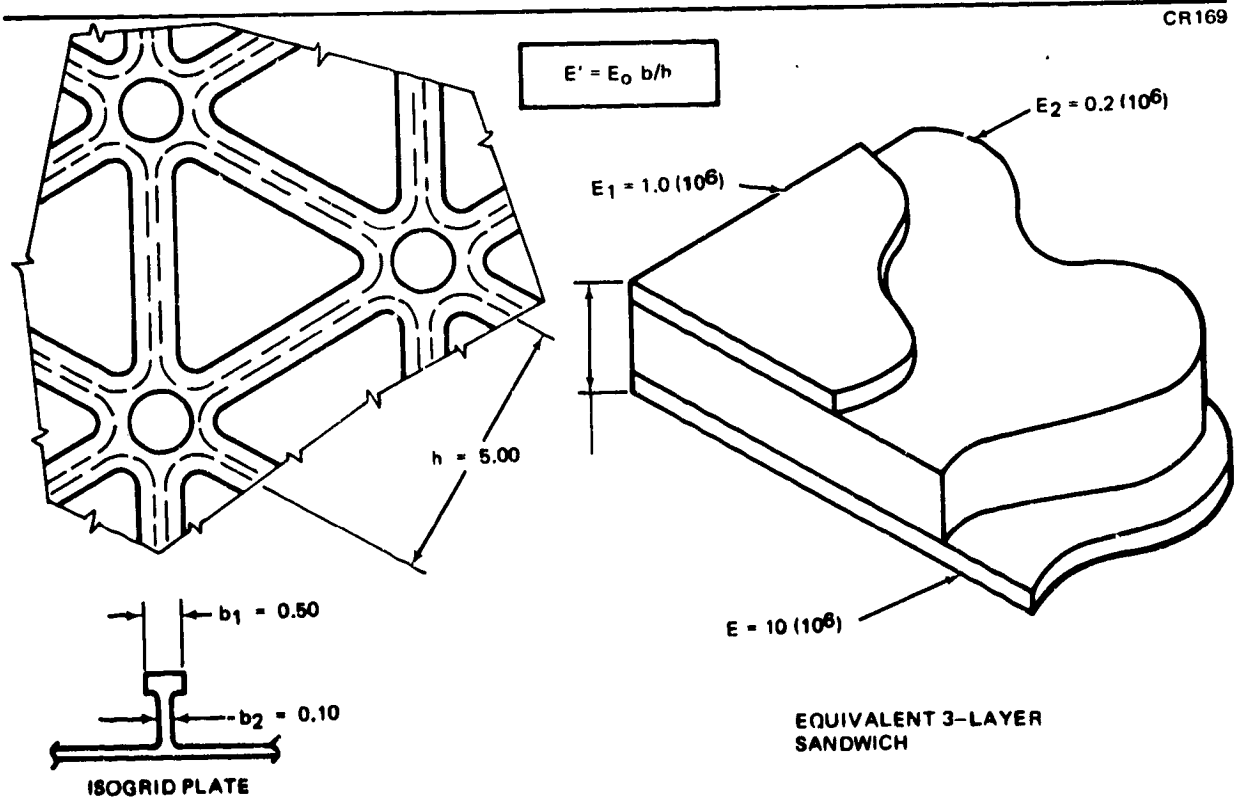

Figure 3-1. Isogrid Is Simple to Analyze

Being easy to analyze, the construction is also readily optimized as will be shown in Section 4. Basic structure sizing over a wide range of load intensities can be accomplished rapidly, allowing a quick and accurate study of the effect of standardizing geometry. As shown in Section 4-13, this technique has been applied to a large integrally stiffened propellant tank to prove that the penalty of geometric standardization is very small – about half of one percent, in a recent phase B shuttle design.

As originally applied in a hardware program (the Orbital Workshop module of the Skylab), isogrid open lattice of standardized geometry forms the walls and floors of the crew quarters and internal experiment space. The intention here was to provide a "pegboard" pattern of equipment mounting points, readily adaptable to change. As can be seen in Figures 3-2 and 3-3, the equipment components are attached at the waffle nodes without structural rework. It is evident that removal of the mounted equipment leaves the substructure exactly as it was, permitting installation of any other installation designed to fit the pattern. This scheme has advantages for a long-term space base that will be periodically refurbished and updated with newly developed advanced equipment.

The design requirement for this construction was a limit load capability of 250 pounds applied normal to the surface at any nodal point. Failure occurred at 750 pounds in static test although the panels are equivalent in weight to a continuous 0.025 aluminum sheet (0.36 pounds per square foot). The geometry is depicted in Figure 3-4.

While substantial local load capability is inherent in unreinforced isogrid, occasionally local reinforcement is required to handle large concentrated loads. How this can be accomplished with minimum weight is shown in Subsections 4.5 and 4.6. As an example of the efficiency provided by ribs and skin working together dissipating load, an 8-foot-diameter cylinder designed for a compressive load intensity of 2,500 pounds per inch required only 4.3 pounds of additional weight to handle a concentrated tangential load of 20,000 pounds. This was distributed within a hexagon 24 inches across the flat (see Figure 3-5).

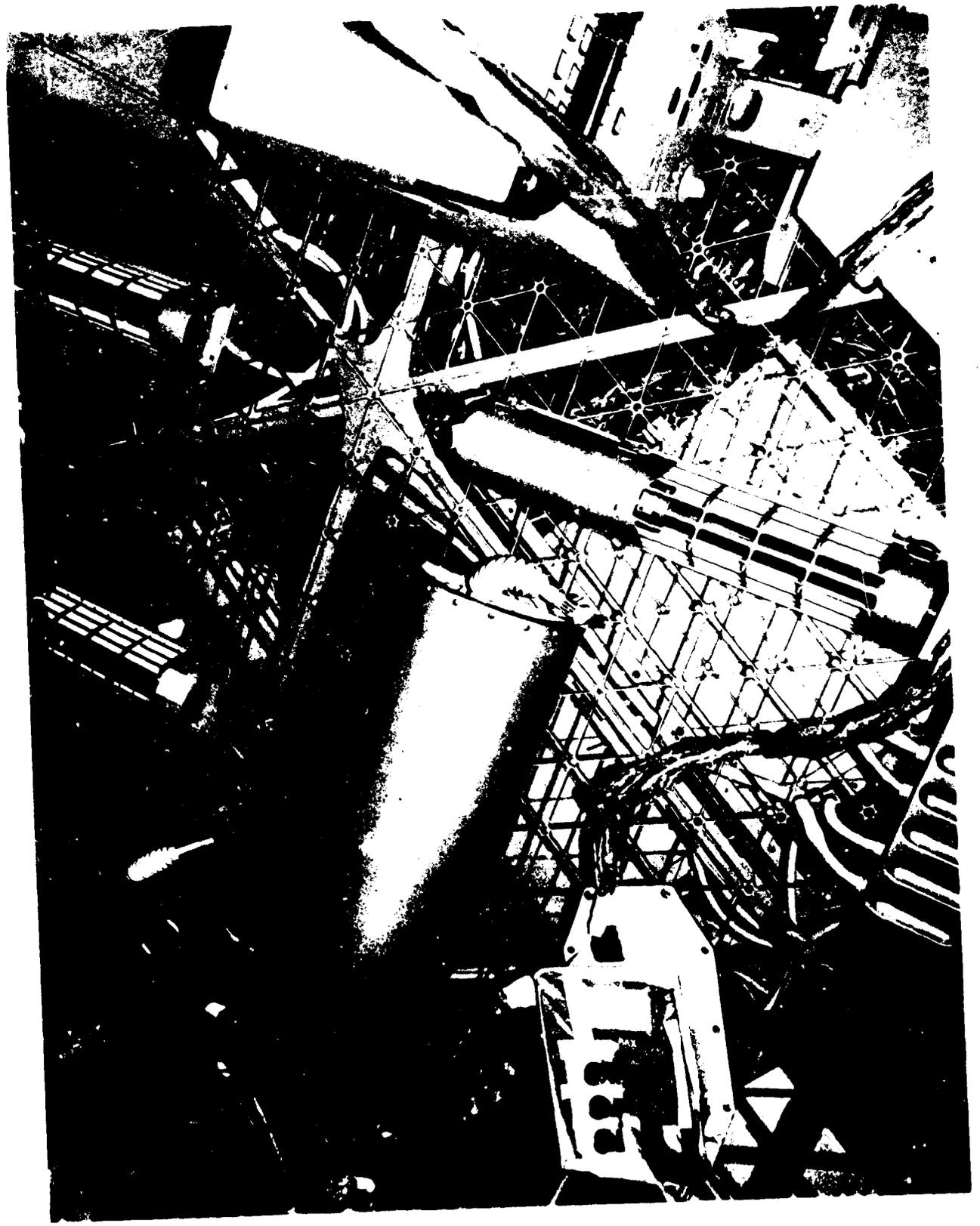

Figure 3-2. Distributing Concentrated Load

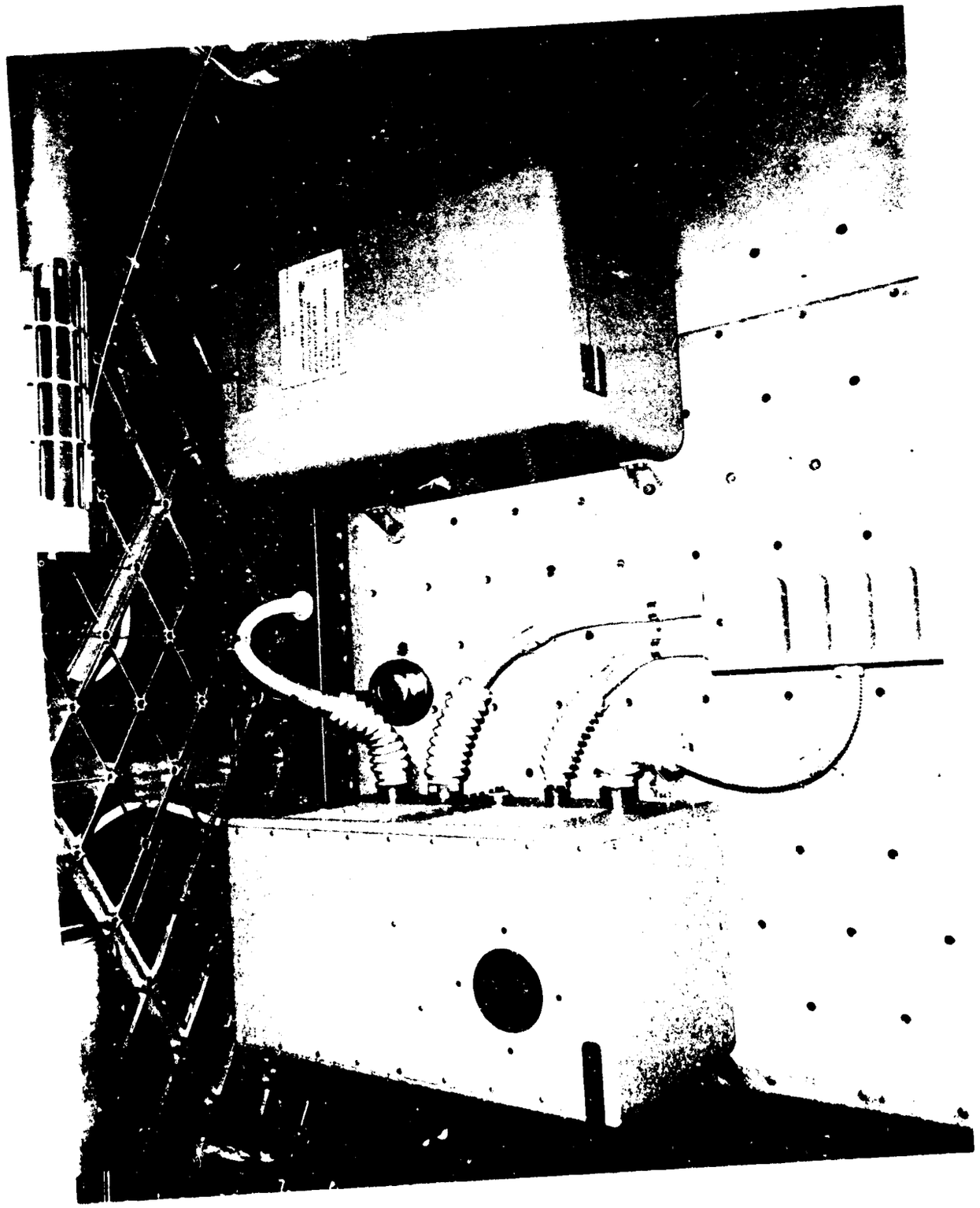

Figure 3-3. Equipment Attached to Nodes

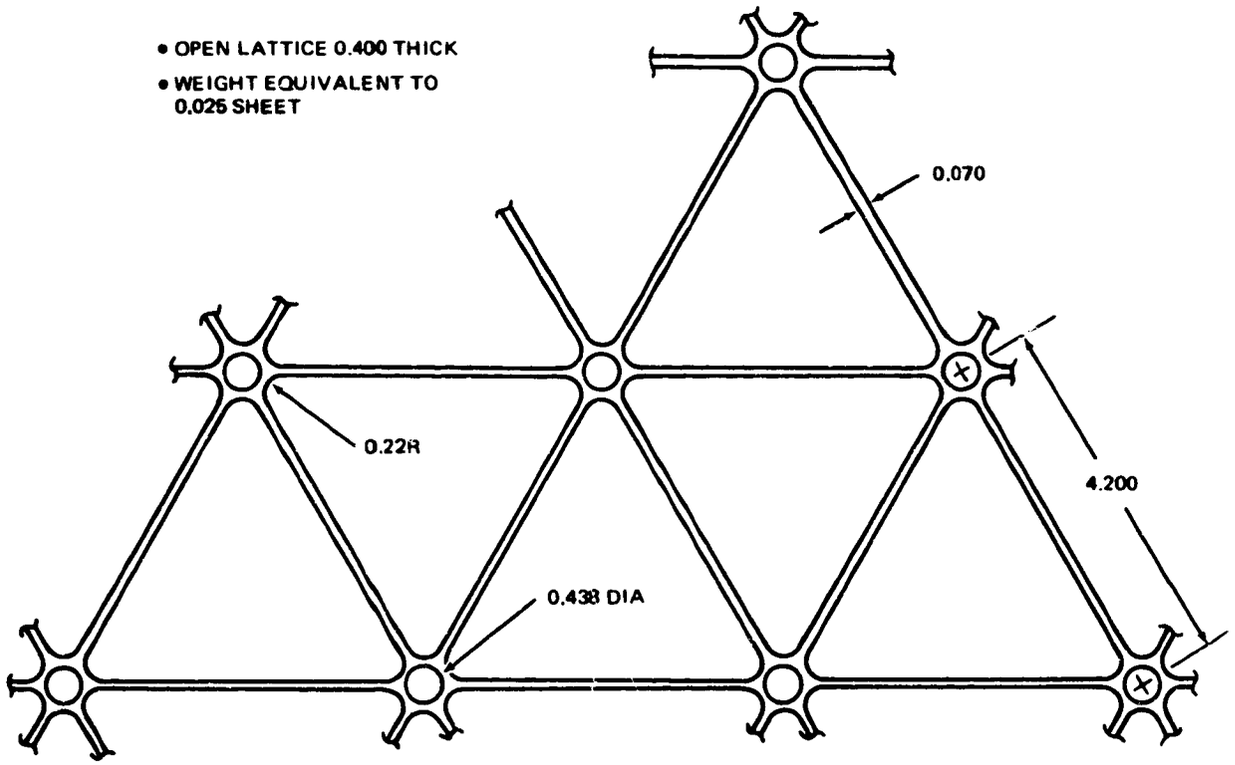

Figure 3-4. Skylab Floor and Wall Grid

As has been mentioned, the isogrid lattice is a complete structure by itself; that is, it can effectively resist tension, compression, shear, and bending loads. Stiffened by such a lattice, a skin has the same capabilities. Therefore, either skin or lattice can be locally reinforced to handle local loads or discontinuities from cutouts. This choice offers more design flexibility than available with rectangular stiffening systems.

Similarly, this redundancy should offer exceptional opportunities to design fail-safe structure. If, for example, the lattice is made separate from the skin and then assembled to it, a crack in either lattice or skin cannot be propagated across the joint. Shear and tensile loads in the skin can be carried around the flaw by the redundant lattice system. Since this is not the case with present rectangular stiffening systems, it should be possible to obtain fail-safe design at lower weight in isogrid, Figure 3-6.

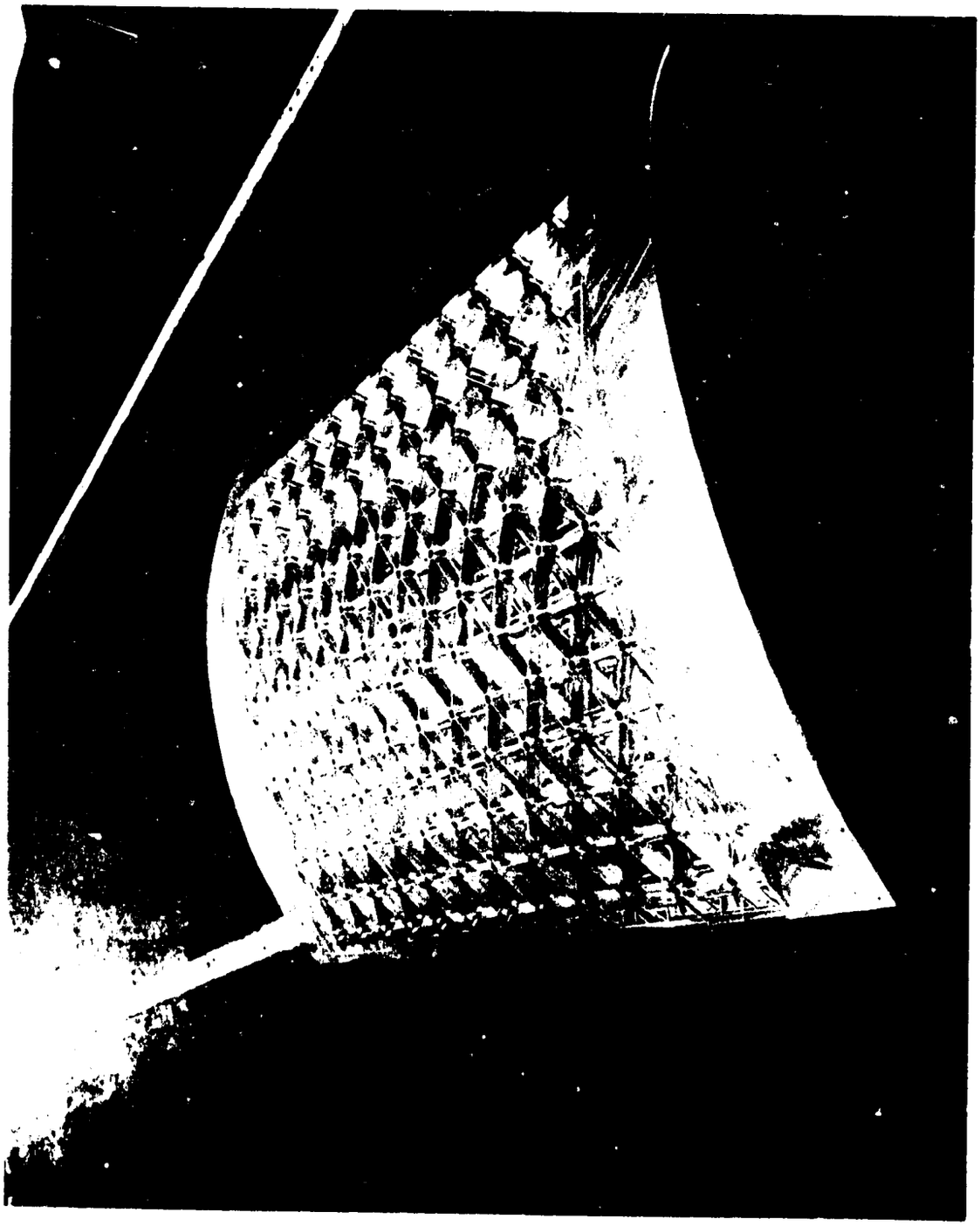

Figure 3-5. Reinforced Hole for Concentrated Load

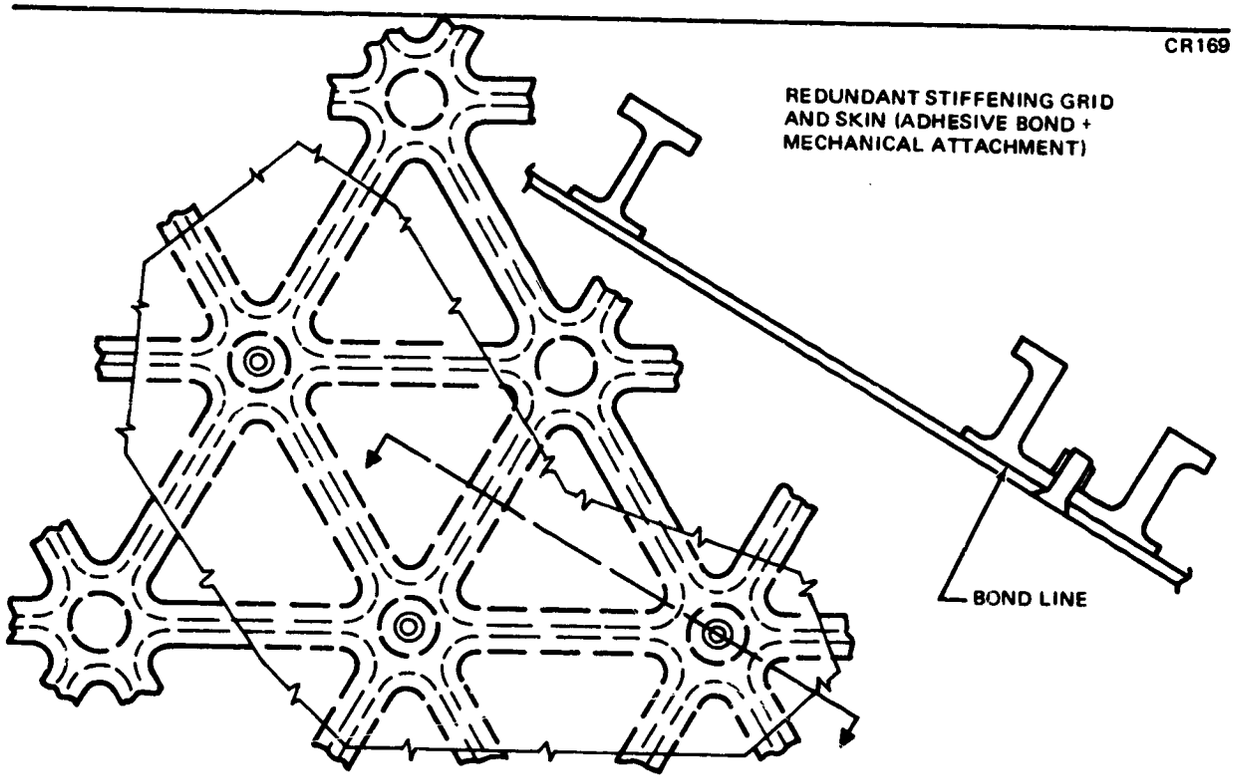

Figure 3-6. Fail-Safe Concept

The rib lattice, carrying shear load and with its centroid spaced away from the skin, in effect forms a second surface of a torque box. Therefore, triangularly stiffened panels are torsionally stiff. This means that situations where torsional stiffness is needed can be met with an isogrid open construction instead of a closed torque box. The advantages of inspectability, access to all surfaces, and elimination of moisture entrapment are obvious. This kind of design can be applied to structural components such as access doors, landing gear doors, door jambs, and speed brakes. Figures 3-7 and 3-8 show typical examples.

In compression-loaded cylinders, isogrid has been found advantageous in another respect: it occupies less depth for the same compressive capability as a rectangular stiffening system. This is true in the case when both kinds of stiffening are in the form of constant depth waffle, even more so when the orthotropic construction is optimum – with frames deeper than the stringers. In a purely structural sense this is not important, but many designs require clear space inside the frames. The deeper they are, the larger the containing shell and therefore the weight. As an example, a recent study

CR169

BUILT-UP SHEET METAL

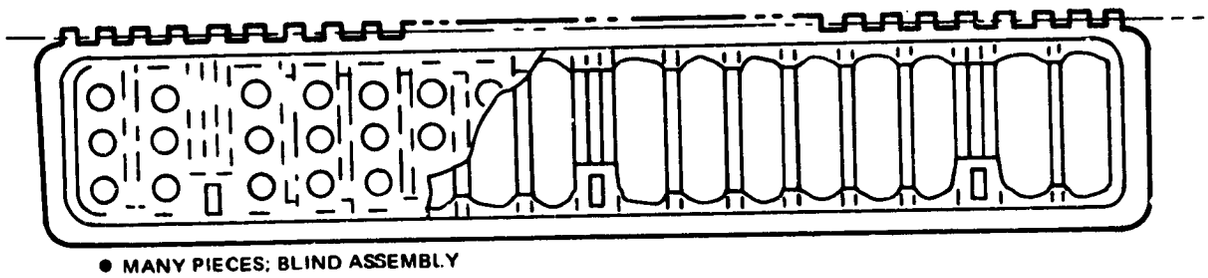

● MANY PIECES; BLIND ASSEMBLY

INTEGRAL WAFFLE

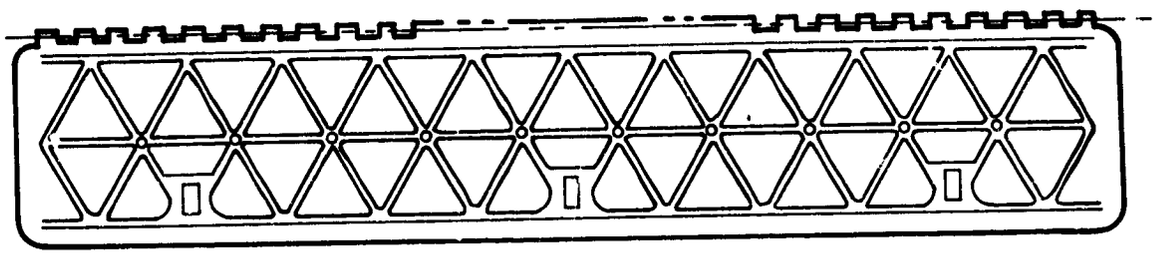

● ONE PIECE

Figure 3-7. Access Door Designs

CR619

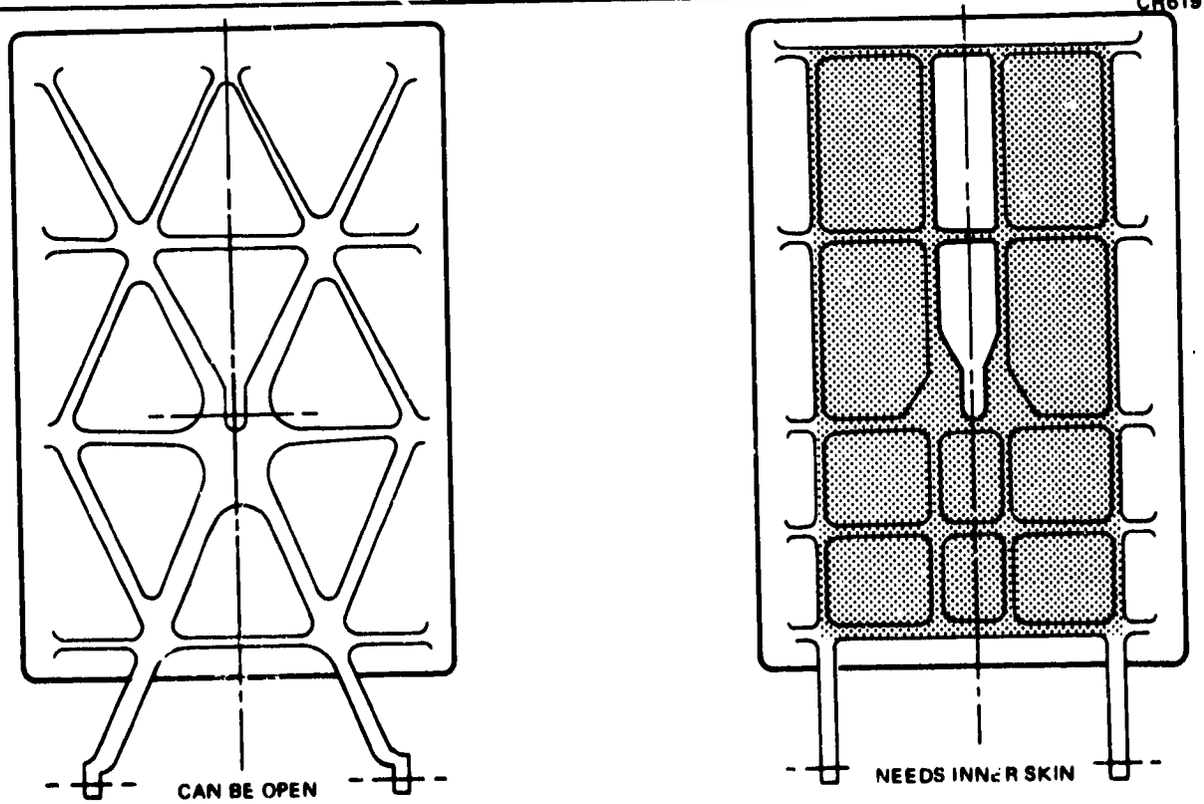

Figure 3-8. Speed Brakes

substituted isogrid for conventional construction in a transport airplane, permitting reduction in fuselage structural depth from 4 inches to 1.5 inches.

The depth of construction noted above was that obtained by the simple optimization technique described in Subsection 4.2. Both weight efficiency and structural space efficiency can be improved if the isogrid ribs are flanged. This was proved in a space shuttle booster study where the depth of construction for a 198-inch radius and 10,000 pounds per inch compressive loading was 2.25 inches. Figures 3-9 and 3-10 show manufacturing samples of this construction and a larger formability test specimen. The analysis does not in this case optimize in a single step with a unique solution. Iterative techniques must be employed. As a design progresses from the preliminary sizing to the final configuration, refinements of this kind are in order.

The practical applications of the advantages of isogrid mentioned above are a few of the cases so far encountered. More are sure to be uncovered with time.

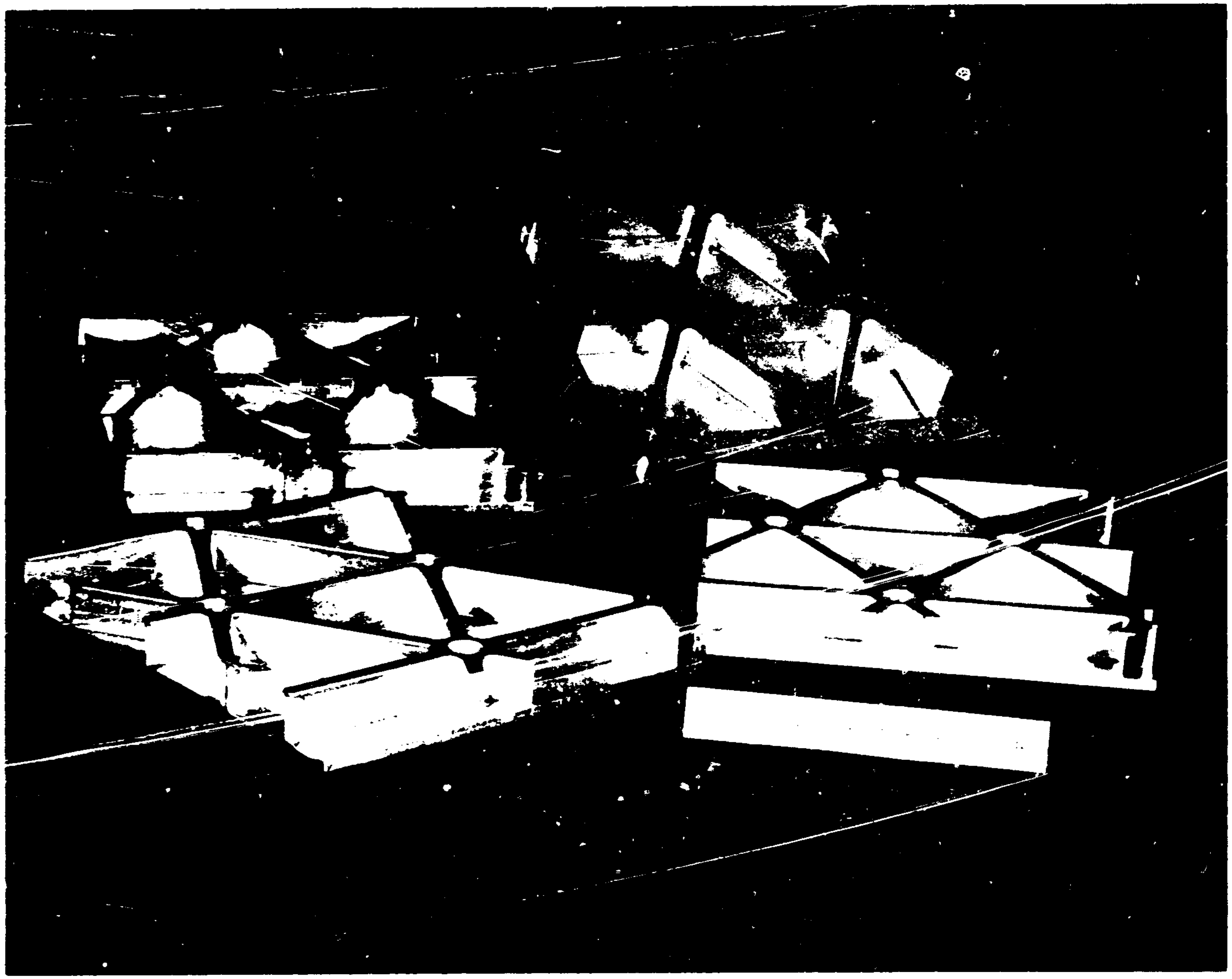

Figure 3-9 Manufacturing Samples of Isogrid

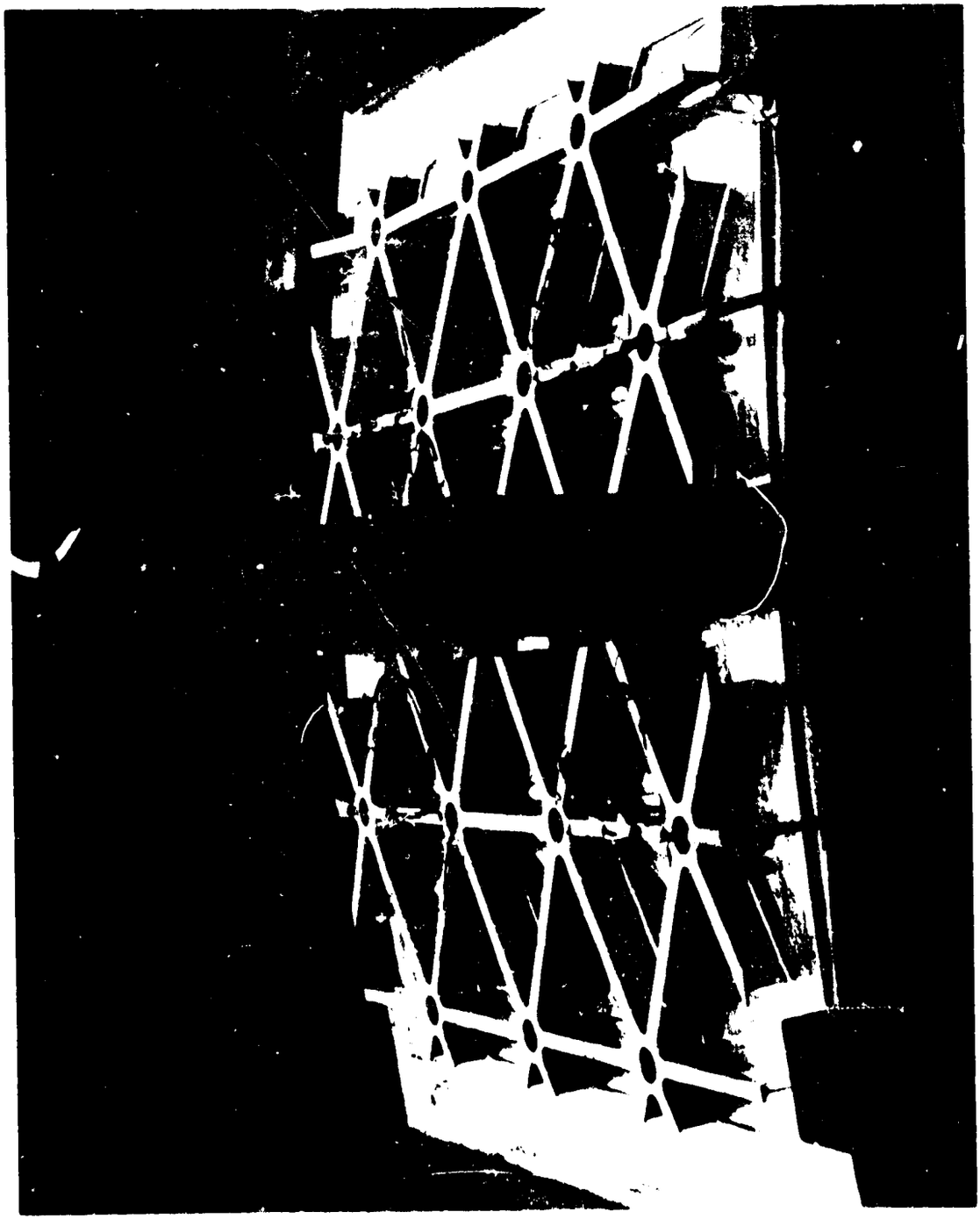

Figure 3.3.0 Forebody Image of Sample

Section 4
ANALYTICAL TECHNIQUES

4.1 SPHERICAL CAP WITH REVERSED PRESSURE

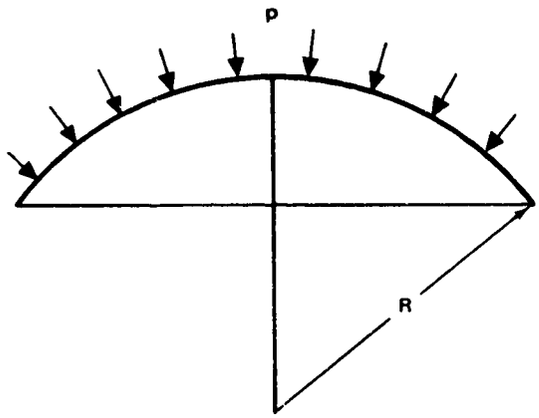

The spherical cap with reversed pressure consists of a portion of a sphere cut off by a plane and loaded by uniform external pressure.

The load/in. in the sphere is uniform in all directions and is given by the equation,

$$N_\phi = N_x = \frac{pR}{2}$$

4.1.1 Typical Design Situations

This situation in design occurs most frequently for common bulkheads used for separating propellants, such as LOX and LH_2 tanks. Considerable vehicle length and skirt material may frequently be saved by such designs. Generally, the bulkheads are designed for tension. For some loading procedures, however, reversed compressive pressure may act upon the bulkhead so that it must also be designed for stability under the compression loading.*

*It was this design condition which initiated the development of isogrid in 1964. (Reference 2-9)

Other design possibilities might be spherical end closures in cylinders subjected to external hydrostatic pressure such as vacuum tanks or submersibles.

4.1.2 Method of Optimization

The optimization technique used assumed that minimum weight occurs when all modes of buckling i.e., general instability, rib-crippling, and skin buckling are equally likely. This optimization principle is popularly known as the "one-horse shay" design principle. It assumes, in particular, that the various modes of buckling failure are uncoupled.

General Instability

Buckling of a complete sphere may be written in the form, Reference 2-4,

$$N_{cr}(1) = \frac{1}{\sqrt{3\,(1-\nu^2)}}\,\frac{E\,t^2}{R} \qquad (4.1.1)$$

Since eq. (4.1.1) is in the form of a stress resultant, the equivalent t* and E* of (2.5.3) and (2.5.4) may be used to transform (4.1.1) into an isogrid formula.

$$N_{cr}(1) = \frac{1}{\sqrt{3\,(1-\nu^2)}}\,\frac{E^*\,t^{*2}}{R}$$

$$= \frac{E\,t^2}{\sqrt{3\,(1-\nu^2)}}\,\frac{(1+\alpha)^2}{\beta}\,\frac{\beta^2}{(1+\alpha)^2}$$

$$N_{cr}(1) = \frac{E\,t^2}{\sqrt{3\,(1-\nu^2)}}\,\beta \qquad (4.1.2)$$

This equation shows the typical form of isogrid equations using α, β and δ, in that the first factor gives the strength of the skin and the second factor shows the nondimensional increase due to the addition of the ribs. For typical optimum designs, $\beta = 16$.

Since test values generally fall below theory, it is customary to apply a "knockdown" or "correlation factor," γ, to eq. (4.1.2), Reference 2-8.

$$N_{cr}(1) = \frac{\gamma}{\sqrt{3\,(1 - \nu^2)}} \frac{E\,t^2}{R} \beta$$

$$N_{cr}(1) = c_0 \frac{E\,t^2}{R} \beta \qquad (4.1.3)$$

With a proper interpretation of c_o to account for the reduction due to boundary effects, eq. (4.1.3) may also be used for spherical caps under external pressure.

Skin Buckling

From Reference 2-9, the buckling stress in an equilateral triangle under equal biaxial loading with simply supported edges is given by the equation,

$$\sigma_{cr} = \frac{k_c\,\pi^2 E}{12\,(1 - \nu^2)} \left(\frac{t}{a}\right)^2 \qquad (4.1.4)$$

$$k_c = 5.0$$

Thus

$$\frac{k_c\,\pi^2}{12\,(1 - \nu^2)} = \frac{5.0\,\pi^2}{12\left(\frac{8}{9}\right)} = 4.62$$

From eq. (2.4.11) the skin stress in terms of the pressure is:

$$\sigma_x = \sigma_y = \frac{p_{cr} R}{2t (1 + \alpha)} \tag{4.1.5}$$

Using eq. (4.1.4),

$$N_{cr}(2) = \frac{p_{cr} R}{2} = 4.62 \, Et \, (1 + \alpha) \left(\frac{t}{a} \right)^2$$

$$N_{cr}(2) = c_1 \, Et \, (1 + \alpha) \, \frac{t^2}{h^2} \tag{4.1.6}$$

where

$$c_1 = \left(\frac{\sqrt{3}}{2} \right)^2 4.62 = 3.47$$

Rib Crippling

From Reference 2-4, the buckling stress in a long plate simply supported on three edges and free on the fourth edge is,

$$\sigma_{cr} = \frac{k_c \, \pi^2 E}{12 (1 - \nu^2)} \left(\frac{b}{d} \right)^2 \tag{4.1.7}$$

$$k_c = 0.456$$

Thus

$$\frac{k_c \, \pi^2}{12 (1 - \nu^2)} = \frac{0.456 \, \pi^2}{12 \left(\frac{8}{9} \right)} = 0.422$$

From eq. (2.4.12) for

$$N_x = N_y = \frac{p_{cr} R}{2} = N_{cr}(3)$$

$$N_{xy} = 0$$

$$\sigma_{cr} = \sigma_1 = \sigma_2 = \sigma_3 = \frac{2}{3t(1+\alpha)} N_{cr}(3) \qquad (4.1.8)$$

Using (4.1.7),

$$N_{cr}(3) = \frac{3}{2} t(1+\alpha)\left[0.422\, E \left(\frac{b}{d}\right)^2\right]$$

$$= c_2 E t (1+\alpha)\left(\frac{b}{d}\right)^2 \qquad (4.1.9)$$

$$c_2 = \frac{3}{2}(0.422) = 0.634$$

Optimum Requirements

Collecting formulas, one now has the system of equations,

$$N_{cr}(1) = c_0 E \frac{t^2}{R} \beta = \frac{p_{cr} R}{2} \qquad (4.1.10)$$

$$N_{cr}(2) = c_1 E t (1+\alpha) \frac{t^2}{h^2} \qquad (4.1.11)$$

$$N_{cr}(3) = c_2 E t (1+\alpha) \frac{b^2}{d^2} \qquad (4.1.12)$$

For optimum requirements, (4.1.10) to (4.1.12) must be simultaneously satisfied. Now these equations are indeterminate, in that four parameters are to be determined, b, d, t, and h, while only three equations are given.

As a fourth equation, one may consider the burst condition,

$$F_{tu} = \frac{pR}{2t\,(1+\alpha)} \qquad (4.1.13)$$

where p is the burst pressure and F_{tu} is the tensile strength of the material. Strictly speaking, eq. (4.1.13) holds only in the elastic region of loading. Its use for burst conditions is conservative, since in the plastic state the ribs will be more highly loaded than for elastic predictions.

It will be found for many design conditions that pressures higher than those given by use of eq. (4.1.13) will yield lower weight designs! For example, there may be no internal pressure. Obviously, some finite skin thickness, t, is required while use of eq. (4.1.13) will give t = 0. The physical interpretation of this phenomenon is that higher pressures mean thicker skins. which in turn implies larger grid sizes, a, so that deeper ribs may result for a given amount of rib material. This will occur for increasing pressures until the increase in skin weight counteracts the increase in general instability due to deeper ribs.

As a consequence, an optimum burst pressure exists which divides all designs into two classes. In the first class are all designs whose burst pressure is less than the optimum pressure. These designs are called " compression-critical" designs. They will have the very desirable property that burst margins are in excess of requirements. This can be a very important effect for prevention of critical growth of flaws in cyclic loading. In the second class are all designs whose optimum pressure is less than the burst pressure. In these cases, the burst pressure dominates. These designs are called "pressure-critical."

To solve eq. (4.1.10) – (4.1.13) simultaneously, introduce the non-dimensional loading parameter, $\overline{N}$.

$$\overline{N} = \frac{p_{cr}}{E}\left(\frac{F_{tu}}{p}\right) \qquad (4.1.14)$$

from (4.1.11), (4.1.13) and (4.1.14),

$$\overline{N} = c_1 \left(\frac{t}{h}\right)^2 \tag{4.1.15}$$

From (4.1.12), (4.1.13) and (4.1.14),

$$\overline{N} = c_2 \left(\frac{b}{d}\right)^2 \tag{4.1.16}$$

Multiplying (4.1.15) and (4.1.16),

$$\overline{N}^2 = c_1 c_2 \frac{b^2 t^2}{h^2 d^2} = c_1 c_2 \left(\frac{bd}{th}\right)^2 \left(\frac{t}{d}\right)^4$$

$$= c_1 c_2 \frac{\alpha^2}{\delta^4}$$

Thus, since α and δ are positive,

$$\overline{N} = \sqrt{c_1 c_2}\, \frac{\alpha}{\delta^2} \tag{4.1.17}$$

Eq. (4.1.17) satisfies the conditions of simultaneous rib-crippling, skin buckling, and burst.

From eq. (4.1.10), (4.1.13) and (4.1.14),

$$\overline{N} = c_0 \frac{t}{R} \frac{\beta}{1+\alpha} = c_0 \frac{p}{F_{tu}} \frac{\beta}{(1+\alpha)^2}$$

or

$$2\overline{N} \frac{F_{tu}}{p} = c_0 \frac{\beta}{(1+\alpha)^2} \tag{4.1.18}$$

Eq. (4.1.18) satisfies the condition of simultaneous general instability and burst.

If the non-dimensional loading parameters

$$x = \frac{\bar{N}}{\sqrt{c_1 c_2}} \left(10^3\right) \tag{4.1.19}$$

$$y = \frac{2 \bar{N} F_{tu}}{c_0 p} \tag{4.1.20}$$

are defined, then eq. (4.1.17) and (4.1.18) become,

$$x = \frac{\alpha}{\delta^2} \left(10^3\right) \tag{4.1.21}$$

$$y = \frac{\beta}{(1 + \alpha)^2} \tag{4.1.22}$$

It is noteworthy that the right-hand sides of these equations are pure functions of the geometry. Boundary conditions for the plate elements and correlation factor are not involved. For this reason it is convenient to stop at this point and consider the solution as a mapping of the α, δ domain into the x, y domain instead of attempting a simultaneous solution. The mapping solution will thus have a validity that is independent of c_0, c_1, and c_2.

The equivalent weight thickness, $\bar{t}$, is,

$$\bar{t} = t (1 + 3\alpha)$$

Using eq. (4.1.13) this becomes,

$$\bar{t} = \frac{p R (1 + 3\alpha)}{2 F_{tu} (1 + \alpha)} \quad , \text{ i.e.,}$$

$$\frac{\bar{t}}{R} = \frac{p}{2 F_{tu}} \left(\frac{1 + 3\alpha}{1 + \alpha}\right) \tag{4.1.23}$$

One now has the complete solution in terms of the nondimensional loading parameters, p/F_{tu} and p_{cr}/E.

By varying p/F_{tu} for a given value of p_{cr}/E, the nondimensional weight curve may be constructed.

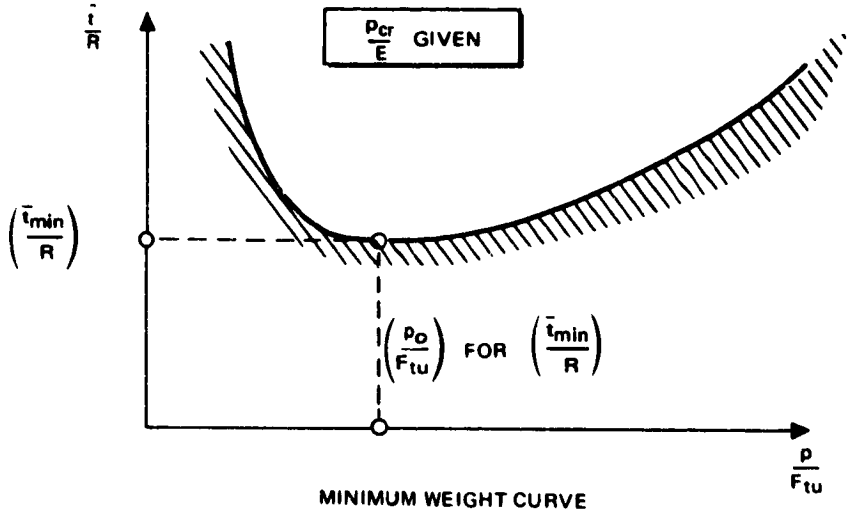

MINIMUM WEIGHT CURVE

Define the pressure for $(\bar{t}_{min}/R)$ as p_o. If $(\bar{t}_{min}/R)$, and (p_o/F_{tu}) are computed for a sequence of values of (pcr/E), a master curve of $(\bar{t}_{min}/R)$. and associated optimum pressures, (p_o/F_{tu}) may be constructed. The graph is given in Figure 4.1-1. As may be seen, these curves plot as straight lines on log-log graph paper.

If only $(\bar{t}_{min}/R)$ is desired and if $p/F_{tu} < p_o/F_{tu}$ this graph is sufficient. Such information is usually all that is required in preliminary design weight studies. On the other hand, if the complete geometry is required, or if the design burst pressure, p, is greater than the minimum weight pressure, p_o, i.e., if the design is pressure critical, it will be necessary to use the x, y; α, δ, graph given on Figure 4.1-2 to obtain $\bar{t}$. This is done in the following steps:

A. Compute x and y and from the graph read off the corresponding α and δ.

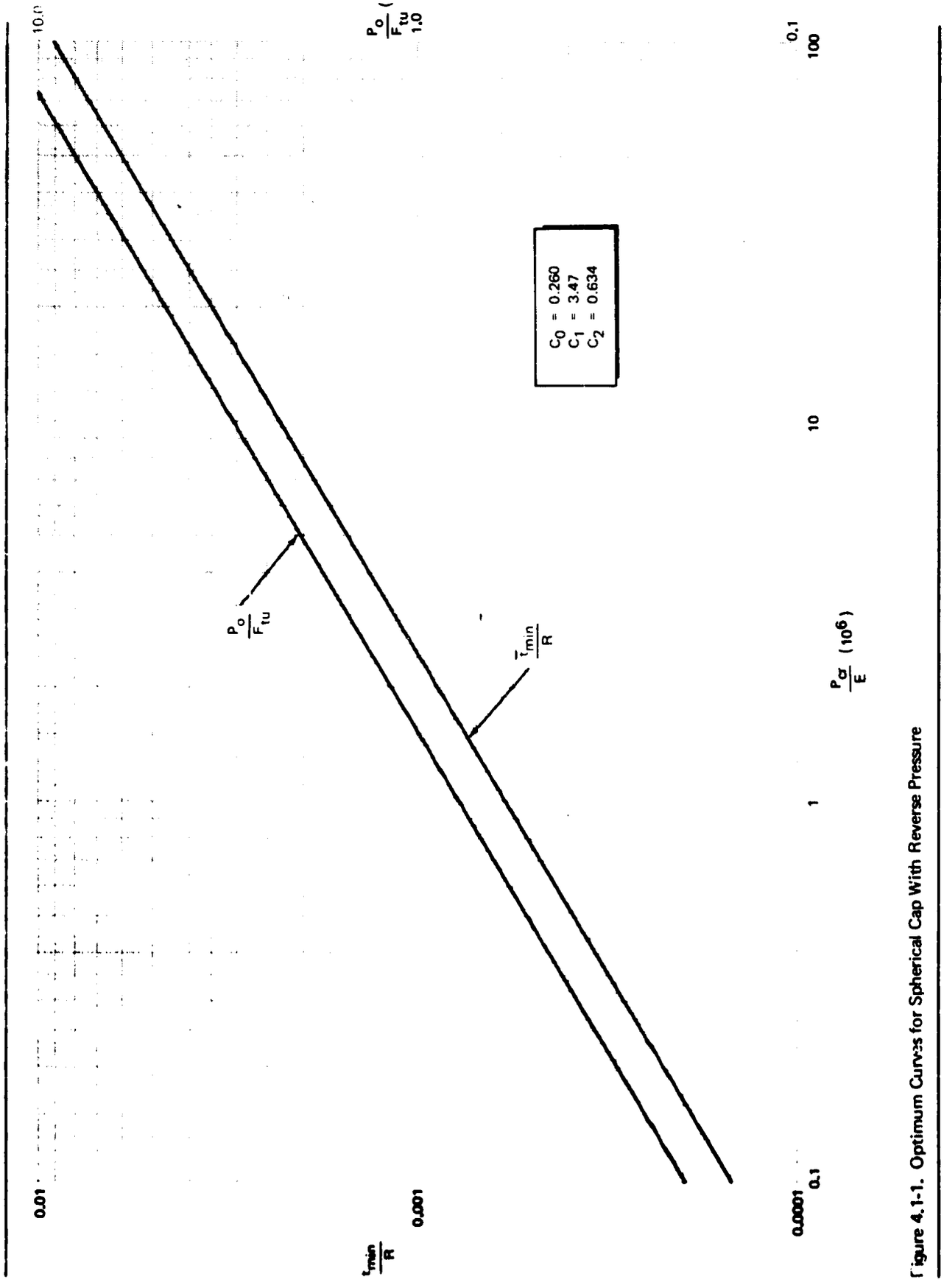

Figure 4.1-1. Optimum Curves for Spherical Cap With Reverse Pressure

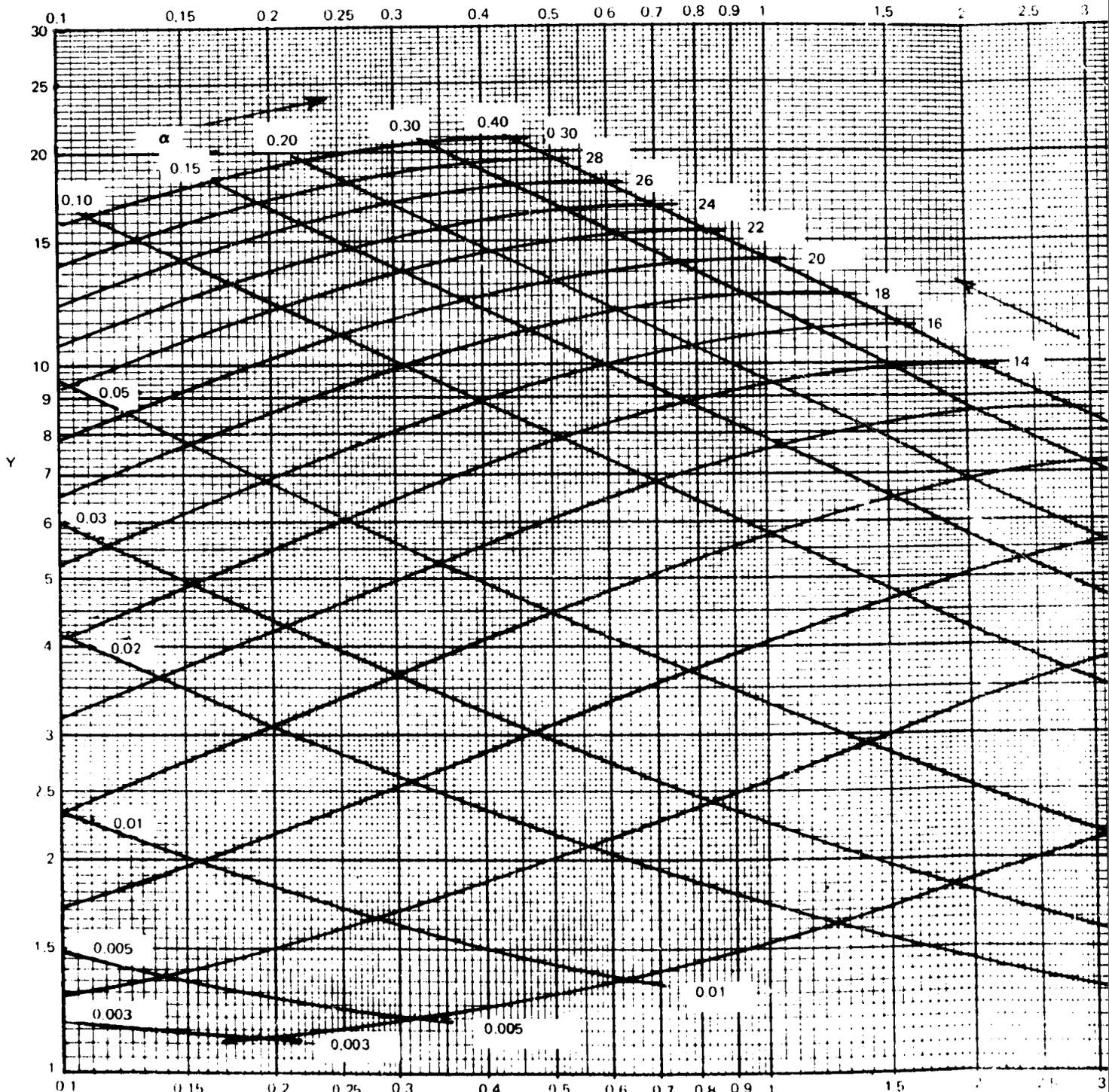

BOLDOUT FRAME

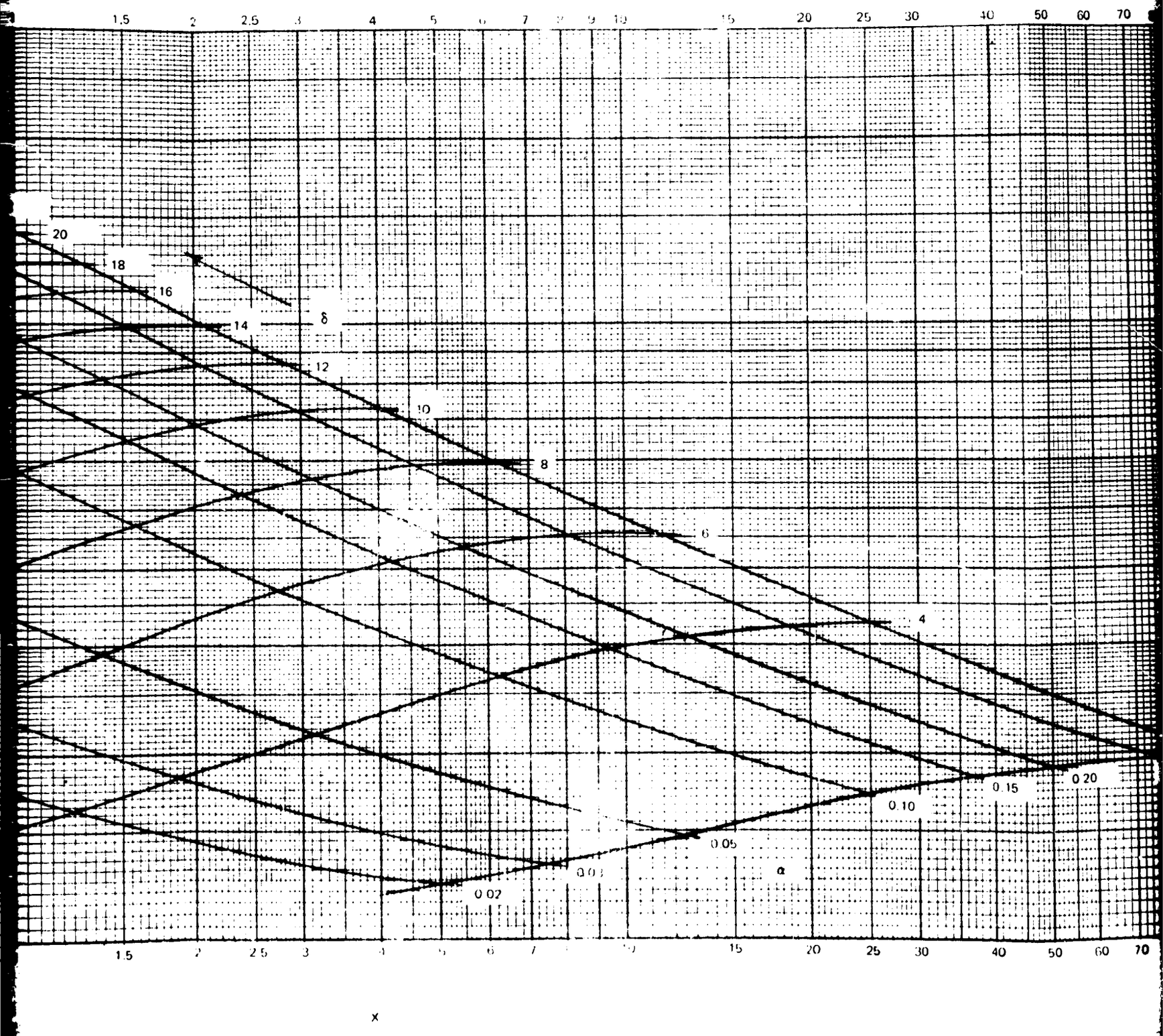

x

FOLDOUT FRAME

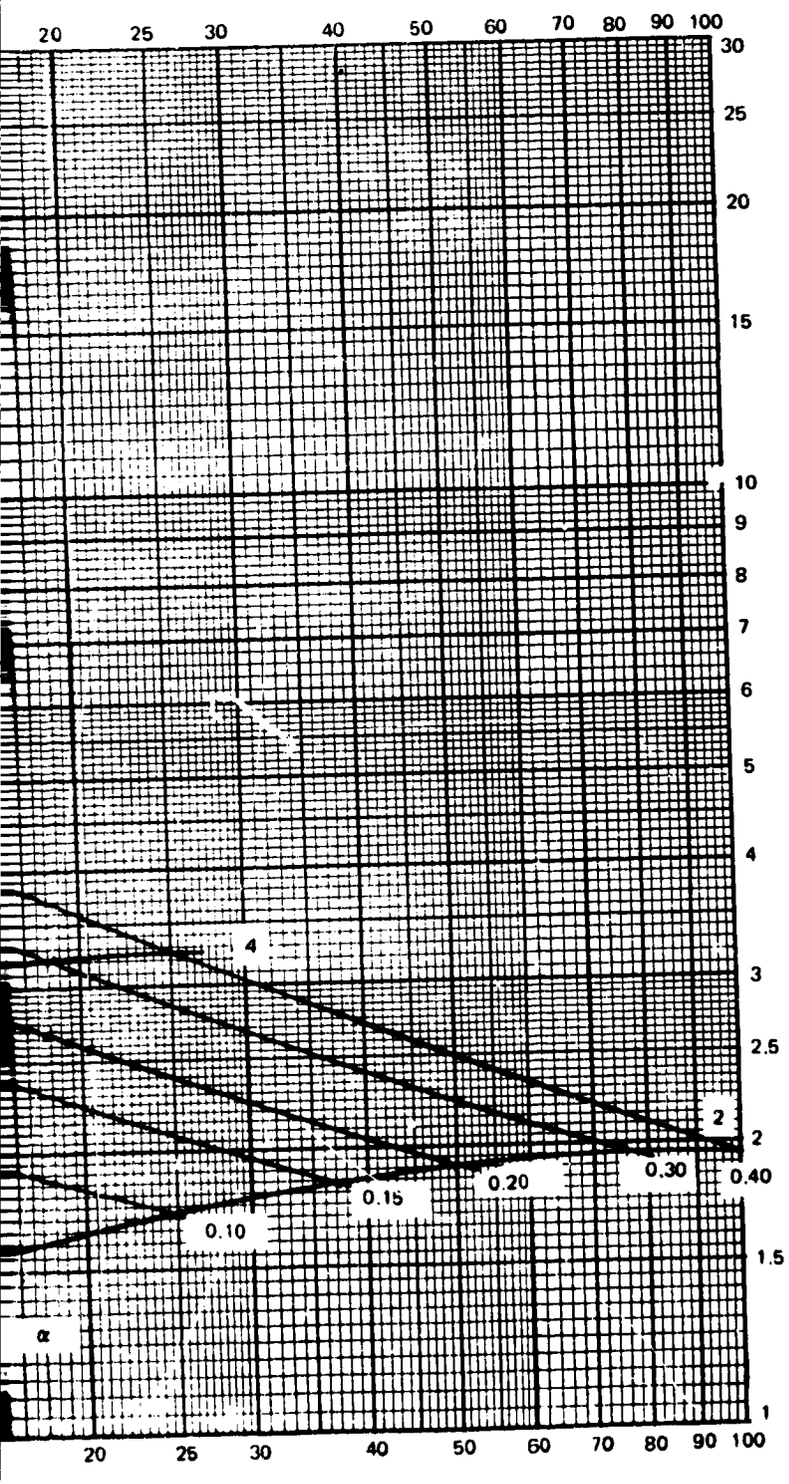

SUMMARY OF DESIGN EQUATIONS FOR SPHERICAL CAP

			REF PAGE
C_o	=	0.260	4.1.011
C_1	=	3.47	4.1.003
C_2	=	0.634	4.1.004

			REF EQ
$\bar{N}$		$\frac{P_{cr}}{E}\left(\frac{F_{tu}}{P}\right)$	(4.1.14)
X	=	$\frac{\bar{N}\ (10^3)}{1.482}$	(4.1.19)
Y	=	$\frac{\bar{N}}{0.130}\left(\frac{F_{tu}}{P}\right)$	(4.1.20)
t	=	$\frac{PR}{2\,F_{tu}\,(1+\alpha)}$	(4.1.13)
d	=	δt	(4.1.26)
b	=	$\sqrt{\frac{\bar{N}}{0.634}}\ d$	(4.1.27)
h	=	$\sqrt{\frac{3.47}{\bar{N}}}\ t$	(4.1.25)

AS A CHECK,

$$\alpha = \frac{bd}{th}$$

$$\bar{t} = t\,(1 + 3\alpha)$$

Figure 4.1-2. Design of Isogrid Spherical Bulkheads

FOLDOUT FRAME
3

B. t may now be computed from the burst condition or from the minimum weight pressure, p_o.

$$t = \frac{pR}{2 F_{tu} (1 + \alpha)} \qquad (4.1.24)$$

C. Knowing t, the triangle height, h may be computed from eq. (4.1.15).

$$h = \sqrt{\frac{c_1}{\bar{N}}}\, t \qquad (4.1.25)$$

D. The rib depth, d, is given by t and δ,

$$d = \delta t \qquad (4.1.26)$$

E. The rib width, b, is computed from eq. (4.1.16).

$$b = \sqrt{\frac{\bar{N}}{c_2}}\, d \qquad (4.1.27)$$

As a check on the computed values, the ratio, bd/th, should agree with the value of α read off the x, y; α, δ graph.

Finally, the value to be used for the correlation factor, γ, may be taken from Reference 2-8 as a function of the ratio, t*/R for lightly stiffened domes. For heavily stiffened domes the result of test in Reference 1-1, gives,

$$\gamma = 0.425$$

$$c_o = 0.612\ \gamma = \underline{0.260}$$

This is the value used for the x, y; α, δ curve in Figure 4.1-2.

4.1.3 Worked Examples

Worked Example 1

p_{cr} = 21 psi

p_{burst} = 60 psi

R = 96 in.

E = 11.6 (10^6) psi

F_{tu} = 78.5 ksi

$$\frac{p_{cr}}{E} = \frac{21}{11.6}(10^{-6}) = 1.81\ (10^{-6})$$

From graph,

$$\left(\frac{p_o}{F_{tu}}\right)10^3 = 1.12 \qquad \frac{\bar{t}_{min}}{R} = 0.000805$$

$$p_o = 1.12\ (78.5) = 87.9 \text{ psi} \quad 60.0 \text{ psi.}$$

The design is compression-critical and the (t_{min}/R) value is valid.

$$\bar{t}_{min} = 0.000805 \times 96 = \underline{0.0772 \text{ in.}}$$

If this is all that is desired, the analysis is completed. However, if the geometry is required,

$$\bar{N} = \frac{p_{cr}}{E}\left(\frac{F_{tu}}{p_o}\right) = \frac{1.81\ (10^{-6})}{1.12\ (10^{-3})} = 1.617\ (10^{-3})$$

$$x = \frac{\bar{N}\ (10^3)}{1.482} = \frac{1.617}{1.482} = 1.09$$

$$y = \frac{\overline{N}}{0.130}\left(\frac{F_{tu}}{p_o}\right) = \frac{1.617\ (10^{-3})}{0.130}\left[\frac{10^3}{1.12}\right]$$

$$= 11.1$$

From graph, $\alpha = 0.275 \quad \delta = 16$

$$t = \frac{p_o R}{2 F_{tu} (1+\alpha)} = \frac{1.12\ (10^{-3})\ (96)}{2\ (1.275)} = \underline{0.0422 \text{ in.}}$$

$$d = \delta t = 16\ (0.0422) = \underline{0.675 \text{ in.}}$$

$$b = \sqrt{\frac{\overline{N}}{0.634}}\ d = \sqrt{\frac{1.617\ (10^{-3})}{0.634}}\ (0.675)$$

$$= 0.0505\ (0.675) = \underline{0.0341}$$

$$h = \sqrt{\frac{3.47}{\overline{N}}}\quad t = \sqrt{\frac{3.47}{1.617}\ (10^3)}\ (0.0422)$$

$$= 46.3\ (0.0422) = \underline{1.95 \text{ in.}}$$

$$a = \frac{2h}{\sqrt{3}} = \frac{2\ (1.95)}{1.732} = \underline{2.25 \text{ in.}}$$

As a check,

$$\frac{bd}{th} = \frac{0.0341\ (0.675)}{0.0422\ (1.95)} = 0.280$$

This is very close to the graph value, $\alpha = 0.275$. As a check on the $\overline{t}_{min}$ value,

$$\overline{t}_{min.} = t\ (1 + 3\alpha) = 0.0422\ [1 + 3\ (0.280)]$$

$$= \underline{0.0777 \text{ in.}}$$

Use of the burst pressure, 60 psi, instead of the optimum pressure, 87.9 psi, would have resulted in thinner skin, smaller triangles, and heavier weight.

Worked Example 2

p_{cr} = 8 psi,

p_{burst} = 75 psi,

R = 120 in.

E = 11 (10^6) psi,

F_{tu} = 76 ksi,

$$\frac{p_{cr}}{E} = \frac{8}{11}(10^{-6}) = 0.726\ (10^{-6})$$

From graph,

$$\left(\frac{p_o}{F_{tu}}\right)10^3 = 0.644\ (\bar{t}_{min}/R) = 0.000466$$

$$p_o = 0.644\ (76) = 48.9 \text{ psi}, < 75 \text{ psi}.$$

This design is pressure-critical since the minimum weight pressure is less than the burst pressure. In this case it will be necessary to use the α, δ curves to obtain $\bar{t}$.

$$\bar{N} = \frac{p_{cr}}{E}\left(\frac{F_{tu}}{p}\right) = 0.726\ (10^{-6})\left[\frac{76\ (10^3)}{75}\right]$$

$$= 0.735\ (10^{-3})$$

$$x = \frac{\bar{N}\ (10^3)}{1.482} = \frac{0.735}{1.482} = 0.496$$

$$y = \frac{\bar{N}}{0.130}\frac{F_{tu}}{p} = \frac{0.735\ (10^{-3})}{0.130}\left[\frac{76\ (10^{3})}{75}\right]$$

$$= 5.73$$

From graph, $\alpha = 0.066$, $\delta = 11.6$

$$t = \frac{pR}{2\,F_{tu}\,(1+\alpha)} = \frac{75\ (120)}{2\ (76)\ (1.066)}\ (10^{-3})$$

$$= 0.555 \text{ in.}$$

$$d = \delta t = 11.6\ (0.0555) = 0.644 \text{ in.}$$

$$b = \sqrt{\frac{\bar{N}}{0.634}}\,d = \sqrt{\frac{7.35\ (10^{-4})}{0.634}}\ (0.644)$$

$$= 0.0341\ (0.644) = 0.219 \text{ in.}$$

$$h = \sqrt{\frac{3.47}{\bar{N}}}\ t = \sqrt{\frac{3.47}{0.735}\ (10^{3})}\ (0.0555)$$

$$= 68.8\ (0.0555) = 3.82 \text{ in.}$$

$$a = \frac{2h}{\sqrt{3}} = \frac{2\ (3.82)}{1.732} = 4.41 \text{ in.}$$

As a check,

$$\frac{bd}{th} = \frac{0.0219\ \ (0.644)}{0.0555\ \ (3.82)} = \underline{0.0666}$$

This is close to the graph value, $\alpha = 0.066$.

The $\bar{t}$ is given by,

$$\bar{t} = t\,(1 + 3\alpha) = 0.0555\ [1 + 3\ (0.0666)]$$

$$= \underline{0.0666 \text{ in.}}$$

If the design had been compression-critical, one would have had,

$$\bar{t}_{min.} = 0.000466\ (120) = \underline{0.0560\ in.}$$

It will be found, for many designs, that the $\bar{t}/R$ curve is fairly flat beyond the optimum p_o/F_{tu} pressure. This means that the skins may be made somewhat thicker than optimum so that larger grid sizes result without excessive weight penalties.

4.1.4 Spherical Grid Layout

The analysis leading to the tables used to lay out the grid is described in detail in Reference 1-1.

The tables developed there and the description of their usage is repeated here for convenience.

Layout of Isogrid

The layout of the triangular gridwork on the spherical surface is accomplished by the following routine.

Consider an icosahedron inscribed in the spherical surface. This regular geometric solid has 20 equilateral triangular faces and is shown in the figure.

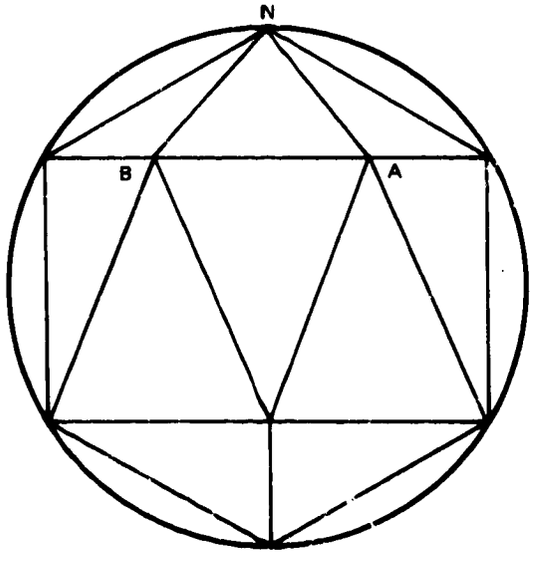

A typical face is labeled NAB, where N is the apex (North Pole) of the sphere. A view of the equilateral triangular whose base plane is NAB is shown in the figure as seen from the apex, N.

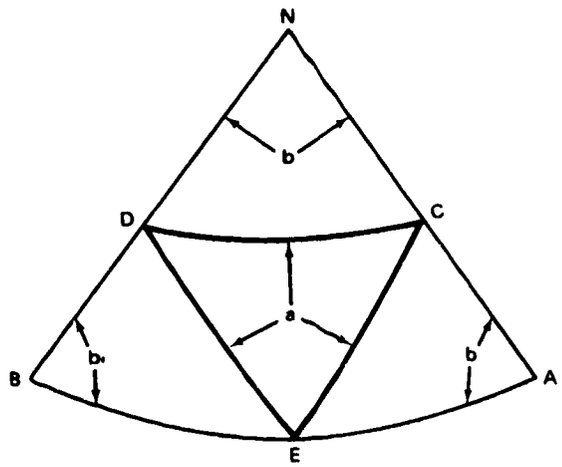

The midpoint of the arcs NA, AB, BN, are designated as C, E, and D. This further subdivides the basic triangle into one central equilateral triangle CED, and three congruent isosceles spherical triangles NCD, AEC, and BDE. The arc lengths, a and b, are symmetrically subdivided from each vertex, i.e. from N or C, etc. and are labeled a_i, b_i for n subdivisions.

From each vertex, corresponding points along the adjacent arcs are connected by great circles.

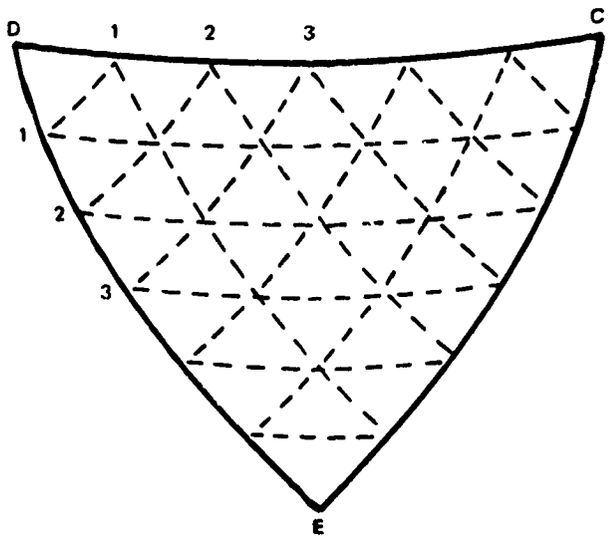

The arcs will intersect in points which define the vertices of the elementary triangles.

The subdivision a_i, b_i have been computed for unit radius, for n = 5 to 20, and are shown, cumulatively added from a vertex, in Table 4-1, to facilitate layout.

For spheres of radius R, multiply tabular values by R.

4.1.5 Summary of Design Equations for Spherical Cap

	Ref. Page
$C_0 = 0.260$	4.1.012
$C_1 = 3.47$	4.1.004
$C_2 = 0.634$	4.1.005

	Ref. Eq.
$\overline{N} = \frac{p_{cr}}{E}\left(\frac{F_{tu}}{p}\right)$	(4.1.14)
$x = \frac{\overline{N}\,(10^3)}{1.482}$	(4.1.19)
$y = \frac{\overline{N}}{0.130}\left(\frac{F_{tu}}{p}\right)$	(4.1.20)
$t = \frac{pR}{2F_{tu}(1+\alpha)}$	(4.1.13)

	Ref. Eq.
$d = \delta t$	(4.1.26)
$b = \sqrt{\frac{\overline{N}}{0.634}}\,d$	(4.1.27)
$h = \sqrt{\frac{3.47}{\overline{N}}}\,t$	(4.1.25)

As a check,

$$\alpha = \frac{bd}{th}$$

$$\overline{t} = t(1 + 3\alpha)$$

Table 4-1

Σa_i

i \ n	5	6	7	8	9	10	11	12	13	14	16	18	20
1	0.1216	0.1008	0.0861	0.0751	0.0666	0.0599	0.0543	0.0497	0.0459	0.0425	0.0372	0.0330	0.0297
2	0.2493	0.2063	0.1758	0.1531	0.1356	0.1216	0.1103	0.1008	0.0929	0.0861	0.0751	0.0666	0.0599
3	0.3791	0.3142	0.2678	0.2331	0.2063	0.1849	0.1675	0.1531	0.1410	0.1306	0.1138	0.1008	0.0905
4	0.5067	0.4221	0.3605	0.3142	0.2781	0.2493	0.2258	0.2063	0.1898	0.1758	0.1531	0.1356	0.1216
5	0.6283	0.5275	0.4525	0.3952	0.3503	0.3142	0.2846	0.2601	0.2393	0.2216	0.1929	0.1707	0.1531
6		0.6283	0.5422	0.4752	0.4221	0.3791	0.3437	0.3142	0.2892	0.2678	0.2331	0.2063	0.1849
7			0.6283	0.5532	0.4928	0.4434	0.4025	0.3683	0.3392	0.3142	0.2736	0.2421	0.2170
8				0.6283	0.5617	0.5067	0.4608	0.4221	0.3890	0.3605	0.3142	0.2781	0.2493
9					0.6283	0.5685	0.5181	0.4752	0.4385	0.4067	0.3548	0.3142	0.2817
10						0.6283	0.5740	0.5275	0.4874	0.4525	0.3952	0.3503	0.3142
11							0.6283	0.5786	0.5354	0.4977	0.4354	0.3862	0.3466
12								0.6283	0.5825	0.5422	0.4752	0.4221	0.3791
13									0.6283	0.5858	0.5145	0.4576	0.4113
14										0.6283	0.5532	0.4928	0.4434
15											0.5911	0.5275	0.4752
16											0.6283	0.5617	0.5067
17												0.5953	0.5378
18												0.6283	0.5685
19													0.5987
20													0.6283

Table 4-1 (Continued)

Σb_i

i \ n	5	6	7	8	9	10	11	12	13	14	16	18	20
1	0.1080	0.0896	0.0766	0.0669	0.0593	0.0533	0.0484	0.0443	0.0409	0.0379	0.0332	0.0294	0.0265
2	0.2200	0.1824	0.1556	0.1357	0.1203	0.1080	0.0979	0.0896	0.0826	0.0766	0.0669	0.0593	0.0533
3	0.3336	0.2768	0.2362	0.2059	0.1824	0.1636	0.1484	0.1357	0.1250	0.1159	0.1011	0.0896	0.0805
4	0.4456	0.3712	0.3173	0.2768	0.2453	0.2200	0.1995	0.1824	0.1680	0.1556	0.1357	0.1203	0.1080
5	0.5536	0.4640	0.3979	0.3477	0.3083	0.2768	0.2510	0.2295	0.2113	0.1958	0.1707	0.1512	0.1357
6		0.5536	0.4770	0.4179	0.3712	0.3336	0.3026	0.2768	0.2549	0.2362	0.2059	0.1824	0.1636
7			0.5536	0.4867	0.4333	0.3899	0.3541	0.3241	0.2986	0.2768	0.2413	0.2138	0.1918
8				0.5536	0.4942	0.4456	0.4052	0.3712	0.3423	0.3174	0.2768	0.2452	0.2200
9					0.5536	0.5003	0.4556	0.4179	0.3856	0.3578	0.3123	0.2768	0.2484
10						0.5536	0.5052	0.4640	0.4286	0.3980	0.3477	0.3084	0.2768
11							0.5536	0.5093	0.4710	0.4377	0.3829	0.3398	0.3052
12								0.5536	0.5127	0.4770	0.4179	0.3712	0.3336
13									0.5536	0.5156	0.4525	0.4024	0.3618
14										0.5536	0.4867	0.4333	0.3899
15											0.5204	0.4640	0.4179
16											0.5536	0.4943	0.4456
17												0.5241	0.4731
18												0.5536	0.5003
19													0.5271
20													0.5536

4.2 CYLINDERS IN COMPRESSION, BENDING

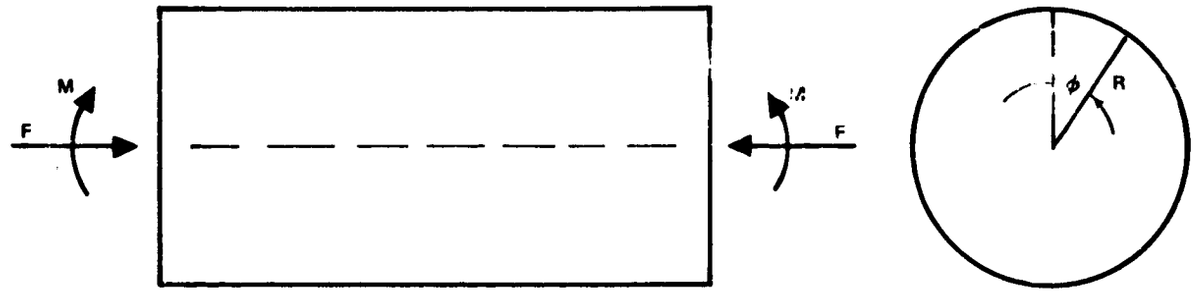

The compression on the cylinder has a resultant force, F, and resultant moment, M, at the two ends of the cylinder. The internal axial load/in., N_x, in the cylinder, is given by the equation,

$$N_x = \frac{F}{2\pi R} + \frac{M}{\pi R^2} \cos \phi$$

The maximum value of N_x occurs for $\phi = 0°$

$$N_x \text{ (max)} = \frac{F}{2\pi R} + \frac{M}{\pi R^2}$$

4.2.1 Typical Design Situations

A very common application occurs in design of fuselages, interstages, tankage, payload and living compartments of space vehicles that are cylindrical in shape and are subjected to maneuver and thrust loading.

The cylindrical configuration is especially attractive from the fabrication point of view since the isogrid may be machined in the flat and then formed into the cylindrical shape.

4.2.2 Method of Optimization

The optimization assumes that minimum weight occurs for simultaneous failure modes in general instability, skin buckling, and rib crippling.

General Instability

In Reference 2-1, it is shown that theoretical values for general instability due to bending may be written in the form,

$$N_{cr}(1) = \frac{1}{\sqrt{3\,(1-\nu^2)}} \frac{Et^2}{R} \qquad (4.2.1)$$

This theoretical formula is independent of the length of the cylinder.

In the case of uniform compression, the theoretical critical load is highly length dependent and is described by a looped "festoon curve," Figure 4.2-1. This curve is dependent on both R/t* and L/R and has been plotted from Reference 2-1 for an R/t* ratio of 85.5, a typical value for isogrid. The length dependence was first noted by R. V. Southwell in 1914 and later by W. Flügge in 1932.

If, however, internal pressure is present or if the loading consists of combined bending and axial compression where the bending component is at least 25 percent of the value given by eq. (4.2.1) and the L/R ratio is equal to or less than 10, then the combined loads are on the linear portion of the interaction curve, then the axial component may also be expressed by eq. (4.2.1) (see Figure 4.2-2).

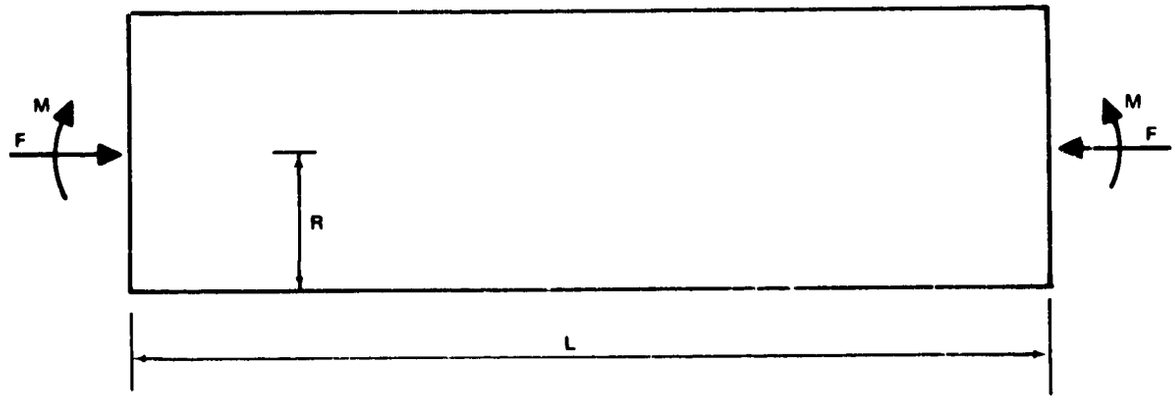

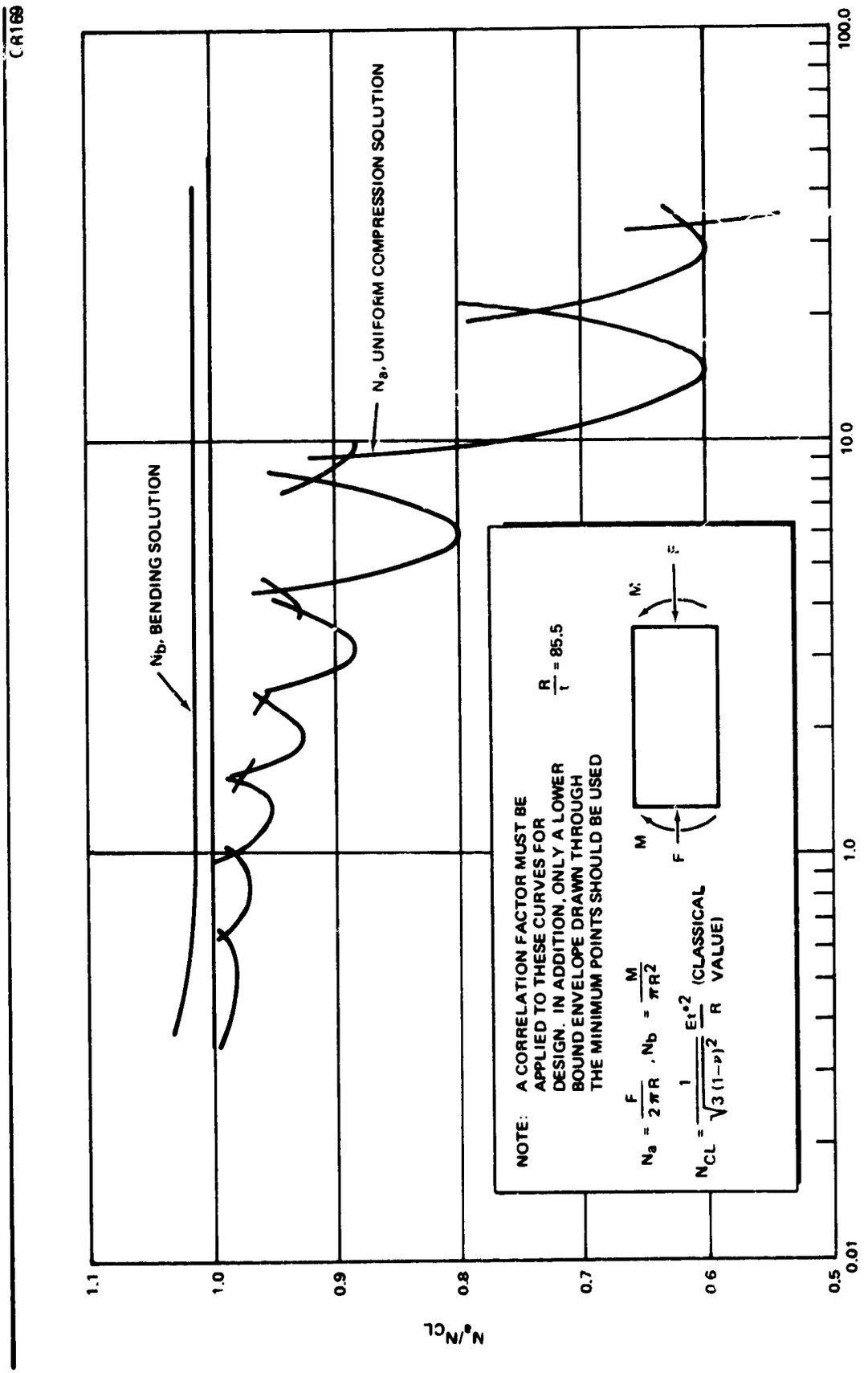

Figure 4.2-1. Length Dependence of Theoretical Axial Compression and Bending Buckling Solutions

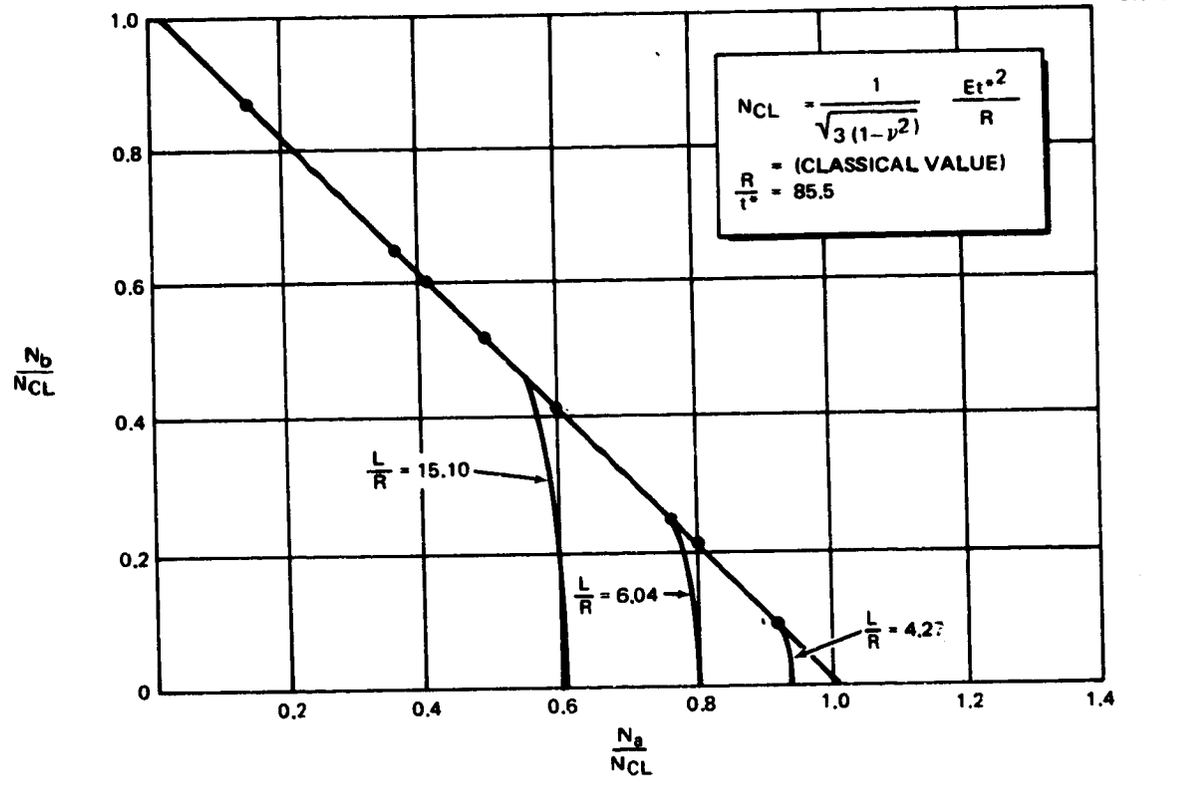

Figure 4.2-2. Interaction Curve Showing the Effect of Length

The axial load/inch, N_a, is given by,

$$N_a = \frac{F}{2\pi R} \tag{4.2.2}$$

The bending load/inch, N_b, is given by,

$$N_b = \frac{M}{\pi R^2} \tag{4.2.3}$$

Assuming the validity condition for uniform compression to be met so that N_a may be given by eq. (4.2.1), the combined loading condition is,

$$N_a + N_b = N_{cr}\,(1) = \frac{1}{\sqrt{3\,(1-\nu^2)}} \frac{E^* t^{*2}}{R} \tag{4.2.4}$$

The theoretical values of eq. (4.2.4) must be multiplied by a "correlation" or "knockdown" factor, γ, ($\gamma < 1.00$) to convert theoretical values to allowable compressive loads/inch. This factor accounts for deviation of geometry, material properties and boundary conditions of test specimen from the ideal condition assumed in the theory. These deviations always reduce the test values below theoretical predictions.

Using the values of E* and t* from eq. (2.5.3) and (2.5.4),

$$N_a + N_b = N_{cr}(1) = \frac{\gamma}{\sqrt{3(1-\nu^2)}} \frac{Et^2}{R} \beta \qquad (4.2.5)$$

where γ is an appropriate correlation factor. For very lightly stiffened cylinders, one may use a γ from Reference 2-6 as a function of t^*/R. For moderate or heavy stiffening a value of

$$\gamma = 0.65$$

is recommended by Reference 2-11. This is the value assumed in the optimization. Thus,

$$N_{cr}(1) = c_0 E \frac{t^2}{R} \beta \qquad (4.2.6)$$

where

$$c_0 = 0.612(\gamma) = 0.397$$

Skin Buckling

The critical stress for skin buckling is given in the form, Reference 2-9,

$$\sigma_{cr} = \frac{k_c \pi^2 E}{12 (1-\nu^2)} \left(\frac{t}{a}\right)^2 \qquad (4.2.7)$$

Using the formulae for isogrid the critical skin buckling load/inch may be written as,

$$N_{cr}(2) = c_1 Et (1 + \alpha) \frac{t^2}{h^2} \qquad (4.2.8)$$

An appropriate value for c_1 established by test on optimum structure, Reference 2-12,

$$c_1 = 10.2$$

Rib Crippling

Since the maximum stresses will occur for principal stress conditions, $N_{xy} = 0$, and eq. (2.4.12) become,

$$\sigma_1 = \frac{1}{t_{eff}} \left(N_x - \frac{1}{3} N_y\right)$$

$$\sigma_{2,3} = \frac{2 N_y}{3 t_{eff}} \qquad (4.2.9)$$

These equations show that if x is chosen as the axial direction, i.e., the 1 ribs are oriented axially, then since

$$N_a + N_b = N_x$$

and if internal pressure is present, then

$$N_y = -\frac{\rho r}{2}$$

thus

$$\sigma_1 = \frac{1}{t_{eff}} \left(N_a + N_b + \frac{pr}{6} \right) \tag{4.2.10}$$

In this case, the internal pressure is contributing an additive load to the 1 rib. It is apparent, that in this case, it would be better to orient the 1 rib in the hoop direction. Then,

$$\sigma_1 = \frac{-1}{t_{eff}} \left[\frac{pr}{2} + \frac{1}{3} (N_a + N_b) \right]$$

$$\sigma_{2,3} = \frac{2}{3\, t_{eff}} (N_a + N_b) \tag{4.2.11}$$

This is a much better arrangement since the 1 rib is now in tension and the 2, 3 ribs are less highly stressed.

In the optimization, it will be assumed that the rib stresses are given by the relation,

$$\sigma_{cr} = \frac{N_a + N_b}{t_{eff}} \tag{4.2.12}$$

thus

$$N_{cr}(3) = c_2 E t (1 + \alpha) \frac{b^2}{d^2} \tag{4.2.13}$$

where

$$N_{cr}(3) = N_{cr}(1)$$

From Reference 2-12, an appropriate value for c_2 is

$$c_2 = 0.616$$

This coefficient is very close to the value for simple support boundary conditions at the attached edges of the plate.

In going from unflanged isogrid ribs to flanged isogrid ribs, the "free" edge would become supported by the flange and the value for c_2 may be expected to improve by a factor of 10.

Collecting formula, one has the system of equations,

$$N_{cr}(1) = c_0 E \frac{t^2}{R} \beta \qquad (4.2.14)$$

$$N_{cr}(2) = c_1 Et (1 + \alpha) \frac{t^2}{h^2} \qquad (4.2.15)$$

$$N_{cr}(3) = c_2 Et (1 + \alpha) \frac{b^2}{d^2} \qquad (4.2.16)$$

where

$$N_{cr}(1) = N_{cr}(2) = N_{cr}(3) = N_a + N_b = N_{cr}$$

Eq. (4.2.14) to (4.2.16) are formally identical to the equations for buckling of the spherical cap and the optimization procedure proceeds in exactly the same way.

To eq. (4.2.14) to (4.2.16) append the "burst" condition where the burst pressure may be regarded as a "free parameter."

$$F_{tu} = \frac{pR}{t (1 + \alpha)} \qquad (4.2.17)$$

Define the non-dimensional loading parameter, N.

$$\bar{N} = \frac{N_{cr}}{ER}\left(\frac{F_{tu}}{p}\right) \tag{4.2.18}$$

From eq. (4.2.15), (4.2.17) and (4.2.18),

$$\bar{N} = c_1\left(\frac{t}{h}\right)^2 \tag{4.2.19}$$

From eq. (4.2.16), (4.2.17) and (4.2.18),

$$\bar{N} = c_2\left(\frac{b}{d}\right)^2 \tag{4.2.20}$$

Multiplying eq. (4.2.19) and (4.2.20),

$$\bar{N}^2 = c_1c_2\frac{b^2t^2}{h^2d^2} = c_1c_2\left(\frac{bd}{th}\right)^2\left(\frac{t}{d}\right)^4 = c_1c_2\frac{\alpha^2}{\delta^4}$$

and since α and δ are positive,

$$\bar{N} = \sqrt{c_1c_2}\ \frac{\alpha}{\delta^2} \tag{4.2.21}$$

Eq. (4.2.20) satisfies the condition of simultaneous rib crippling, skin buckling and burst.

From eq. (4.2.14), (4.2.17) and (4.2.18),

$$\bar{N} = c_0\frac{t}{R}\frac{\beta}{1+\alpha} = c_0\frac{p}{F_{tu}}\frac{\beta}{(1+\alpha)^2}$$

or

$$\overline{N}\left(\frac{F_{tu}}{p}\right) = c_0 \frac{\beta}{(1+\alpha)^2} \tag{4.2.22}$$

Eq. (4.2.22) satisfies the condition of simultaneous general instability and burst.

Define the non-dimensional loading,

$$x = \frac{\overline{N}}{\sqrt{c_1 c_2}} (10^3) \tag{4.2.23}$$

$$y = \frac{\overline{N} F_{tu}}{c_0 p} \tag{4.2.24}$$

then eq. (4.2.21) and (4.2.22) become,

$$x = \frac{\alpha}{\delta^2} (10^3) \tag{4.2.25}$$

$$y = \frac{\beta}{(1+\alpha)^2} \tag{4.2.26}$$

The right hand side of eq. (4.2.25) and (4.2.26) are identical to equations of the spherical cap and the same x, y; α, δ mapping graphs may be used.

The equivalent weight thickness, $\overline{t}$, is

$$\overline{t} = t\,(1 + 3\alpha)$$

Using eq. (4.2.16) this becomes,

$$\overline{t} = \frac{pR}{F_{tu}} \frac{1 + 3\alpha}{1 + \alpha}$$

or

$$\frac{\bar{t}}{R} = \frac{p}{F_{tu}} \frac{1 + 3\alpha}{1 + \alpha} \qquad (4.2.27)$$

As in the case of the sphere, the quantity $\bar{t}/R$ may be minimized as a function of p/F_{tu} for a given value of N_{cr}/ER.

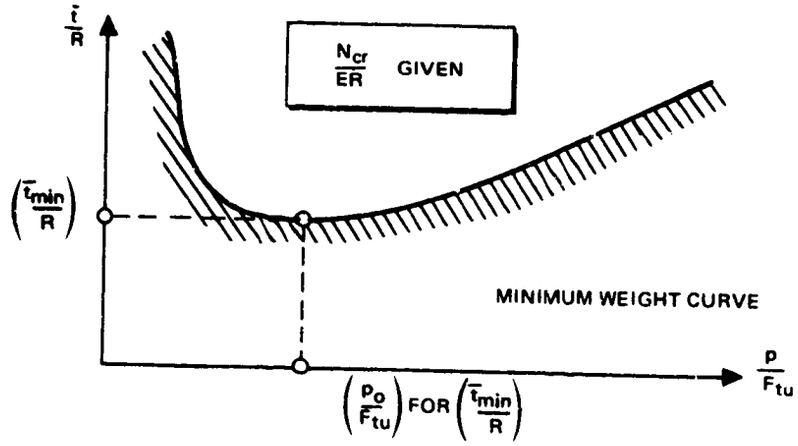

As before this will divide all design into two classes.

A. For

$$\frac{p \text{ burst}}{F_{tu}} < \frac{p_o}{F_{tu}}$$

the minimum weight is given by p_o and the construction is "compression-critical." Use of p_o will thus give lighter weight designs and additional burst safety factors so that crack propagation effects due to cyclic loading on flaws are less severe.

B. For

$$\frac{p_{burst}}{F_{tu}} > \frac{p_o}{F_{tu}}$$

the burst pressure must be used. These designs are "pressure-critical."

If a family of $(\bar{t}_{min}/R)$ and associated (p_o/F_{tu}) values are computed for different (N_{cr}/ER) a master non-dimensional curve may be constructed. This is shown in Figure 4.2-3.

The complete geometry is determined by the following procedure:

A. Compute x and y and from Figure 4.2-4 read off the corresponding α and δ.

B. t may now be computed from the burst condition or from the minimum weight pressure, p_o.

$$t = \frac{pR}{F_{tu}(1+\alpha)} \tag{4.2.28}$$

where p is the larger value of p_{burst} or p_o.

C. Knowing t, the triangle height, h, may be computed from (4.2.19)

$$h = \sqrt{\frac{c_1}{\bar{N}}}\, t \tag{4.2.29}$$

D. The rib depth, d, is given from t and δ.

$$d = \delta t \tag{4.2.30}$$

E. The rib width, b, is computed from eq. (4.2.20).

As a check on the computed values, bd/th should agree with the value of α read off the α, δ graph.

4.2.3 Worked Examples

Worked Example 1

R = 48.0 in.

E = 11.0 (10^6) psi

F = 390 k

M = 8000 k in.

p_{burst} = 55 psi

F_{tu} = 67.0 ksi.

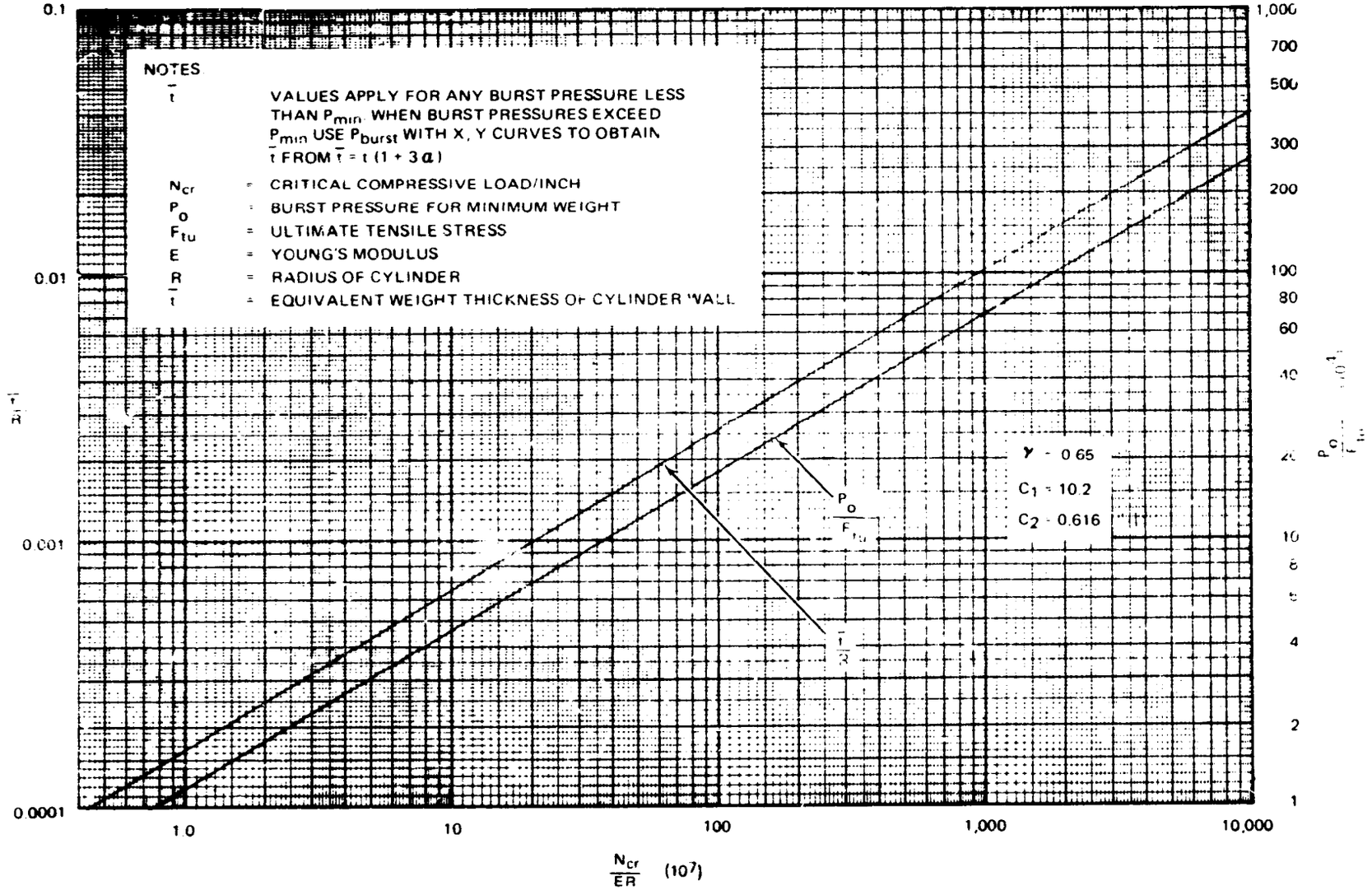

Figure 4.2-3. Weight of Optimized Compression-Critical Isogrid Cylinders

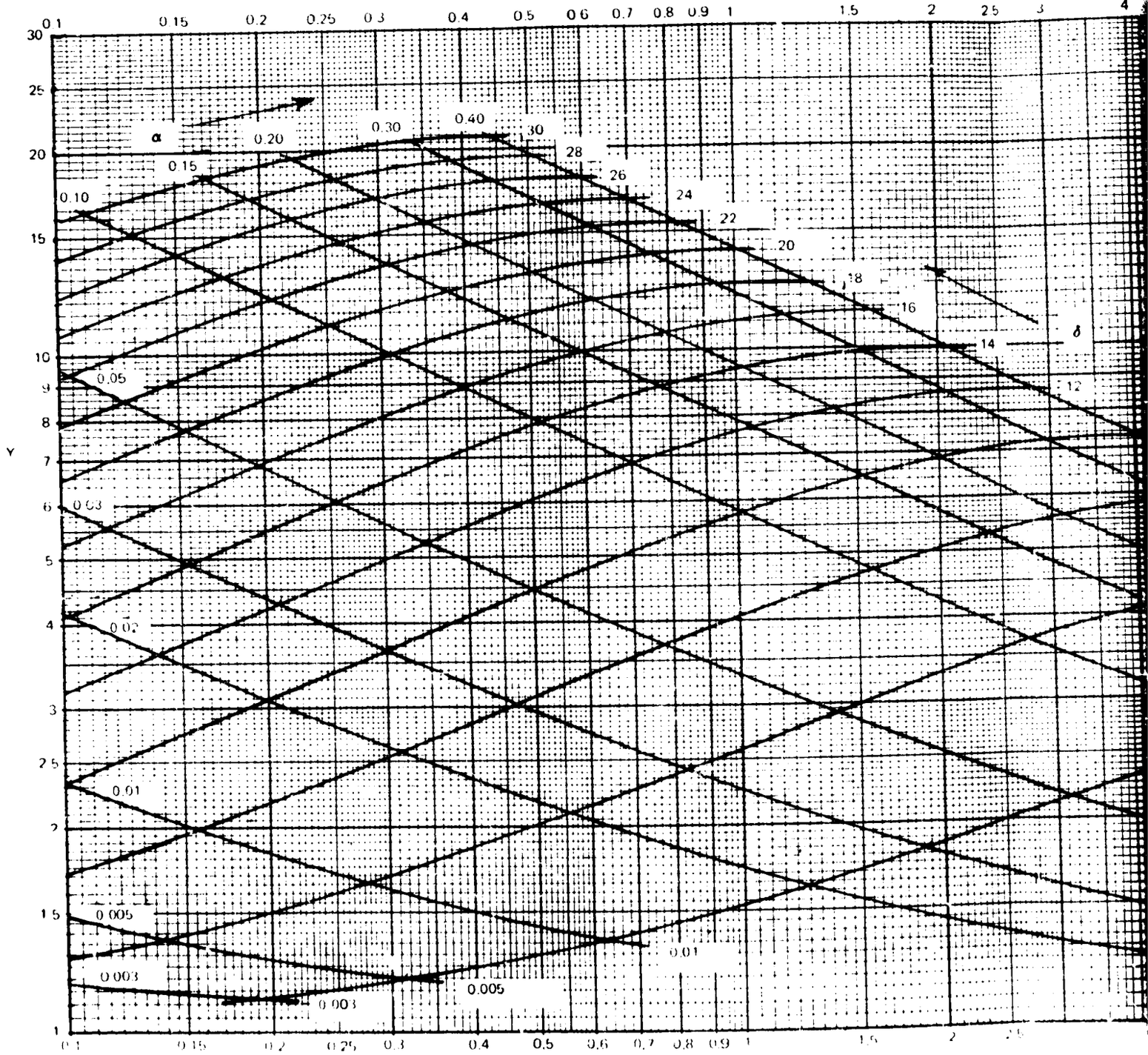

FOLDOUT FRAME

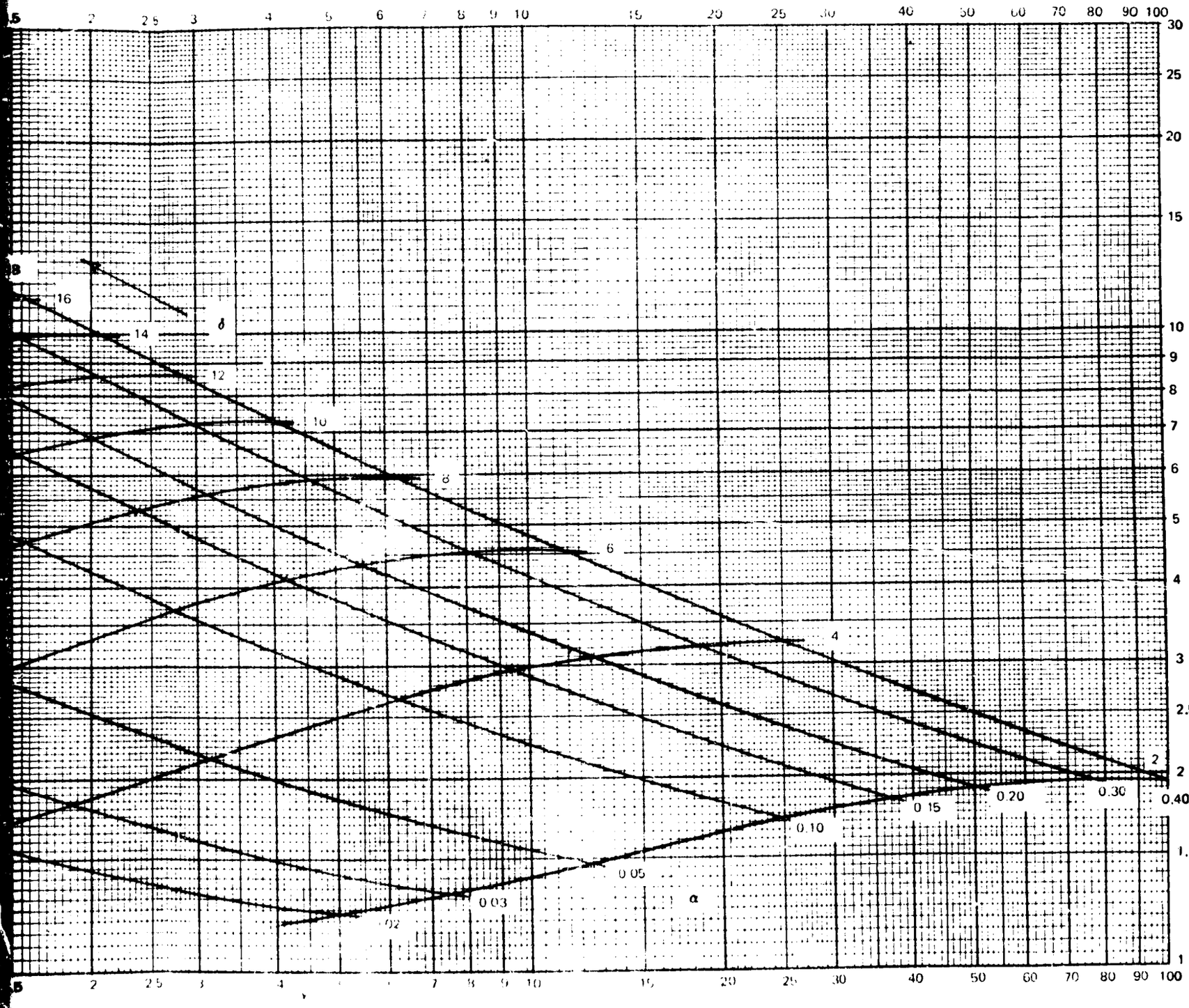

FOLDOUT FRAME

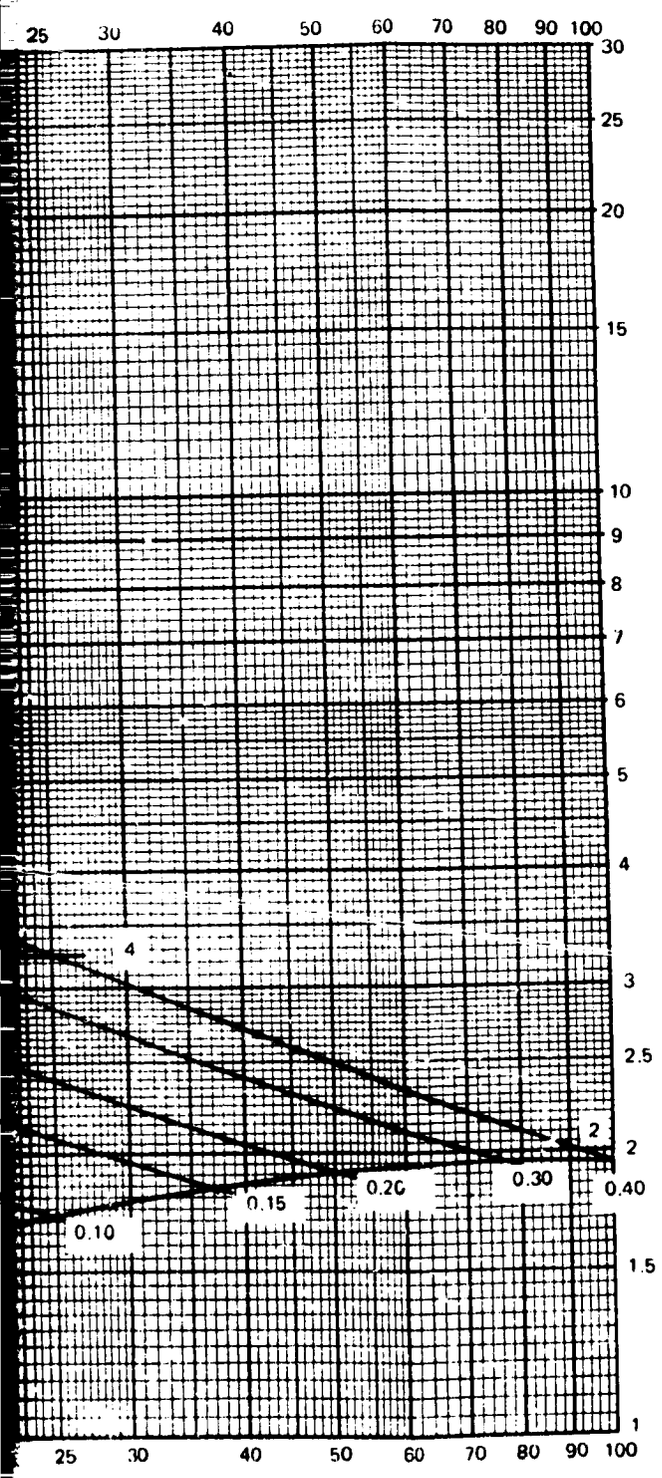

SUMMARY OF DESIGN EQUATIONS FOR CYLINDER UNDER AXIAL COMPRESSION AND BENDING

			REF PAGE
C_o	=	0.397	4.2.005
C_1	=	10.2	4.2.006
C_2	=	0.616	4.2.008
			REF EQ
$\bar{N}$	=	$\frac{N_{cr}}{ER}\left(\frac{F_{tu}}{P}\right)$	(4.2.17)
X	=	$\frac{\bar{N}\ (10^3)}{2.505}$	(4.2.22)
Y	=	$\frac{\bar{N}}{0.397}\left(\frac{F_{tu}}{P}\right)$	(4.2.23)
t	=	$\frac{PR}{F_{tu}\ (1+\alpha)}$	(4.2.27)
d	=	δ t	(4.2.29)
b	=	$\sqrt{\frac{\bar{N}}{0.616}}$ t	(4.2.19)
h	=	$\sqrt{\frac{10.2}{\bar{N}}}$ t	(4.2.28)

AS A CHECK,

$\alpha = \frac{bd}{th}$

$\bar{t} = t(1+3\alpha)$

Figure 4.2-4. Design of Isogrid Cylinders

FOLDOUT FRAME

3

$$N_a = \frac{F}{2\pi R} = \frac{300}{2\pi(48)} = 0.993 \text{ k/in.}$$

$$N_b = \frac{M}{\pi R^2} = \frac{8000}{\pi(48)^2} = 1,106 \text{ k/in.}$$

$$N_{cr} = 2.099 \text{ k/in.}$$

Since $N_b > N_{cr}(1)/4$, the assumption for validity of

$$N_a + N_b = N_{cr} = \frac{1}{\sqrt{3\,(1-\nu^2)}} \frac{E^* t^{*2}}{R}$$

is fulfilled.

$$\frac{N_{cr}}{ER} = \frac{2099}{11\ (48)} \left(10^{-6}\right) = 39.7 \left(10^{-7}\right)$$

From the graph,

$$\left(\frac{\bar{t}_{min}}{R}\right) = 0.00149 \qquad \left(\frac{p_o}{F_{tu}}\right) 10^4 = 10.3$$

$$p_o = 1.03\ (67.0) = 69.0 \text{ psi} > 55 \text{ psi.}$$

The design is <u>compression-critical</u> since $p_o > p_{burst}$ and the minimum weight is obtained by using p_o. Also, the $(\bar{t}_{min}/R)$ graph, based upon p_o is valid and,

$$\bar{t}_{min} = 0.00149\,(48) = \underline{0.0715 \text{ in.}}$$

$$\bar{N} = \frac{N_{cr}}{ER}\left(\frac{F_{tu}}{p_o}\right)$$

$$= 3.97(10^{-6})\ \frac{67.0\ (10^3)}{69.0} = 3.85\ (10^{-3})$$

$$x = \frac{\bar{N}(10^3)}{2.505} = \frac{3.85}{2.505} = 1.535$$

$$y = \frac{\bar{N}}{0.397}\left(\frac{F_{tu}}{p}\right) = \frac{3.85(10^{-3})}{0.397}\left[\frac{67.0(10^3)}{69.0}\right]$$

$$= 9.42$$

From the α, δ graph,

$$\alpha = 0.273, \quad = 13.5$$

$$t = \frac{p_o R}{F_{tu}(1+\alpha)} = \frac{69.0(48.0)}{67.0(1.273)}(10^{-3}) = 0.0388 \text{ in.}$$

$$d = \delta t = 13.5(0.0388) = 0.524 \text{ in.}$$

$$b = \sqrt{\frac{\bar{N}}{0.616}}\, d = \sqrt{\frac{38.5(10^{-4})}{0.616}}(0.524) = 0.0791(0.524) = 0.0415 \text{ in.}$$

$$h = \sqrt{\frac{10.2}{\bar{N}}}\, t = \sqrt{\frac{10.2}{0.385}(10^2)}(0.0388) = 51.5(0.0388) = 2.00 \text{ in.}$$

$$a = \frac{2}{\sqrt{3}} h = \frac{2(2.00)}{1.732} = 2.31 \text{ in.}$$

As a check,

$$\frac{bd}{th} = \frac{0.0415(0.524)}{0.0388(2.00)} = 0.280$$

$$\bar{t} = t(1 + 3\alpha) = 0.0388\left[1 + 3(0.280)\right] = 0.0714 \text{ in.}$$

Worked Example 2

$R = 150$ in.

$E = 10.5(10^6)$ psi.

$M = 59.5(10^6)$ lb in.

$p_{burst} = 60$ psi.

$F_{tu} = 71.0$ ksi.

$$N_b = \frac{M}{\pi R^2} = \frac{59.5\,(10^6)}{\pi(150^2)} = \frac{59.5\,(10^6)}{70700} = 842 \text{ lb/in.}$$

$$\frac{N_{cr}}{ER} = \frac{842}{10.5\,(150)}\,(10^{-6}) = 5.35\,(10^{-7})$$

From the graph,

$$\left(\frac{t_{min}}{R}\right) = 0.000444, \qquad \left(\frac{p_o}{F_{tu}}\right)\,10^4 = 3.10$$

$$p_o = 0.310\,(71.0) = 22.0 \text{ psi} < 60 \text{ psi} = p_{burst}$$

In this case the cylinder is pressure-critical and p_{burst} must be used.

$$\overline{N} = \frac{N_{cr}}{ER}\left(\frac{F_{tu}}{p_{burst}}\right) = 5.35\,(10^{-7})\left[\frac{71.0\,(10^3)}{60}\right] = 6.33\,(10^{-4})$$

$$x = \frac{\overline{N}\,(10^3)}{2.505} = \frac{0.633}{2.505} = 0.262$$

$$y = \frac{\overline{N}}{0.397}\left(\frac{F_{tu}}{p}\right) = \frac{0.633}{0.397}\left(\frac{71.0}{60.0}\right) = 1.89$$

From graph, $\alpha = 0.0118$, $\delta = 6.8$

$$t = \frac{pR}{F_{tu}(1+\alpha)} = \frac{60\,(150)}{71\,(1.0118)}\,(10^{-3}) = 0.1252 \text{ in.}$$

$$d = \delta t = 6.8\,(0.1252) = 0.852 \text{ in.}$$

$$b = \sqrt{\frac{\bar{N}}{0.616}}\, d = \sqrt{\frac{6.33\ (10^{-4})}{0.616}}\ (0.852) = 0.0321\ (0.0852) = 0.0273 \text{ in.}$$

$$h = \sqrt{\frac{10.2}{\bar{N}}}\, t = \sqrt{\frac{10.2}{6.33}\ (10^{4})}\ (0.1252) = 127\ \ (0.1252) = 15.9 \text{ in.}$$

$$a = \frac{2}{\sqrt{3}}\, h = \frac{2\ (15.9)}{1.732} = 18.38 \text{ in.}$$

As a check,

$$\frac{bd}{th} = \frac{0.0273\ (0.852)}{0.1252\ (15.9)} = 0.0117$$

For the equivalent weight thickness,

$$\bar{t} = t\ (1 + 3\alpha)$$

$$= 0.1252\ \left[1 + 3\ (0.0117)\right]$$

$$\bar{t} = 0.1297 \text{ in.}$$

If the cylinder had been compressive critical, one would have had,

$$\bar{t}_{min} = 0.000444\ \ (150)$$

$$= 0.0666 \text{ in.}$$

4.2.4 Summary of Design Equations for Cylinder Under Axial Compression and Bending

	Ref. page
$c_0 = 0.397$	4.2.005
$c_1 = 10.2$	4.2.006
$c_2 = 0.616$	4.2.008

	Ref. eq.
$\bar{N} = \frac{N_{cr}}{ER}\left(\frac{F_{tu}}{p}\right)$	(4.2.18)
$x = \frac{\bar{N}\,(10^3)}{2.505}$	(4.2.23)
$y = \frac{\bar{N}}{0.397}\left(\frac{F_{tu}}{p}\right)$	(4.2.24)
$t = \frac{pR}{F_{tu}(1+\alpha)}$	(4.2.28)
$d = \delta t$	(4.2.30)
$b = \sqrt{\frac{\bar{N}}{0.616}}\,d$	(4.2.20)
$h = \sqrt{\frac{10.2}{\bar{N}}}\,t$	(4.2.29)

As a check,

$$\alpha = \frac{\upsilon d}{th}$$

$$\bar{t} = t(1+3\alpha)$$

4.3 CYLINDERS UNDER TORSIONAL SHEAR

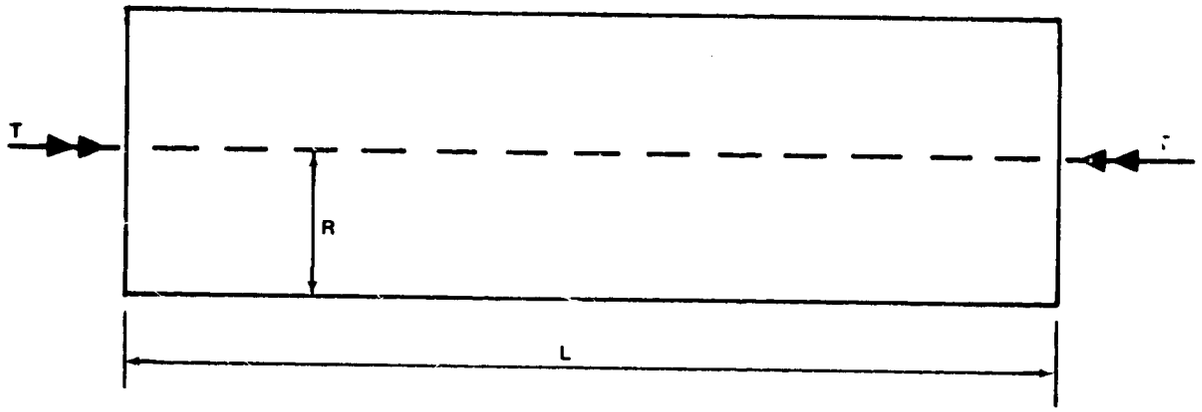

The cylinder is loaded by a resultant torque, T, on the two opposite ends. The internal shear load/in., $N_{x\phi}$, is given by the equation,

$$N_{x\phi} = \frac{T}{2\pi R^2} = V_{cr}$$

where R is the cylinder radius.

4.3.1 Typical Design Situation

High torque may occur because of maneuver loads control fins or because of spin torques applied for flight stability purposes. The analysis may also be used to approximate the required dimensions around the neutral axis due to transverse shear accompanying bending, References 2-13 and 2-14. Reference 2-1 shows that the shear buckles are located in neutral axis region.

4.3.2 Method of Optimization

The optimization method assumes simultaneous general instability, skin buckling, and rib crippling. An auxiliary burst pressure is introduced which is varied to obtain minimum weight of the design. This defines an optimum pressure which divides the design into two classes. In the first class are all designs whose burst pressure (which may be zero) is less than the optimum pressure. In the second class are all designs whose burst pressure

exceeds the optimum pressure. In these cases, the higher pressure must be used for the design.

General Stability

From Reference 2-6, the general instability torsional shear, V_{cr}, is given by,

$$V_{cr}(1) = \frac{c_0 E^* t^*}{\left(\frac{R}{t^*}\right)^{5/4} \left(\frac{L}{R}\right)^{1/2}} \qquad (4.3.1)$$

where

$$c_0 = 0.747 \gamma^{3/4}$$

The recommended value for $\gamma^{3/4}$ is 0.67.

Thus

$$c_0 = 0.50$$

Note that E^* and t^* may be used since eq. (4.3.1) is in terms of a stress resultant, V_{cr}.

Substituting

$$E^* = E \frac{(1+\alpha)^2}{\beta}$$

$$t^* = t \frac{\beta}{1+\alpha}$$

into eq. (4.3.1),

$$V_{cr}(1) = \frac{c_o Et}{\left(\frac{R}{t}\right)^{5/4}\left(\frac{L}{R}\right)^{1/2}} \frac{\beta^{5/4}}{(1+\alpha)^{1/4}} \qquad (4.3.2)$$

Skin Buckling

The skin buckling equation appears in the form,

$$\tau_{cr} = \frac{k_s \pi^2 E t^2}{12(1-\nu^2)\, h^2}$$

An unpublished investigation by B. R. Lyons indicates that

$k_s = 35.0$ for clamped edges

$k_s = 20.1$ for simply supported edges

It will be assumed, for the purpose of the section, that the edge fixity is such that

$$k_s = 25.0$$

then from eq. (2.4.11)

$$V_{cr}(2) = t(1+\alpha)\,\sigma_{cr} = c_1 E(1+\alpha)\,\frac{t^3}{h^2} \qquad (4.3.3)$$

where

$$c_1 = \frac{25.0\ (\pi^2)}{12\ \ (8/9)} = 23.1$$

Rib Crippling

From eq. (2.4.12)

$$\sigma_2 = -\sigma_3 = \pm \frac{2N_{xy}}{\sqrt{3}\, t(1+\alpha)}$$

$$N_{xy} = \frac{\sqrt{3}}{2}\, t(1+\alpha)\, \sigma_2$$

From eq. (4.2.13) one then obtains

$$V_{cr}(3) = c_2 \, Et \, (1 + \alpha) \frac{b^2}{d^2} \tag{4.3.4}$$

where

$$c_2 = \frac{\sqrt{3}}{2} \, (0.616)$$

$$= 0.533$$

A summary of the critical load is,

$$V_{cr}(1) = \frac{c_0 \, Et}{\left(\frac{R}{t}\right)^{5/4} \left(\frac{L}{R}\right)^{1/2}} \, \frac{\beta^{5/4}}{(1 + \alpha)^{1/4}} \tag{4.3.5}$$

$$V_{cr}(2) = c_1 \, E \, t \, (1 + \alpha) \frac{t^2}{h^2} \tag{4.3.6}$$

$$V_{cr}(3) = c_2 \, E \, t \, (1 + \alpha) \frac{b^2}{d^2} \tag{4.3.7}$$

To these are now added the burst pressure, p, which is regarded as a free parameter.

$$F_{tu} = \frac{pR}{t \, (1 + \alpha)} \tag{4.3.8}$$

Define the non-dimensional parameter,

$$\overline{V} = \frac{V_{cr}}{ER} \left(\frac{F_{tu}}{p}\right) \tag{4.3.9}$$

From eq. (4.3.6), (4.3.8), and (4.3.9),

$$\overline{V} = c_1 \left(\frac{t}{h}\right)^2 \tag{4.3.10}$$

From eq. (4.3.7), (4.3.8), and (4.3.9),

$$\bar{V} = c_2 \left(\frac{b}{d}\right)^2 \tag{4.3.11}$$

Multiplying (4.3.10) and (4.3.11)

$$\bar{V}^2 = c_1 c_2 \frac{t^2 b^2}{h^2 d^2} = \left(\frac{bd}{th}\right)^2 \left(\frac{t}{d}\right)^4$$

$$\bar{V} = \sqrt{c_1 c_2}\, \frac{\alpha}{\delta^2} \tag{4.3.12}$$

From eq. (4.3.5) and (4.3.9)

$$V_{cr} = \bar{V}\, ER \left(\frac{p}{F_{tu}}\right) = \frac{c_0 E t}{\left(\frac{R}{t}\right)^{5/4} \left(\frac{L}{R}\right)^{1/2}} \frac{\beta^{5/4}}{(1+\alpha)^{1/4}}$$

or

$$\frac{\bar{V} p}{c_0 F_{tu}} \left(\frac{R}{t}\right)^{9/4} \left(\frac{L}{R}\right)^{1/2} = \frac{\beta^{5/4}}{(1+\alpha)^{10/4}}$$

Using eq. (4.3.8),

$$\frac{\bar{V} p}{c_0 F_{tu}} \left(\frac{L}{R}\right)^{1/2} \left(\frac{F_{tu}}{p}\right)^{9/4} (1+\alpha)^{9/4} = \frac{\beta^{5/4}}{(1+\alpha)^{10/4}}$$

or

$$\frac{\bar{V}}{c_0} \left(\frac{L}{R}\right)^{1/2} \left(\frac{F_{tu}}{p}\right)^{5/4} = \frac{\beta^{5/4}}{(1+\alpha)^{10/4}}$$

$$\left[\frac{\bar{V}}{c_0}\sqrt{\frac{L}{R}}\right]^{4/5}\frac{F_{tu}}{p} = \frac{\beta}{(1+\alpha)2} \qquad (4.3.13)$$

Now set

$$x = \frac{\bar{V}\left(10^3\right)}{\sqrt{c_1 c_2}} = \frac{\alpha}{\delta^2}\left(10^3\right) \qquad (4.3.14)$$

$$y = \left[\frac{\bar{V}}{c_0}\sqrt{\frac{L}{R}}\right]^{4/5}\frac{F_{tu}}{p} = \frac{\beta}{(1+\alpha)^2} \qquad (4.3.15)$$

The x, y; α, δ dependence is seen to be the same as previous graphs. The equivalent weight thickness, $\bar{t}$, is

$$\bar{t} = t(1+3\alpha)$$

Using eq. (4.3.8) this becomes,

$$\frac{\bar{t}}{R} = \frac{p}{F_{tu}}\left(\frac{1+3\alpha}{1+\alpha}\right) \qquad (4.3.16)$$

As in previous cases, the quantity, $\bar{t}/R$, may be minimized as a function of p/F_{tu} for a given value of V_{cr}/ER and L/R.

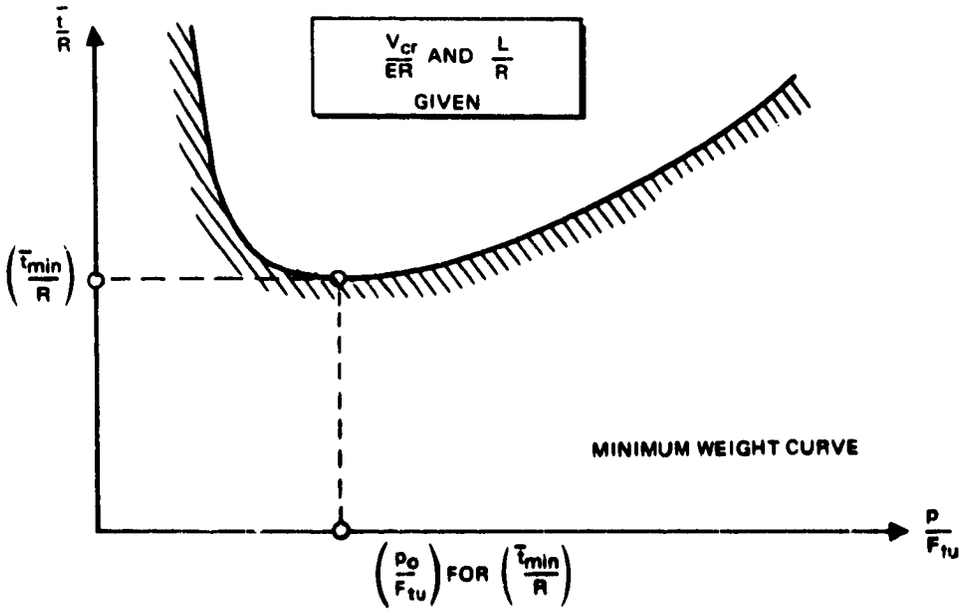

This will again divide all designs into two classes:

1. For $\frac{p_{burst}}{F_{tu}} \leq \frac{p_o}{F_{tu}}$

These are the compression-critical cases.

2. For $\frac{p_{burst}}{F_{tu}} > \frac{p_o}{F_{tu}}$

In this case the design is pressures-critical and the boost pressure must be used.

A master curve may now be constructed of $(\bar{t}_{min}/R)$ and associated (p_o/F_{tu}) values for different V_{cr}/ER and L/R. This is shown in Figures 4.3-1 and 4.3-2.

The complete geometry is determined by the following procedure:

1. Compute x and y, and from the graph read off the corresponding α and δ, Figure 4.3-3.

2. t may now be computed from the burst condition or from the minimum weight pressure, p_o, whichever is larger.

$$t = \frac{pR}{F_{tu}(1+\alpha)} \qquad (4.3.17)$$

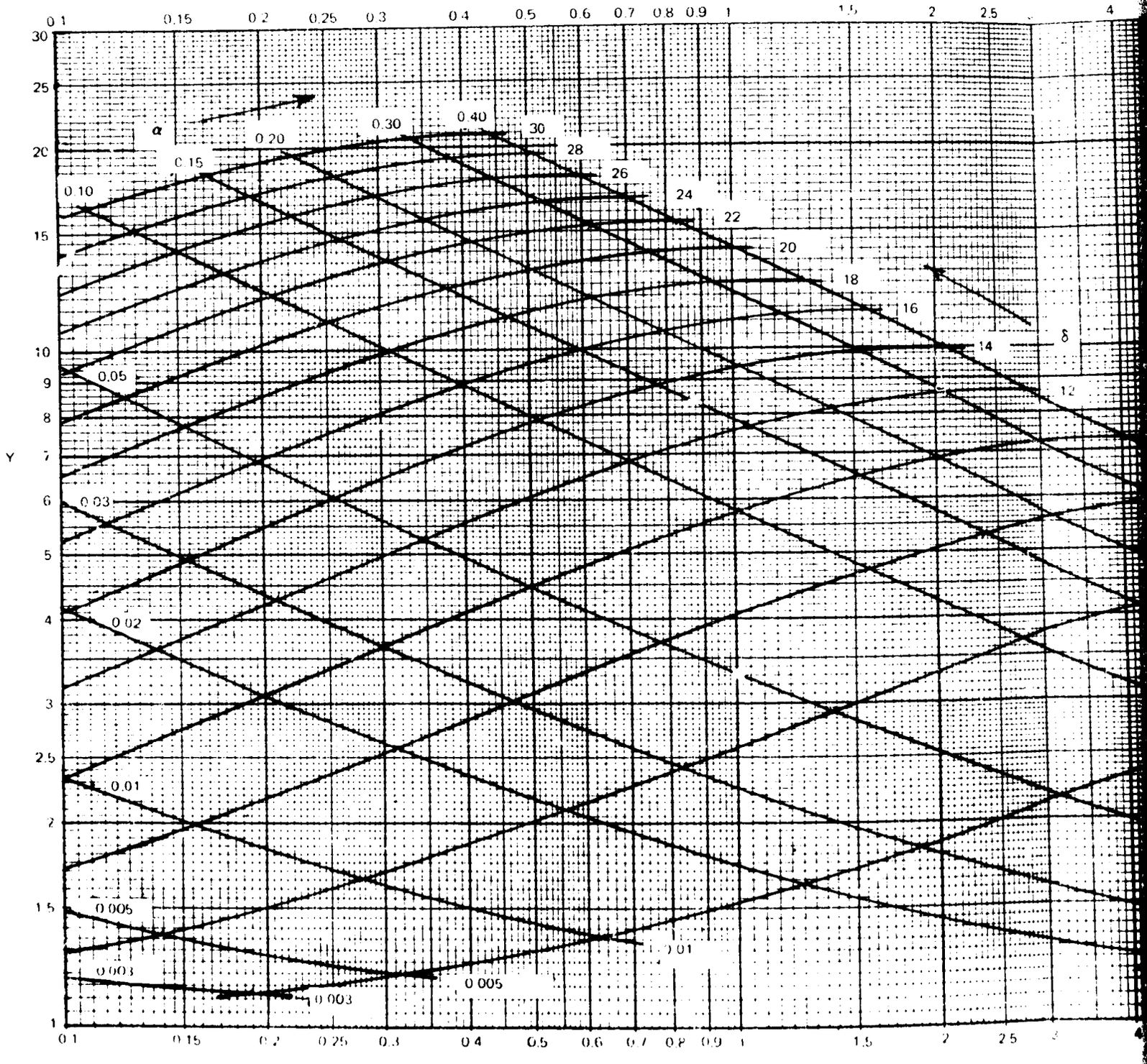

FOLDOUT FRAME

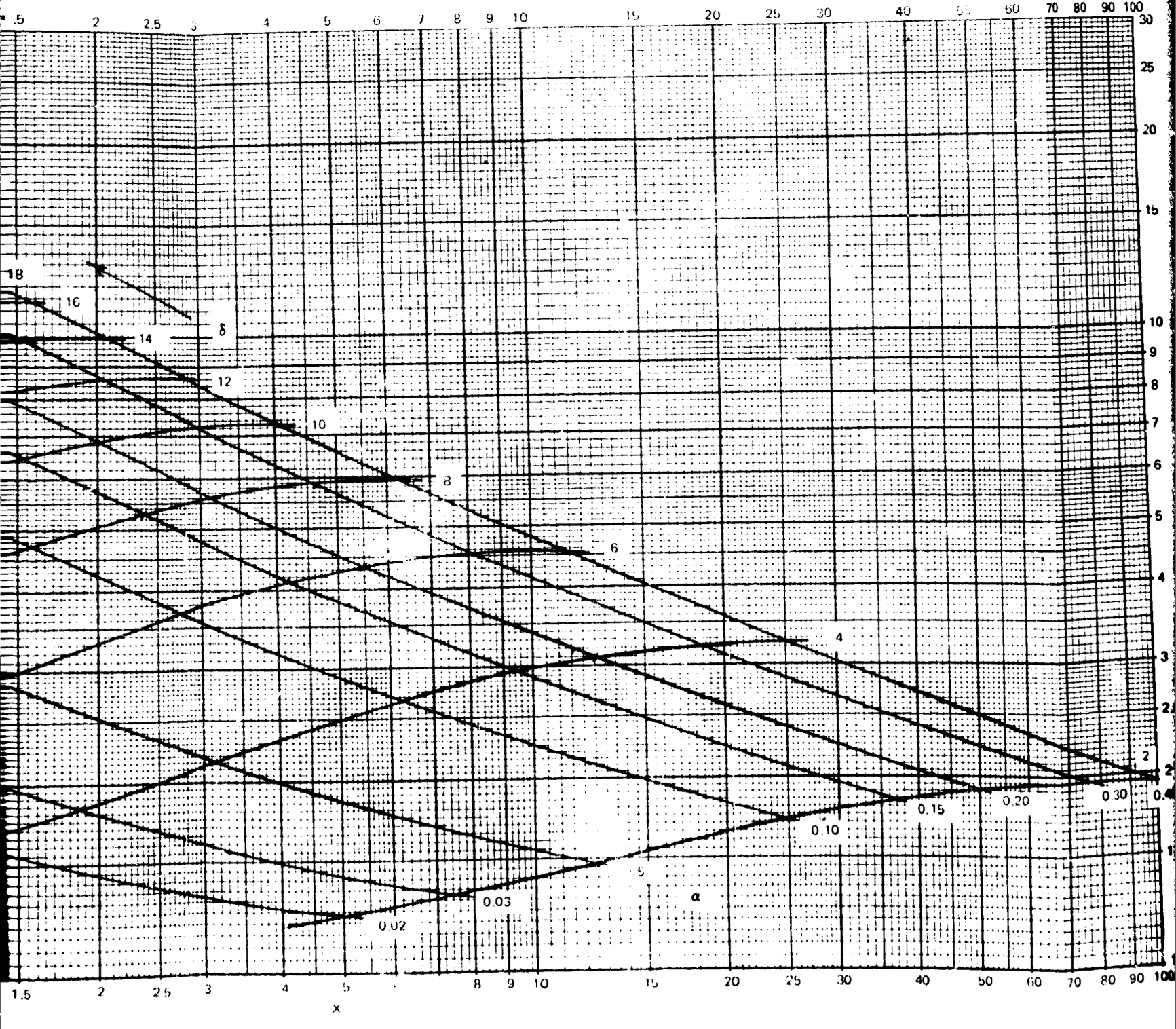

FOLDOUT FRAME

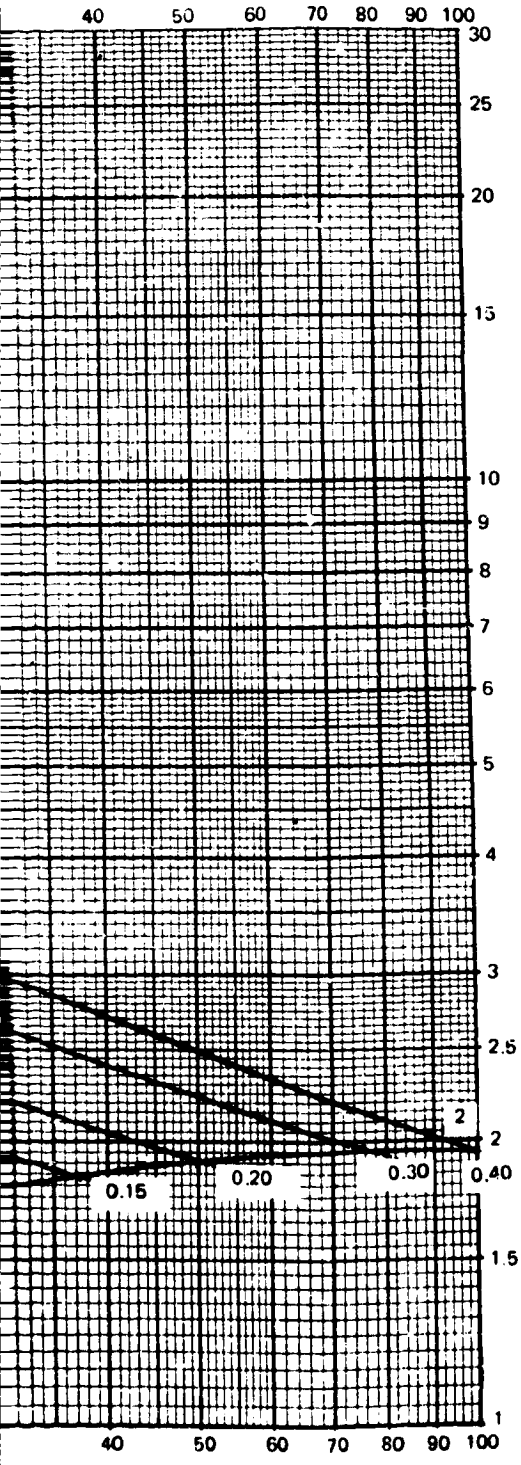

SUMMARY OF DESIGN EQUATIONS FOR CYLINDER UNDER TORSIONAL SHEAR

	REF PAGE
$C_0 = 0.50$	4.3.002
$C_1 = 23.1$	4.3.003
$C_2 = 0.533$	4.3.004
$\bar{V} = \frac{V_{cr}}{E_r}\left(\frac{F_{tu}}{P}\right)$	REF EQ (4.3.9)
$X = \frac{\bar{V}\ (10^3)}{3.51}$	(4.3.14)
$Y = \left[\frac{\bar{V}}{0.50\sqrt{\frac{L}{R}}}\right]^{4/5} \frac{F_{tu}}{P}$	(4.3.15)
$t = \frac{PR}{F_{tu}(1+\alpha)}$	(4.3.17)
$d = \delta t$	(4.3.18)
$b = \sqrt{\frac{\bar{V}}{0.533}}\ d$	(4.3.19)
$h = \sqrt{\frac{23.1}{\bar{V}}}\ t$	(4.3.20)

AS A CHECK,

$$\alpha = \frac{bd}{th}$$

$$\bar{t} = t(1+3\alpha)$$

Figure 4.3-1. X, Y, α, δ Curves for Cylinders Under Torsional Shear

FOLDOUT FRAME

3

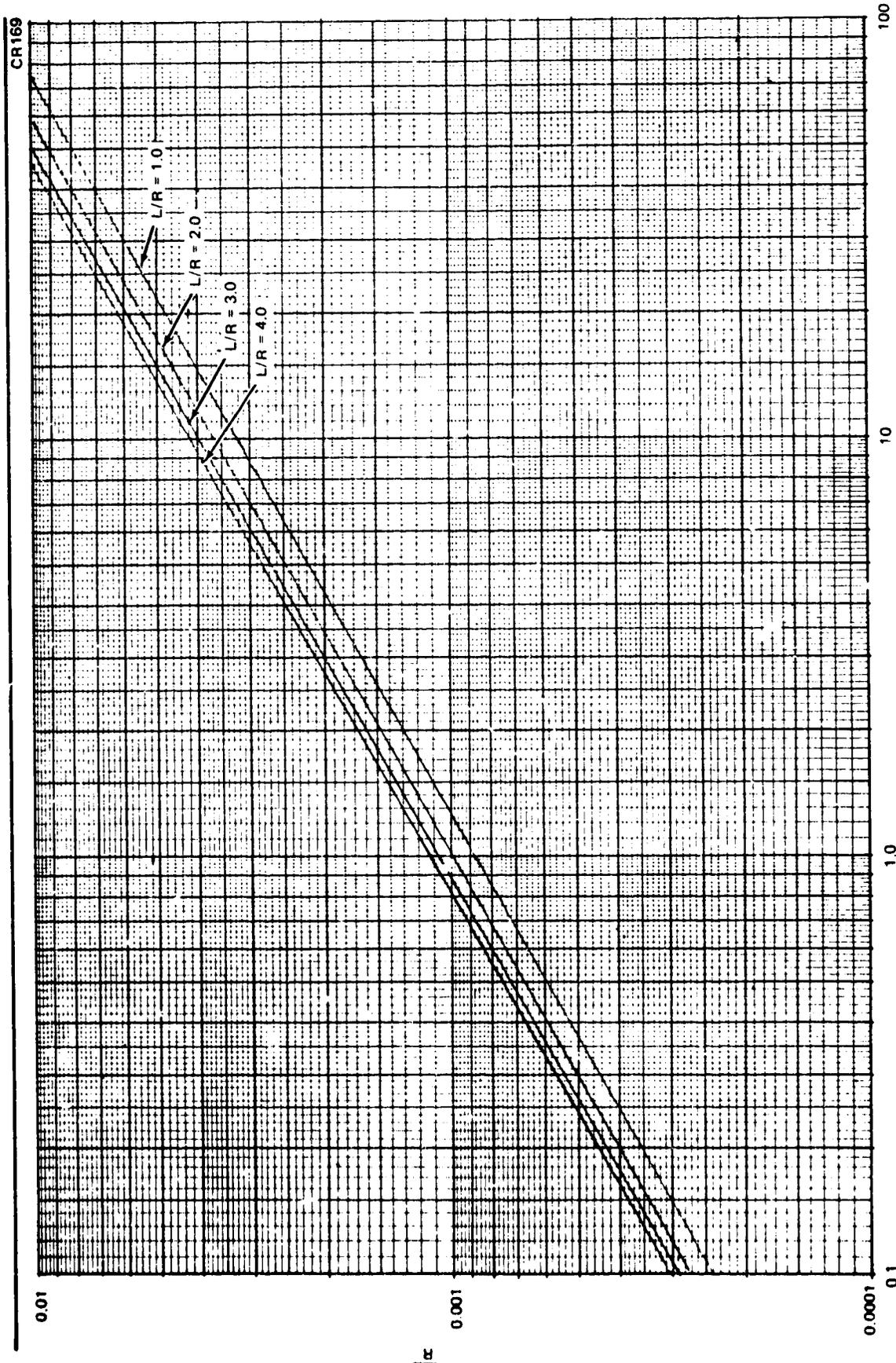

Figure 4.3-2. Master Curves for Torsional Shear

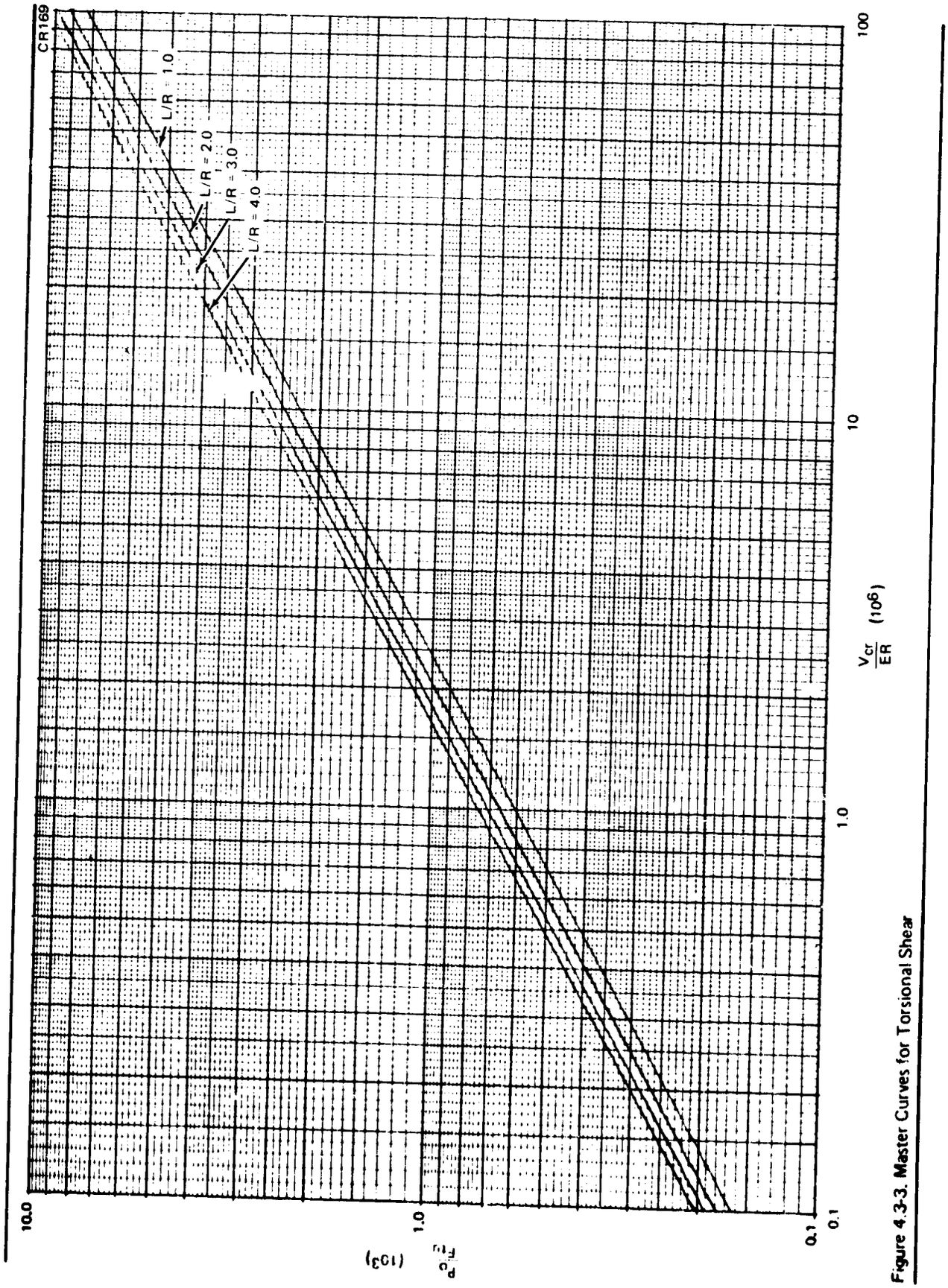

Figure 4.3-3. Master Curves for Torsional Shear

3. Knowing t, the rib depth, d, is obtained from δ.

$$d = \delta t \tag{4.3.18}$$

4. The rib width, b, is computed from eq. (4.3.11).

$$b = \sqrt{\frac{\bar{V}}{c_2}}\, d \tag{4.3.19}$$

5. The triangle height, h, is computed from eq. (4.3.10).

$$h = \sqrt{\frac{c_1}{\bar{V}}}\, t \tag{4.3.20}$$

As a check on the computation and graph reading, now compare the computed value of α from

$$\alpha = \frac{bd}{th}$$

with the value read off from the graph

4.3.3 Worked Example

$R = 48.0$ in.

$E = 11.0\ (10^6)$ psi

$T = 30\ (10^6)$ lb in.

$L = 198$ in.

$L/R = 4.0$

$p_{burst} = 40.0$ psi

$F_{tu} = 67.0$ ksi

$$V_{cr} = \frac{T}{2\pi R^2} = \frac{30\ (10^6)}{2\pi\ (48)^2} = 2075 \text{ lb/in.}$$

$$\frac{V_{cr}}{ER} = \frac{2075}{11.0 \quad (48.0)} \quad (10^{-6}) = 3.93 \quad (10^{-6})$$

From graph,

$$\frac{p_o}{F_{tu}} \quad (10^3) = 1.67$$

$$\frac{\bar{t}_{min.}}{R} = 0.00247$$

$$p_o = 1.67 \quad (67.0) = 112 \text{ psi} > 40$$

The design is compression-critical,

$$\bar{t}_{min} = 0.00247 \quad (48) = 0.1186 \text{ in.}$$

$$\bar{V} = \frac{V_{cr}}{ER} \left(\frac{F_{tu}}{p}\right) = \frac{3.93 \quad (10^{-6})}{1.67 \quad (10^{-3})} = 2.35 \quad (10^{-3})$$

$$y = \left[\frac{\bar{V}}{0.50} \sqrt{\frac{L}{R}}\right]^{4/5} \left(\frac{F_{tu}}{p}\right) = \left[\frac{2.35 \quad (2)}{0.50} \quad (10^{-3})\right]^{4/5} \left(\frac{10^3}{1.67}\right)$$

$$= 14.38$$

$$x = \frac{\bar{V} \quad (10^3)}{3.51} = \frac{2.35}{3.51} = 0.668$$

From α, δ graph,

$$\alpha = 0.285,$$

$$\delta = 20.7$$

$$t = \frac{pR}{F_{tu}(1+\alpha)} = \frac{1.67\ (10^{-3})\ (48.0)}{1.285} = \underline{0.0625 \text{ in.}}$$

$$d = \delta t = 20.7\ (0.0625) = 1.290 \text{ in.}$$

$$b = \sqrt{\frac{\overline{V}}{0.533}}\ d = \sqrt{\frac{23.5\ (10^{-4})}{0.533}}\ (1.290)$$

$$b = 0.0858 \text{ in.}$$

$$h = \sqrt{\frac{23.1}{\overline{V}}}\ t = \sqrt{\frac{23.1\ (10^{3})}{2.35}}\ (0.0625)$$

$$h = 6.19 \text{ in.}$$

As a check on the dimension,

$$\alpha = \frac{bd}{th} = \frac{0.0858}{0.0625}\frac{(1.290)}{(6.19)} = 0.287$$

$$\overline{t} = t(1+3\alpha) = 0.0625\ \ (1.862) = 0.1163 \text{ in.}$$

As an additional check on all strength calculations, from the β curve, Figure 2-1.

$\alpha = 0.287$
$\delta = 20.7$
$\beta = 24.0$

From eq. (4.3.5), (4.3.6), and (4.3.7),

$$V_{cr}(1) = \frac{c_0 Et}{\left(\frac{R}{t}\right)^{5/4}\left(\frac{L}{R}\right)^{1/2}}\ \ \frac{\beta^{5/4}}{(1+\alpha)^{1/4}}$$

$$= \frac{0.50\ (11.0)\ (10^{6})\ 0.0625}{\left(\frac{48.0}{0.0625}\right)^{5/4}\left(\frac{192}{48.0}\right)^{1/2}}\ \ \frac{(24.0)^{5/4}}{(1.287)^{1/4}} = 2030 \text{ lb/in.}$$

$$V_{cr}(2) = c_1 Et(1+\alpha)\left(\frac{t}{h}\right)^2$$

$$= 23.1 \quad (11.0)\ (10^6)\ (0.0625)\ (1.287)\ \left(\frac{0.0625}{6.19}\right)^2$$

$$= 2080 \text{ lb/in.}$$

$$V_{cr}(3) = c_2 Et(1+\alpha)\left(\frac{b}{d}\right)^2$$

$$= 0.533 \quad (11.0)\ (10^6)\ (0.0625)\ \left(\frac{0.0858}{1.29}\right)^2 = 2080 \text{ lb/in.}$$

4.3.4 Summary of Design Equations for Cylinder Under Torsional Shear

	Ref. page
$c_0 = 0.50$	4.3.002
$c_1 = 23.1$	4.3.003
$c_2 = 0.533$	4.3.004

	Ref. eq.
$\overline{V} = \frac{V_{cr}}{ER}\left(\frac{F_{tu}}{p}\right)$	(4.3.9)
$x = \frac{\overline{V}\ (10^3)}{3.51}$	(4.3.14)
$y = \left[\frac{\overline{V}}{0.50}\sqrt{\frac{L}{R}}\right]^{4/5}\left(\frac{F_{tu}}{p}\right)$	(4.3.15)
$t = \frac{pR}{F_{tu}(1+\alpha)}$	(4.3.17)

$$d = \delta t \qquad (4.3.18)$$

$$b = \sqrt{\frac{\overline{V}}{0.533}}\, d \qquad (4.3.19)$$

$$h = \sqrt{\frac{23.1}{\overline{V}}}\, t \qquad (4.3.20)$$

As a check,

$$\alpha = \frac{bd}{th}$$

$$\overline{t} = t\,(1 + 3\alpha)$$

4.4 CYLINDER UNDER UNIFORM EXTERNAL PRESSURE

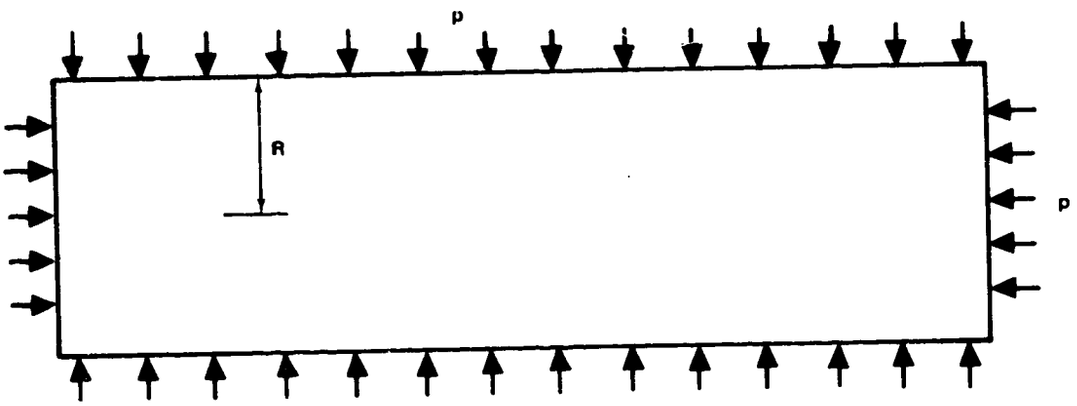

The loading of the cylinder consists of a condition of uniform external pressure over the side walls and ends of the cylinder.

If N_x is the internal axial load/in. and N_ϕ is the internal hoop load/in. in the cylinder, then,

$$N_x = \frac{pR}{2}$$

$$N_\phi = pR$$

where p is the uniform external pressure and R is the radius of the cylinder.

4.4.1 Typical Design Situations

The most common design situations for this condition of loading occur for submersibles or vacuum tanks. In some cases, small additional axial loads or more commonly small bending loads are superimposed upon the external pressure loading. In these cases, the subsequent analysis may be used for a "first cut" at the design. Usually only small modifications are necessary to accommodate the additional loading.

4.4.2 Method of Optimization

The method of optimization assumes simultaneous failure for rib-crippling,

skin buckling, and general instability. A burst pressure parameter is introduced and is varied to obtain minimum weight of the cylinder. This determines an allowable burst pressure for minimum tank weight and divides all designs into two classes. In the first class are all designs whose actual burst pressure (which may be zero) is less than the minimum weight pressure. In the second class are all designs whose burst pressure exceeds the pressure for minimum weight. In these cases the actual burst pressure must be used.

General Instability

Two cases are considered. These are,

1. The "long" cylinder
2. The "intermediate length" cylinder.

According to Reference 2-6, the intermediate length cylinder lies in the range,

$$10^2 \leq 0.562 \left(\frac{L}{R}\right)^2 \left(\frac{R}{t^*}\right) \sqrt{1-\nu^2} \leq 4\left(10^3\right)$$

and since

$$\sqrt{1-\nu^2} = \sqrt{\frac{8}{9}} = 0.943$$

$$t^* = t\,\frac{\beta}{1+\alpha}\,, \quad 10^2 \leq 0.530 \left(\frac{L}{R}\right)^2 \left(\frac{R}{t}\right) \frac{\beta}{1+\alpha} \leq 4\left(10^3\right) \tag{4.4.1}$$

For the long cylinder, the general instability pressure, p_{cr}, is given by Reference 2-6.

$$p_{cr} = c_0 E \left(\frac{t}{R}\right)^3$$

where

$$c_0 = \frac{\gamma}{4(1-\nu^2)} = \frac{0.90}{4\left(\frac{8}{9}\right)} = 0.253$$

Thus,

$$N_{cr}\,(1a) = p_{cr}R = c_0 E^* R \left(\frac{t^*}{R}\right)^3$$

$$N_{cr}\,(1a) = c_0 ER \left(\frac{t}{R}\right)^3 \frac{\beta^2}{1+\alpha} \qquad (4.4.2a)$$

For the <u>intermediate length</u> cylinder, Reference 2-6

$$p_{cr} = \frac{c_0 E}{\left(\frac{R}{t}\right)^{5/2}\left(\frac{L}{R}\right)}$$

where

$$c_0 = \frac{0.855\sqrt{\gamma}}{(1-\nu^2)^{3/4}} = \frac{0.855\,(0.75)}{\left(\frac{8}{9}\right)^{3/4}} = 0.702$$

Thus,

$$N_{cr}\,(1b) = p_{cr}R = \frac{c_0 E^* R}{\left(\frac{R}{t^*}\right)^{5/2}\left(\frac{L}{R}\right)}$$

$$N_{cr}\,(1b) = \frac{c_0 ER}{\left(\frac{R}{t}\right)^{5/2}\left(\frac{L}{R}\right)} \frac{\beta^{3/2}}{(1+\alpha)^{1/2}} \qquad (4.4.2b)$$

Skin Buckling

Tests by Jenkins, Reference 2-13 have shown that the biaxial interaction curve for skin buckling is linear in the range of interest.

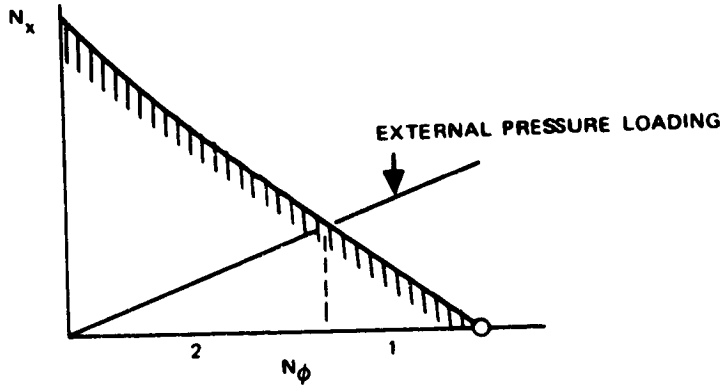

SKIN BUCKLING INTERACTION CURVE

From the interaction diagram,

$$N_\phi \text{ (External Pressure)} = \frac{2}{3} N_\phi \text{ (Uniaxial)}$$

Thus taking 2/3 of the allowable from Reference 2-12.

$$N_{cr}(2) = c_1 E (1 + \sigma) \cdot \frac{t^3}{h^2} \qquad (4.4.3)$$

where

$$c_1 = \frac{2}{3} (10.2) = 6.80$$

Rib Crippling

Eq. (2.4.12) shows that one may conservatively set $N_{cr}(2) = N_x$ for the 1 ribs in either circumferential or longitudinal direction. In this case, one has the same rib crippling allowable as for uniaxial loading.

$$N_{cr}(3) = c_2 E (1 + \alpha) \left(\frac{b}{d}\right)^2 t \qquad (4.4.4)$$

where

$$c_2 = 0.616$$

Burst

The burst pressure is given by the equation, $F_{tu} = pR/t(1 + \alpha)$

Collecting formula,

$$N_{cr}(1a) = p_{cr}R = c_0 ER \left(\frac{t}{R}\right)^3 \frac{\beta^2}{1 + \alpha} \qquad (4.4.5a)$$

$$N_{cr}(1b) = p_{cr}R = \frac{c_0 ER}{\left(\frac{R}{t}\right)^{5/2} \left(\frac{L}{R}\right)} \frac{\beta^{3/2}}{(1 + \alpha)^{1/2}} \qquad (4.4.5)$$

$$N_{cr}(2) = c_1 E (1 + \alpha) \frac{t^3}{h^2} \qquad (4.4.6)$$

$$N_{cr}(3) = c_2 E (1 + \alpha) \frac{b^2 t}{d^2} \qquad (4.4.7)$$

$$F_{tu} = \frac{pR}{t(1 + \alpha)} \qquad (4.4.8)$$

Define the auxiliary variable, $\overline{N}$.

$$\overline{N} = \frac{p_{cr}}{E} \left(\frac{F_{tu}}{p}\right) \qquad (4.4.9)$$

From (4. 4. 6), (4. 4. 8), and (4. 4. 9),

$$\bar{N} = c_1 \frac{t^2}{h^2} \qquad (4.4.10)$$

From (4. 4. 7), (4. 4. 8), and (4. 4. 9),

$$\bar{N} = c_2 \frac{b^2}{d^2} \qquad (4.4.11)$$

Multiplying (4. 4. 10) and (4. 4. 11)

$$\bar{N}^2 = c_1 c_2 \frac{b^2 t^2}{h^2 d^2} = c_1 c_2 \left(\frac{bd}{th}\right)^2 \left(\frac{t}{d}\right)^4 = c_1 c_2 \frac{\alpha^2}{\delta^4}$$

$$\bar{N} = \sqrt{c_1 c_2}\ \frac{\alpha}{\delta^2} \qquad (4.4.12)$$

The positive root is taken since $\bar{N}$, α, and δ are all positive.

Equation (4. 4. 12) satisfies skin buckling, rib crippling and burst conditions.

From eq. (4. 4. 5a), (4. 4. 8), and (4. 4. 9),

$$\frac{P_{cr}}{E} = c_0 \left(\frac{p}{F_{tu}} \cdot \frac{1}{1+\alpha}\right)^3 \left(\frac{\beta^2}{1+\alpha}\right)$$

$$= \left(c_0 \frac{p}{F_{tu}}\right)^3 \frac{\beta^2}{(1+\alpha)^4}$$

$$\bar{N} \left(\frac{p}{F_{tu}}\right)\left(\frac{1}{c_0} \frac{F_{tu}}{p}\right)^3 = \frac{\beta^2}{(1+\alpha)^4}$$

$$\frac{\bar{N}}{c_0^3}\left(\frac{F_{tu}}{p}\right)^2 = \frac{\beta^2}{(1+\alpha)^4}$$

$$\left(\frac{\bar{N}}{c_0}\right)^{1/2}\frac{F_{tu}}{p} = \frac{\beta}{(1+\alpha)^2} \qquad (4.4.13a)$$

Eq. (4.4.13a) satisfies burst and general instability for a long cylinder.

From eq. (4.4.5b), (4.4.8), and (4.4.9),

$$N_\phi = \bar{N}ER\left(\frac{p}{F_{tu}}\right) = \frac{c_0 ER}{\left(\frac{R}{t}\right)^{5/2}\left(\frac{L}{R}\right)}\left[\frac{\beta^{3/2}}{(1+\alpha)^{1/2}}\right]$$

$$\frac{\bar{N}}{c_0}\left(\frac{p}{F_{tu}}\right)\left(\frac{L}{R}\right) = \frac{1}{\left(\frac{R}{t}\right)^{5/2}}\left[\frac{\beta^{3/2}}{(1+\alpha)^{1/2}}\right]$$

But

$$\frac{R}{t} = \frac{F_{tu}}{p}(1+\alpha),$$

Thus

$$\frac{\bar{N}}{c_0}\left(\frac{F_{tu}}{p}\right)^{3/2}\left(\frac{L}{R}\right) = \frac{\beta^{3/2}}{(1+\alpha)^3}$$

or

$$\left[\frac{\bar{N}}{c_0}\left(\frac{L}{R}\right)\right]^{2/3}\left(\frac{F_{tu}}{p}\right) = \frac{\beta}{(1+\alpha)^2} \qquad (4.4.13b)$$

Eq. (4.4.13b) satisfies burst and general instability for buckling of an intermediate length cylinder

Equations (4.4.12), (4.4.13a), and (4.4.13b) satisfy all instability and burst conditions, moreover, they are seen to be similar to eq. (4.2.25) and (4.2.26) for buckling of the cylinder. As a consequence, the same x, y; α, δ curves may be used. Thus define the quantities,

$$x = \frac{\bar{N}\ (10^3)}{\sqrt{c_1\ c_2}} = \frac{\alpha}{\delta^2}\left(10^3\right) \qquad (4.4.14)$$

and

$$y_a = \left[\frac{\bar{N}}{c_0}\right]^{1/2} \frac{F_{tu}}{p} = \frac{\beta}{(1+\alpha)^2} \qquad (4.4.15a)$$

or

$$y_b = \left[\frac{\bar{N}}{c_0}\frac{L}{R}\right]^{2/3} \frac{F_{tu}}{p} = \frac{\beta}{(1+\alpha)^2} \qquad (4.4.15b)$$

to be used with the x, y; α, δ curves.

The equivalent weight thickness, $\bar{t}$, is

$$\bar{t} = t\,(1 + 3\alpha)$$

Using eq. (4.4.9) this becomes,

$$\bar{t} = \frac{pR}{F_{tu}} \left(\frac{1 + 3\alpha}{1 + \alpha}\right)$$

or

$$\frac{\bar{t}}{R} = \frac{p}{F_{tu}} \left(\frac{1 + 3\alpha}{1 + \alpha}\right) \qquad (4.4.16)$$

As in the previous cases, the quantity $\bar{t}/R$ may be minimized as a function of p/F_{tu} for a given value of p_{cr}/E and L/R.

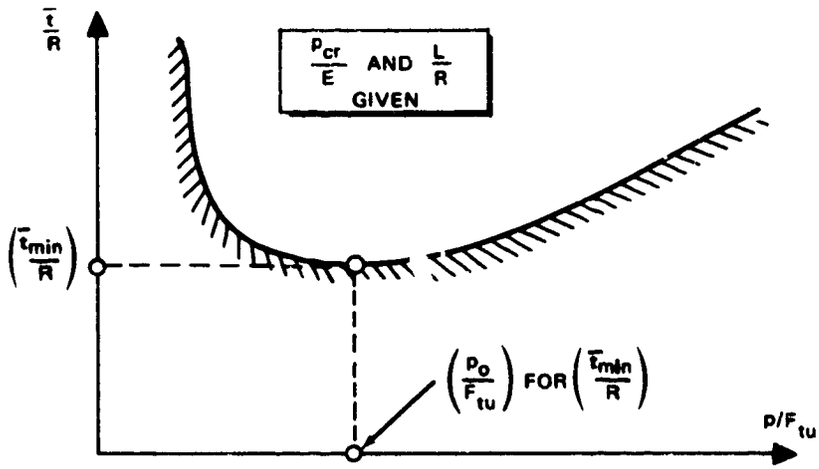

MINIMUM WEIGHT CURVE

If a family of $(\bar{t}_{min}/R)$ and associated (p_o/F_{tu}) values are computed for different p_{cr}/E and L/R, a master nondimensional curve may be constructed. This is shown on pp. 4.4.019 and 4.4.020.

The complete geometry is determined by the following procedure:

1. Compute x and y and from the graph read off the corresponding α and δ, Figure 4.4-1.

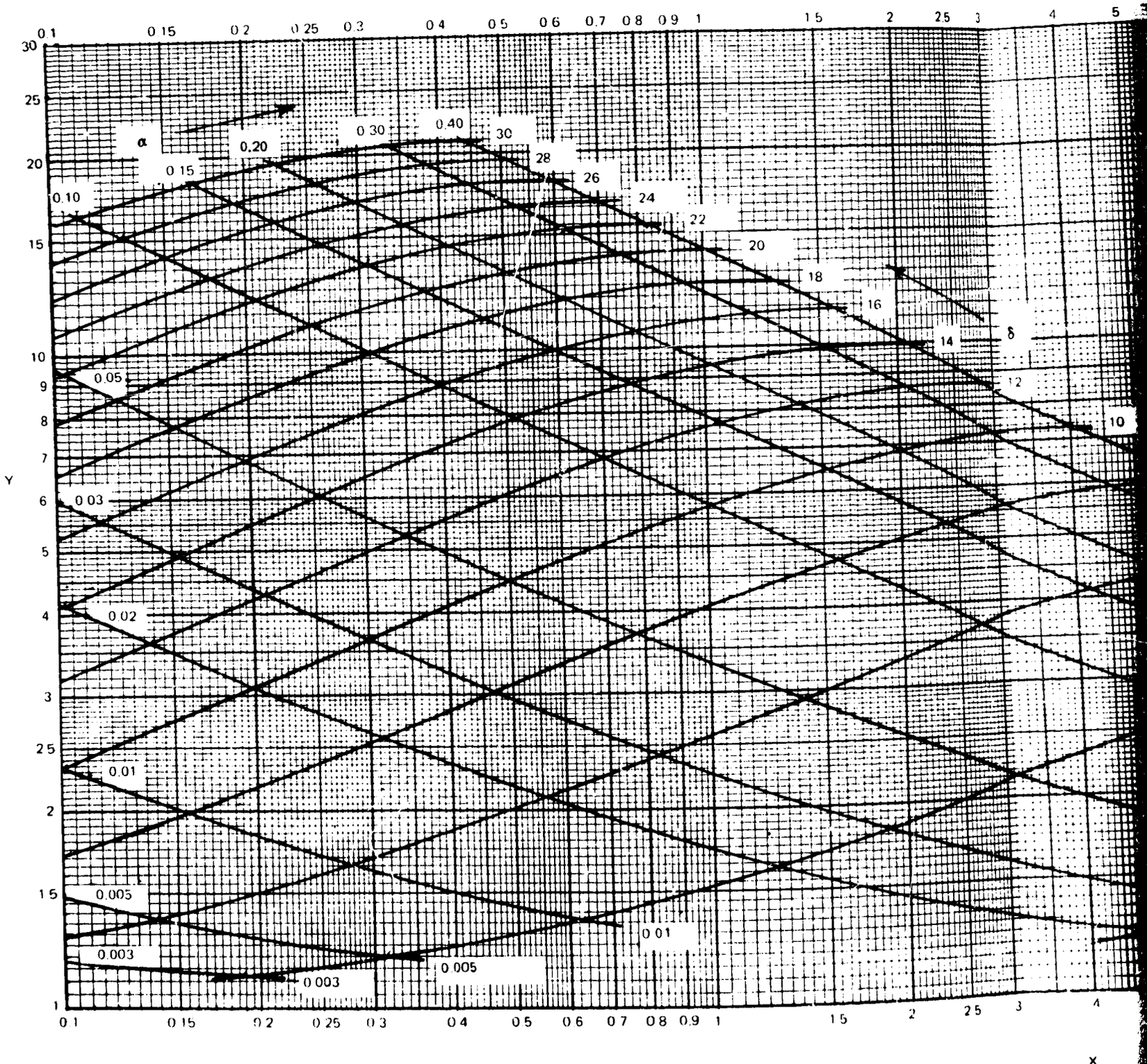

FOLDOUT FRAME

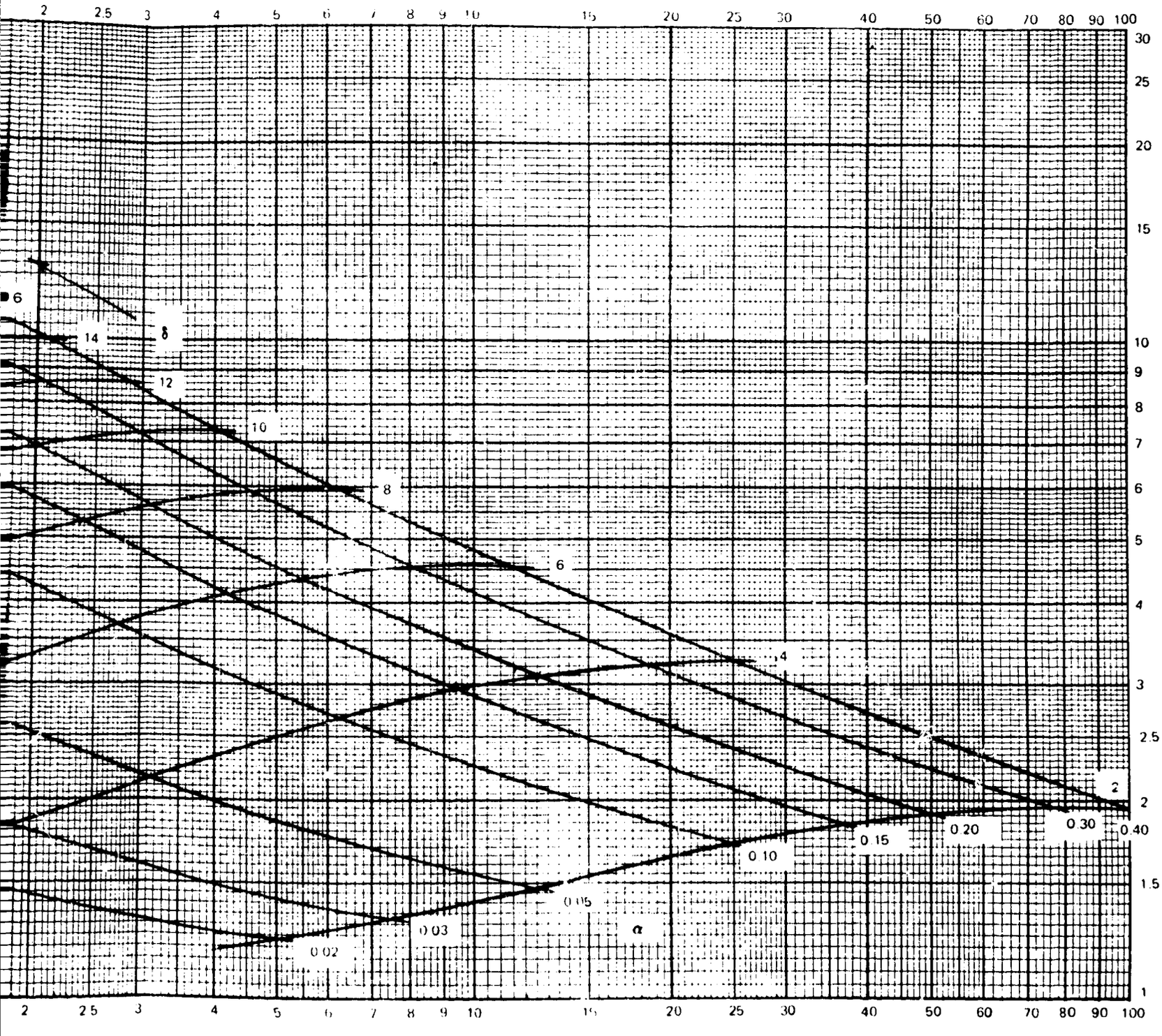

x

FOLDOUT FRAME

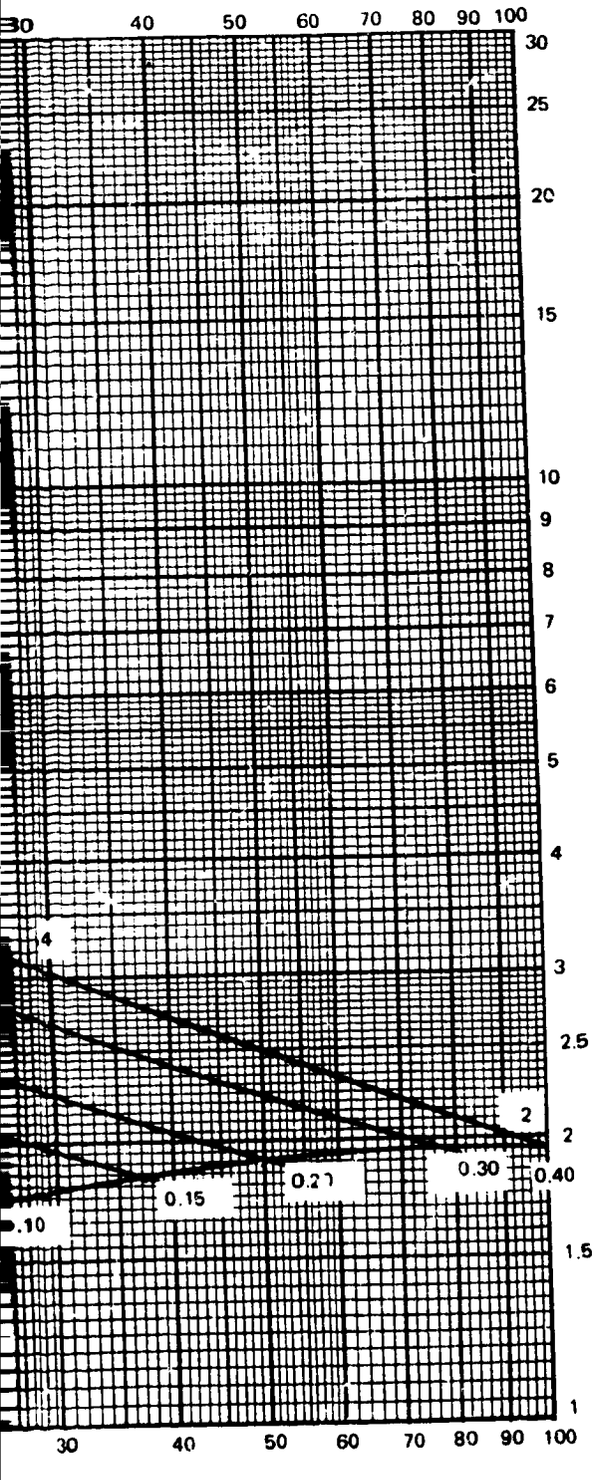

SUMMARY OF DESIGN EQUATIONS FOR CYLINDER UNDER UNIFORM EXTERNAL PRESSURE

$$A = 0.530 \left(\frac{L}{R}\right)^2 \left(\frac{R}{t}\right) \frac{\beta}{1+\alpha}$$

	INTERMEDIATE CYL $10^2 \leq A \leq 4\,(10^3)$	LONG CYL $A > 4 \times 10^3$	REF PAGE
C_o =	0.702	0.253	4.4.003
C_1 =	6.80	6.80	4.4.004
C_2 =	0.616	0.616	4.4.005

			REF EQ
$\bar{N} = \frac{P_{cr}}{E}\left(\frac{F_{tu}}{P}\right)$			(4.4.9)
$X = \frac{\bar{N}\,(10^3)}{2.04}$			(4.4.14)
$Y_a = \left[\frac{\bar{N}}{0.253}\right]^{1/2}\left(\frac{F_{tu}}{P}\right)$		(LONG CYL)	(4.4.15a)
$Y_b = \left[\frac{\bar{N}}{0.702}\left(\frac{L}{R}\right)\right]^{2/3}\left(\frac{F_{tu}}{P}\right)$		(INTERMED CYL)	(4.4.15b)
$t = \frac{PR}{F_{tu}(1+\alpha)}$			(4.4.17)
$d = \delta t$			(4.4.18)
$b = \sqrt{\frac{\bar{N}}{0.616}}\, d$			(4.4.20)
$h = \sqrt{\frac{6.80}{\bar{N}}}\, t$			(4.4.19)

AS A CHECK,

$$\alpha = \frac{bd}{th}$$

$$\bar{t} = t(1+3\alpha)$$

Figure 4.4-1. X, Y, α, δ Curves for Cylinders Under Uniform External Pressure

FOLDOUT FRAME 3

2. t may now be computed from the minimum weight pressure, p_o, or the burst pressure, whichever is larger.

$$t = \frac{pR}{\overline{F}_{tu}(1+\alpha)} \qquad (4.4.17)$$

3. Knowing t, and δ, the rib depth, d, is computed from,

$$d = \delta t \qquad (4.4.18)$$

4. The triangle height is computed from eq. (4.4.11)

$$h = \sqrt{\frac{c_1}{\overline{N}}}\ t \qquad (4.4.19)$$

5. The rib width is computed from eq. (4.4.12).

$$b = \sqrt{\frac{\overline{N}}{c_2}}\ d \qquad (4.4.20)$$

As a check on the computed values of b, d, t, h and the accuracy of the reading of the graph, the quantity (bd/th) should equal the value of α read off from the x, y; α, δ graph, Figure 4.4-1.

4.4.3 Worked Examples

Case of Long Cylinder

Long cylinder.

p_{cr} = 600 psi

p_{burst} = 0

R = 10.5 in.

E = 18.0 (10^6) psi

$$\frac{P_{cr}}{E}\ (10^6) = \frac{600}{18.0} = 33.3$$

From long cylinder graph, Figures 4.4-2 and 4.4-3

$$\frac{\bar{t}}{R} = 0.016$$

$$\frac{p_o}{F_{tu}}\ (10^3) = 10.7$$

$$\bar{t} = 0.016\ (10.5) = 0.168 \text{ in.}$$

$$\bar{N} = \frac{P_{cr}}{E}\left(\frac{F_{tu}}{p}\right) = \frac{33.3\ (10^{-3})}{10.7} = 3.11\ (10^{-3})$$

$$y_a = \left[\frac{\bar{N}}{0.253}\right]^{1/2}\left(\frac{F_{tu}}{p}\right)\left[\frac{3.11\ (10^3)}{0.253}\right]^{1/2}\left(\frac{10^3}{10.7}\right)$$

$$= 10.37$$

$$x = \frac{3.11}{2.04} = 1.523$$

From graph,

$\alpha = 0.320$

$\delta = 14.5$

$$c = \frac{pR}{F_{tu}\ (1+\alpha)} = \frac{10.7\ (10^{-3})(10.5)}{1.320} = 0.0852 \text{ in.}$$

$$d = \delta t = 14.5\ (0.0852) = 1.235 \text{ in.}$$

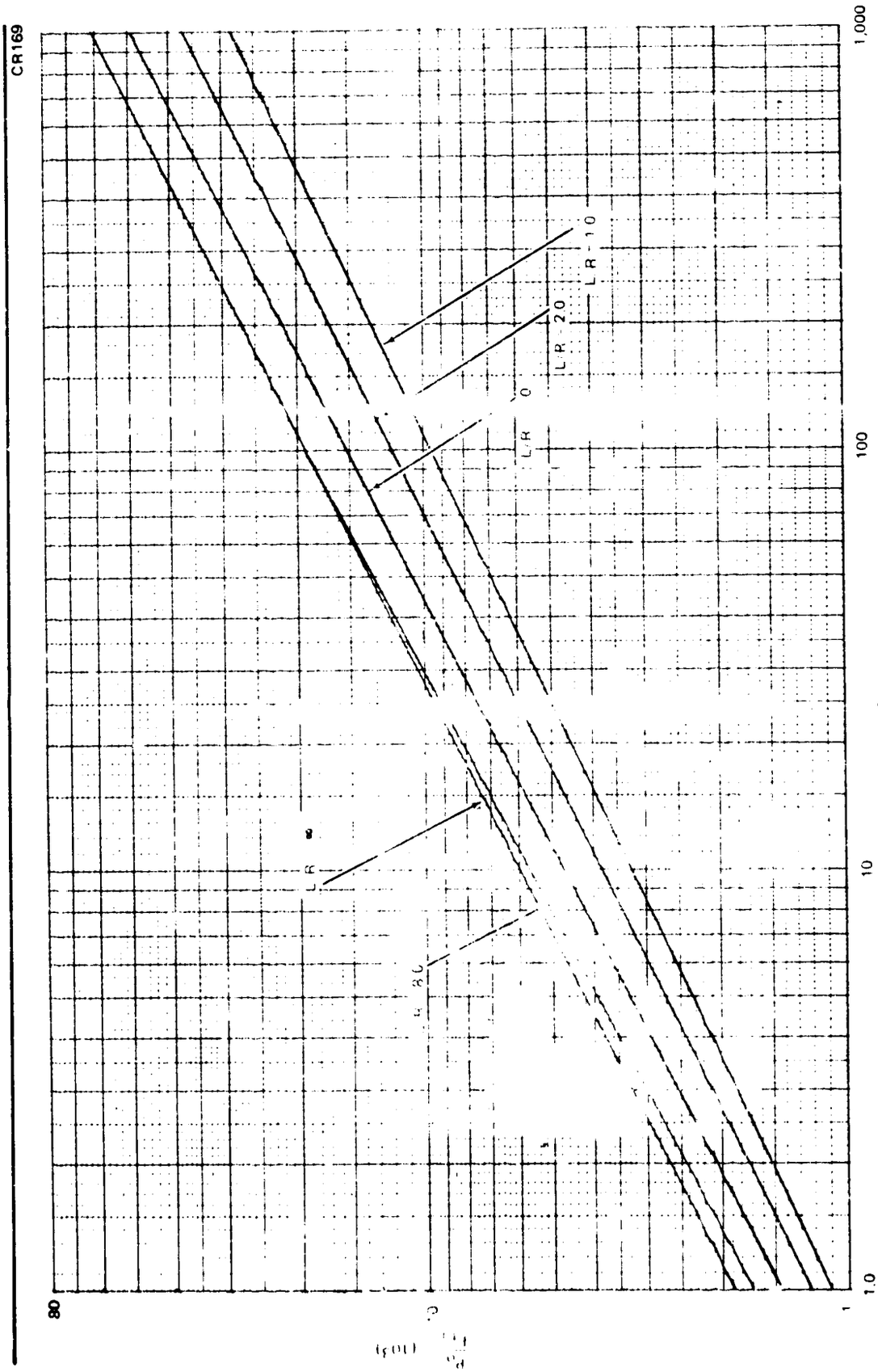

Figure 4.4.2 Master Curves for Uniform External Pressure

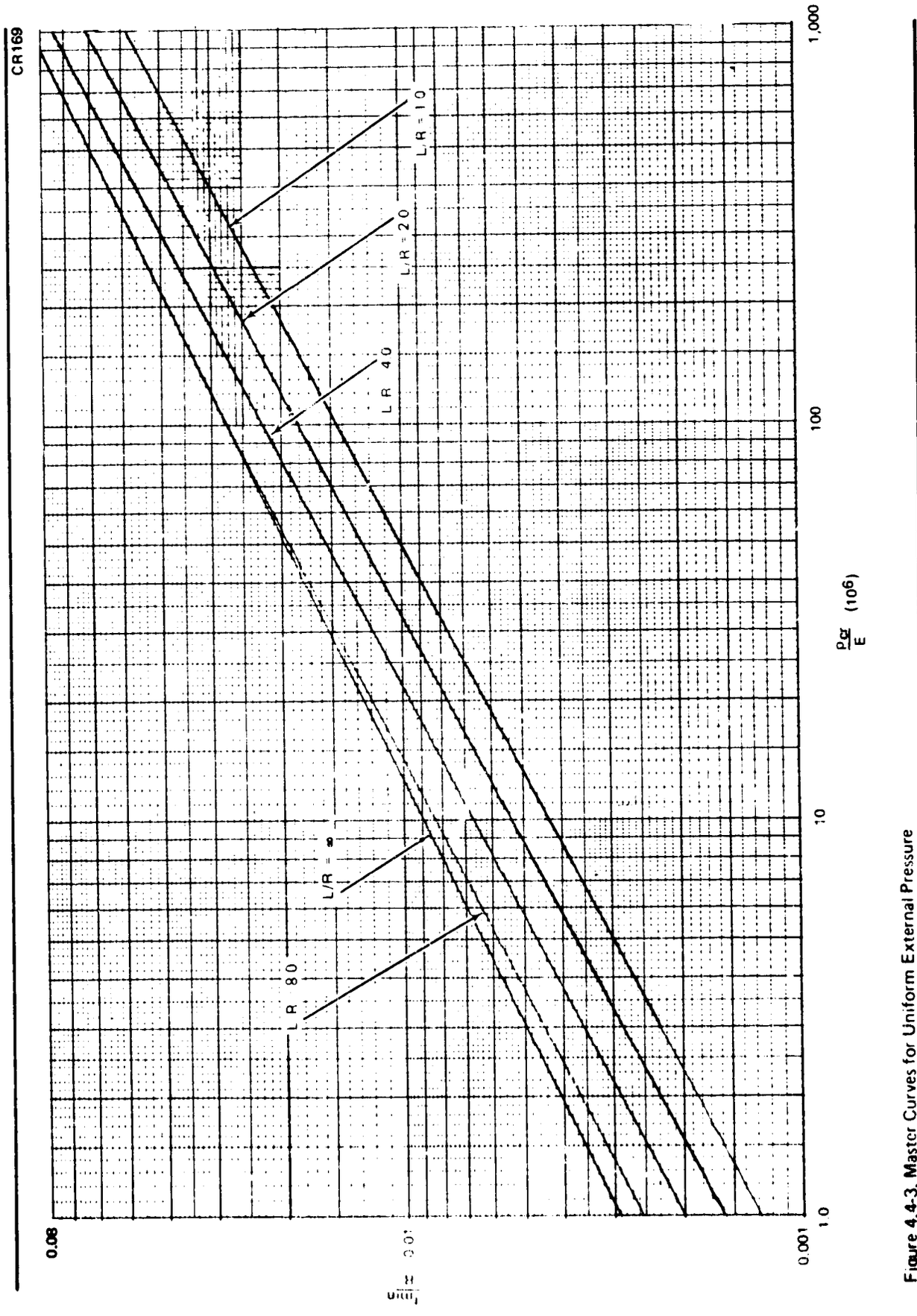

Figure 4.4-3. Master Curves for Uniform External Pressure

$$b = \sqrt{\frac{\overline{N}}{0.616}} \qquad d = \sqrt{\frac{3.11\,(10^3)}{0.616}}\,(1.235) = 0.0877 \text{ in.}$$

$$h = \sqrt{\frac{6.80}{\overline{N}}} \qquad t = \sqrt{\frac{6.80\,(10^3)}{3.11}}\,(0.0852) = 3.99 \text{ in.}$$

As a check,

$$\alpha = \frac{bd}{th} = \frac{0.0877\,(1.235)}{0.0852\,(3.99)} = 0.318$$

$$\overline{t} = t\,(1 + 3\alpha) = 0.0852\,(1.953) = 0.1665 \text{ in.}$$

$$p_{cr}\,R = 600\,(10.5) = 6300 \text{ lb/in.}$$

From the α, δ, β graph, Figure 2-1,

$$\alpha = 0.318, \quad \delta = 14.5, \quad \beta = 18$$

Using eq. (4.4.5a), (4.4.6) and (4.4.7)

$$N_{cr}\,(1) = 0.253\,ER\left(\frac{t}{R}\right)^3 \frac{\beta^2}{1+\alpha}$$

$$= 0.253\,(18.0)(10^6)(10.5)\left(\frac{0.0852}{10.5}\right)^3 \frac{(18)^2}{1.318}$$

$$= 6250 \text{ lb/in.}$$

$$N_{cr}\,(2) = 6.80\,E\,(1+\alpha)\,\frac{t^3}{h^2}$$

$$= 6.80(18.0)(10^6)(1.318)\,\frac{(0.0852)^3}{(3.99)^2} = 6250 \text{ lb/in.}$$

$$N_{cr}(3) = 0.615\, E\,(1+\alpha)\, t\, \frac{b^2}{d^2}$$

$$= 0.616\,(18.0)\,(10^6)\,(1.318)(0.0852)\left(\frac{0.0877}{1.235}\right)^2$$

$$= 6260 \text{ lb/in.}$$

Worked Example 2

p_{cr}	= 100 psi	F_{tu}	= 67.0 ksi
p_{burst}	= 0	L	= 192 in.
R	= 48.0		
E	= 10.7 (10^6) psi		
L/R	= $\frac{192}{48}$ = 4.0		
$\frac{p_{cr}}{E}(10^6)$	= $\frac{100}{10.7}$ = 9.35		

From graph,

$$\frac{p_o}{F_{tu}}(10^3) = 4.55$$

$$\frac{\bar{t}_{min}}{R} = 0.0065$$

The optimum burst pressure, p_o is,

$$p_o = 4.55\,(67.0) = 305 \text{ psi.}$$

The minimum equivalent weight thickness, $\bar{t}_{min}$, is,

$$\bar{t}_{min} = 0.0065\,(48) = 0.312 \text{ in.}$$

$$\bar{N} = \frac{p_{cr}}{E}\left(\frac{F_{tu}}{p}\right) = \frac{9.35\ (10^{-6})}{4.55\ (10^{-3})} = 2.05\ (10^{-3})$$

$$x = \frac{\bar{N}\ (10^{3})}{2.04} = \frac{2.05}{2.04} = 1.01$$

$$y_b = \left[\frac{\bar{N}}{0.702}\left(\frac{L}{R}\right)\right]^{2/3}\left(\frac{F_{tu}}{p}\right)$$

$$= \left[\frac{2.05\ (10^{-3})}{0.702}\ (4)\right]^{2/3}\left(\frac{10^{3}}{4.55}\right) = 11.30$$

From x, y; α, δ graph, Figure 4.4-1

$\alpha = 0.27$

$\delta = 16.6$

$$t = \frac{pR}{F_{tu}(1+\alpha)} = \frac{4.55\ (10^{-3})\ 48.0}{1.27} = 0.172 \text{ in.}$$

$$d = \delta t = 16.6\ (0.172) = 2.85 \text{ in.}$$

$$b = \sqrt{\frac{\bar{N}}{0.616}}\ d = \sqrt{\frac{2.05\ (10^{-3})}{0.616}}\ (2.85) = 0.1645$$

$$h = \sqrt{\frac{6.80}{\bar{N}}}\ t = \sqrt{\frac{6.80\ (10^{3})}{2.05}}\ (0.172) = 9.91 \text{ in.}$$

As a check,

$$\alpha = \frac{bd}{th} = \frac{0.1645\ (2.85)}{0.172\ (9.91)} = 0.275$$

$$\bar{t} = t(1 + 3\alpha) = 0.172\,(1.81) = 0.311 \text{ in.}$$

$$N_{cr} = p_{cr} R = 100\,(48) = 4800 \text{ lb/in.}$$

From the β graph, Figure 2-1

$$\alpha = 0.275, \quad \delta = 1.6.6, \quad \beta = 18.8$$

Using eq. (4.4.5b), (4.4.6) and (4.4.7),

$$N_{cr}(1) = \frac{0.702\,ER}{\left(\frac{R}{t}\right)^{5/2} \frac{L}{R}} \left[\frac{\beta^{3/2}}{(1+\alpha)^{1/2}}\right]$$

$$= \frac{0.702\,(10.7)\,(10^6)\,(48.0)}{\left(\frac{48.0}{0.172}\right)^{5/2} \frac{192}{48}} \frac{(18.8)^{3/2}}{(1.275)^{1/2}} = 4980 \text{ lb/in.}$$

$$N_{cr}(2) = 6.80E\,(1+\alpha)\frac{t^3}{h^2}$$

$$= 6.80\,(10.7)\,(10^6)\,1.275\,\frac{(0.172)^3}{(9.91)^2} = 4800 \text{ lb/in.}$$

$$N_{cr}(3) = 0.616E\,(1+\alpha)\,t\,\frac{b^2}{d^2}$$

$$= 0.616\,(10.7)\,(10^6)\,(1.275)\,(0.172)\,\frac{(0.1645)^2}{(2.85)^2}$$

$$= 4820 \text{ lb/in.}$$

4.4.4 Summary of Design Equations for Cylinder Under Uniform External Pressure

Ref. page

$$A = 0.530 \left(\frac{L}{R}\right)^2 \left(\frac{R}{t}\right) \frac{\beta}{1+\alpha}$$ 4.4.002

Intermediate Cyl	Long Cyl	Ref. page
$10^2 \le A \le 4\ (10^3)$	$A > 4\ (10^3)$	4.4.002
$c_0 = 0.702$	0.253	4.4.003

Intermediate Cyl	Long Cyl	Ref. page
$c_1 = 6.80$	6.80	4.4.004
$c_2 = 0.616$	0.616	4.4.005

Ref. q.

$$\bar{N} = \frac{p_{cr}}{E} \left(\frac{F_{tu}}{p}\right)$$ (4.4.9)

$$x = \frac{\bar{N}\ (10^3)}{2.04}$$ (4.4.14)

$$y_a = \left[\frac{\bar{N}}{0.253}\right]^{1/2} \left(\frac{F_{tu}}{p}\right)$$ (Long Cyl) (4.4.15a)

$$y_b = \left[\frac{\bar{N}}{0.702} \left(\frac{L}{R}\right)\right]^{2/3} \frac{F_{tu}}{p}$$ (Intermed. Cyl) (4.4.15b)

$$t = \frac{pR}{F_{tu}(1+\alpha)}$$ (4.4.17)

$$d = \delta t$$ (4.4.18)

$$b = \sqrt{\frac{\bar{N}}{0.616}}\, d$$ (4.4.20)

$$h = \sqrt{\frac{6.80}{\overline{N}}}\ t \qquad (4.4.19)$$

As a check,

$$\alpha = \frac{bd}{th}$$

$$\overline{t} = t\,(1 + 3\alpha)$$

4.5 IN-PLANE CONCENTRATED LOAD IN INFINITE SHEET

As noted in Subsection 2.4, if changes of curvature are negligible, the stresses in isogrid may be easily determined if N_x, N_{xy}, and N_y are known. For the case of the in-plane concentrated load for an isotropic sheet in plane stress, the solution, due to Mitchell, is immediately obtainable from Reference 2-2.

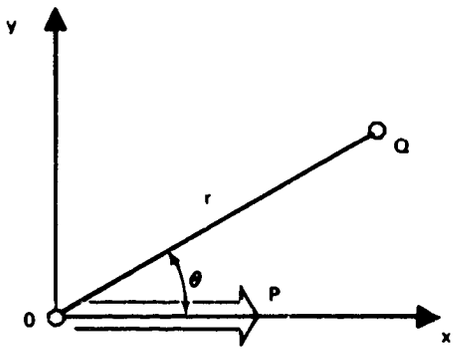

Let the point O, at which the stresses are to be computed, be a distance r from the origin and make an angle θ with the x axis. The concentrated load, P, is applied at the origin, 0, and is directed along the positive x axis. The stress resultants are given by the expressions,

$$N_x = \frac{P}{4\pi}\frac{\cos\theta}{r}\left[-(3+\nu)+2(1+\nu)\sin^2\theta\right] \qquad (4.5.1)$$

$$N_y = \frac{P}{4\pi}\frac{\cos\theta}{r}\left[1-\nu-2(1+\nu)\sin^2\theta\right] \qquad (4.5.2)$$

$$N_{xy} = -\frac{P}{4\pi}\frac{\sin\theta}{r}\left[1-\nu+2(1+\nu)\cos^2\theta\right] \qquad (4.5.3)$$

Although N_x, N_y, and N_{xy} become infinite at r = 0, this is no problem since stresses will not be computed closer than the reinforcing around the hole in the node. At this point, all stresses are finite. The solution will be used to size ribs and skin around the attachment. Strictly speaking, eq. (4.5.1) to (4.5.3) were developed using an Airy stress function in polar coordinates for constant sheet thickness; however, if the thickness variation is rotationally symmetric and not too drastic, it may be expected to give results sufficiently accurate for the majority of design problems.

4.5.1 Typical Design Situations

Main structural loads carried by the shell of the vehicle arise from thrust, airload, inertia, and gravity effects. The inertia and gravity loads resulting from mass properties of the component parts may be directly transmitted to the shell wall or through intermediate floors or bulkheads. For most cases it is desirable to avoid bending stresses to minimize weight. In general, this may be done if the loads are transmitted tangentially into the wall of the isogrid plate or shell.

Typical design situations will arise from equipment in interstages between tanks, tank baffles, pipe supports, etc. In one case (Figure 4.5-1), a side load on a tank was transmitted tangentially into the tank by means of an internal A-shaped frame in a structural test, Reference 2-12.

CR169

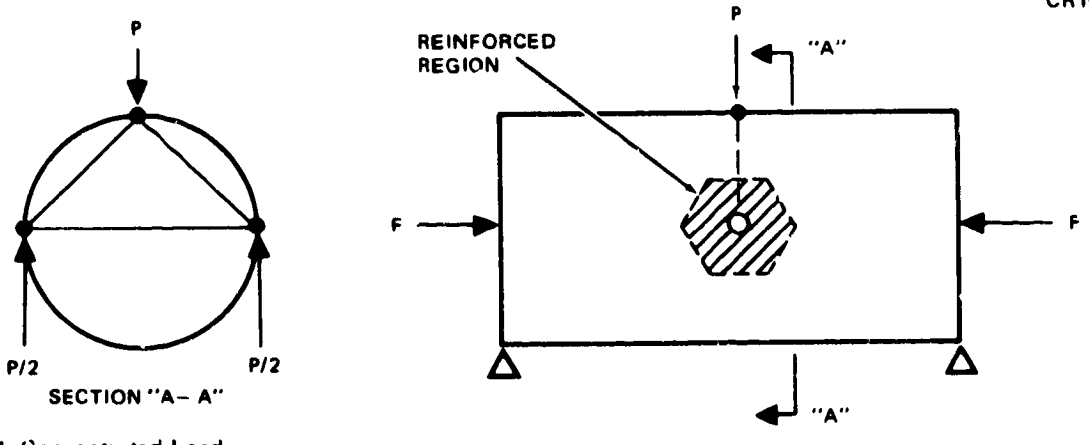

Figure 4.5-1. Concentrated Load

The reinforced region in the first pocket and first set of ribs away from the loaded node was designed according to the analysis developed in this section. No extra reinforcing was indicated beyond this point. However, from the point of view of fabrication, in particular for bending from a flat sheet to circular curvature, the "beef up" was feathered out for another 5 pockets to prevent a flat spot in forming. This extra material served a double purpose to distribute the local load as well as to provide local reinforcement.

A more exact shell analysis using Fourier series was able to account for the changes of curvature of the shell wall. This analysis is sensitive to the size of the loaded region. Strain gage readings showed that the reinforcing served

as a "hard pad" to distribute the load over the entire reinforced area. The total pad weight involved was very small.

The cylindrical wall of the 8-foot-diameter tank was designed for an axial loading of 2,500 lb in. without any side loading. The reinforcing at each pad amounted to only 6 lb with a pad diameter of 24 in. The failure load was 40,000 lb side loading, i.e., 20,000 lb at each pad and an axial loading of 2,400 lb/in., only 100 lb/in. less that the design load for no side loading. Moreover, failure did not penetrate the reinforced region.

4.5.2 Method of Analysis

Since $\nu = 1/3$ for isogrid, eq. (4.5.1) to (4.5.3) become,

$$N_x = \frac{P}{6\pi} \frac{\cos\theta}{r} (-5 + 4\sin^2\theta) \tag{4.5.4}$$

$$N_y = \frac{P}{6\pi} \frac{\cos\theta}{r} (1 - 4\sin^2\theta) \tag{4.5.5}$$

$$N_{xy} = -\frac{P}{6\pi} \frac{\sin\theta}{r} (1 + 4\cos^2\theta) \tag{4.5.6}$$

Skin Stresses

These are immediately obtainable from eq. (2.4.11)

$$\begin{Bmatrix} \sigma_x \\ \sigma_y \end{Bmatrix} = \frac{P}{6\pi} \frac{\cos\theta}{rt(1+\alpha)} \begin{Bmatrix} -5 + 4\sin^2\theta \\ 1 - 4\sin^2\theta \end{Bmatrix} \tag{4.5.7}$$

$$\tau_{xy} = -\frac{P}{6\pi} \frac{\sin\theta}{rt(1+\alpha)} (1 + 4\cos^2\theta) \tag{4.5.8}$$

Stresses will be a maximum along the load direction where $\theta = 0$.

$$\sigma_{x,y\,max} = \sigma_x(\phi = 0) = -\frac{5P}{6\pi} \frac{1}{t(1+\alpha)}$$

Behind the load, where θ = 180 degrees,

$$\sigma_x(\theta = 180°) = + \frac{5P}{6\pi} \frac{1}{rt\,(1+\alpha)} \qquad (4.5.9)$$

Rib Stresses (P in x direction)

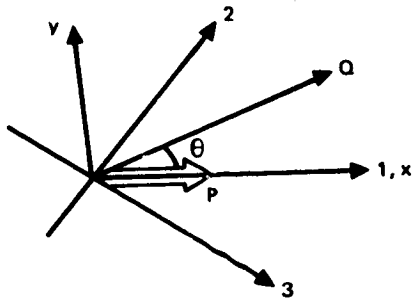

Rib stresses are obtainable from eq. (2.4.12)

$$\sigma_1 = - \frac{8}{9\pi} \frac{P \cos^3\theta}{rt\,(1+\alpha)} \qquad (4.5.10)$$

$$\sigma_{2,3} = \left\{\frac{P}{9\pi\, rt\,(1+\alpha)}\right\} \left\{\cos\theta - 4\sin^2\theta\cos\theta \pm \sqrt{3}\right.$$

$$\left.(\sin\theta + 4\sin\theta\cos^2\theta)\right\} \qquad (4.5.11)$$

Rib Stress (P in y direction)

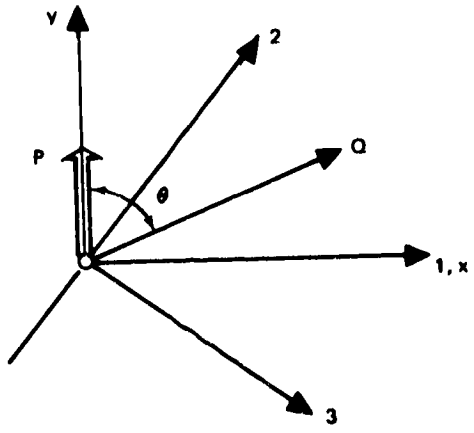

RIB STRESS (P IN y DIRECTION)

In this case exchange of x and y is eq. (4.5.4) to (4.5.6) gives

$$N_x = \frac{P}{6\pi}\frac{\cos\theta}{r}\ (1 - 4\sin^2\theta) \qquad (4.5.12)$$

$$N_y = \frac{P}{6\pi}\frac{\cos\theta}{r}\ (-5 + 4\sin^2\theta) \qquad (4.5.13)$$

$$N_{xy} = -\frac{P}{6\pi}\frac{\sin\theta}{r}\ (1 + 4\cos^2\theta) \qquad (4.5.14)$$

Note that θ is now measured from the y axis toward the x axis.

Eq. (2.4.12) now gives

$$\sigma_1 = \frac{4}{9}\frac{P\cos\theta}{\pi r t\,(1+\alpha)}\ (1 - 2\sin^2\theta) \qquad (4.5.14)$$

$$\sigma_{2,3} = \frac{P}{9\pi r t\,(1+\alpha)}\left\{-5\cos\theta + 4\sin^2\theta\cos\theta \mp \sqrt{3}\right.$$
$$\left.(\sin\theta + 4\sin\theta\cos^2\theta)\right\} \qquad (4.5.15)$$

Recommend Design Procedure

The maximum rib stresses will occur for the 1 ribs for loads in the x direction.

$$\sigma_{1\,max} = \frac{8}{9\pi}\frac{P}{rt\,(1+\alpha)} \qquad (4.5.16)$$

From eq. (4.5.9) the maximum skin stresses are,

$$\sigma_{x,y\,max} = \frac{5}{6\pi}\frac{P}{rt\,(1+\alpha)} \qquad (4.5.17)$$

As previously explained, the reinforcing of ribs and skin will be in such a manner that the reinforcing is rotationally symmetric with respect to the

loaded point. It is further recommended that the nominal value of α, say α_o, in the unreinforced region be maintained in the reinforced region.

Since

$$\frac{8}{9\pi} = 0.283$$

and

$$\alpha_o h = \frac{bd}{t} = \frac{A}{t}$$

where $A = bd$ = rib area,

then a conservative sizing of skin and ribs will be given by the equations,

$$t_{req} = 0.283 \frac{P}{F_{tu}\, r\, (1 + \alpha_o)} \qquad (4.5.18)$$

$$A_{req} = \alpha_o\, h\, t \qquad (4.5.19)$$

or

$$A_{req} = 0.283\, \alpha_o h \frac{P}{F_{tu}\, r\, (1 + \alpha_o)} \qquad (4.5.20)$$

Eq. (4.5.18) and (4.5.20) will satisfy dimensional requirements for loads in either x or y directions. Since t_{req} and A_{req} are inversely proportional to r, the reinforced regions and additional weights are very small. If the loads are applied as in Figure 4.5-1, where some curvature changes may

be expected, the increase in dimension may be "feathered out" over a larger region than that required by (4.5.18) and (4.5.20) to "spread" the load and reduce the curvature changes. If this is done the additional weight will still be small.

It may be necessary to check for local skin buckling or rib crippling using the equations:

$$\sigma \text{ (skin allowable)} = 10.2\ E \frac{t^2}{h^2} \qquad (4.5.21)$$

$$\sigma_i \text{ (rib allowable)} = 0.616\ E \frac{b^2}{d^2} \qquad (4.5.22)$$

4.5.3 Worked Example

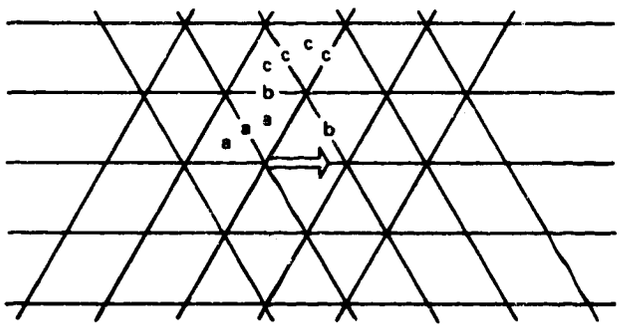

$P = 30\ k$

$\alpha_o = 0.31$

$h = 4.1$ in.

$F_{tu} = 61.0$ ksi

$\alpha_o h = 0.31\ (4.1) = 1.27 = \frac{A}{t}$

$$\frac{0.283\ P}{F_{tu}(1+\alpha_o)} = \frac{0.283\ (30)}{61.0\ (1.31)} = 0.116 \text{ in.}^2,$$

Rib	r	A
a	$\frac{h}{3} = 1.365$	0.0988
b	4.1	0.0329
c	$\frac{4}{3}h = 5.47$	0.0247

Skin	r	t
a	$\frac{h}{3} = 1.365$	0.0778
c	$\frac{4}{3}h = 5.47$	0.0194

On the actual design it will be necessary to check the final dimensions for skin buckling and rib crippling according to eq. (4.5.21) and (4.5.22).

4.6 IN-PLANE CONCENTRATED LOAD AT EDGE OF SHEET

4.6.1 Typical Design Situations

Typical design situations where this type of loading occurs are interstage attachments and local edge load due to engine thrust. Many connections are predominantly loadings of this type.

4.6.2 Method of Optimization

For the case of the concentrated in-plane load at the edge of an isogrid sheet in generalized plane stress, the solution, due to Flamant, is obtainable from Reference 2-2. It should be noted that eccentricity of load is not included.

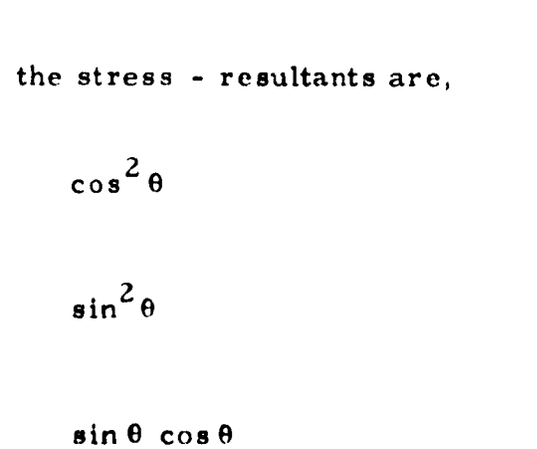

Let the point Q at which the stresses are to be computed, be a distance r from the origin, 0, and make an angle θ with the x axis. The concentrated load, P, is applied at the origin, 0, and is directed along the positive x axis.

From Reference 2-2, the stress - resultants are,

$$N_x = \frac{2P\cos\theta}{\pi r}\cos^2\theta \qquad (4.6.1)$$

$$N_y = \frac{2P\cos\theta}{\pi r}\sin^2\theta \qquad (4.6.2)$$

$$N_{xy} = \frac{2P\cos\theta}{\pi r}\sin\theta\cos\theta \qquad (4.6.3)$$

Although N_x, N_y and N_{xy} become infinite at $r = 0$, the stresses will not be evaluated closer than the reinforcing around the hole at the node. At this point all stresses are finite. The solution will be used to size ribs and skin around the attachment. Although the solution assumed constant thickness, it is probably a very good approximation for reinforced sheet provided that the reinforcing does not depend upon the angle θ, i.e., at each half circle, $r = r_i$, the reinforcing is constant around the half-circle.

Skin Stress

The skin stress is immediately obtainable from eq. (2.4.11).

$$\begin{Bmatrix} \sigma_x \\ \sigma_y \\ \tau_{xy} \end{Bmatrix} = \frac{2P\cos\theta}{\pi r t (1+\alpha)} \begin{Bmatrix} \cos^2\theta \\ \sin^2\theta \\ \sin\theta\cos\theta \end{Bmatrix} \qquad (4.6.4)$$

Rib Stress (1-Bars in x direction)

The rib stresses will depend upon whether the 1 bars are in the x direction or in the y direction.

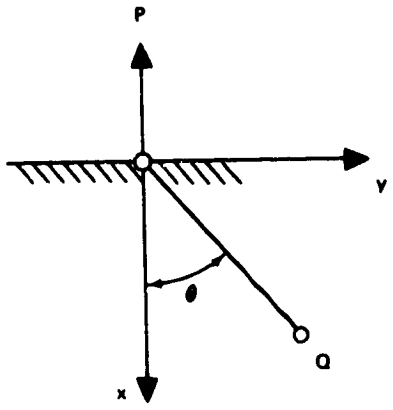

LOADING

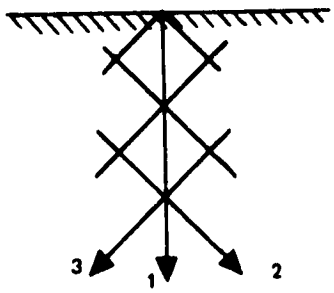

BAR ORIENTATION

From eq. (2.4.12),

$$\sigma_1 = \frac{2P\cos\theta}{3\pi r t (1+\alpha)} (4\cos^2\theta - 1) \qquad (4.6.5)$$

$$\sigma_{2,3} = \frac{4\,P \sin\theta \cos\theta}{3\pi r t\,(1+\alpha)} \left(\sin\theta \pm \sqrt{3}\cos\theta\right) \qquad (4.6.6)$$

Rib Stress (1 = Bars in y direction)

In this case the subscripts x and y in eq. (2.4.12) must be interchanged.

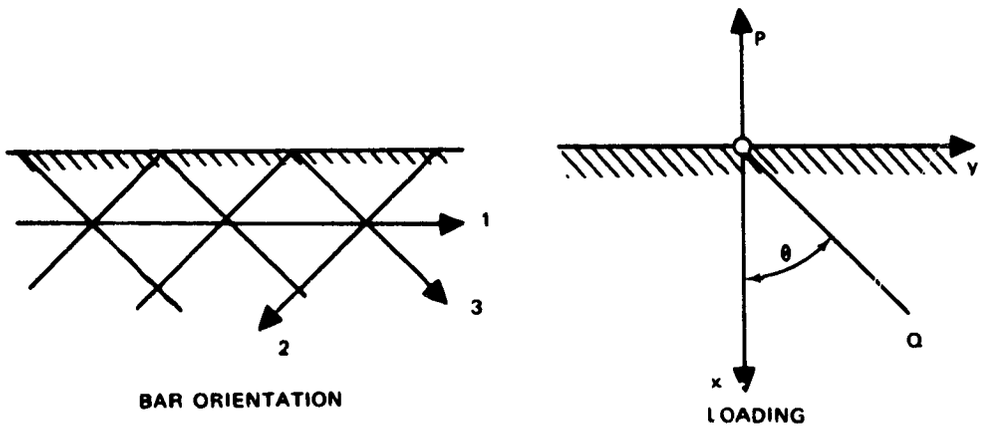

$$\sigma_1 = \frac{2\,P \cos\theta}{3\pi r t\,(1+\alpha)} \left(4\sin^2\theta - 1\right) \qquad (4.6.7)$$

$$\sigma_{2,3} = \frac{4\,P \sin\theta \cos\theta}{3\pi r t\,(1+\alpha)} \left(\cos\theta \pm \sqrt{3}\sin\theta\right) \qquad (4.6.8)$$

Recommended Reinforcement

The maximum value of the stresses computed from eq. (4.6.4) to (4.6.8) will not exceed the value, σ, from the eq.

$$\sigma = \frac{2P}{\pi r t\,(1+\alpha)} \qquad (4.6.8)$$

It is recommended that α be held constant at the nominal value, α_o

Then,

$$t_{req} = 0.637\,\frac{P}{F_{tu}\,r\,(1+\alpha_o)} \qquad (4.6.9)$$

and

$$\alpha = \frac{A}{th} = \alpha_o$$

where

$A = bd$ = rib area.

Thus

$$A_{req} = 0.637\, \alpha_o\, h\, \frac{P}{F_{tu}\, r\, (1 + \alpha_o)} \qquad (4.6.10)$$

If P is a compression load it will be necessary to check the ribs and skin for rib crippling and skin buckling using the equations,

$$\sigma_x \text{ (skin allowable)} = 10.2\, E \frac{t^2}{h^2} \qquad (4.6.11)$$

$$\sigma_{rib} \text{ (allowable)} = 0.616\, E \frac{b^2}{d^2} \qquad (4.6.12)$$

where σ_x is computed from eq. (4.6.4) and σ_{rib} is computed from the maximum value σ_i from eq. (4.6.5) and (4.6.6) or (4.6.7) and (4.6.8) dependent upon the rib orientation. Maximum rib stresses will lie in the load direction, x.

4.6.3 Worked Example

F_{tu} = 67.0 ksi 1 Bars parallel to edge.

h = 3.5 in.

α_o = 0.30

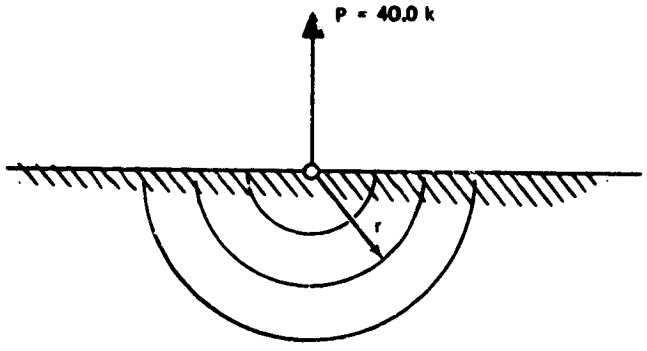

$$\alpha_o h = \frac{A}{t} = 0.30\ (3.5) = 1.05 \text{ in.}$$

From eq. (4.6.9) and (4.6.10)

$$\frac{0.637\ P}{F_{tu}\ (1 + \alpha_o)} = \frac{0.637\ (40.0)}{67.0\ (1.3)} = 0.293 \text{ in.}^2$$

No. Pockets	r	t	A = 1.05 t
1	3.5	0.0837	0.0880
2	7.0	0.0420	0.0440
3	10.5	0.0280	0.0293

4.7 CUTOUT REINFORCEMENT

4.7.1 Typical Design Situations

Cutouts are provided for access and are assumed to be hexagonal in shape to match the grid. It is assumed that the plate is uniaxially loaded.

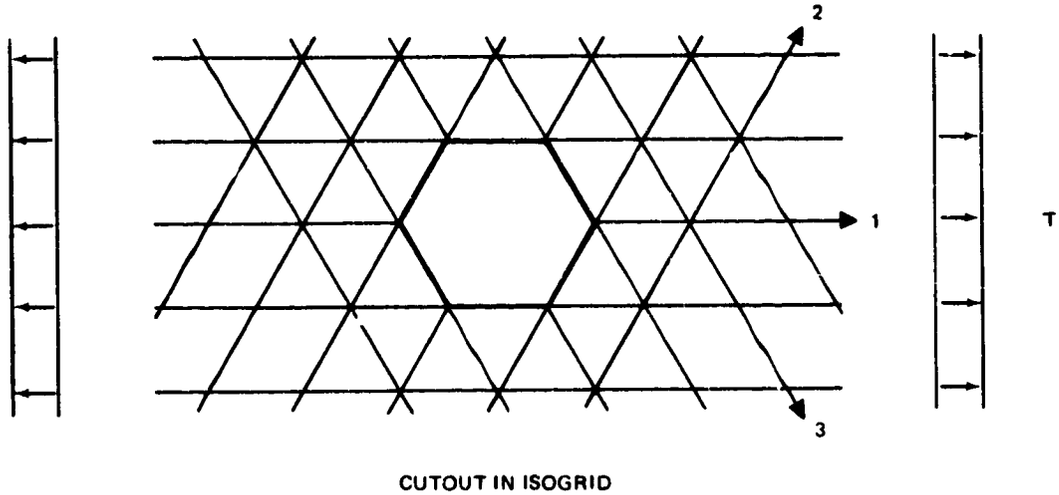

CUTOUT IN ISOGRID

Although the grid hole is hexagonal, the bar pattern around the hole will concentrate the forces at the bars and the stress concentrations at the nodes should be of the order of secondary stresses. The analysis used the solution of G. Kirsch for the stress around a circular hole in generalized plane stress, Reference 2-2.

It should be noted that the use of rectangular or square cutouts in isogrid is inefficient. Large doublers are required to redistribute the load around these cutouts when it is more effective to use the hexagonal rib pattern already provided by isogrid, stiffening these ribs if required. In additions, if circular holes are needed, the skin material should be removed to the rib, again making a hexagonal cutout, to prevent stress concentrations and possible tearing of the unsupported skin.

4.7.2 Method of Optimization

The Kirsch solution, in polar coordinates, is

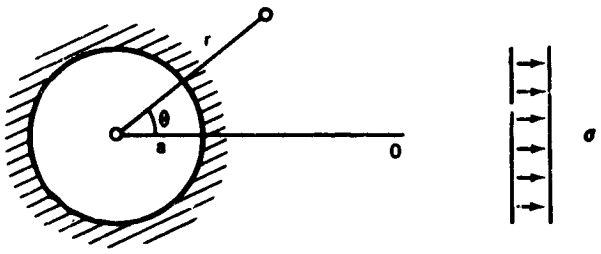

COORDINATES AND LOADING

$$\sigma_{rr} = \frac{\sigma}{2}\left(1 - \frac{a^2}{r^2}\right) + \frac{\sigma}{2}\left(1 - 4\frac{a^2}{r^2} + 3\frac{a^4}{r^4}\right)\cos 2\theta \qquad (4.7.1)$$

$$\sigma_{\theta\theta} = \frac{\sigma}{2}\left(1 + \frac{a^2}{r^2}\right) - \frac{\sigma}{2}\left(1 + 3\frac{a^4}{r^4}\right)\cos 2\theta \qquad (4.7.2)$$

$$\sigma_{r\theta} = -\frac{\sigma}{2}\left(1 + 2\frac{a^2}{r^2} - 3\frac{a^4}{r^4}\right)\sin 2\theta \qquad (4.7.3)$$

where σ is the nominal stress and a is the hole radius.

In order to apply the solution to isogrid, it will be necessary to express (4.7.1)-(4.7.3) in cartesian coordinates to obtain the bar stresses.

Consider the rotation of axes,

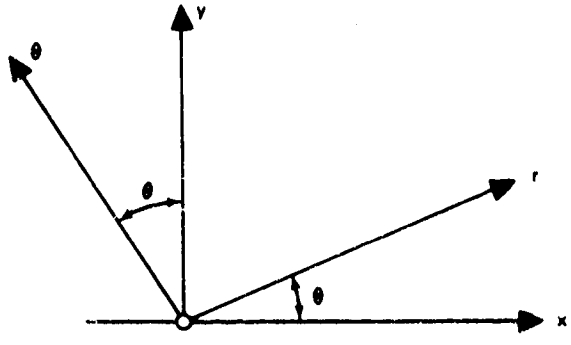

COORDINATE AXES

Define the direction cosines, a^i_j,

$$a^r_x = \cos\theta = c$$

$$a^r_y = \sin\theta = s$$

$$a^\theta_x = -\sin\theta = -s \qquad (4.7.4)$$

$$a^\theta_y = \cos\theta = c$$

The transformation equations are:

$$\sigma_{xx} = \sigma_{rr}\, a^r_x a^r_x + \sigma_{r\theta}\, a^r_x a^\theta_x + \sigma_{\theta r}\, a^\theta_x a^r_x + \sigma_{\theta\theta}\, a^\theta_x a^\theta_x$$

$$= \sigma_{rr}\, c^2 - 2\,\sigma_{r\theta}\, sc + \sigma_{\theta\theta}\, s^2 \qquad (4.7.5)$$

$$\sigma_{xy} = \sigma_{rr}\, a^r_x a^r_y + \sigma_{r\theta}\, a^r_x a^\theta_y + \sigma_{\theta r}\, a^\theta_x a^r_y + \sigma_{\theta\theta}\, a^\theta_x a^\theta_y$$

$$= (\sigma_{rr} - \sigma_{\theta\theta})\, sc + \sigma_{r\theta}\,(c^2 - s^2) \qquad (4.7.6)$$

$$\sigma_{yy} = \sigma_{rr}\, a^r_y a^r_y + \sigma_{r\theta}\, a^r_y a^\theta_y + \sigma_{\theta r}\, a^\theta_y a^r_y + \sigma_{\theta\theta}\, a^\theta_y a^\theta_y$$

$$= \sigma_{rr}\, s^2 + 2\,\sigma_{r\theta}\, sc + \sigma_{\theta\theta}\, c^2 \qquad (4.7.7)$$

Now define the quantity,

$$\boxed{\frac{a}{r} = \xi} \qquad (4.7.8)$$

The eq. (4.7.1)-(4.7.3) become,

$$\frac{2}{\sigma}\,\sigma_{rr} = (1 - \xi^2) + (1 - 4\xi^2 + 3\xi^4)\,(c^2 - s^2)$$

$$\frac{2}{\sigma}\,\sigma_{\theta\theta} = (1+\xi^2) - (1+3\xi^4)(c^2 - s^2)$$

$$\frac{2}{\sigma}\,\sigma_{r\theta} = -(1+2\xi^2-3\xi^4)(2sc)$$

Multiplying by the plate thickness and using (4.7.5)-(4.7.7) these become,

$$\frac{2}{T}\,N_x = 2+\xi^2(1-6c^2+16s^2c^2) + \xi^4(3-24s^2c^2) \qquad (4.7.9)$$

$$\frac{2}{T}\,N_{xy} = \xi^2 sc(6-16c^2) - 12\xi^4 sc(1-2c^2) \qquad (4.7.10)$$

$$\frac{2}{T}\,N_y = \xi^2(3-2c^2-16s^2c^2) + \xi^4(-3+24s^2c^2) \qquad (4.7.11)$$

where $(2/\sigma)\,\sigma_{xx} = (2/T)N_x$, etc., N_x is stress resultant around the hole while T is the nominal stress resultant.

Skin Stresses

The skin stresses are immediately obtainable from eq. (4.7.9) to (4.7.11) or from eq. (4.7.1) to (4.7.3) expressed in stress resultants by substituting into eq. (2.4.11), e.g.,

$$\sigma_x = \frac{N_x}{t(1+\alpha)}, \quad \sigma_y = \frac{N_y}{t(1+\alpha)}, \quad \tau_{xy} = \frac{N_{xy}}{t(1+\alpha)} \qquad (4.7.12)$$

Rib Stresses

The rib stresses for the 1 bars in the x direction are obtainable from eq. (2.4.12).

$$\sigma_1 = \frac{1}{3t(1+\alpha)}(3N_x - N_y)$$

$$\sigma_2 = \frac{2}{3t(1+\alpha)}(N_y + \sqrt{3}\,N_{xy})$$

$$\sigma_3 = \frac{2}{3\,t\,(1+\alpha)}\,(N_y - \sqrt{3}\,N_{xy}) \qquad (4.7.13)$$

If the 1 bars are in the y direction, exchange x and y in eq. (4.7.13).

Recommended Reinforcement

Solution (4.7.1) to (4.7.3) was obtained under the assumption of constant plate thickness using polar coordinates. One may expect this solution to give a good approximation to the reinforced plate provided that the reinforcement does not depend upon θ and that the variation in the r direction is not too rapid.

For this purpose, the reinforcement will be computed along the line where stresses are a maximum. This will be along the y axis, Reference 2-2. Along this line, s = 1 and c = 0.

Along the y axis (4.7.9) to (4.7.11) become,

$$\frac{2}{T}\,N_x = 2 + \xi^2 + 3\xi^4$$

$$\frac{2}{T}\,N_{xy} = 0 \text{ (Principal stress requirement)}$$

$$\frac{2}{T}\,N_y = 3\xi^2 - 3\xi^4 \qquad (4.7.14)$$

Skin Stress along y axis

$$\sigma_x = \frac{T}{2\,t\,(1+\alpha)}\,(2 + \xi^2 + 3\xi^4) \qquad (4.7.15)$$

$$\sigma_y = \frac{3T}{2\,t\,(1+\alpha)}\,(\xi^2 - \xi^4)$$

$$\tau_{xy} = 0$$

At the edge of the hole, $\xi = 1$ and

$$\sigma_x = \frac{3T}{t(1+\alpha)} \qquad (4.7.16)$$

$$\sigma_y = \tau_{xy} = 0 \text{ (Boundary condition)}$$

1 Rib Stress along y axis

From eq. (4.7.13) and (4.7.14)

$$\sigma_1 = \frac{T}{t(1+\alpha)}(1+2\xi^4) \qquad (4.7.17)$$

At the edge of the hole, $\xi = 1$ and

$$\sigma_1 = \frac{3T}{t(1+\alpha)} \qquad (4.7.18)$$

It is recommended that α be held constant at nominal value, α_o. The required skin thickness is thus,

$$t_{req} = \frac{T}{2F_{tu}(1+\alpha_o)}(2+\xi^2+3\xi^4) \qquad (4.7.19)$$

$$\alpha_o = \frac{A}{th}$$

when A = rib area = bd

$$A = \alpha_o th$$

or

$$A_{req} = \frac{\alpha_o \, h \, T}{2 \, F_{tu} \, (1 + \alpha_o)} \, (2 + \xi^2 + 3 \xi^4) \qquad (4.7.20)$$

Equations (4.7.19) and (4.7.20) can be simplified if one notes that:

$$t_o = \frac{T}{F_{tu} \, (1 + \alpha)}$$

then

$$t_{req} = t_o \, (1 + \tfrac{1}{2} \xi^2 + \tfrac{3}{2} \xi^4) \qquad (4.7.21)$$

and since

$$\frac{A_o}{t_o} = \frac{A}{t} = \alpha_o \, h$$

$$A_{req} = A_o \, (1 + \tfrac{1}{2} \xi^2 + \tfrac{3}{2} \xi^4) \qquad (4.7.22)$$

4.7.3 Worked Example

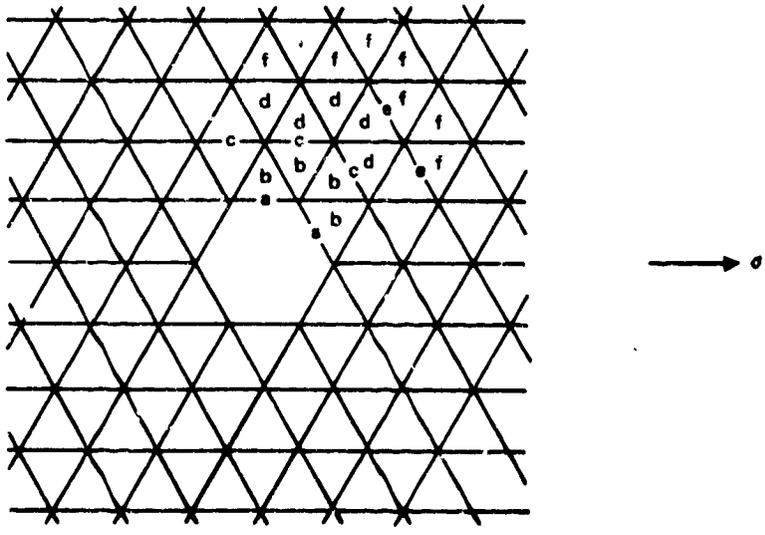

4.7.007

Let the a bars be the bars around the edge of the hole,
The c and e bars are parallel to the a bars.

The skin and the b bars are in the first set of triangles around the hole.

The skin and the d bars are in the second set of triangles around the hole.

The skin and the f bars are in the third set of triangles around the hole.

For the skin and skin-related bars, b, d, and f, the distance from the hole will be calculated at 1/3 of the triangle height.

Assume the hole radius equal to the triangle height and the load in the direction of the l bars.

The following ratios of A/A_o and t/t_o may be calculated from eq. (4.7.21) and (4.7.22).

Bar	ξ	A/A_o
a	1	3.0
b	3/4	1.745
c	1/2	1.219
d	3/7	1.142
e	1/3	1.075
f	3/10	1.046

Skin	ξ	t/t_o
b	3/4	1.745
d	3/7	1.142
f	3/10	1.046

4.8 OPEN ISOGRID SHEAR WEBS

The open isogrid construction consists of a gridwork of ribs alone. This may be desirable from the point of view of free flow of fluid or air or for access, routing of control lines, etc.

Unlike the 0- to 90-degree grid pattern, the isogrid pattern is structurally stable and possesses a remarkable degree of torsional rigidity.

The stress strain properties are immediately obtainable either by considering it as a sheet of solid material with Young's modulus, $\overline{E}$, given by

$$\overline{E} = E \frac{b}{h} \tag{4.8.1}$$

and Poisson's ratio, $\nu = 1/3$, or by considering the limiting cases in previous formula when $t \to 0$.

For example, for stress calculations,

$$\lim_{t \to 0} t(1 + \alpha) = \lim_{t \to 0} \left(t + \frac{bd}{h} \right) = \frac{bd}{h} \tag{4.8.2}$$

and for weight calculation,

$$\lim_{t \to 0} \overline{t} = \lim_{t \to 0} \left(t + 3 \frac{bd}{h} \right) = 3 \frac{bd}{h} \tag{4.8.3}$$

Eq. (4.8.2) may be used in eq. (2.4.12) to obtain the stresses in the ribs.

$$\sigma_1 = \frac{h}{3\,bd} (3N_x - N_y) \tag{4.8.4}$$

$$\sigma_{2,3} = \frac{2h}{3\,bd} (N_y \pm \sqrt{3}\, N_{xy}) \tag{4.8.5}$$

The twisting strength of isogrid plate may be calculated from eq. (4.8.1), (2.2.5) and (2.2.10).

$$D = \frac{\overline{E}d^3}{12(1 - \nu^2)} = \frac{3}{32}\frac{Ebd^3}{h} \qquad (4.8.6)$$

$$M_{xy} = \frac{1}{3} D (2\chi_{xy})$$

$$M_{xy} = \frac{1}{32}\frac{Ebd^3}{h} (2\chi_{xy}) \qquad (4.8.7)$$

The bending and extensional stiffness of open isogrid has been verified by test.

4.8.1 Typical Design Situations

This sort of design situation usually occurs for webs of beams, such as wing spars, girders, etc. In some cases, the entire panel, such as a wall, is required to carry the shearing forces. When solid members are used, it is frequently necessary to penetrate the shear web by holes which usually have to be reinforced around the edges to prevent edge crippling. Isogrid provides for great flexibility in hole location as well as considerable redundancy in case of damaged members. Because of its high twisting rigidity and strength, it can easily accommodate unanticipated wracking loads.

Open grid construction for shear webs would be useful for wing rib and spar webs when fuel containment is not a concern, for transport aircraft floor beams where cables, wires, and ventilation ducts are routed down the fuselage (Figure 4.8-1), and for beam systems distributing thrust from multiple engine clusters in large space boosters.

Apart from the general need for structural efficiency, these design situations require a structure which can be penetrated without excessive penalty as well as one with frequent opportunities for attachment of

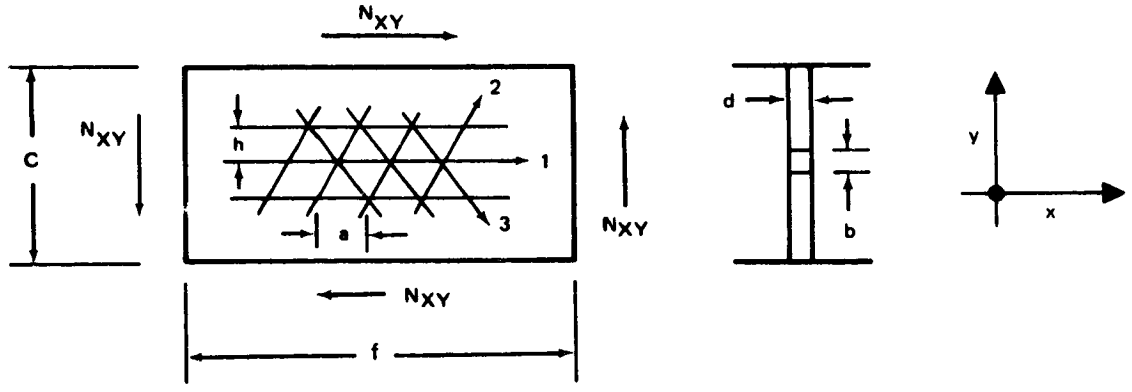

Figure 4.8-1. Shear Panel

support brackets or equipment components. Open construction is also desirable for free flow of ventilation or purge gases.

Support beams extending over long spans also tend to be laterally unstable, requiring several supports along the span to prevent rolling under load. This requirement can be minimized if the beam is a symmetrical section and torsionally stiff. Both of these characteristics are inherent in integrally machined open isogrid panels.

4.8.2 Methods of Optimization

The method of optimization assumes that general instability and in-plane Euler column buckling of the ribs are equally likely, see Figure 4.8-1. Under these assumptions the weight, plate thickness, d, and the ratio, $\beta = \frac{b}{a}$ = rib width/grid spacing, see Figure 4.8.1, are determined.

The magnitude of the rib width, b, and grid spacing, a, are determined to satisfy β and make the plate depth, c, and integral multiple of the triangle height, h, and so that d > b to prevent Euler column buckling of the ribs out of the plane of the plate.

Consider a rectangular plate of length f, width c and thickness d,

General Instability

From reference 2.9 for gross buckling of the plate, $N_{cr}(1)$,

$$N_{xy} = N_{cr}(1) = \frac{k_s \pi^2 \bar{E} d^3}{12(1-\nu^2) c^2} \qquad (4.8.8)$$

where k_s is the buckling coefficient of the plate which depends upon c/f and the plate boundary conditions.

Using the effective modulus E and Poisson's ratio from (4.8.1),

$$N_{cr}(1) = \frac{3\pi^2}{32} k_s \frac{Ebd^3}{c^2 h} \qquad (4.8.9)$$

$$= 1.10\, k_s \frac{Ebd^3}{ac^2}$$

since

$$h = \frac{\sqrt{3}}{2} a$$

Now define

$$\beta = \frac{b}{a} \qquad (4.8.10)$$

$$N_{cr}(1) = 1.10\, k_s \frac{E\beta d^3}{c^2} \qquad (4.8.11)$$

In-Plane Euler Column Buckling of Rib

From eq. (4.8.5)

$$\sigma_1 = 0$$

$$\sigma_{2,3} = \pm \frac{\pm 2h}{\sqrt{3}\, bd} N_{xy} = \frac{P_{2,3}}{bd} \qquad (4.8.12)$$

$$P_{2,3} = \pm a\, N_{xy}$$

P_3 will be critical for compression.

The Euler column load for P_3 is,

$$P_3 = -\frac{k_c \pi^2 EI}{a^2}$$

where k_c is the column fixity for in-plane buckling.

Thus,

$$\frac{k_c \pi^2 Edb^3}{12\, a^2} = 0.822 \frac{k_c Edb^3}{a^2} = a\, N_{xy}$$

or using (4.8.10),

$$N_{xy} = N_{cr}(2) = 0.822\, k_c Ed\beta^3 \qquad (4.8.13)$$

Equating (4.8.13) and (4.8.11),

$$1.10\, k_s \beta \frac{d^3}{c^2} = 0.822\, k_c\, d\beta^3$$

$$\frac{1.10\ k_s}{0.822\ k_c} = \beta^2 \frac{c^2}{d^2} = 1.34 \frac{k_s}{k_c}$$

i.e.,

$$\beta = \frac{d}{c}\sqrt{1.34 \frac{k_s}{k_c}} \qquad (4.8.14)$$

Substituting (4.8.14) into (4.8.11),

$$N_{xy} = 1.10\ k_s\ E \frac{d^4}{c^3}\sqrt{1.34 \frac{k_s}{k_c}}$$

$$\frac{N_{xy}}{Ec} = 1.272\left(\frac{d}{c}\right)^4 \frac{k_s^{3/2}}{k_c^{1/2}}$$

Solving for d,

$$\boxed{d = 0.943\left[\frac{N_{xy}}{Ec}\frac{k_c^{1/2}}{k_s^{3/2}}\right]^{1/4} c} \qquad (4.8.15)$$

Since c is given and d is determined by (4.8.15); β may be computed from d/c and eq. (4.8.14).

The equivalent weight thickness, $\bar{t}$, is determined using eq. (4.8.3) and β.

$$\bar{t} = 3\frac{bd}{h} = 2\sqrt{3}\frac{bd}{a}$$

$$\boxed{\bar{t} = 2\sqrt{3}\beta d} \qquad (4.8.16)$$

Since both β and d have been determined, $\bar{t}$ has been determined.

4.8.3 Worked Example

$N_{xy} = 8000$ lb/in $\qquad E = 10.5 \ (10^6)$ psi

$c = 20$ in

$d >> c$ and simple support boundary.

From Reference 2-4.

$$k_s = 5.35$$

Since eq. (4.8.4) and (4.8.5) show that the 1 bars are unloaded and the 2 bars have tensile loads equal to the compressive loads in the 3 bars, assume that the bar fixity, k_c is 2.0.

Thus

$$k_s^{3/2} = 12.40$$

$$k_c^{1/2} = 1.414$$

$$\frac{k_c^{1/2}}{k_s^{3/2}} = \frac{1.414}{12.40} = \frac{1}{8.77}$$

From eq. (4.8.15),

$$d = \frac{0.943}{1.72}\left(\frac{N_{xy}}{Ec}\right)^{1/4} c$$

$$\frac{d}{c} = 0.548\left[\frac{8000\ (10^{-6})}{10.5\ (20)}\right]^{1/4}$$

$$0 = 4.30\ (10^{-2})$$

$$d = 0.860 \text{ in.}$$

From eq. (4.8.14),

$$\beta = 4.30\ (10^{-2})\ \sqrt{1.34\left(\frac{5.35}{2.0}\right)}$$

$$= 0.0814 = \frac{b}{a}$$

From eq. (4.8.16)

$$\bar{t} = 3.47\ (0.0814)\ (0.860) = 0.243 \text{ in.}$$

As a check, from eq. (4.8.11),

$$N_{cr}(1) = 1.10\ (5.35)\ (10.5)\ (10^6)\ (0.0814)\left(\frac{0.860}{20^2}\right)$$

$$= 8000 \text{ lb/in}$$

From eq. (4.8.13),

$$N_{cr}(2) = 0.822\ (2)\ (10.5)\ (10^6)\ (0.860)\ (0.0814)^3$$

$$= 8000 \text{ lb/in.}$$

For the b/a dimensions, try 4 pockets.

$$4h = c = 20 \text{ in.},$$
$$h = 5.00 \text{ in.}$$

$$a = \frac{2}{\sqrt{3}}\ h = 5.77 \text{ in.}$$

$$b = \beta a = 0.0814\ (5.77)$$

$$b = 0.473 \text{ in.}$$

Since b/d = 0.473/0.860 = 0.551, this should be sufficient to prevent buckling of the bars out of the plane of the figure between the nodes.

For a weight comparison with monocoque construction, for a monocoque d_o,

$$N_{cr}(1) = 0.924\ k_1 \frac{E d_o^{\,3}}{c^2}$$

$$8000 = 0.924\ (5.35)\ \frac{10.5\ (10^6)\left(d_o^{\,3}\right)}{20^2}$$

$$= 12.98\ (10^4)\ d_o^{\,3}$$

$$d_o = \sqrt[3]{\frac{8\ (10^3)}{0.1298\ (10^6)}} = 0.395 \text{ in.}$$

The relative weights are,

$$\frac{\bar{t}}{t_o} = \frac{0.243}{0.395} = 0.616$$

The isogrid shear panel weighs approximately 61.6 percent of the weight of a solid sheet neglecting nodal weight.

In the case of a built-up tension field beam, the web gage is determined by the ultimate shear strength of the material corrected for loss of material (about 20 percent) caused by penetrations for attachment.

For a 7075-T6 web where

$$F_{su} = 46,000 \text{ psi}$$

$$t_w = \frac{N_{xy}}{F_{su}}\left(\frac{1}{0\,8}\right) = \frac{8000}{(46000)(0.8)} = 0.217$$

If the beam is efficiently designed, the ratio of stiffener weight to web weight is approximately 0.35.

Applying this correction,

$$\bar{t} = 1.35\ t_w = 0.293$$

For this case, then, the relative weights are,

$$\frac{\bar{t}}{t_o} = \frac{0.293}{0.395} = 0.742$$

Relative weights of the 3 shear web constructions are:

Shear Resistant	1.000
Tension Field	0.742
Open Isogrid	0.615

If the tension field design were to be evaluated without loss of material for attachment, that is, as an integrally stiffened structure, its weight would theoretically be only 0.593 times that of a shear resistant web. However, integral constructions need to be shear resistant because the interruption of tension field wrinkles at the stiffener produces undesirably high local stress concentrations, particularly risky when fatigue life is a consideration.

In any case, as mentioned previously, the continuous shear web designs suffer severe weight penalties when, as internal structure, they must inevitably be penetrated for useful service in a real-life vehicle.

4.9 OPEN ISOGRID CYLINDERS IN COMPRESSION, BENDING

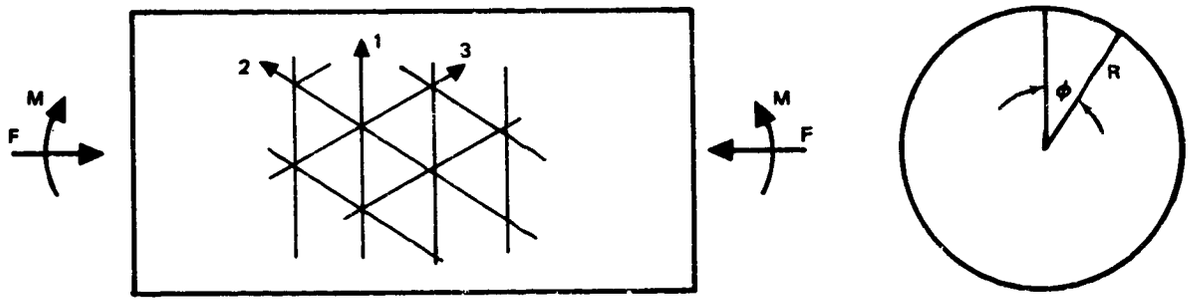

The open isogrid cylinder, consisting of a gridwork of ribs without skin, is loaded by a resultant force, F, and resultant moment, M, at the ends of the cylinder. The internal axial load/inch, N_x, is given by

$$N_x = \frac{F}{2\pi R} + \frac{M}{\pi R^2} \cos \phi$$

The maximum value of N_x occurs for $\phi = 0$ degree.

$$N_x \text{ (Max.)} = \frac{F}{2\pi R} + \frac{M}{\pi R^2}$$

The elastic properties of the gridwork are obtained by considering it as a sheet of solid material with Young's modulus, $\bar{E}$, and Poisson's ratio, ν, given by:

$$\bar{E} = E \frac{b}{h}$$

$$\nu = 1/3 \qquad (4.9.1)$$

For flanged isogrid, each flange and the web is treated as a layer whose individual modulus is given by (4.9.1) for each b.

The rib stresses are given by eq. (4.8.4) and (4.8.5).

For the 1 ribs in the x direction,

$$\sigma_1 = \frac{h}{A_o} N_x \text{ and } \sigma_{2,3} = 0 \qquad (4.9.2)$$

where A_o is the rib cross sectional area. A_o = bd for unflanged isogrid. For the 1 rib in the ϕ direction,

$$\sigma_1 = - \frac{h}{3A_o} N_x$$

$$\sigma_{2,3} = \frac{2h}{3A_o} N_x \qquad (4.9.3)$$

The preferred direction for the ribs is the 1 ribs in the ϕ direction.

4.9.1 Typical Design Situations

Typical uses for open isogrid cylinders would be for interstages and thrust structures where accessibility is important. Isogrid slosh baffles would be another good potential application. The open isogrid pattern will reduce the number of parts, complexity, and cost for such structures, compared to built-up design, as well as provide a regular pattern of attachment points for equipment. Refer to Section 5 for information on nodal geometry and to Section 7 for information on machining of isogrid, including the nodes.

4.9.2 Method of Optimization

The method of optimization assumes that minimum weight occurs when general instability and Euler column buckling of the ribs within the cylindrical profile are equally likely.

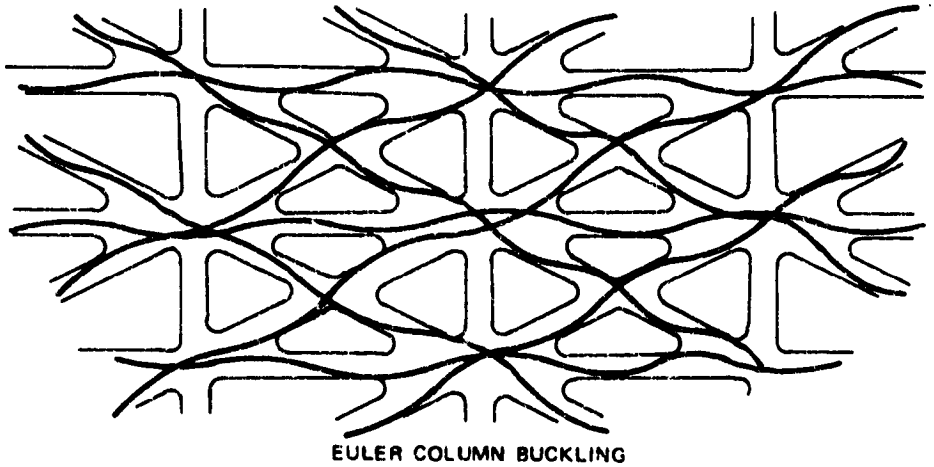

EULER COLUMN BUCKLING

Under these assumptions, equivalent weight thickness, $\bar{t}$, the plate thickness, d, and the ratio of rib width, grid spacing,

$$\beta = \frac{b}{a}$$

are determined. The magnitude of the rib width, b, and the grid spacing, a, are determined to satisfy β, make the triangle size an integral multiple of the circumference and make the rib depth, d > b, the rib width, so that local Euler column buckling of the ribs in the radial direction of the cylinder will not occur.

General Instability

In Reference 2-1 it is shown that general instability due to bending may be written in the form,

$$N_{cr}(1) = \frac{1}{\sqrt{3(1-\nu^2)}} \frac{E^* t^{*2}}{R} \qquad (4.9.4)$$

which is independent of the cylinder length.
For uniform compression, F, the cylinder is highly length dependent, see Figure 4.2-1.

Let

$$N_x = N_a + N_b$$

where

$$N_a = \frac{F}{2\pi R} \quad , \quad N_b = \frac{M}{\pi R^2} \quad ; N_b \geq \frac{1}{4} N_a$$

then it is shown in Reference 2-1 that the buckling strength of the cylinder is independent of the cylinder length and may be given by the simple formula,

$$N_x = N_a + N_b = N_{cr}(1) \qquad (4.9.5)$$

t^* and E^* from eq. (2.5.3) and (2.5.4) may be substituted into eq. (4.9.4).

$$N_{cr}(1) = \frac{2\gamma}{\sqrt{1-\nu^2}} \frac{E}{R}\sqrt{AI}$$

$$= 2.12 \frac{\gamma E}{R}\sqrt{AI} \qquad (4.9.6)$$

where γ is the "correlation factor". In eq. (4.9.6) A and I are the "transformed" area and moment of inertia.

If A_o and I_o are the actual rib area and moment of inertia, then since A and I are linearly proportional to the width,

$$A = \frac{A_o}{h} \quad , \quad I = \frac{I_o}{h}$$

giving,

$$N_{cr}(1) = \frac{2.12\gamma E}{Rh} \sqrt{A_o I_o} \qquad (4.9.7)$$

For Rectangular Stiffeners

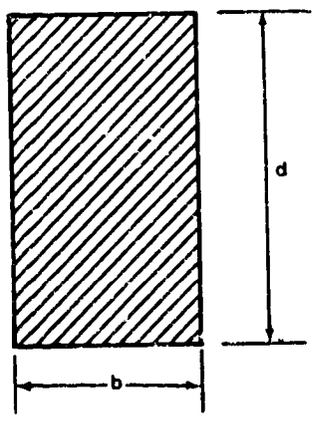

$A_o = bd$

$I_o = \frac{bd^3}{12}$

$$N_{cr}(1) = 0.612 \gamma E \frac{bd^2}{Rh} \qquad (4.9.8)$$

For All Material in Flanges

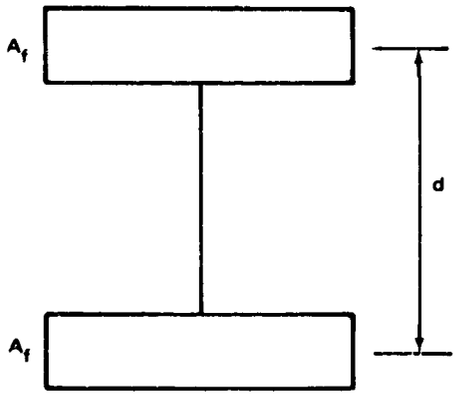

$$A_o = 2A_f$$

$$I_o = 2A_f\left(\frac{d}{2}\right)^2 = \frac{A_f d^2}{2}$$

$$A_o I_o = A_f^2 d^2$$

From (4.9.7),

$$N_{cr} = \frac{2.12\ \gamma E}{Rh} A_f d \qquad (4.9.8)$$

Only the Rectangular Stiffeners Will Be Optimized

From (4.9.8) for $\gamma = 0.65$ and $h = \frac{\sqrt{3}}{2}a$,

$$N_{cr}(1) = 0.460\ \frac{Ebd^2}{a}$$

Define the ratio,

$$\boxed{\beta = \frac{b}{a}}$$

then,

$$\boxed{N_{cr}(1) = 0.460\ \frac{E\beta d^2}{R}} \qquad (4.9.9)$$

Euler Column Buckling of Ribs

Assume the 1 ribs in the ϕ direction

From eq. (4.9.3)

$$\sigma = \frac{2h}{3bd} N_x = \frac{P}{bd}$$

$$P = \frac{2}{3} h N_x = \frac{a}{\sqrt{3}} N_x$$

By the Euler formula,

$$P = \frac{k_c \Pi^2 EI}{a^2} = k_c \Pi^2 \frac{Edb^3}{12a^2}$$

where k_c is the column fixity.

Thus

$$N_x = \frac{\sqrt{3}}{a} \frac{k_c \Pi^2 Edb^3}{12 a^2}$$

$$= 1.422 \frac{k_c E db^3}{a^3}$$

$$\boxed{N_{cr}(2) = 1.422 k_c E d \beta^3} \qquad (4.9.10)$$

Equating (4.9.9) for general instability and (4.9.10) for Euler column buckling,

$$0.460 \frac{d}{R} = 1.422 k_c \beta^2$$

$$\beta^2 = \frac{0.323}{k_c} \frac{d}{R} \qquad (4.9.11)$$

Equation (4.9.11) for β may now be substituted into eq. (4.9.9)

$$N_x^2 = \frac{0.212 (0.323)}{k_c} \frac{E^2 d^5}{R^3}$$

$$\left(\frac{N_x}{ER}\right)^2 = \frac{0.0683}{k_c} \left(\frac{d}{R}\right)^5$$

$$\frac{d}{R} = \left[14.62\ k_c \left(\frac{N_x}{ER} \right)^2 \right]^{1/5} \qquad (4.9.12)$$

After d has been found from eq. (4.9.12), d/R can be substituted into (4.9.11) and $\beta = b/a$ may be determined.

Since

$$\bar{t} = 3\,\frac{bd}{h} = 2\sqrt{3}\,\frac{bd}{a}$$

$$\bar{t} = 2\sqrt{3}\,\beta\,d \qquad (4.9.13)$$

So that the equivalent weight thickness, $\bar{t}$, has now been determined.

4.9.3 Worked Examples

Isogrid with flanges

Since this case is not optimized, it is assumed that Euler column buckling of the bars is not critical.

$N_x = 9{,}000$ lb/in

$E = 10.6\ (10^6)$ psi

$R = 198$ in.

$d = 2.00$ in.

$h = 10.00$ in.

$\gamma = 0.65$

From eq. (4.9.8)

$$N_{cr} = \frac{2.12\,(0.65)\,(10.6)}{198\,(10.00)}\,(2.00\,A_f)$$

$$9000 = 1.475\,(10^4)\,A_f$$

$$A_f = \frac{9.00}{14.75} = 0.610 \text{ in.}^2$$

The equivalent weight thickness, $\bar{t}$, is

$$\bar{t} = \frac{6A_f}{h} = \frac{6.0}{10.0}\,(0.610) = 0.366 \text{ in.}$$

For comparison with monocoque with the same γ, (actually $\gamma = 0.65$, Reference 2-11 is valid for stiffened cylinders only; for unstiffened cylinders, Reference 2-6, γ values are lower), using t_o for the monocoque thickness, from eq. (4.9.4).

$$N_{cr} = 0.612\,\frac{Et_o^2}{R}$$

$$9000 = \frac{0.612\,(10.6)\,10^6}{198}\,t_o^2 = 0.328\,(10^5)\,t_o^2$$

$$t_o^2 = \frac{9.00}{32.8} = 0.275$$

$$t_o = 0.524$$

The ratio of open isogrid/monocoque is,

$$\frac{\bar{t}}{t_o} = \frac{0.366}{0.524} = 0.698$$

Unflanged Isogrid (Optimized)

$N_x = 9,000$ lb/in.

$E = 10.6\ (10^6)$ psi

$R = 198$ in.

$\gamma = 0.65$

From eq. (4.9.12)

$$\frac{d}{R} = \left[14.62\ k_c \left(\frac{N_x}{ER}\right)^2 \right]^{1/5}$$

Assume $k_c = 2.00$

$$\left(\frac{N_x}{ER}\right)^2 = \left[\frac{9.0\ (10^3)}{10.6\ (10^6)\ (198)}\right]^2 = \left[4.28\ (10^{-6})\right]^2 = 18.35\ (10^{-12})$$

$$\left(\frac{d}{R}\right)^5 = 14.62\ (2)\ 18.35\ (10^{-12}) = 537\ (10^{-12}) = 5.37\ (10^{-10})$$

$$\frac{d}{R} = 1.400\ (10^{-2})$$

$$d = 1.400\ (198)\ 10^{-2} = 2.77 \text{ in.}$$

From eq. (4.9.11).

$$\beta^2 = \frac{0.323}{2.00}\ (1.4)\ 10^{-2} = 0.226\ (10^{-2})$$

$$\beta = 0.0475 = \frac{b}{a}$$

Since one should have $d > b$, it is evident that a value of $a < 40$ in. would be about right.

The circumference c, is,

$$c = 2\Pi R = 2\Pi (198) = 1243 \text{ in.}$$

Take 35 pockets around the circumference*

Then

$$a = \frac{1243}{35} = 35.5 \text{ in.}$$

and

$$b = \beta a = 0.0475 (35.5) = 1.690 \text{ in.} < 2.77 \text{ in.}$$

The equivalent weight thickness is,

$$\overline{t} = 3 \frac{bd}{h} = 2 \sqrt{3} \beta d$$

$$\overline{t} = 3.47 (0.0475) 2.77 = 0.456 \text{ in.}$$

The relative $\overline{t}$'s are now:

Construction	$\overline{t}$
Monocoque	0.524 in.
Unflanged Isogrid	0.456 in.
Flanged Isogrid	0.366 in.

*If the spacing a, is too large, it will be necessary to check for between frame buckling.

The unflanged isogrid example shows that the grid spacing of the flanged isogrid may be opened up considerably.

As a check on the unflanged example, substitute the derived dimension into eq. (4.9.9) and (4.9.10).

$$N_{cr}(1) = 0.460\,(10.6)\,(10^6)\,(0.0475)\,\frac{2.77^2}{198} = 9000 \text{ lb/in.}$$

$$N_{cr}(2) = 1.422\,(2.0)\,(10.6)\,(10^6)\,(2.77)\,(0.0475)^3$$

$$= 8950 \text{ lb/in.} \quad \text{(close enough)}$$

4.10 OPEN AND SKINNED ISOGRID PLATES

For stiffened plate supported or loaded locally with rectangular, circular, triangular, or irregular boundaries, the isogrid construction possesses some important structural advantages. Specifically, these are the high twisting rigidity of the construction which acts to distribute the loading over a wide region; its isotropic character so that no weak directions exist; and the uncoupling of the bending and in plane stress resultants, M and N. These latter two properties make it possible to immediately apply the many available solutions of classical plate theory, Reference 2-3.

4.10.1 Typical Design Situation

Some typical design situations would be doors, floors, walls, containers, etc., in short, all flat surfaces which are subjected to bending loads. If accessibility and free flow of fluids is required, the construction is unskinned. The construction may be integral for thin plates two inches or less in depth or it may be built up with an isogrid pattern web. Open face isogrid sandwich plates may be constructed with mechanically attached ribs since the web area is accessible. In such construction the reliability is high since all areas are open for fabrication and inspection.

From the constructional point of view, lightening holes drilled out at the centers of the grid points where the fillet material tends to build up, serve as natural attachment points for stud insert to secure equipment and transfer local loads to the plate.

4.10.2 Analyses

Skinned Isogrid

From eq. (2.2.4) and (2.2.5),

$$\begin{Bmatrix} M_x \\ M_y \end{Bmatrix} = -D \begin{bmatrix} 1 & \upsilon \\ \upsilon & 1 \end{bmatrix} \begin{bmatrix} \chi_x \\ \chi_y \end{bmatrix} \tag{4.10.1}$$

$$M_{xy} = \frac{1-\upsilon}{2} D (2\chi_{xy}) \tag{4.10.2}$$

Solving for the change of curvature,

$$\begin{Bmatrix} \chi_x \\ \chi_y \end{Bmatrix} = -\frac{1}{D(1-\upsilon^2)} \begin{bmatrix} 1 & -\upsilon \\ -\upsilon & 1 \end{bmatrix} \begin{Bmatrix} M_x \\ M_y \end{Bmatrix}$$

$$(2\chi_{xy}) = \frac{2}{D(1-\upsilon)} M_{xy}$$

Using eq. (2.2.3) these become,

$$\begin{Bmatrix} \epsilon_x \\ \epsilon_y \end{Bmatrix} = -Z \begin{Bmatrix} \chi_x \\ \chi_y \end{Bmatrix} = \frac{Z}{D(1-\nu^2)} \begin{bmatrix} 1 & -\upsilon \\ -\upsilon & 1 \end{bmatrix} \begin{Bmatrix} M_x \\ M_y \end{Bmatrix}$$

$$\gamma_{xy} = -Z(2\chi_{xy}) = -\frac{2Z}{D(1-\nu)} M_{xy}$$

Now define the section modulus, S, by,

$$ES = \frac{D(1-\nu^2)}{Z} \qquad (4.10.3)$$

then,

$$\begin{Bmatrix} \epsilon_x \\ \epsilon_y \end{Bmatrix} = \frac{1}{ES} \begin{bmatrix} 1 & -\nu \\ -\nu & 1 \end{bmatrix} \begin{Bmatrix} M_x \\ M_y \end{Bmatrix} \qquad (4.10.4)$$

$$\gamma_{xy} = -\frac{2(1+\nu)}{ES} M_{xy} \qquad (4.10.5)$$

Section Moduli

The maximum fiber stresses requires the distance, Z, from the neutral axis to the extreme fibers.

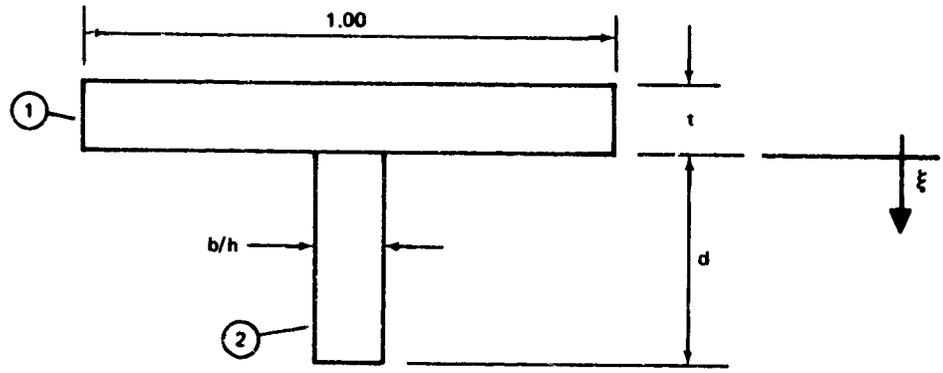

TRANSFORMED SECTION

Part	A_i	ξ_i	$A_i\xi_i$
(1)	t	$-t/2$	$-t^2/2$
(2)	$\frac{bd}{h}$	$d/2$	$bd^2/2h$

$$A = \Sigma A_i = t + \frac{bd}{h} = t\,(1+\alpha)$$

$$A\bar{\xi} = \Sigma A_i \xi_i = \frac{bd^2}{2h} - \frac{t^2}{2} = \frac{t}{2}\left(\frac{\alpha\delta - 1}{1+\alpha}\right) \qquad (4.10.6)$$

The neutral axis at a distance Z_o from $\xi = o$ is given by,

$$Z_o = \frac{\Sigma A_i \xi_i}{\Sigma A_i} = \frac{t}{2} \quad \frac{\alpha\delta - 1}{1+\alpha}$$

The fiber distance, c_1, of the skin from the neutral axis is,

$$c_1 = -(t + Z_o) = -\left(\frac{t}{2} \quad \frac{2\alpha + \alpha\delta + 1}{1+\alpha}\right) \qquad (4.10.7)$$

The section modulus, S_1, of the skin is given by (4.10.7), (4.10.3) and (2.3.5).

$$S_1 = -\frac{t^2}{6} \frac{\beta^2}{2\alpha + \alpha\delta + 1} \qquad (4.10.8)$$

The fiber distance, c_2, of the ribs from the neutral axis is,

$$c_2 = d - Z_o = \frac{t}{2} \quad \frac{2\delta + \alpha\delta + 1}{1 + \alpha} \tag{4.10.9}$$

The section modulus, S_2, of the ribs is given by (4.10.7), (4.10.3), and (2.3.5).

$$S_2 = \frac{t^2}{6} \quad \frac{\beta^2}{2\delta + \alpha\delta + 1} \tag{4.10.10}$$

Note that the first factor of (4.10.8) and (4.10.10) is the section modulus of the skin without ribs and the second factor is a nondimensional amplification factor due to the rib grid.

Thus for monocoque construction,

$$\beta \to 1 \ , \ \alpha \to 0 \ , \ \delta \to 0 \ \text{ and } S_1 = -S_2 = \frac{t^2}{6}$$

the familiar value.

Skin Stresses

From Hooke's law for the skin (2.4.6)

$$\begin{Bmatrix} \sigma_x \\ \\ \sigma_y \end{Bmatrix} = \frac{E}{1-\nu^2} \begin{bmatrix} 1 & \nu \\ \\ \nu & 1 \end{bmatrix} \begin{Bmatrix} \epsilon_x \\ \\ \epsilon_y \end{Bmatrix} \tag{4.10.11}$$

$$\tau_{xy} = \frac{E}{2(1+\nu)} \gamma_{xy} \tag{4.10.12}$$

Substituting (4.10.4) and (4.10.5) into this relation,

$$\begin{Bmatrix} \sigma_x \\ \\ \sigma_y \end{Bmatrix} = -\frac{1}{S_1} \begin{Bmatrix} M_x \\ \\ M_y \end{Bmatrix} \tag{4.10.13}$$

$$\tau_{xy} = -\frac{M_{xy}}{S_1} \tag{4.10.14}$$

Rib Stresses

Because of the uniaxial character of the ribs, the rib stresses are given by,

$$\sigma_i = E\, e_i$$

where e_i is obtained from (2.1.2)

$$\begin{Bmatrix} \sigma_1 \\ \sigma_2 \\ \sigma_3 \end{Bmatrix} = \frac{E}{4} \begin{bmatrix} 4 & 0 & 0 \\ 1 & \sqrt{3} & 3 \\ 1 & -\sqrt{3} & 3 \end{bmatrix} \begin{Bmatrix} \epsilon_x \\ \gamma_{xy} \\ \epsilon_y \end{Bmatrix} \tag{4.10.15}$$

From (4.10.4), (4.10.5)

$$\begin{Bmatrix} \epsilon_x \\ \gamma_{xy} \\ \epsilon_y \end{Bmatrix} = \frac{1}{ES} \begin{bmatrix} 1 & 0 & -\nu \\ 0 & 2(1+\nu) & 0 \\ -\nu & 0 & 1 \end{bmatrix} \begin{Bmatrix} M_x \\ M_{xy} \\ M_y \end{Bmatrix} \tag{4.10.16}$$

Substituting (4.10.16) into (4.10.15),

$$\begin{Bmatrix} \sigma_1 \\ \sigma_2 \\ \sigma_3 \end{Bmatrix} = \frac{1}{4S_2} \begin{bmatrix} 4 & 0 & -4\nu \\ (1-3\nu) & 2\sqrt{3}\,(1+\nu) & (3-\nu) \\ (1-3\nu) & -2\sqrt{3}\,(1+\nu) & (3-\nu) \end{bmatrix} \begin{Bmatrix} M_x \\ M_{xy} \\ M_y \end{Bmatrix}$$

and since $\nu = 1/3$,

$$\begin{Bmatrix} \sigma_1 \\ \sigma_2 \\ \sigma_3 \end{Bmatrix} = \frac{1}{S_2} \begin{bmatrix} 1 & 0 & -\frac{1}{3} \\ 0 & \frac{2}{3}\sqrt{3} & \frac{2}{3} \\ 0 & -\frac{2}{3}\sqrt{3} & \frac{2}{3} \end{bmatrix} \begin{Bmatrix} M_x \\ M_{xy} \\ M_y \end{Bmatrix} \qquad (4.10.17)$$

Section Modulus Graph

To facilitate the calculation, the section moduli are written in the form,

$$S_1 = -\frac{t^2}{6} k_1 \qquad (4.10.18)$$

$$k_1 = \frac{\beta^2}{2\alpha + \alpha\delta + 1} \qquad (4.10.19)$$

$$S_2 = \frac{t^2}{6} k_2 \qquad (4.10.20)$$

$$k_2 = \frac{\beta^2}{2\delta + \alpha\delta + 1} \qquad (4.10.21)$$

where $t^2/6$ is the section modulus of the skin alone and

$$k_1 = k_1(\alpha, \delta)$$

$$k_2 = k_2(\alpha, \delta)$$

are the rib amplification factors in non-dimensional form which are given by the graphs in Figures 4.10-1 and 4.10-2.

When $\alpha \to 0$ but δ = constant $\neq 0$, the ribs have constant depth but the rib width becomes very small.

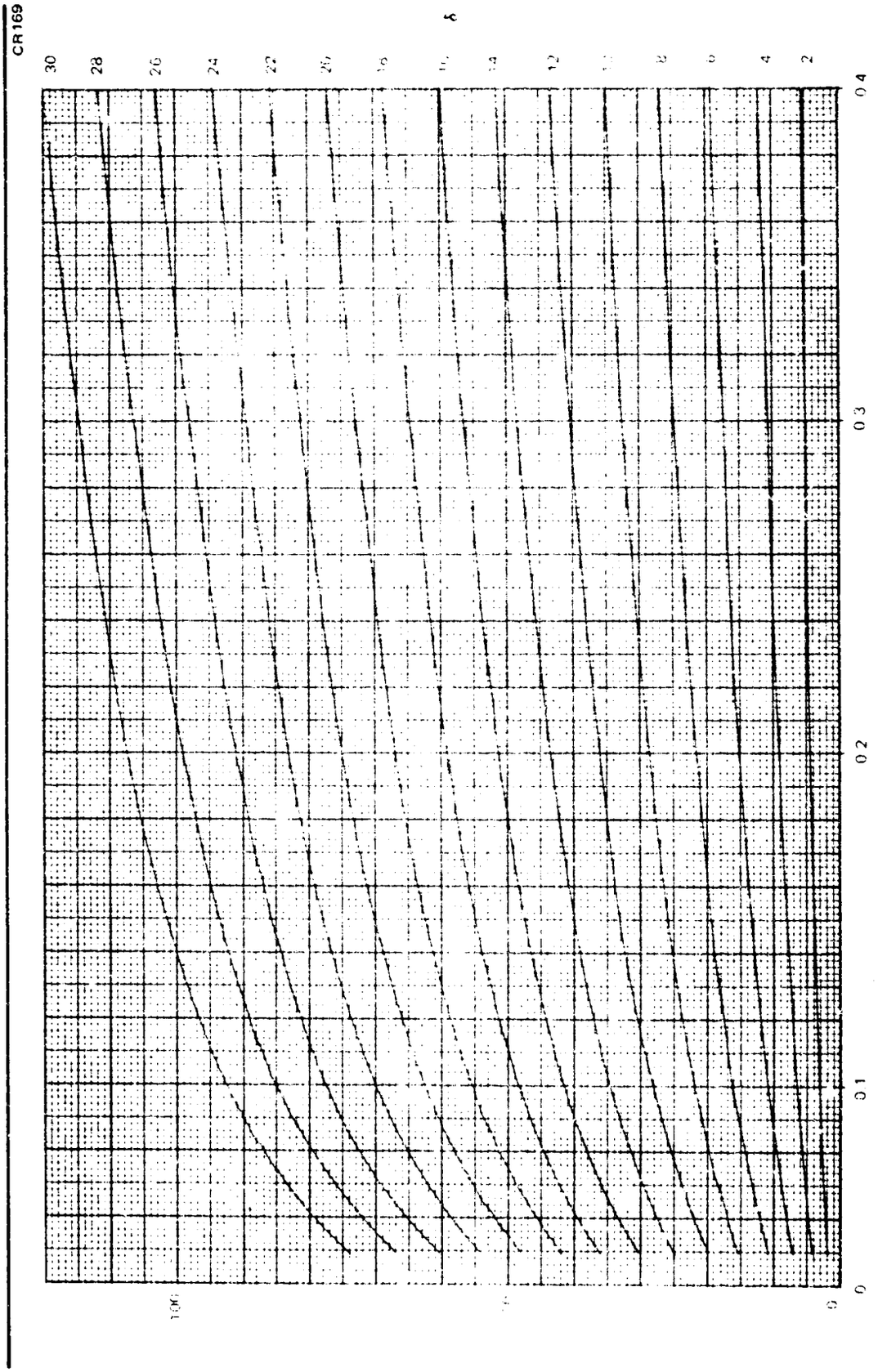

Figure 4.10-1 K_1, α, δ Curves

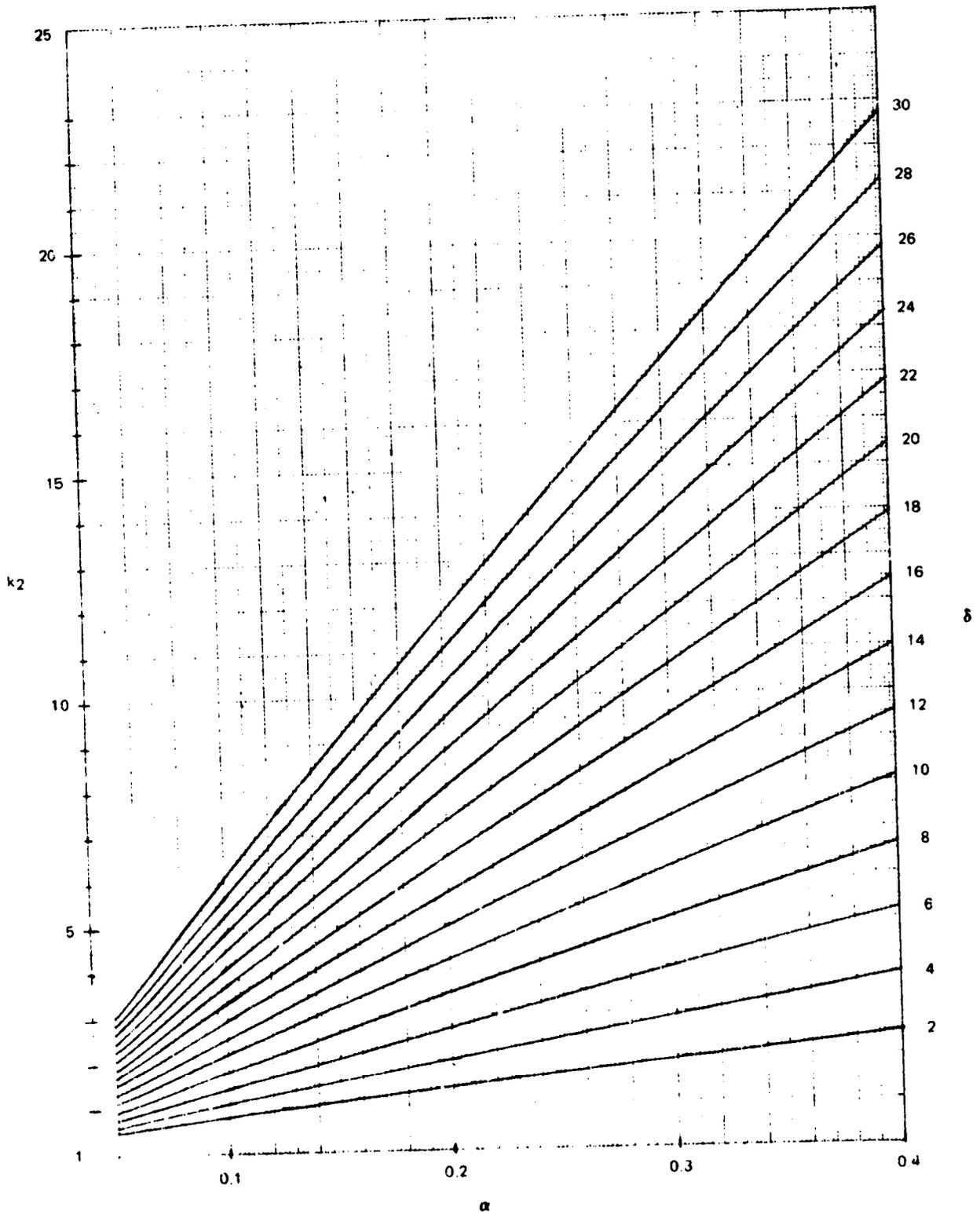

Figure 4.10-2. k_2, α, δ Curves

In such cases, stresses at the outstanding edge of a very thin deep rib attached to the skin actually weaken the structure, stresswise. These pathological cases on the graph occur in the domain where $k < 1.00$ and should be avoided for stress critical structure.

Open Isogrid

In this case, the skin eq. (4.10.13) and (4.10.14) drop out. The rib equations are now given by (4.10.17) where S_2 is given by (4.10.10) from the limiting case,

$$\bar{S}_2 = \lim_{t \to 0} S_2$$

From eq. (4.10.10) and (2.3.2),

$$S_2 = \frac{1}{6} \frac{\left[3 \frac{bd}{h} (t \cdot d)\, t^2 + (t + \frac{bd}{h}) (t^3 + \frac{bd}{h} d^2) \right]}{2\, dt + \frac{bd^2}{h} + t^2}$$

$$\boxed{\bar{S}_2 = \lim_{t \to 0} S_2 = \frac{1}{6} \frac{bd^2}{h}} \qquad (4.10.22)$$

and

$$\bar{S}_1 = -\bar{S}_2 \qquad (4.10.23)$$

4.10.3 Worked Examples

Skinned isogrid

Simply supported

Circular plate

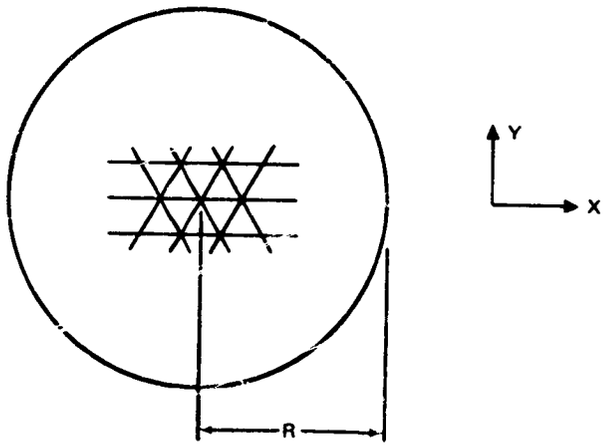

$R = 36$ in.

$q = 3$ psi

$F_{tu} = 60$ ksi

$E = 10.7\ (10^6)$ psi

From Reference 2-3, the maximum stresses at the center of the plate are,

$$M_x = M_y = \frac{3 + \nu}{16} qR^2$$

$$= \frac{3.333}{16} (3)\ 36^2$$

$$= 808 \text{ lb in}$$

Assume $\delta = 10$, $\alpha = 0.20$

From the k_1, k_2 graphs,

$$k_1 = 28.8$$

$$k_2 = 4.25$$

$$S_1 = -\frac{t^2}{6} k_1 = -\frac{28.8}{6} t^2 = -4.81\ t^2$$

$$S_2 = \frac{t^2}{6} k_2 = \frac{4.25}{6} t^2 = 0.710\ t^2$$

Assume ribs on tension side. Then, from eq. (4.10.17)

$$\sigma_1 = \sigma_2 = \sigma_3 = \frac{2}{3} \frac{808}{0.710 t^2} = 60\ 000$$

$$t^2 = \frac{2\ (808)}{3\ (0.710)\ 60\ 000} = 1.267\ (10^{-2})$$

$$t = 0.113 \text{ in}$$

$$d = \delta t = 10\,(0.113) = 1.13 \text{ in.}$$

$$\alpha = \frac{bd}{th} = \delta \frac{b}{h}$$

$$h = \frac{\delta}{\alpha} b = \frac{10}{0.20} b = 50b$$

Let

$$b = \frac{d}{10} \text{ say. Then}$$

$$b = 0.113 \text{ in.}$$

$$h = 50\,(0.113) = 5.65 \text{ in.}$$

The grid size, a, is given by,

$$a = \frac{h}{0.866} = \frac{5.65}{0.866} = 6.53 \text{ in}$$

As a check on the skin stresses, from (4.10.13)

$$\sigma_x = \sigma_y = -\frac{808}{4.81\,(0.113)^2} = -13,150 \text{ psi.}$$

The allowable skin buckling stress, Reference 2 9, is

$$\sigma_{cr} = \frac{12.0\,\pi^2 E}{12(1-\nu^2)} \left(\frac{t}{a}\right)^2 = 11.10E \left(\frac{t}{a}\right)^2$$

$$\sigma_{cr} = 11.10\,(10.7)\,(10^6) \left(\frac{0.113}{6.53}\right)^2$$

$$= 35,000 \text{ psi} > 13,500$$

The equivalent weight thickness, $\bar{t}$, is.

$$\bar{t} = t\,(1 + 3\alpha)$$

$$= 0.113\,(1.60) = 0.181 \text{ in.}$$

4.11 MINIMUM OVERALL WEIGHT FOR CYLINDER SUBJECTED TO AXIAL COMPRESSION AND BENDING

In general, the envelope of maximum N_{cr} and p_{burst} as well will vary along the length of the cylinder. Although b, d and t may be varied to reflect the variation of load, the grid triangle height, h, must usually be held constant, for fabrication reasons and the problem becomes that of minimizing the weight for h held constant along the length of the tank. To accomplish this, select N_{cr} (i) at i points along the tank axis where N_{cr} is changing most rapidly and determine the associated distance, Δ_i at mid-stations between the point.

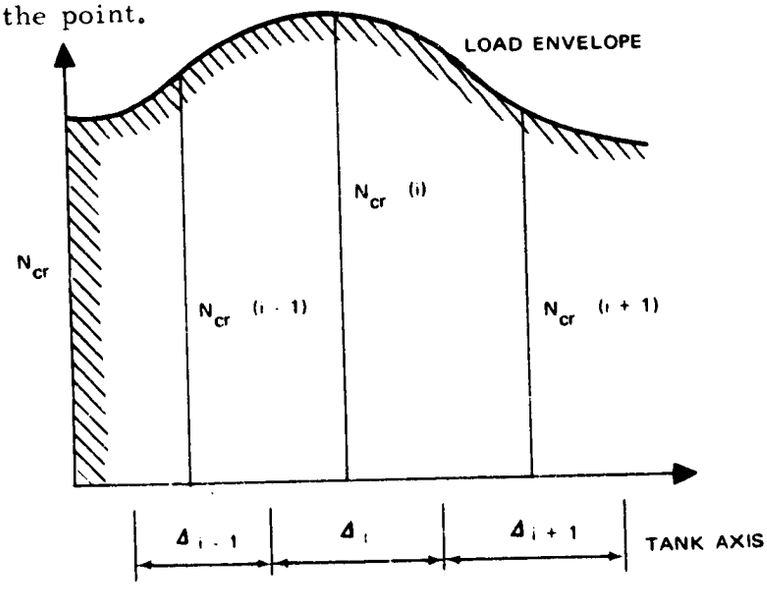

LOAD ENVELOPE

Next construct a set of graphs of $\bar{t}$ vs h as functions of p for each station, i, for the given value of N_{cr} (i).

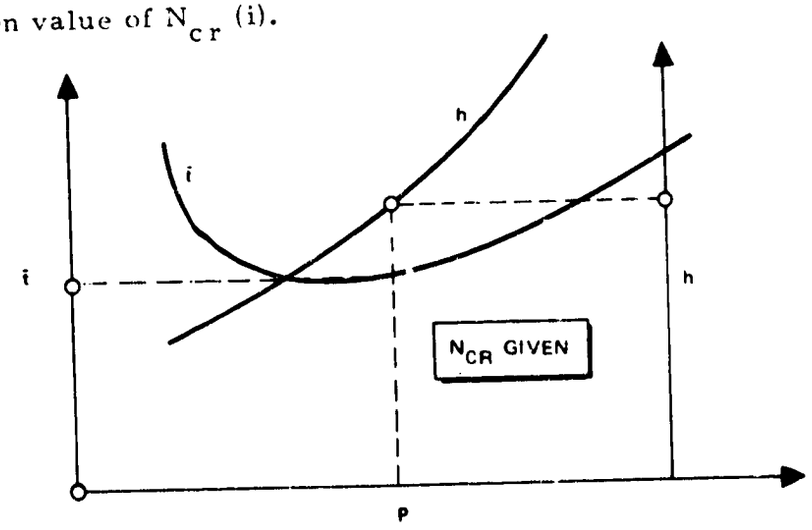

$\bar{t}$/h GRAPH

From the set of $\bar{t}$, h graphs for the i^{th} station along the tank axis, the relative tank weight may be determined for various value of h.

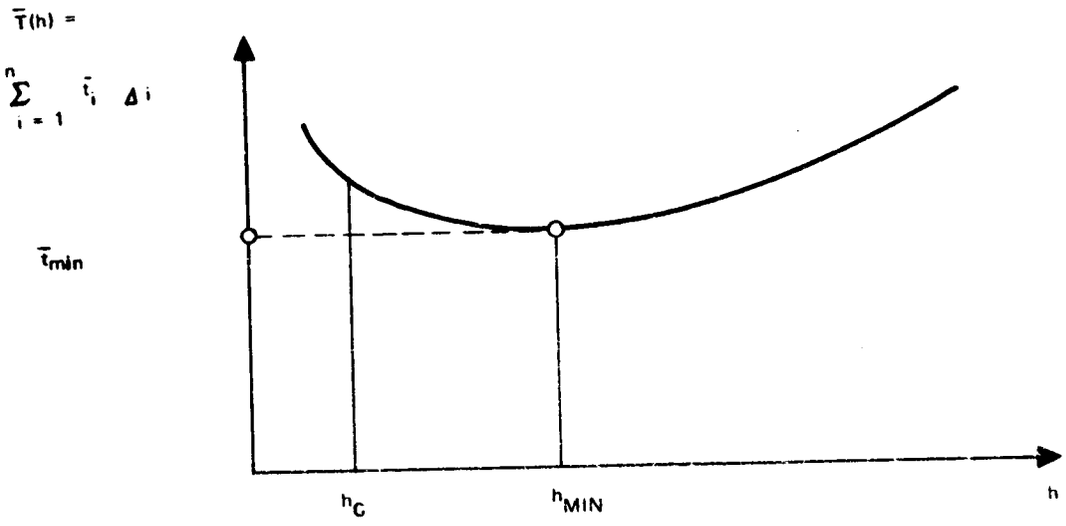

$\bar{T}$ (h) GRAPH

The initial value of h, called h_o, must be selected as the smallest value of h which satisfied all the burst conditions at the n stations along the tank axis. Since the graph of $\bar{t}$ in the neighborhood of t_o (the value for minimum weight at each station) is quite flat, considerable variation in h may be allowed with only minor changes in $\bar{t}$ so that the requirement that h remain constant over the entire tank does not impose a significant weight penalty on the design.

4.12 NOTE ON USE OF x, y; α, δ CURVES

Although the α, δ curves are fairly easy to interpolate along the δ direction, by eye, since the variation is approximately linear, it is not easy to interpolate by eye along the α direction. This is because the variation is approximately exponential.

It will be found that distance in the α direction along the curves $\delta = 2$ or $\delta = 30$ at the extreme edges of the graph are practically identical. Moreover, these scales almost coincide with the portion of the x scales at the bottom of the graph between the values $x = 0.50$ and $x = 3.0$.

A procedure which will be found to be most convenient is as follows:

A. Locate the α, δ point by pencil and then move up a small piece of paper so that its edge is aligned along the δ curve direction.

B. Mark the edge of the paper at the α, δ point and also mark the grid values of α to the left and right of the point.

C. The edge of the paper may now be transferred to the x scale with the grid values superimposed upon the x scale values. The intermediate α may now be readily interpolated on the x scales.

If the above procedure is not followed, checked calculated values of α from computed bd/th will rarely agree with initial graph values since the graph cannot otherwise be read with sufficient precision.

4.13 OFF-OPTIMUM ISOGRID

For many applications, constraints due to plate thickness availability, cost of machining etc., require that the gridwork design be other than that indicated by the optimum. Usually it is required that the plate thickness be less than the optimum thickness and that the gridwork triangle size be larger than the optimum. These are the basic assumptions underlying the following off-optimum analysis.

4.13.1 Method of Analysis

When the total plate thickness is less than the optimum and the grid triangle size is greater than the optimum, it follows that the rib dimensions will be thicker than optimum and consequently not critical for rib crippling.

The critical requirements are general instability and skin buckling.

General Instability

The critical loading conditions assumed are either the spherical cap under external pressure or the circular cylinder under combined axial compression and bending. (Reference Subsections 4.1 and 4.2.) Thus,

$$N_{cr}(1) = C_o \frac{E t^2}{R} \beta \qquad (4.13.1)$$

where

$$N_{cr}(1a) = \frac{P_{cr} R}{2}$$

$$C_o = 0.260 \qquad (4.13.2)$$

for the spherical cap.

$$N_{cr}(1b) = N_x = \frac{F}{2\pi R} + \frac{M}{\pi R^2}$$

$$C_o = 0.397 \qquad (4.13.3)$$

for the circular cylinder.

Skin Buckling

For skin buckling,

$$N_{cr}(2a) = C_1 \, Et(1+\alpha) \frac{t^2}{h^2}$$

$$C_1 = 3.47 \qquad (4.13.4)$$

for the spherical cap, and,

$$C_1 = 10.2 \qquad (4.13.5)$$

for the circular cylinder.

Collecting requirements,

$$N_{cr}(1) = C_o \frac{E\,t^2}{R} \beta \qquad (4.13.6)$$

$$N_{cr}(2) = C_1 \, Et(1+\alpha) \frac{t^2}{h^2} \qquad (4.13.7)$$

Given: $S = t+d \leq S_o$ (4.13.8)

Given: $h \geq h_o$ (4.13.9)

Equations (4.13.6) to (4.13.9) consist of four equations for the four required geometric dimensions, b, d, t and h. Of these, h is already given. The remaining three dimensions are determined as follows:

From (4.13.8)

$$S = t+d = t(1+\delta)$$

$$t = \frac{S}{1+\delta} \qquad (4.13.10)$$

Substituting (4.13.10) into (4.13.6),

$$N_{cr} = C_o \frac{E}{R} \frac{s^2 \beta}{(1+\delta)} 2$$

$$\frac{N_{cr} R}{C_o E s^2} = \frac{\beta}{(1+\delta)} 2 \qquad (4.13.11)$$

From (4.13.10) and (4.13.7),

$$N_{cr} = C_1 E (1+\alpha) \frac{s^3}{h^2 (1+\delta)^3} \qquad (4.13.12)$$

$$\frac{N_{cr} h^2}{C_1 E s^3} = \frac{1+\alpha}{(1+\delta)^3}$$

Define,

$$x = \frac{N_{cr} h^2}{C_1 E s^3} \qquad (4.13.13)$$

$$y = \frac{N_{cr} R}{C_o E s^2} \qquad (4.13.14)$$

then

$$x = \frac{1+\alpha}{(1+\delta)^3} \qquad (4.13.15)$$

$$y = \frac{\beta}{(1+\delta)^2} \qquad (4.13.16)$$

This defines a mapping of the α, δ domain into the x, y domain and is given in Figure 4.13-1 on a log plot. This mapping, it may be noted, is purely geometric and does not depend upon the values used for C_o and C_1.

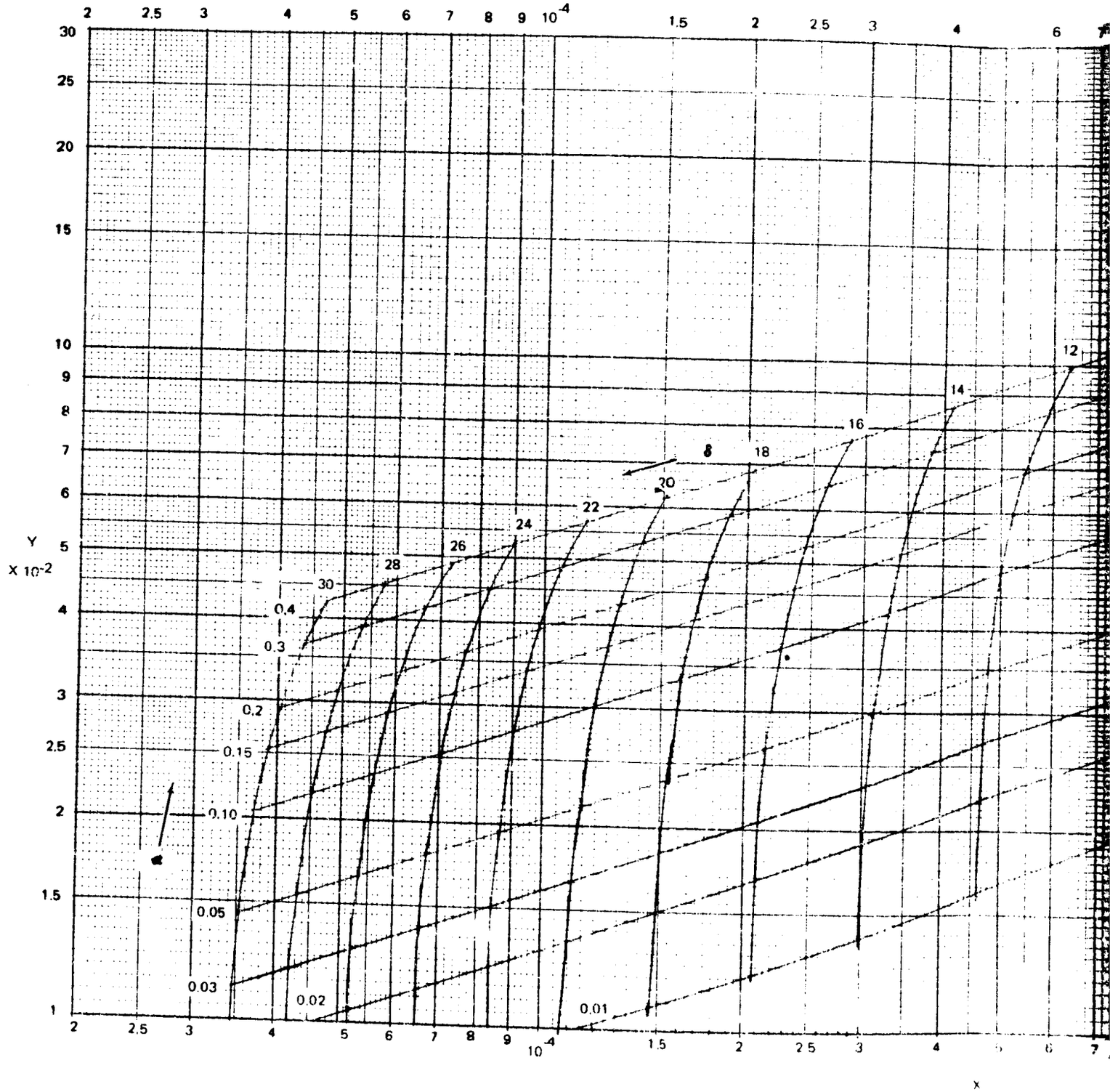

FOLDOUT FRAME

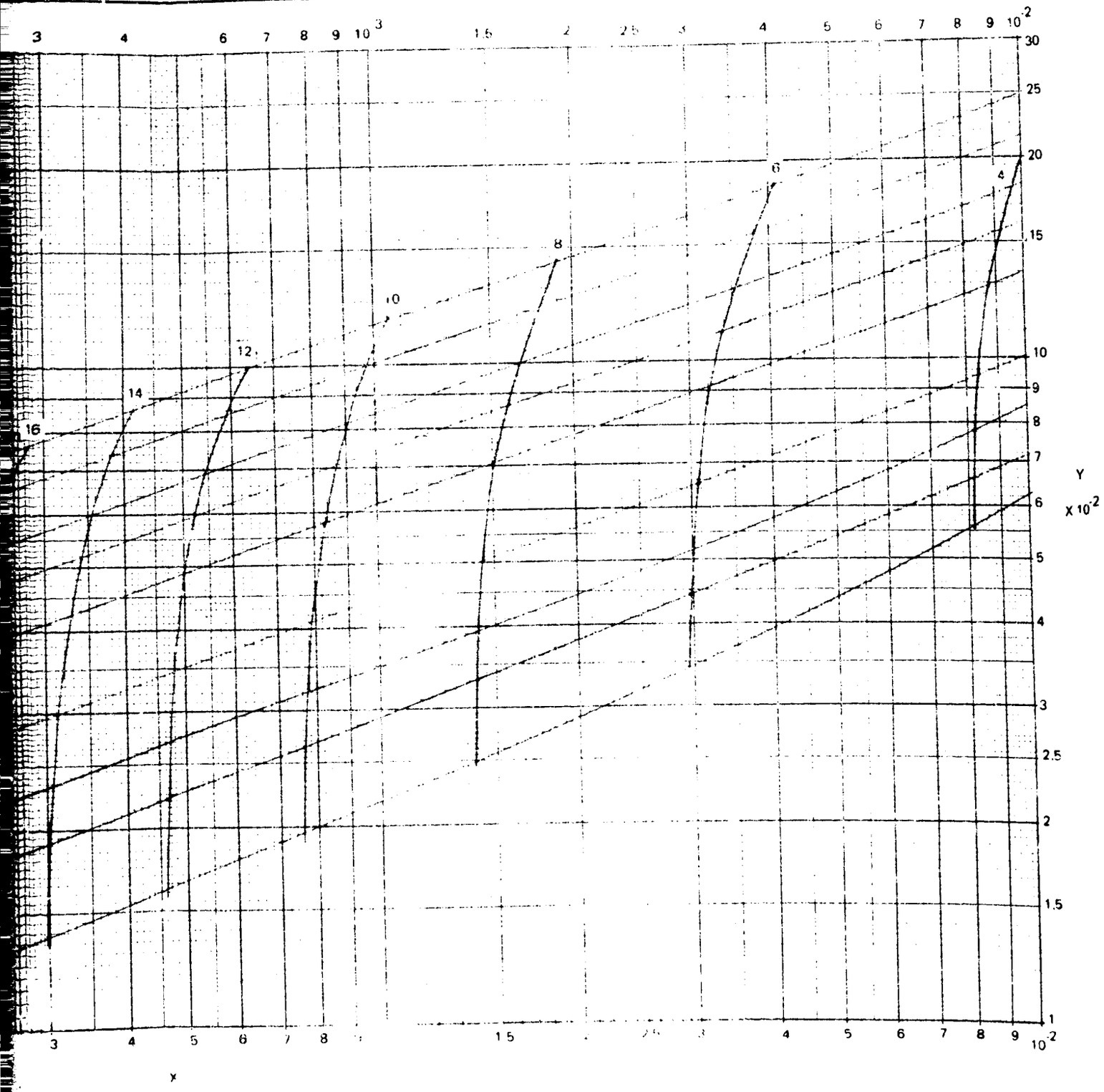

NORMAL PRE
SPHERICAL C

C_0 = 0.26

C_1 = 3.47

C_2 = 0.63

$S = d + t \leq S$

$h \geq h$ OPTIMU

$X = \frac{N}{C_1}$

$Y = \frac{N}{C_0}$

$t = \frac{}{1}$

$d = \delta$

$b = \alpha$

AS A CHEC

N_{cr}

FOLDOUT FRAME

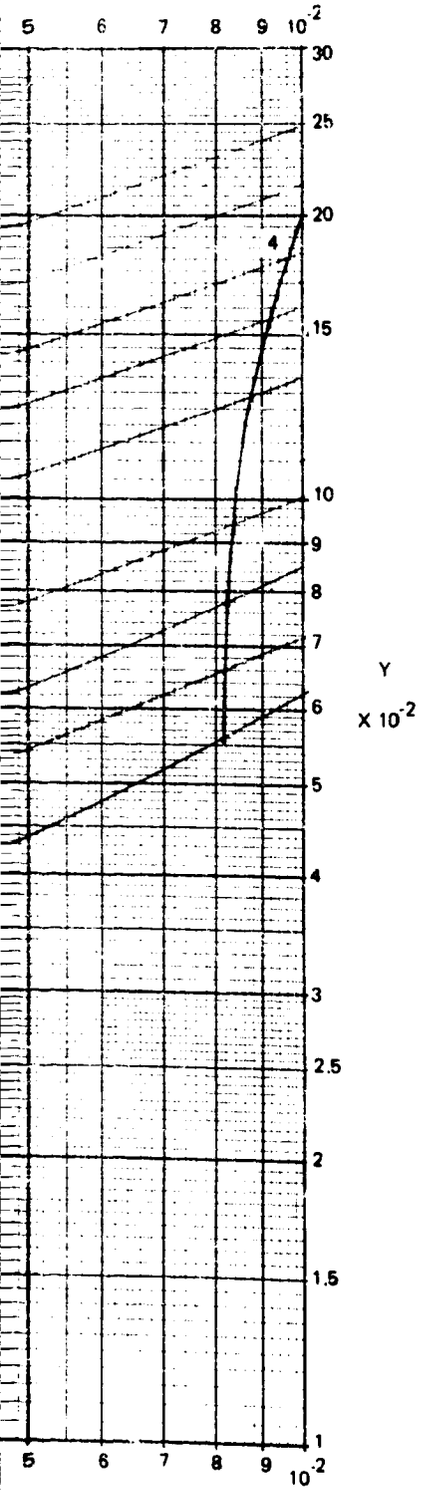

SUMMARY OF OFF-OPTIMUM EQUATIONS

NORMAL PRESSURE ON SPHERICAL CAP	CYLINDER UNDER AXIAL COMPRESSION AND BENDING	REFERENCE
$C_0 = 0.260$	0.397	p. 4.13.001
$C_1 = 3.47$	10.2	p. 4.13.002
$C_2 = 0.634$	0.616	P. 4.13.006
$S = d + t \leq S_{OPTIMUM}$		
$h \geq h_{OPTIMUM}$		
$X = \frac{N_{cr} h^2}{C_1 E S^3}$		Eq. 4.13.13
$Y = \frac{N_{cr} R}{C_0 E S^2}$		Eq. 4.13.14
$t = \frac{S}{1 + \delta}$		Eq. 4.13.10
$d = \delta t$		p. 4.13.005
$b = \alpha \frac{th}{d}$		p. 4.13.005

AS A CHECK,

$$N_{cr}\ (\text{RIB CRIPPLING}) = C_2 E t (1 + \alpha) \left(\frac{b}{d}\right)^2 \geq N_{cr}$$

Figure 4.13-1. X, Y, α, δ Curves

FOLDOUT FRAME

2

The design procedure is as follows:

A. Calculate x and y from eq. (4.13.13) and (4.13.14).

B. Read off α and δ from the α, δ graph. (Logarithmic interpolation is required here.)

C. Calculate t from equation (4.13.10) $t = \frac{s}{1+\delta}$

D. Calculate d from $d = \delta t$

E. Calculate the rib width from α, $b = \alpha \frac{th}{d}$

Thus all dimensions have been determined. As a check, determine rib crippling from the equation,

$$N_{cr}(3) = C_2 \, E \, t \, (1+\alpha) \left(\frac{b}{d}\right)^2 \qquad (4.13.17)$$

where

$C_2 = 0.634$ for the

spherical cap and,

$C_2 = 0.616$ for the

circular cylinder.

4.13.2 Worked Example

Spherical cap with the following requirements:

$P_{cr} = 33.6$ psi

$R = 198$ in

$F_{tu} = 71.2$ ksi,

$E = 11.6 \ (10^6)$psi

An optimum design will first be obtained and the weight penalty involved in holding the plate thickness constant while opening up the grid will be determined.

$$\frac{p_{cr}}{E} = \frac{33.6}{11.6}(10^{-6}) = 2.90\,(10^{-6})$$

From the graph in Figure 4.1-1.

$$\frac{p_o}{F_{tu}}(10^3) = 1.48\,,\quad \frac{t_{min}}{R} = 0.00107$$

thus

$$p_o = 1.48\,(71.2) = 105.3 \text{ psi}$$

$$\bar{t} = 0.00107\,(189) = 0.202 \text{ in.}$$

$$\bar{N} = \frac{p_{cr}}{E}\frac{F_{tu}}{p} = \frac{2.90\,(10^{-6})}{1.48\,(10^{-3})} = 1.96\,(10^{-3})$$

$$x = \frac{\bar{N}\,(10^3)}{1.482} = \frac{1.96}{1.482} = 1.323$$

$$y = \frac{\bar{N}}{0.130}\frac{F_{tu}}{p} = \frac{1.96\,(10^{-3})}{0.130}\frac{10^3}{1.48} = 10.2$$

From the α, δ graph in Figure 4.1-2.

$$\alpha = 0.29,\quad \delta = 14.6$$

then,

$$t = \frac{pR}{2F_{tu}(1+\alpha)} = \frac{1.48\,(10^{-3})\,189}{2\,(1.28)} = 0.1092 \text{ in.}$$

$$d = \delta t = 14.6\,(0.1092) = 1.594 \text{ in.}$$

$$b = \sqrt{\frac{\bar{N}}{0.634}}\,d = \sqrt{\frac{1.96\,(10^{-3})}{0.634}}\,(1.594)$$

$$= 0.0888 \text{ in.}$$

$$h = \sqrt{\frac{3.47}{\bar{N}}}\, t = \sqrt{\frac{3.47}{1.96\,(10^{-3})}}\,(0.1092)$$

$$= 4.59 \text{ in.}$$

as a check,

$$\alpha = \frac{bd}{th} = \frac{0.0888\,(1.594)}{0.1092\,(4.59)} = 0.282$$

$$\bar{t} = t(1 + 3\alpha) = 0.1092\,(1.846) = 0.202 \text{ in.}$$

As a check from the off-optimum curve, Figure 4.13-1.

$$S = d + t = 1.594 + 0.1092 = 1.703 \text{ in.}$$

$$N_{cr} = \frac{p_{cr}R}{2} = \frac{33.6\,(189)}{2} = 3180 \text{ lb/in.}$$

$$y = \frac{N_{cr}R}{0.260ES^2} = \frac{3.18\,(1.89)\,10^5}{0.260\,(11.6)\,(10^6)\,(1.703)^2} = 0.0678$$

$$x = \frac{N_{cr}h^2}{3.47\,ES^3} = \frac{3.18\,(10^3)\,(4.59)^2}{3.47\,(11.6)\,(10^6)\,(1.703)^3} = 0.337\,(10^{-3})$$

From the α, δ curve,

$$\alpha = 0.28, \quad \delta = 14.7$$

This checks with the previous values using the graph from Subsection 4.1.

For the first off-optimum design,

$$S = 1.703 \text{ in.} \quad h = 10.0 \text{ in.}$$

$$S = S_o \qquad h > h_o$$

then,

$$y = 0.0687 \quad \text{as before, and}$$

$$x = 0.337\ (10^{-3}) \left(\frac{10.0}{4.59}\right)^2 = 1.60\ (10^{-3})$$

From the α, δ graph, Figure 4.13-1.

$$\alpha = 0.085, \quad \delta = 7.8$$

$$t = \frac{s}{1+\delta} = \frac{1.703}{8.8} = 0.1935 \text{ in.}$$

$$d = \delta t = 7.8\ (0.1935) = 1.510 \text{ in.}$$

$$b = \alpha \frac{th}{d} = 0.085 \left[\frac{0.1935\ (10.0)}{1.510}\right]$$

$$= 0.109 \text{ in.}$$

$$\bar{t} = t(1 + 3\alpha) = 0.1935\ (1.255)$$

$$= 0.243 \text{ in.}$$

As a check on strength,
From the β curve, Figure 2-1

$$\alpha = 0.085, \quad \delta = 7.8, \quad \beta = 5.2$$

$$N_{cr}(1) = c_o E \frac{t^2}{R} \beta$$

$$= \frac{0.260\ (11.6)\ (10^6)\ (0.1935)^2}{189} (5.2)$$

$$= 3110 \text{ lb/in.}$$

$$N_{cr}(2) = c_1 E t(1 + \alpha) \frac{t^2}{h^2}$$

$$= 3.47\ (11.6)\ (10^6)\ (1.085)\ \frac{(0.1935)^3}{(10.0)^2}$$

$$= 3160 \text{ lb/in.}$$

$$N_{cr}(3) = c_2\ Et\ (1 + \alpha)\ \frac{b^2}{d^2}$$

$$= 0.634\ (11.6)\ (10^6\ (1.085)\ 0.1935\ \left(\frac{0.109}{1.51}\right)^2$$

$$= 8050 \text{ lb/in.}$$

Note that the rib crippling allowable, $N_{cr}(3)$ is not critical.

For the second off-optimum design,

$s = 1.703$ in. , $h = 15.0$ in.

$s = s_o$ $h > h_o$

$y = 0.0687$, as before, and

$$x = 0.337\ (10^{-3})\ \left(\frac{15.0}{4.59}\right)^2 = 3.60\ (10^{-3})$$

From the α, δ curves, Figure 4.13-1.

$\alpha = 0.05$, $\delta = 5.6$

$$t = \frac{s}{1+\delta} = \frac{1.703}{6.6} = 0.258 \text{ in.}$$

$$d = \delta t = 5.6\ (0.258) = 1.445 \text{ in.}$$

$$b = \alpha\ \frac{th}{d} = 0.05\ \frac{(0.258)\ (15.0)}{1.445}$$

$$= 0.1340 \text{ in.}$$

$$\bar{t} = t(1 + 3\alpha) = 0.258\ (1.15) = 0.296 \text{ in.}$$

Summary of results

$s = d + t = 1.703$ in.

h	b	d	t	α	δ	$\bar{t}$
* 4.59	0.0888	1.594	0.1092	0.282	14.6	0.202
10.0	0.109	1.510	0.1935	0.085	7.8	0.243
15.0	0.1340	1.445	0.258	0.05	5.6	0.296

*Optimum design

Note that b increases while d decreases. This is the reason why the ribs become non-critical.

4.13.3 Summary of Off-Optimum Equations

Normal Pressure on Spherical Cap	Cylinder Under Axial Compression and Bending	Reference
$c_o = 0.260$	0.397	Eq. 4.13.2, 4.13.3
$c_1 = 3.47$	10.2	Eq. 4.13.4, 4.13.5
$c_2 = 0.634$	0.616	p. 4.13.005
$s = d + t \leq S$ optimum		
$h \geq h$ optimum		
$x = \frac{N_{cr} h^2}{C_1 E s^3}$		Eq. 4.13.13
$y = \frac{N_{cr} R}{c_o E s^2}$		Eq. 4.13.14
$t = \frac{s}{1 + \delta}$		Eq. 4.13.10
$d = \delta t$		p. 4.13.005

Reference

$$b = \alpha \frac{th}{d}$$

p. 4.13.005

As a check,

$$N_{cr}\,(\text{Rib Crippling}) = C_2\, Et(1+\alpha)\left(\frac{b}{d}\right)^2 \geq N_{cr}$$

Section 5
NODAL GEOMETRY

The point where the isogrid ribs intersect is called a node, Figure 5-1. In the manufacture of isogrid, extra material is left at the nodes because the milling cutters cannot cut to the center of the intersection without cutting into the ribs. The weight penalty of this extra material is reduced by drilling a hole in the center of each node. These node holes are ideal points of attachment for other structures or for fittings carrying concentrated loads. Examples of their use in current practice are given in Section 3.

The nodal region in isogrid deserves special consideration because the nodes are flexible and cause a local redistribution of stresses in the area. As stated in Sections 2 and 4, the analysis of isogrid is based on "smearing out" the ribs so that the stiffened structure can be analyzed as a solid continuous sheet of material with appropriate elastic properties. This method has the advantage of being able to use the equations which have been developed for monocoque structures while providing accurate information for the sizing of isogrid structure. However, the "smeared-out" analysis ignores the flexibility of the nodes and its effect on the stress distribution. These local stresses may be very important in the detail design of critical areas. For example, in an area experiencing a considerable amount of cyclic loading,

CR169

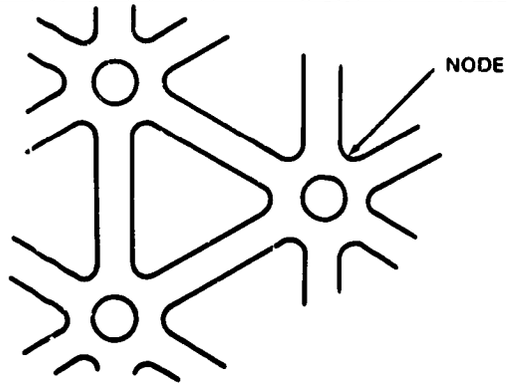

Figure 5-1. Isogrid Node

the stress concentrations should be determined to assess the possibility of initiating and growing cracks which could adversely affect the service life of the structure.

There are at least two methods which can be used to accurately determine the local stress distribution in the nodal area. One method is to use a finite element analysis and another is to use three-dimensional photoelasticity.

There are many excellent general references on finite element analysis methods in the literature, e.g., References 5-1 and 5-2, which the reader may refer to for basic information. Reference 5-3 describes NASTRAN, a widely-used general-purpose computer code for structural analysis based on the finite element method. An application of NASTRAN to isogrid analysis is described in Reference 1-2 for the Delta launch vehicle. A description of photoelastic analysis can be found in Reference 5-4.

The amount of stress redistribution due to node flexibility is, of course, a function of the geometry of the stiffening pattern and must be determined for each design. However, the following example from Reference 5-5 will illustrate the effect of flexibility for one particular geometry. The analysis method used was three-dimensional photoelasticity.

Two identical isogrid panels were fabricated from Hysol 4290 epoxy resin. Both panels were loaded in uniaxial tension, one in the direction of the 0 degree stiffening rib and the other 90 degree to the 0 degree rib. Three-dimensional photoelastic analysis was used to determine the stresses in the panels and the values were then compared with analysis, Reference 5-5. The panel skin was 0.075 inch thick. The ribs were 0.045 inch thick with a flange at the top that was 0.300 inch wide and 0.162 inch thick. The nodes were 5-inch on-centers with a node hole of 0.75-inch diameter. The milling cutter radius of the ribs at the node was 0.375 inch and was 0.248 inch at the flanges. For this configuration, the skin stresses were approximately 30 percent greater than "monocoque" analysis and the rib stresses were approximately 20 percent less. For uniaxial loading, a stress concentration of approximately 2.1 times the skin stress occurred at the node. Using superposition for a one-to-two biaxial loading, the stress concentration at the node was

1.3 times the skin stress. Finally, using superposition for a one-to-one biaxial loading, a stress concentration of approximately 1.2 times the stress in the skin away from the ribs occurred in the skin directly beneath the 0-degree and 60-degree ribs. Other values would, of course, be found for panels with a different geometry. For example, adding material at the nodes of the test panels described above, could significantly alter the results.

In addition to the local stress distributions, the bending and extensional stiffnesses of isogrid configurations should be verified by test for designs with very flexible nodes, e.g., very large center holes. This determination can be made simply and economically using a Lexan plastic panel subjected to a tension load to verify the extensional stiffness and to a bending load to verify the bending stiffness. Stiffness is, of course, essentially a gross property of a structure and is not as sensitive to local concentration effects as is the stress distribution. Buckling tests of Lexan isogrid cylinders, Reference 5-7, showed excellent agreement with theory for an isogrid configuration in which the hole diameter was 60 percent of the total distance across the node.

Section 6
TESTING

In order to verify assumptions of the theory and assess the effect of fabrication variables on the design, it is necessary to test representative components and shells in small scale, subscale or full-scale size. Buckling tests, in particular, are very sensitive to fabrication variables of a random nature which can only be assessed by subscale or full-scale testing. On the other hand, small scale model tests in polyvinyl chloride, or Lexan plastic can be made virtually free of random fabrication variables. Moreover, such Lexan model tests are non-destructive so that small, relatively cheap models may be repeatedly tested to check out interaction and multiple loading affects.

6.1 MODEL TESTS

Since fabrication variable effects are generally insignificant for models, it is recommended that verification of theoretical assumptions be made by model tests. For example, effects of nodal geometry on the elastic constants, reinforcement around holes, stress concentration around nodes, interaction curve verification and influence of thermal gradient on buckling values, are all examples of tests which are best conducted on small scale models. In some cases, where buckling effects of the order of 10 or 15 percent are to be investigated, such models are the only practical means of obtaining objective data which would be entirely masked by the random effects of fabrication typical of larger scale metal specimens which is of the same order as the effect to the investigated.

Instrumentation of the models may vary widely ranging from simple load deflection readouts to elaborate three dimensional photoelastic investigations. Because of the low elastic moduli of polyvinyl chloride and Lexan, internal pressure effects may be obtained by pulling a vacuum on the interior of the model.

Temperature control and an accurate determination of elastic moduli are important features of model testing. The influence of glued joints may present problems in softening the moduli of the material and should be accounted for.

The proper scaling factor for the models is also important. For models with uniform walls, it is necessary to obtain the correct bending stiffness, D and extensional stiffness, K. As shown in Section 2, an equivalent monocoque model may be substituted for isogrid using the equivalent E^* and t^*. In buckling of cylinders it may be shown that the buckling strength depends upon the R/t and L/R ratios in a non-linear manner and upon E linearly. Thus the proper modeling is

$$\frac{R}{t} \quad \text{monocoque} = \frac{R}{t^*}$$

$$\frac{L}{R} \quad \text{monocoque} = \frac{L}{R}$$

and

$$\frac{N_{cr}}{E} \quad \text{monocoque} = \frac{N_{cr}}{E^*}$$

The N_{cr}/E effects may thus be ratioed from the test values by analysis while the proper R/t and L/R must be built into the model.

Rib crippling and skin buckling effects, of course, cannot be obtained from equivalent monocoque models which are of value, primarily, for general instability characteristics.

6.2 SUB-SCALE AND FULL-SCALE TESTS

Since sub-scale and full-scale tests can be very expensive, it is important to examine all aspects of the influence of fabrication and peculiarities of the test setup on the expected test results. Reference 2-12 gives a good account of typical problems to the expected. Some of these are repeated here for convenience.

A. Examine the specimen carefully for bent and undersize ribs and skins. Straighten bent ribs and patch understrength defects. Make sure the specimen is protected from atmospheric corrosion.

B. Check specimen for roundness and straightness.

C. Conduct analysis to assess the effects of tolerance on the various modes of failure. Very local undersize regions may be "bridged over" by the high degree of redundancy of isogrid provided that fatigue is not an important consideration.

D. Check bearing fit between specimen and loading head. "High spots" can result in large local overloads in the specimen.

E. Monitor rib crippling and skin buckling by back-to-back strain gages located on outstanding edges of ribs and centers of skin panels.

Back-to-back gage readouts on monitoring equipment should be read together so that divergence of gages indicating local change of curvature or ribs and skin may be directly identified.

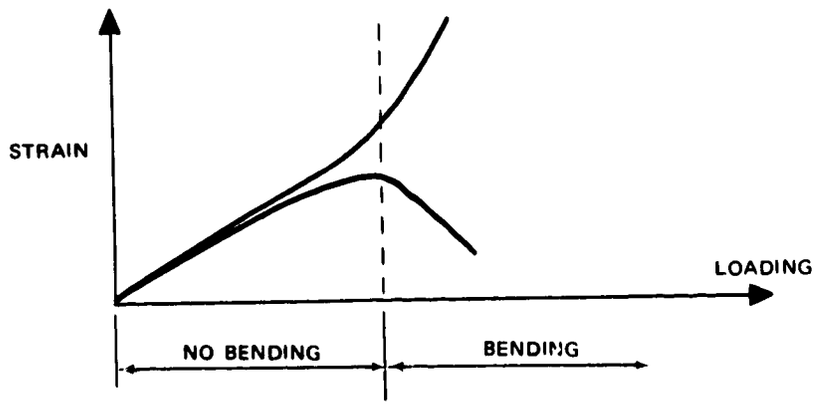

In specimens which are weaker in rib crippling and skin buckling than in general instability, such gage readings, properly located on the specimen, are invaluable in predicting not only rib crippling and skin buckling but are excellent indication of the ultimate load to be expected.

Section 7
MANUFACTURING TECHNIQUES

7.1 INTRODUCTION

To date, waffle construction, unless it is very shallow and used for parts with compound curvature, has been machined in the flat and subsequently formed. The open grid in the Orbital Workshop of the Skylab, since it forms walls and floors, was left flat. The same would apply to beams, frames, and wing ribs. The shallow ribs on compound curved parts are usually chemically milled. In one known case, a small spherical segment dome constructed for testing under NASA contract NAS8-11542, a compound curved spun part was sculptured after forming with a template-guided hand operated router. In general, therefore, integral structure deep enough to be structurally competitive with built-up structure has been applied to simple flat or singly curved shapes - flat elements, cylinders, cones and the slightly curved surfaces of wings and control surfaces in aircraft.

7.2 MACHINING

In the aerospace industry, integral construction generally means machining. Intricate shapes are most economically produced by casting, but the mechanical properties are not competitive with wrought material. Forging properties are usually the best obtainable, but the process does not deliver the close tolerances and thin stiffening ribs required for weight effective structure. This is particularly true for very large structural elements in the sizes necessary for achievement of economy and combining enough structural features to legitimize the word "integral". Forgings require finish machining. Machining limitations are, therefore, of prime importance in the design of integral structures, especially so for waffle construction.

Isogrid, like all other types of waffle, is pocket milled. An end mill traces the inside contour of the pocket and cleans out all the material in the center. See Figure 7.2-1. When the stiffening ribs are flanged, a fashioned cutter is used wherein the cutter extends beyond it shank, Figure 7.2-2. These are the two basic variations so far employed; they have provided adequate geometric latitude to cover a wide range of design load intensities and local reinforcement.

Six abutting triangular pockets, with corners appropriately rounded by cutter dimensions, define the geometry of a waffle node. When the pockets are small and the waffle nodes large severe weight penalties result. Therefore careful attention must be given to nodal geometry. Holes are drilled in the nodes to reduce weight. It should be noted that other methods may be used to make the hole, e.g., milling, electrical discharge machining.

For adequate cutter rigidity, the deeper a cutter penetrates to cut a waffle pocket, the larger the cutter diamater must be. Rigidity is required to obtain close tolerances or the reasonably smooth surface finishes which

CR169

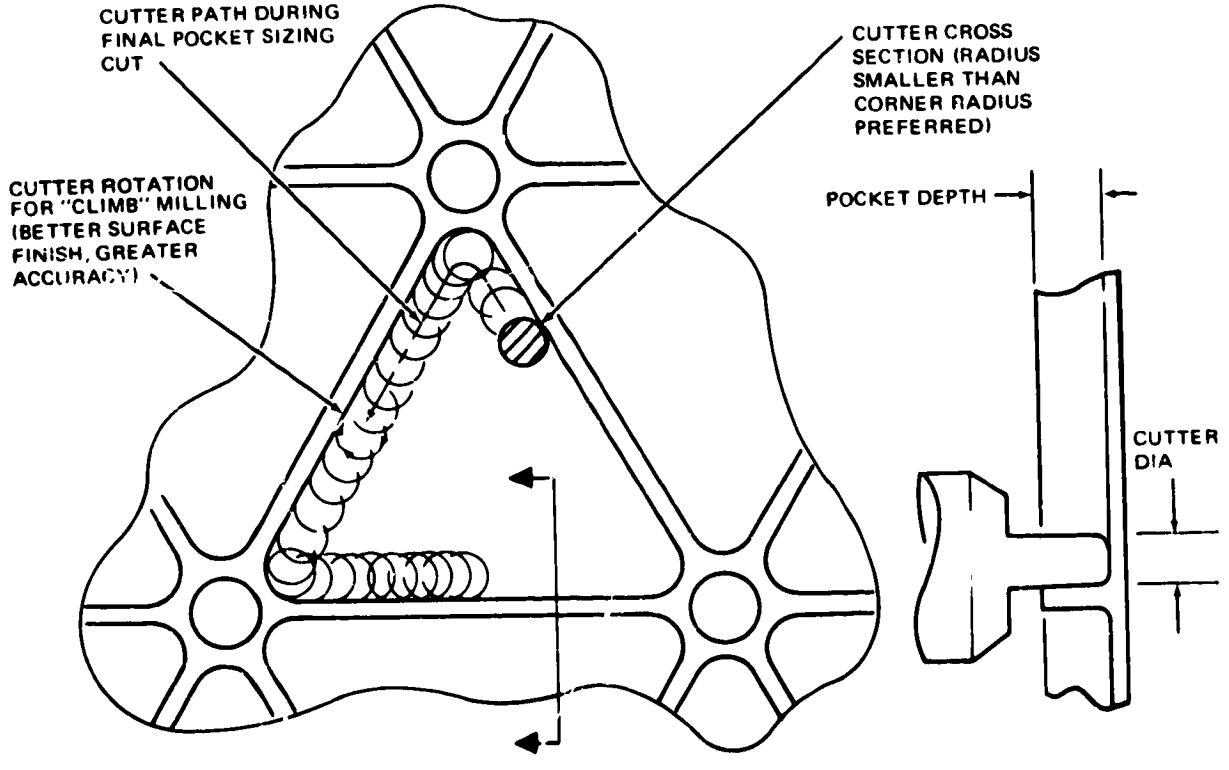

Figure 7.2-1. Machining Isogrid With Unflanged Ribs

CR169

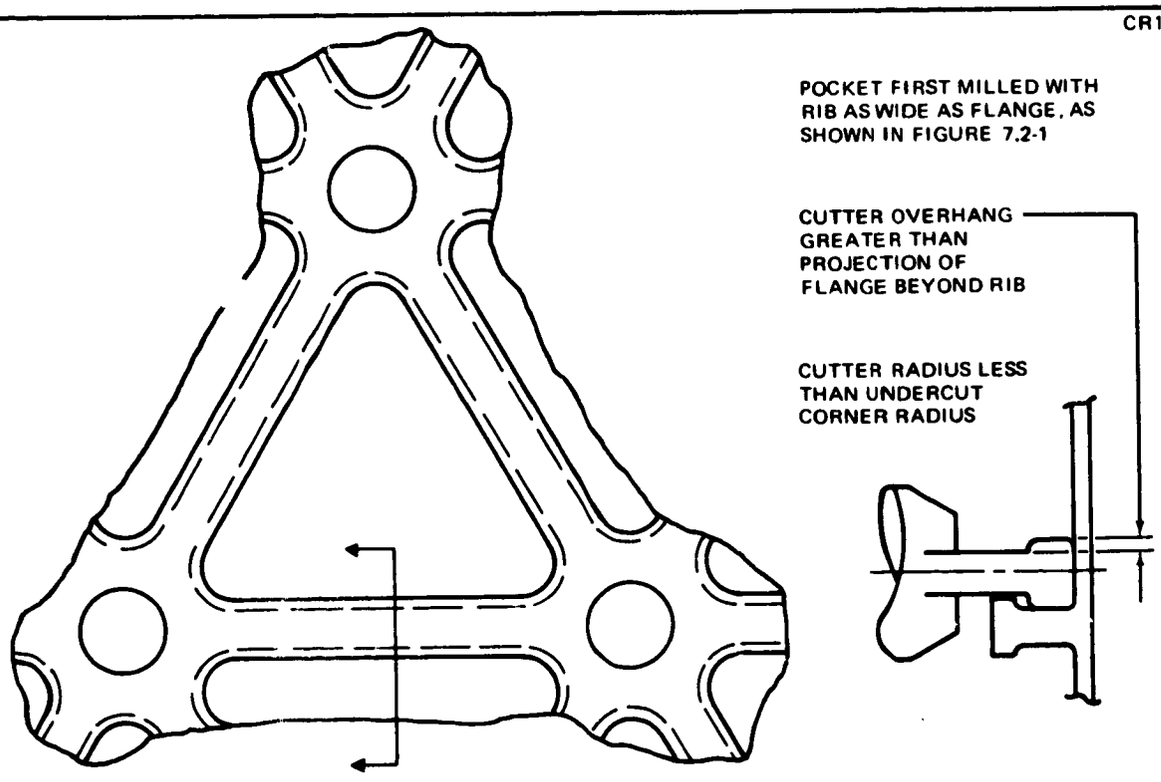

Figure 7.2-2. Machining Isogrid With Flanged Ribs

contribute to structural fatigue resistance. Cutter diameter should therefore be about 0.75 times the pocket depth or 0.5 as an absolute minimum. The smaller cutter diameters require a light finishing pass at high cutter rotational speed.

When the pocket corner radius is the same as the cutter radius, the cutter path stops on a point before resuming its movement down another leg of the triangle. During this "dwell" a cutter, especially a small one, drags against the wall of the pocket, chatters, enlarging the hole it occupies, and undercuts one of the stiffening ribs. This undesirable situation is best avoided by making the corner radius larger than the cutter radius. The path of the cutter centerline then describes a small radius at each corner. Slow cutter feed rates at the corner also contribute to better finish and accuracy especially in numerical controlled machining.

Both of the machining limitations mentioned above conspire to increase the size of waffle nodes with some loss in structural efficiency. Some weight penalty, however, is acceptable, because, as has been mentioned before, one of the functions of structure is to support system components. There is a benefit in both cost and weight if the structural system provides a pattern of predictably located strong natural attachment fittings which can perform the support function without necessitating structural changes. The geometry depicted in Figure 7.2-3 involves a nodal penalty of about 7 percent weight increase above that of a stiffening lattice whose equivalent weight thickness is defined by $t = t_s (1 + \alpha)$. Structural weight penalties of 10 to 15 percent provide equivalent secondary support capability are not uncommon in built-up structure. It should be noted that for very wide triangles, additional attachment points may be provided by putting bosses in the flanges of the flanged ribs.

Quite often in structures optimized for high compressive load intensities, the secondary capability of a waffle node may exceed any requirements the other systems impose on it. In such cases, refinements to reduce nodal

CR169

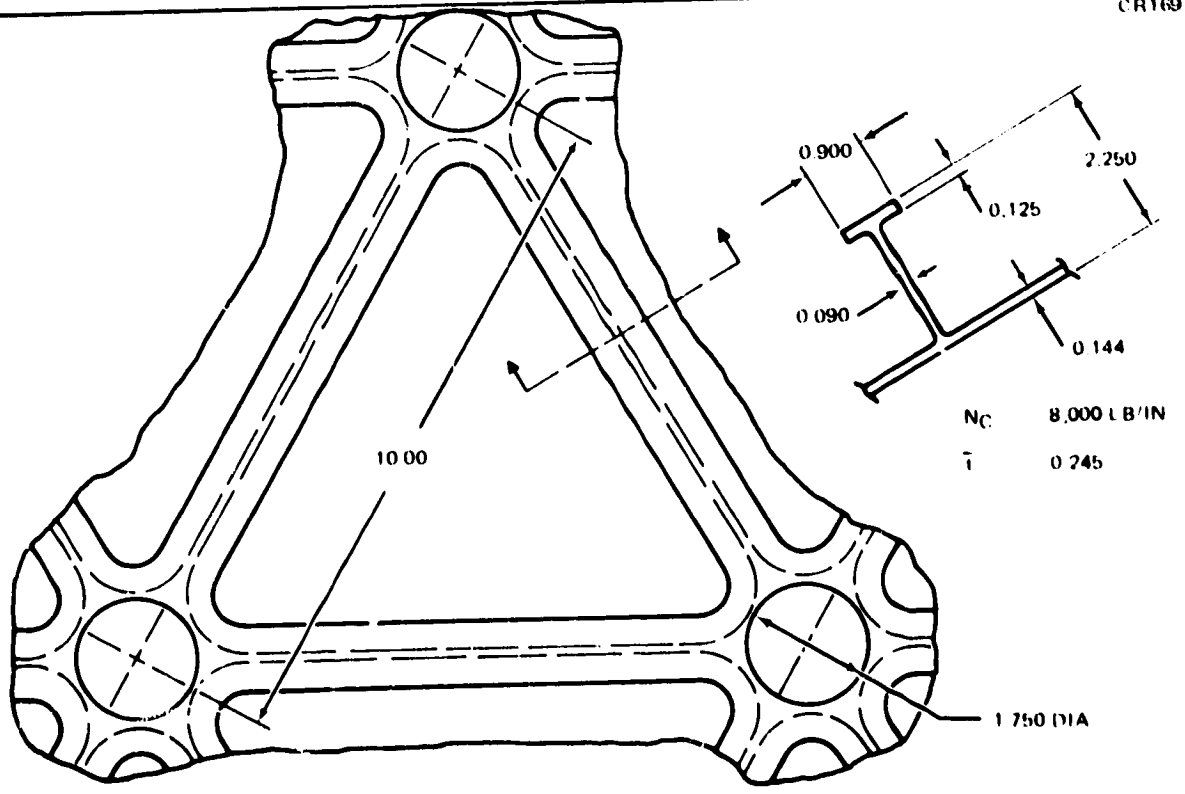

Figure 7.2-3. A Tank Wall Configuration

weight are in order. Electrical discharge or electro-chemical machining may provide a means of achieving such refinement. Because the shape of an electrode determines the shape of an impression rather than a rotating cutter, an almost unlimited range of shapes can be produced. The designer is cautioned, however, to apply this versatility with restraint. Such stress-raising configurations as keyways and spliced holes are not recommended; nor is complete elimination of the hole with attendant sharp corners at the rib intersections. Some practical recommendations are shown in Figure 7.2-4.

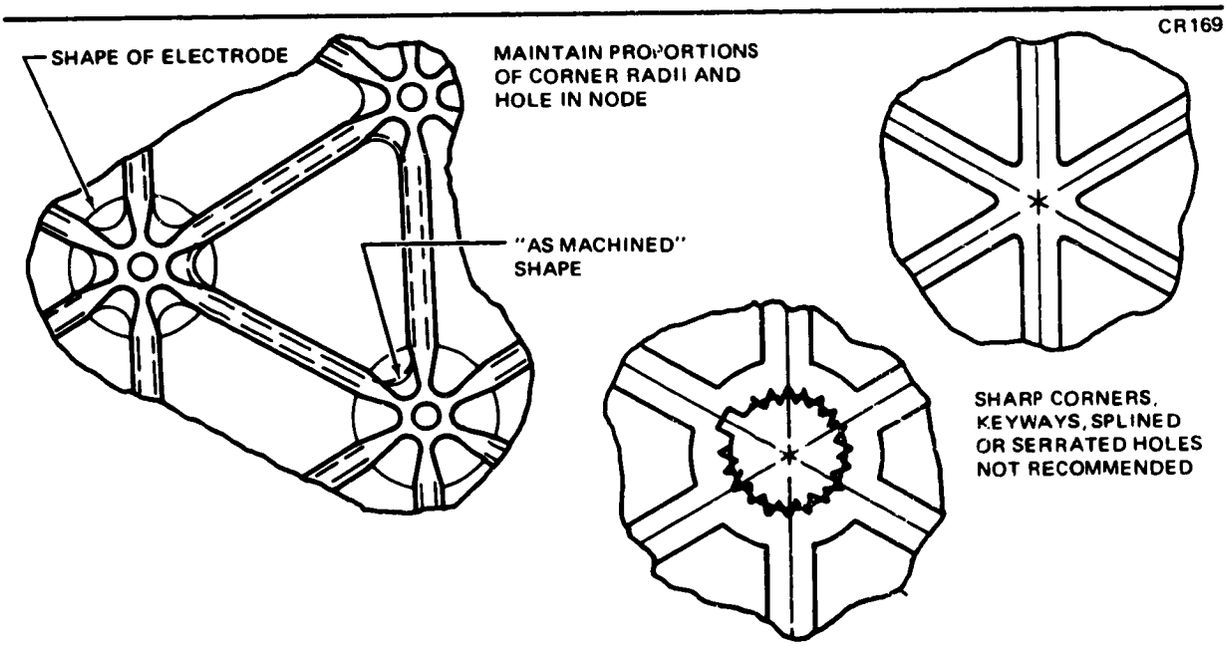

Figure 7.2-4. Electrical Discharge (EDM) or Electrochemical (ECM) Machining to Reduce Isogrid Nodal Size and Weight

7.3 FORMING

7.3.1 Power Brake Forming

One of the more common processes for forming simply curved surfaces is progressive pinching in a power brake. Still effective and often used, it accomplishes its objective by successively creasing line elements of the curved surface, Figure 7.3-1. The line elements may be parallel as in

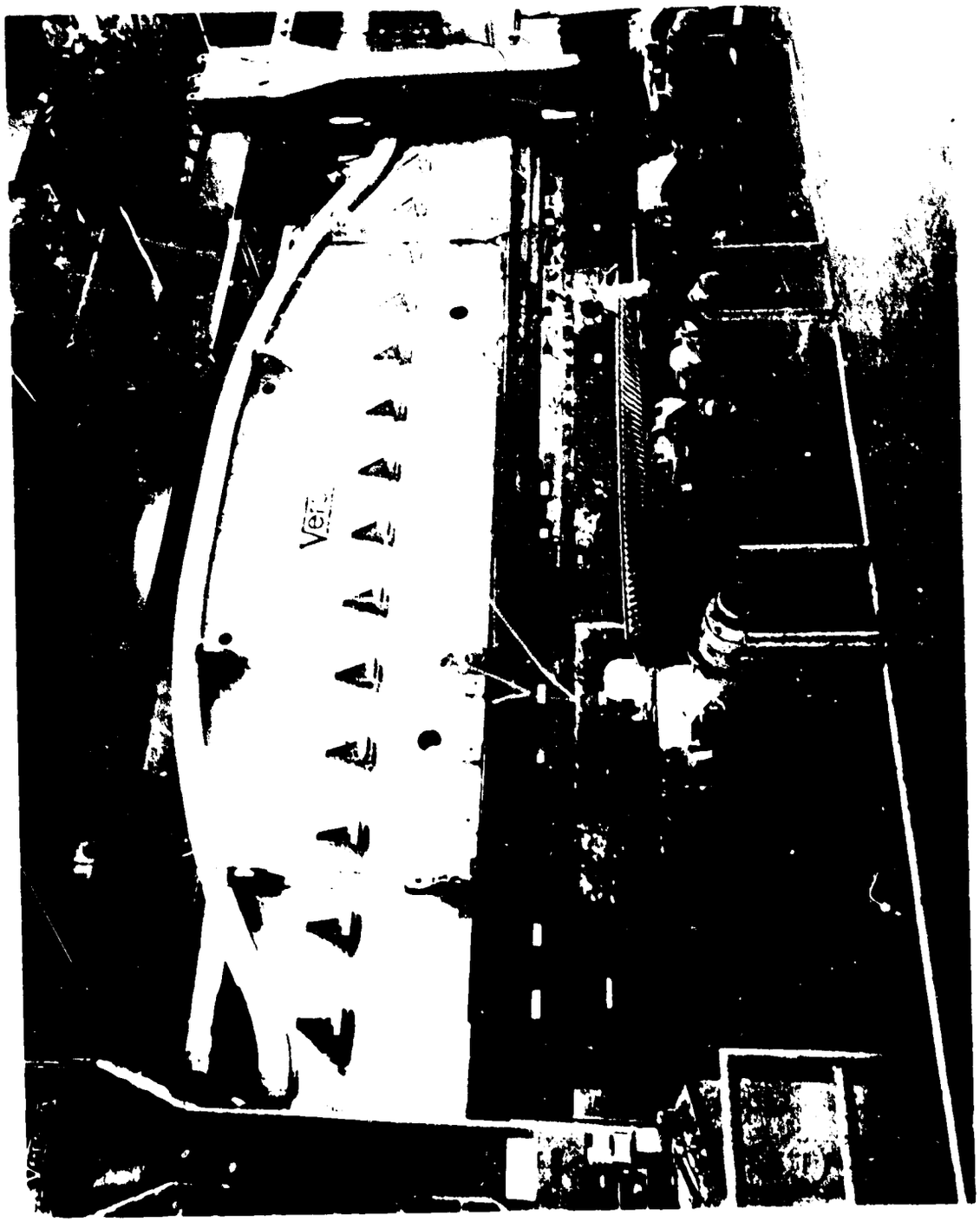

the case of a cylinder or converging as they are on a cone or the surface of a tapered wing.

The fundamental limitation in this type of forming is the permissible elongation without fracture of the material being formed. Room temperature properties apply since the final formed shape is that assumed after the material springs back, considerable (and somewhat unpredictable) over-forming is necessary. The process must therefore be carefully developed for each stiffening configuration. In general, forming difficulties may be expected if the plate depth exceeds about 1.5 percent of the final formed radius. Internal ribs are subject to buckling at higher ratios, external ribs are likely to crack at the nodal intersections. Local high pressure on the tops of the ribs can accentuate either of these problems. Removable support blocks in the pockets have been successful in alleviating these conditions, but they complicate the process.

The highest ratio of plate depth to radius so far attempted is 1.5 percent. This was the ratio on a compression cylinder tested under NASA Contract NAS 8-26016. The ribs were external and the forming was accomplished with no support blocks in the pockets, Figure 3-5. While some of the ribs were slightly deformed in the process, they were straightened quite easily and adequately, Figure 7.3-2. The size and geometry of the waffle shell is shown in Figure 7.3-3. It should be noted that the method used to straighten deformed ribs depend upon the amount of deformation. e.g. ribs can be "bridged" to maintain column buckling capability. The internal ribs configuration of the Thor-Delta vehicle required widening of the stiffening ribs from 0.060 to 0.080 to avoid compression buckling, Figures 7.3-4 and 7.3-5. In this case, the plate depth was 1.04 percent of the shell radius of curvature.

Fortunately optimized isogrid in cases typical for space boosters and aircraft tends to stay within these geometric limitations. Where simple unflanged rib designs tend to be deeper, the depth can be reduced by incorporating flanges.

Figure 7.3-2 Hardware Photograph

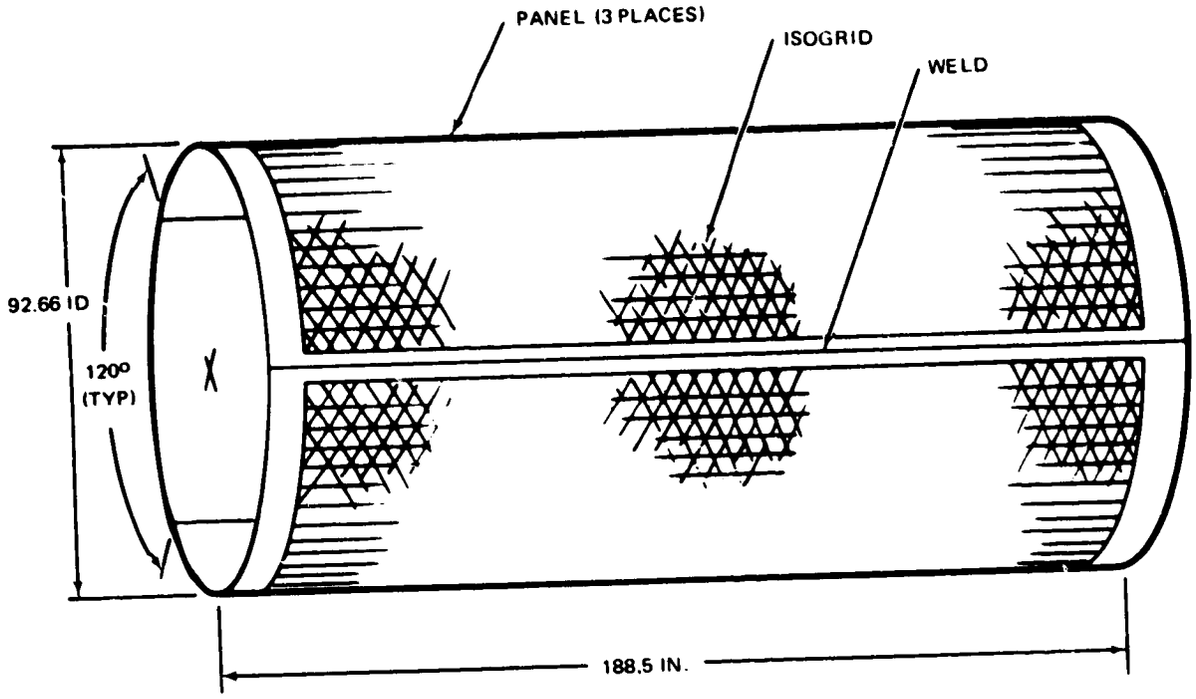

Figure 7.3-3. Test Cylinder

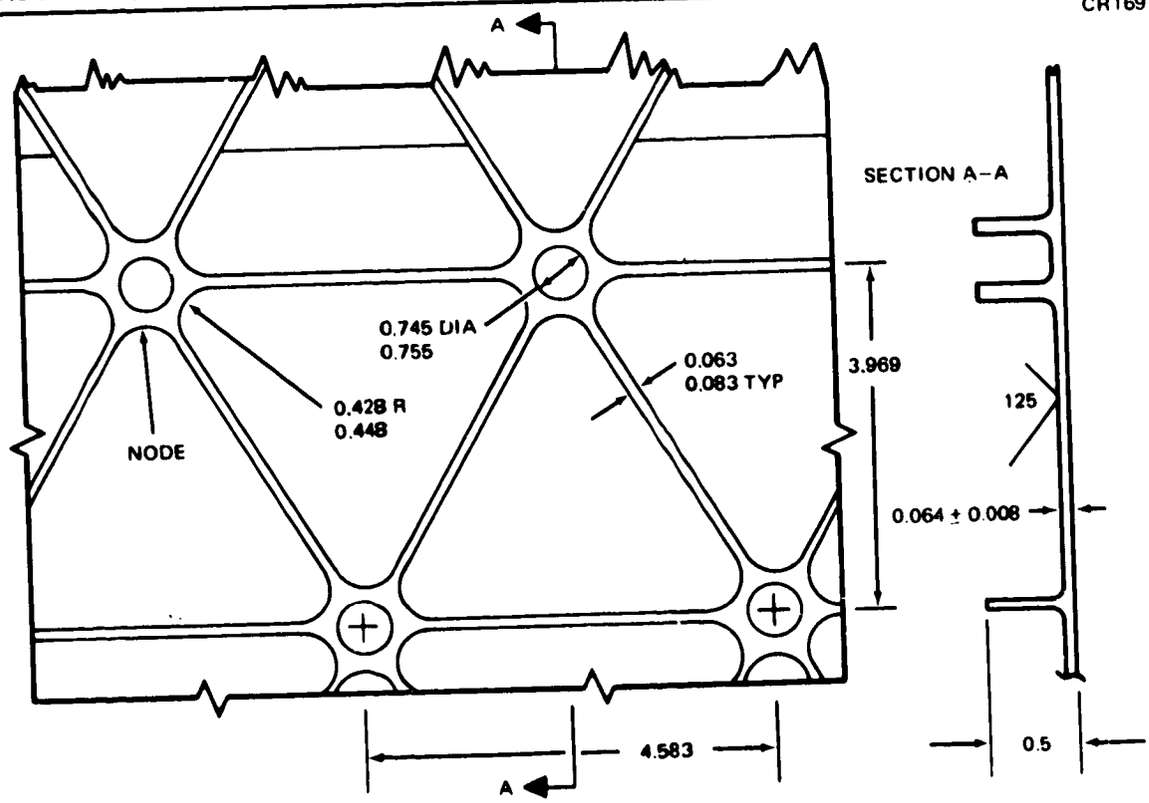

Figure 7.3-4. Thor Delta Isogrid Geometry

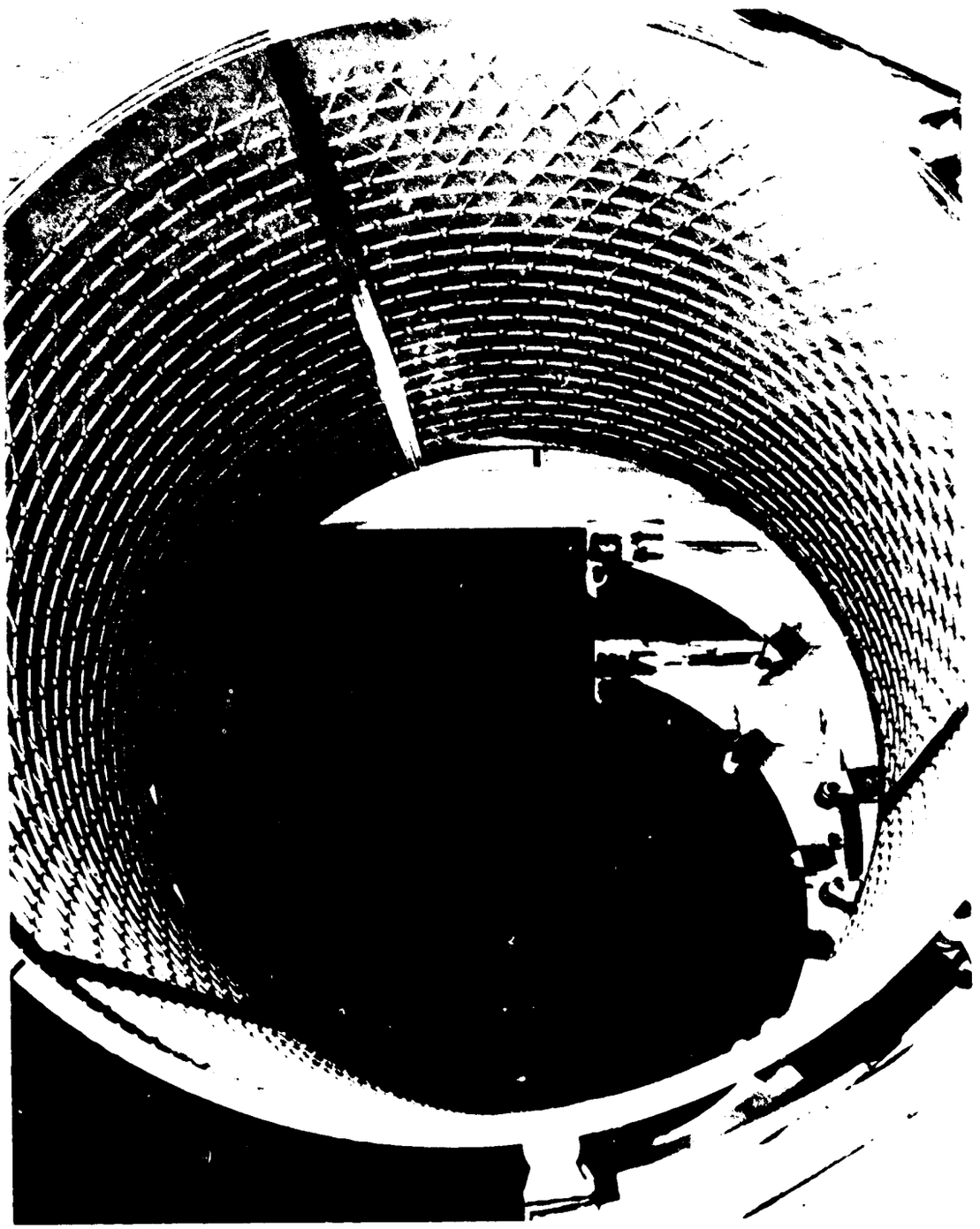

Although the brake forming process is in some respects more of an art than a science, the results after a few development parts have been made, are quite good. This has been verified by the successful production of waffle skins for the Thor-Delta boosters, the Saturn S-IV and S-IVB and the crew compartment shell of MOL. For such work quite large and powerful equipment is needed. An example of this is the 40-foot power brake illustrated in Figure 7.3-1.

An additional forming method that may be applicable is roll forming. For this method the isogrid pockets should be filled with a suitable filler material to prevent buckling of the members.

7.3.2 Creep and Age Forming

A more advanced forming method, which treats the material more gently, promises more accuracy and consistency, and may produce parts with compound curvature, is creep forming. When the part, usually aluminum, creeps to final shape at the heat treatment aging temperature, two processes are performed simultaneously and the part is said to be age formed. It should be noted that this is not a standard 'day-to-day' process but one that must be developed by the individual user.

In this process, the part to be formed is clamped to a fixture and held at elevated temperature until it creeps to its predetermined final shape. Allowance for some springback is made in the shape of the fixture. Such a fixture and the part formed on it is shown in Figures 7.3-6 and 3-10. In this case, a segment of a cylindrical wall, it was found that springback was practically eliminated and consistency improved by applying a tensile force along the edges of the part. Though the final tensile elongation was small, allowance would have to be made in the machined shape for an accurate production part. Where the part must assume a final shape quite different than its machined starting point (e.g., a 120-degree arc), the process may require multiple staging, either in several creep forming steps (preferably in the same fixture), with appropriate consideration of over-aging, or by initial rough forming with the power brake. Creep forming offers, among other advantages, an opportunity to reduce residual stresses.

Figure 7.3.6. Isogrid in Creep Forming Fixture

2219-T37 Aluminum isogrid has been successfully formed by this process.

7.3.3 Compound Curvature

Compound curvature is difficult to achieve with integrally stiffened parts mainly because a flat pattern cannot be developed for such shapes. This means that parts machined in the flat are subject to unpredictable, and sometimes unrepeatable, distortions. Each configuration must therefore be developed individually. Each curvature has special problems requiring special solutions.

Machining after forming offers similar difficulties. Even moderate forming leaves residual stresses in parts. Subsequent machining, locally relieving these stresses, causes distortions. Tolerances are difficult, if not impossible to hold. Costs are escalated by rigid - and probably multiple- holding fixtures as well as the higher amortization costs of the more elaborate machines capable of doing the work.

Fairly large contour changes can be approximated with truncated cones as shown in Figure 7.3-7. This diagram is representative of ogive noses on large missiles or aircraft; similar geometry defines taper of the aft end. A very small bulge outside the straight conical line element is enough to produce an accurate faired final contour. This much double curvature should be achievable with creep forming. Whether such an accurate contour is actually worth making is a question to be raised in these circumstances.

In summary, standard manufacturing techniques have been applied to the fabrication of isogrid structures. Machining, power-brake forming, and creep and age forming have been used to successfully form structure which is flat or has a single curvature. The forming of compound curvature can be difficult but the problems are those associated with all integrally stiffened structures and are not peculiar to isogrid.

7.4 NON-DESTRUCTIVE INSPECTION FOR MANUFACTURING ACCEPTANCE

Standard non-destructive inspection techniques should be suitable for accepting manufactured isogrid parts. Fluorescent dye penetrant was used to

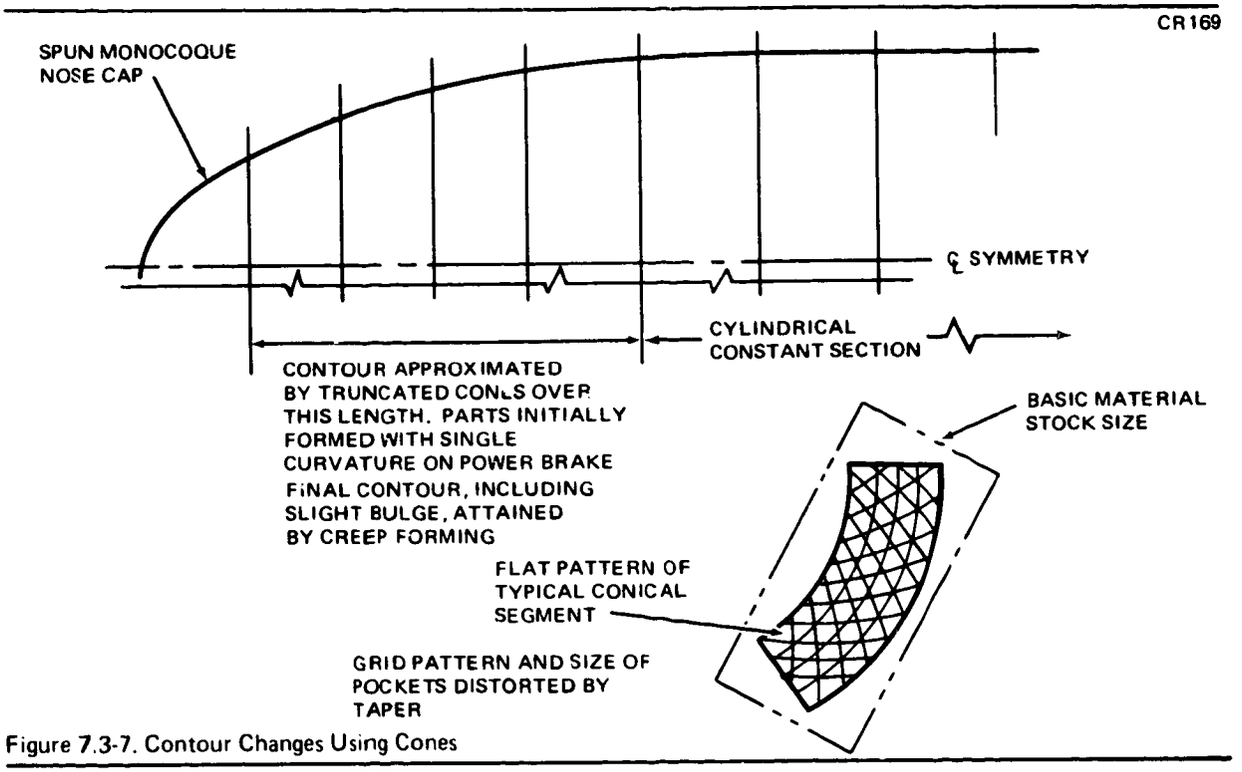

Figure 7.3-7. Contour Changes Using Cones

inspect isogrid parts for Delta. The parts were handled in an automatic penetrant facility in which the parts were handled and the penetrant applied automatically. Visual inspection of the parts was then used; sometimes with 5x-10x magnification. Other inspection techniques may be developed by the individual user, e.g., dye penetrant which was used to look for forming cracks in the SIVB waffle skins.

REFERENCES

1-1 Meyer, R. R. and R. J. Bellinfante, "Fabrication and Experimental Evaluation of Common Domes having Waffle-like Stiffening", Douglas Report SM-47742, November 1964.

1-2 Knighton, D. J., "Delta Launch Vehicle Isogrid Structure NASTRAN Analysis", NASTRAN: User Experiences. NASA TMX-2637. Presented at the Second Colloquium held at Langley Research Center. Hampton, Va., Sept. 11-12, 1972. Sept. 1972. pp. 121-143.

2-1 Meyer, R. R., "Buckling of Stiffened Cylindrical Shells Subjected to Combined Axial Compression, Normal Pressure, Bending and Shear Loading." Ph. D. Dissertation. June 1972. UCLA.

2-2 Timoshenko, S. and J. N. Goodier, "Theory of Elasticity." 2nd Ed. McGraw-Hill, 1951.

2-3 Timoshenko, S. and Woinowsky-Krieger, "Theory of Plates and Shells." 2nd Ed. McGraw-Hill, 1959.

2-4 Timoshenko, S. and J. M. Gere, "Theory of Elastic Stability." 2nd Ed. McGraw-Hill, 1971.

2-5 Flugge, W., "Stresses in Shells," Springler-Verlag, New York Inc. 3rd Printing 1966.

2-6 Weingarten, V., P., Seide, and J. P. Peterson, "Buckling of Thin-Walled Circular Cylinders." NASA SP-8007. Sept. 1965, revised August 1968.

2-7 Weingarten, V. and P. Seide, "Buckling of Thin Walled Truncated Cones." NASA SP-8019, Sept. 1968.

2-8 Weingarten, V. and P. Seide, "Buckling of Thin Walled Doubly Curved Shells." NASA SP-8032, August 1969.

2-9 Gerard, G. and H. Becker, "Handbook of Structural Stability, Part I - Buckling of Flat Plates," NACA TN-3781, July 1957.

2-10 Jenkins, W. C., "Determination of Critical Buckling Loads for Isogrid Stiffened Cylinders," McDonnell Douglas Report Number MDC G2792, Feb. 1972.

2-11 Peterson, J. P. "Buckling of Stiffened Cylinders in Axial Compression & Bending - A Review of Test Data," NASA TN-5561, December 1969.

2-12 Meyer, R. R. and H. A. Anderson, "Space Shuttle Isogrid Tank Buckling Test. Vol. I, Design and Analysis," McDonnell Douglas Report MDC G24804, February 1972.

2-13 Gerard, G. and H. Becker, "Handbook of Structural Stability, Part III - Buckling of Curved Plates and Shells," NACA TN-3783, August 1957.

2-14 Peterson, J. P. and R. G. Updograff, "Tests of Ring Stiffened Circular Cylinders Subjected to Transverse Shear Load," NACA TN 4403, September 1958.

5-1 Rubinstein, M. F., "Matrix Computer Analysis of Structures," Prentice Hall, Inc., Englewood Cliffs, N. J., 1966.

5-2 Przemieniecki, J. S., "Theory of Matrix Structural Analysis," McGraw-Hill Book Company, New York, N. Y. 1968.

5-3 MacNeal, R. H. (Editor), "The NASTRAN Theoretical Manual," NASA SP-221, September 1970.

5-4 Heywood, R. B., "Designing by Photoelasticity", Chapman and Hall, Ltd., London, England, 1952.

5-5 Jenkins, W. C., "Three-Dimensional Photoelastic Analysis of the Stress Distribution in Isogrid Stiffened Panels." McDonnell Douglas Report MDC-G2496, March 1972.

5-6 Jenkins, W. C., "Determination of Critical Buckling Loads for Isogrid Stiffened Cylinders," McDonnell Douglas Report MDC G2792, March 1972.

ADDENDUM

Section 8

EXPERIMENTAL RESULTS FROM MODEL TESTS

Analyses of isogrid as presented in this handbook are primarily concerned with the prediction of buckling instability and of states of stress that occur in isogrid under the action of loads, singularly applied or applied in combination. The validity of such analyses can only be verified by tests conducted on isogrid structures. These tests may be either tests of full-scale metal structures or tests on subscale models. Full-scale metal tests of structural components have certain characteristics which make them undesirable for theory verification, e.g., plastic deformation upon buckling, small buckling "knock-down" factors, and wide data scatter. During recent years, the fabrication and testing of models, made from Lexan polycarbonate plastic, have shown that the use of such models has several advantages over the use of full-scale metal test models. These advantages are summarized as follows:

a. Lexan models are relatively inexpensive compared to full-scale metal models

b. The large ratio of strain-to-yield stress of Lexan results in elastic buckling of the models, thereby allowing the repeated testing of a single model

c. Past programs with Lexan models have shown that such models have buckling "knock-down" factors approaching unity versus typical metal "knock-down" factors of 0.6 to 0.7

d. Past programs have shown that buckling data from Lexan models have negligible data scatter

e. Lexan can be bonded with solvent adhesives (ethylene dichloride or methylene chloride) thereby facilitating the construction of models as well as allowing the simulation of weld joints.

f. Lexan, unlike other plastics, is an extremely tough material and does not require special handling during machining or special handling of the completed model.

This section will be devoted to a documentation of the results of such subscale plastic model tests and a comparison of the results of these tests with the results from analyses as presented in Section 4 of this handbook.

8.2 LEXAN MODEL BUCKLING TESTS OF SKINNED AND UNSKINNED ISOGRID CYLINDERS SUBJECTED TO COMBINED LOADING OF COMPRESSION, BENDING, AND TORSION

8.2.1 Background

Generally, a vehicle structure will be subjected to a combination of loading in the fulfillment of its mission objectives. As is well known, the buckling stability of a structure under such loads is affected by the proportions of the individual types of loads applied to the structure at any given moment, i.e., compression, bending, shear, torsion, and internal pressure. The manner in which the loads interact to affect the buckling stability are characterized in interaction equations as presented in Reference 8-1. As this reference indicates, the interaction equations are empirically determined. It is therefore important to assess the accuracy of such equations in the prediction of the response of isogrid cylinders.

as a partial verification of such interaction equations, a program was conducted consisting of the design, fabrication, and testing of two isogrid cylinders, one without skin (unskinned) and one with skin (skinned) for the determination of buckling behavior under the action of compression, compression-bending and torsion.

8.2.2 Design and Fabrication of Models

Both cylinders were designed to buckle in general instability. This was accomplished using the analyses given in Section 4 of this handbook for the skinned cylinder for compression, compression-bending, and torsion buckling and for the unskinned cylinder for compression and compression-bending buckling. Torsion buckling of the unskinned isogrid cylinder was determined by an analysis developed by McDonnell Douglas Astronautics Company. All equations employed are summarized in Table 8.2-1. In all cases, the "knock-down" factors were taken as unity. Circumferential isogrid was used in both cylinders to minimize rib stresses. For the case of the skinned cylinder, an external isogrid configuration was employed. No attempt was made to optimize either cylinder. Customary units were used in all calculations. In this section, all results of experimental and theoretical calculations are given in both the International System of Units and in customary units.

The fabrication of each cylinder consisted of the machining of the appropriate isogrid configuration in three flat plates of Lexan. These plates were subsequently heat formed into curved configurations constituting one-third of a cylinder each. For a given cylinder, three of these curved pieces, hereinafter referred to as segments, were solvent bonded such that each cylinder had three longitudinal joints. The philosophy of the design of the longitudinal joints was

to design a joint that would realistically simulate the weld joint of a full-scale metal prototype. The final measured dimensions of the cylinders are shown in Figures 8.2-1 and 8.2-2. The calculated buckling stress resultants for these dimensions using the equations of Table 8.2-1 are shown in Table 8.2-2. As can be seen from this table, both cylinders were conservatively designed to buckle in general instability before either rib or skin buckling.

8.2.3 Test Set-up

Both models were mounted in aluminum end fixtures that penetrated into the cylinders a distance of 5.08 cm (2 inches). To assure the transfer of torsion loads to the cylinder, end bands were used to clamp the cylinders to the end fixtures. Compression and compression-bending were applied to the test cylinders by a compression test machine acting through a steel sphere located in conical depressions in the upper end fixture. Application of the load in a depression at the center of the end fixture resulted in pure compression to the cylinder. Combined compression-bending of the cylinders was achieved by off-axial loading of the cylinders at depressions located approximately one-quarter the radius (R/4) and one-half the radius (R/2) from the cylinder axis. For a monocoque cylinder, such off-axial loading would correspond to an f_b/f_c ratio of 0.5 and 1.0, respectively, where f_b is the maximum bending stress and f_c is the axial stress. Torsion load was applied by a hydraulic jack acting through moment arms on the upper end fixture. The manner in which these loads were applied is shown in Figure 8.2-3. As also shown in this figure, three load cells were employed in monitoring the loads applied to the cylinders, one for the axial load and two for the torsion loads. During cylinder loading, the outputs of these cells were continually recorded on a dual pen X-Y recorder.

...4 Test Sequence, Results, and Discussion of Results

Both cylinders were initially buckled in pure axial compression and in pure torsion to determine buckling behavior for these loadings. The resulting buckling patterns for the skinned cylinder are shown in Figures 8.2-4 and 8.2-5. As can be seen in Figure 8.2-4 the post-buckle pattern of the skinned cylinder under pure axial compression indicated that buckles occurred in the joints as well as in the isogrid. Subsequent tests of the cylinder, using a dual beam oscilloscope and electrical contacts at buckle centers, indicated that the buckles were initiating in the isogrid rather than in the joint. The buckles in the joints were therefore of no further concern. Figure 8.2-5 indicates that considerable deformation to the skinned cylinder occurred in torsional buckling. A subsequent examination of this cylinder indicated that one circumferential rib had fractured and the possibility existed that other ribs had experienced plastic deformation. Although the fractured rib was repaired by solvent bonding, average maximum axial load after rib fracture was 7557 N (1699 pounds) compared to a maximum load of 8095 N (1820 pounds) before rib fracture. To prevent further damage to this cylinder, the hydraulic system used to apply torque to the cylinder was configured in such a manner that the torsion load could be immediately released at the onset of buckling, thus preventing the cylinder from undergoing large displacements. Interestingly, the maximum torsion buckling load was found not to have been affected by the rib fracture.

Axial buckling of the unskinned cylinder indicated that buckling was initiated at the joints. This problem was overcome by the bonding of longerons, shown in Figure 8.2-6, to the inside and outside of the joints. These longerons had the effect of greatly increasing the bending stiffness of the joint without a

corresponding increase in extensional stiffness. Measurements made on tensile samples, designed to simulate the joint, indicated that the addition of the double longerons increased the effective extensional stiffness of the joints by approximately 53 percent. The buckling patterns of the modified unskinned isogrid cylinder for pure axial loading and pure torsion loading are shown in Figures 8.2-7 and 8.2-8. No damage occurred to this cylinder from torsion buckling as had occurred for the skinned cylinder. Nevertheless, all subsequent tests for torsion buckling of the unskinned cylinder employed the quick load release system previously described for the skinned cylinder.

A total of 54 buckling tests were performed on each cylinder to determine the buckling interaction of combined compression, compression-bending, and torsion. This was accomplished by the application and maintenance of a torsion load while axial load was applied until buckling occurred. Torsion loads were varied from zero to 100 percent of maximum torsion load in approximately 20 percent increments. Axial loads were applied along the cylinder axis, for zero bending, and at two off-axial load points (R/4 and R/2), for combined compression-bending. To prevent anomalies in the data from local trisector variation, all load combinations were performed for buckling on each trisector and the results were averaged. The data from these tests are summarized in the graphs of Figures 8.2-9 and 8.2-10 in terms of average compression stress ratios ($R_c = f_c/F_c$ where f_c is the compression buckling stress and F_c is the maximum compression buckling stress) and average torsion stress ratios ($R_{st} = f_{st}/F_{st}$ where f_{st} is the torsion buckling stress and F_{st} is the maximum torsion buckling stress) as functions of the compression-bending ratio f_b/f_c.

To determine the effect of the order in which loads were applied, both cylinders were also loaded by application of axial compression followed by torsion. The results of this reverse load order were essentially identical to the original loading order.

Reference 8-1 gives an interaction equation for compression, bending, and torsion of

$$R_c + R_b + R_{st}^2 = 1 \qquad (8.2.1)$$

where R_b is the bending stress ratio. This interaction equation is plotted in Figure 8.2-11 for ratios of f_b/f_c of 0, 0.5, and 1. A comparison of Figure 8.2-11 with the experimental data of Figures 8.2-9 and 8.2-10 indicate that excellent correlation is obtained for an f_b/f_c ratio of zero but that the experimental curves for f_b/f_c of 0.5 and 1 both lie above the theoretical curves. The excellent correlation for $f_b/f_c = 0$ partially results because the end points of the experimental results are defined to be the same as the theoretical values, i.e., $R_c = 1$ at $R_{st} = 0$ and $R_c = 0$ at $R_{st} = 1$. In like manner the end point for $R_{st} = 1$ and $R_c = 0$ is by definition the same for both theory and experiment for the two remaining ratios of f_b/f_c.

The end points of the theoretical curves may be equated to the remaining experimental end points by modifying Equation (8.2.1) as follows

$$k(R_c + R_b) + R_{st}^2 = 1 \qquad (8.2.2)$$

where $k = (R_c)_{th}/(R_c)_{exp}$ and $(R_c)_{th}$ and $(R_c)_{exp}$ are the R_c values for theory and experiment, respectively, for $R_{st} = 0$ and for the appropriate ratio of f_b/f_c. A comparison of the results of Equation (8.2.2) with the experimental results indicate excellent correlation as shown in Figures 8.2-12 and 8.2-13 for all ratios of f_b/f_c for both cylinders.

This excellent agreement indicates that the shape of the curves given by equation (8.2.1) is essentially correct for both skinned and unskinned isogrid cylinders. There are a number of reasons why the original data varies from the theoretical values. These reasons will be mentioned in later paragraphs that deal with correlation between theoretical and experimental buckling loads for pure axial compression and pure torsion. The practicality of the excellent correlation of the adjusted data is that only the end points of the interaction curves need be ascertained in order to completely define the entire interaction curves.

The average values of axial load were 7557 N (1699 pounds) and 7167 N (1611 pounds) for the skinned and unskinned cylinders, respectively, and the average values of the torsion loads were 479 M-N (353 ft-lbs) and 353 M-N (260 ft-lbs) for the skinned and unskinned cylinders, respectively. The comparison of these measured values with the theoretical values of Table 8.2-2 require the reduction of the total loads to equivalent stress resultants. This is necessary in that the cylinder joints supported a portion of the load applied to the cylinders. This reduction is relatively straight-forward for axial compression in that a uniform axial strain may be assumed by virtue of the rigid aluminum end fixtures. Given a uniform axial strain, the stress resultant in the isogrid may be shown to be

$$N_{cr} = \frac{P_{cr}}{A} t\ (1 + \alpha) \qquad (8.2.3)$$

where N_{cr} is the critical buckling force per unit length, A is the total effective extensional area, P_{cr} is the total buckling load, and t and α are as previously defined in this handbook.

Application of the appropriate values from Figure 8.2-1 for the skinned cylinder and from Figure 8.2-2 for the unskinned cylinder will give

$$N_{cr} \text{ (skinned)} = (0.728\ M^{-1})\ P_{cr}$$

$$N_{cr} \text{ (unskinned)} = (0.417\ M^{-1})\ P_{cr}$$

An average load of 7557 N (1699 pounds) for the skinned cylinder will then give an N_{cr} of 5500 N/M (31.4 lb/in) corresponding to 76.1 percent of the theoretical values of 7230 N/M (41.3 lb/in). As previously mentioned, the maximum load carried by the skinned cylinder was 8095 N (1820 lbs) prior to cylinder damage from torsion loading. This load corresponds to 81.5 percent of the theoretical load. In like manner an average axial load of 7167 N (1611 lbs) for the unskinned cylinder gave an N_{cr} of 2990 N/M (17.1 lb/in) for 89.5 percent of the theoretical values of 3340 N/M (19.1 lb/in).

A comparison of the theoretical torsion buckling loads to the experimental values is not as straight-forward as the axial case just treated in that the relationship between torsional shear strain and the torsional load carried by the joints is not known. If the assumption is made that the isogrid buckles in torsion at a critical shear strain (i.e., $V_{cr}(1)$ is the proportional to $\theta_{cr}(1)$ where $\theta_{cr}(1)$ is the critical shear strain) then the following relationship can be derived that relates the experimentally determined torsional rigidity, defined as the shear strain per unit torque, to the theoretical torsional rigidity of a 360-degree isogrid cylinder.

$$T = \left[\left(\frac{\theta}{T}\right)_{th} / \left(\frac{\theta}{T}\right)_{exp} \right] T_{cr} \qquad (8.2.4)$$

where T is the expected torsion load, $(\theta/T)_{th}$ is the theoretical torsional rigidity, $(\theta/T)_{exp}$ is the experimentally determined torsional rigidity, and

is the theoretical critical torsion load. Application of the measured and theoretical torsional rigidities will give

$$T \text{ (skinned)} = 1.19\ T_{cr}$$

$$T \text{ (unskinned)} = 1.36\ T_{cr}$$

For the skinned cylinder the calculated value of V_{cr} is 1460 N/M (8.31 lb/in) (Table 8.2-2) corresponding to a T_{cr} of 374 M-N (276 ft-lbs), for an expected torsion buckling load of 445 M-N (328 ft-lbs). The experimental value was 480 M-N (354 ft-lbs), a value 8 percent greater than the expected value. In like manner, the calculated V_{cr} for the unskinned cylinder is 786 M/N (4.49 lb/in) for a T_{cr} of 204 M-N (151 ft-lbs), giving an expected torsion load of 278 M-N (205 ft-lbs). Actual torsion load was 353 M-N (260 ft-lbs), 27 percent greater than the expected value.

There are a number of buckling considerations that relate to the discrepancies between the theoretical and experimental compression and torsion buckling loads and the discrepancies between the theoretical and unadjusted experimental interaction curves.

The buckling equations, given in Table 8.2-1 and taken from Section 4 of this handbook, assume simply supported end conditions. Furthermore, these equations do not consider the effects of prebuckling bending, rib torsional rigidity, the inclusions of joints, or the festoon curve predicted by the Flügge equations. For the models tested in this program the ends of the cylinders were clamped in order to transmit the torsion loads to the cylinders. Clamped end conditions will increase the buckling loads for both torsion and compression over simply

supported end conditions. It is thought that these clamped end conditions were responsible for the experimental torsion load of the skinned cylinder being 8 percent greater than the expected torsion load. As can be seen in Figure 8.2-5, the torsion buckle pattern traverses a joint in the skinned cylinder. For the unskinned cylinder, on the other hand, the bending stiffness of the joints was increased by the longerons to the point that buckling in the joints did not occur, thereby restricting all buckles to the isogrid portion of the cylinder (Figure 8.2-8). It is thought that this restriction, in conjunction with the effect of the clamped ends, resulted in the 27 percent increase in the torsion buckling load over the expected value.

The festoon curve effect, mentioned in Section 4.2, as well as prebuckling bending, will tend to decrease the compression buckling for pure axial compression. These effects do not apply to torsion loading and have little or no effect for off-axial loading (compression-bending).

It is thought that these effects were responsible for the displacement of the unadjusted experimental data away from the theoretical interaction curves. For example, the skinned cylinder under off-axial loading for $f_b/f_c = 0.5$ buckled at 89.5 percent of the load for pure axial compression but classical theory indicates that this ratio of compression bending should result in a buckling load of 66.7 percent of that for pure axial compression.

The torsional rigidity of the isogrid ribs contribute to the load carrying capability of an isogrid cylinder but this effect is not included in the equations of this handbook. In the majority of cases, such torsional rigidity would have a minor effect as the cross section of typical isogrid ribs is

relatively small. For the unskinned cylinder of this program, however, the width of the ribs was approximately 90 percent of the deptn of the rib, thereby giving the ribs of this cylinder significant torsional rigidity. It is thought that the increase in buckling load by this torsional rigidity resulted in the relatively high N_{cr} for the unskinned cylinder of 89.5 percent of the calculated value versus the N_{cr} of 81.5 percent of the calculated value (prior to rib damage) of the skinned cylinder.

The previous paragraphs indicate that the theory of Section 4 is conservative in relation to the effects of clamped ends and rib torsion rigidity and also for the effects of joints, provided that buckling is not initiated in the joints. The theory is unconservative in relation to the Flügge festoon-curve effect and the effects of prebuckling bending. In practice, account is generally made of these effects, as well as the effects of structural imperfections, by all inclusive "knock-down" factors determined by tests on representative full-scale metal structures.

The above departures from the theories presented in this handbook as related to this test program, as well as the specifics of the test program described in this section (Section 8.2), are presented in detail in the engineering test report of reference 8-2.

[illegible]

[illegible] of the experimental program indicate that the interaction curves [illegible] equation (8.2.1) adequately describe the response of skinned and [illegible] isogrid cylinders subjected to combined compression, compression-bending, and torsion provided the end points of the theoretical curves are

equated to the experimental data. In practice, this means that tests must be performed on metal specimens of a proposed configuration for buckling loads under pure torsion and under various combinations of compression-bending. The data from these tests combined with Equation (8.2.2) in the manner described in Section 8.2.4 will completely define the interaction curves.

It should also be realized that effects other than those analyzed in Section 4 influence the buckling stability of a configuration and that these secondary effects are generally handled by a "knock-down" factor determined by tests of representative full-scale metal structures.

REFERENCES

3-1 Bruhn, E. F., "Analysis and Design of Flight Vehicle Structures," Tri-State Offset Company, Cincinnati, Ohio, 1965.

3-2 Sneff, A. T., "Experimental Determination of the Buckling Interaction of Skinned and Unskinned Isogrid Cylinders Subjected to Compression, Compression-Bending, and Torsion," McDonnell Douglas Report MDC G5238, August 1974.

Table 3.2-1

STRESS RESULTANT BUCKLING FORMULAE USED IN THE DESIGN OF THE SKINNED AND UNSKINNED ISOGRID CYLINDERS

		COMPRESSION-BENDING		TORSION	
		FORMULA	SOURCE	FORMULA	SOURCE
GENERAL INSTABILITY BUCKLING	SKINNED	$N_{cr}(1)=0.612\gamma E\beta\frac{t^2}{R}$	I.D.H. Eq. 4.2.6	$V_{cr}(1)=\frac{0.747\,\gamma^{3/4}E^*t^*}{(\frac{R}{t^*})^{5/4}(\frac{L}{R})^{1/2}}$	I.D.H. Eq. 4.3.7
	UNSKINNED	$N_{cr}(1)=0.612\,\gamma E\,\frac{bd^2}{Rh}$	I.D.H. Eq. 4.9.8	$V_{cr}(1)=0.753ER(\gamma^{3/2}\frac{R}{L})^{1/2}(\frac{b}{h})(\frac{d}{R})^{9/4}$	McDonnell Douglas Analysis
SKIN BUCKLING	SKINNED	$N_{cr}(2)=C_1Et(1+\alpha)\frac{t^2}{h^2}$ $C_1=10.2$	I.D.H. Eq. 4.2.8	$V_{cr}(2)=C_1Et(1+\alpha)\frac{t^2}{h^2}$ $C_1=23.1$	I.D.H. Eq. 4.3.3
RIB BUCKLING	SKINNED	$N_{cr}(3)=C_2Et(1+\alpha)\frac{b^2}{d^2}$ $C_2=0.616$	I.D.H. Eq. 4.2.13	$V_{cr}(3)=C_2Et(1+\alpha)\frac{b^2}{d^2}$ $C_2=0.533$	I.D.H. Eq. 4.3.2
	UNSKINNED	$N_{cr}(3)=1.422k_cEd(\frac{b}{a})^3$ $k_c=2$	I.D.H. Eq. 4.9.10	$V_{cr}(3)=\frac{\sqrt{3}\pi^2}{32}Ed(\frac{b}{h})^3$	McDonnell Douglas Analysis

I.D.H. refers to the Isogrid Design Handbook

Table 8.2-2

[illegible] STRESS RESULTANTS FOR SKINNED AND UNSKINNED CYLINDERS

		COMPRESSION-BENDING	TORSION
GENERAL INSTABILITY BUCKLING	SKINNED	7.23×10^3 N/M (41.3 lb/in)	1.46×10^3 N/M (8.31 lb/in)
	UNSKINNED	3.34×10^3 N/M (19.1 lb/in)	7.86×10^2 N/M (4.49 lb/in)
SKIN BUCKLING	SKINNED	1.27×10^4 N/M (72.8 lb/in)	2.89×10^5 N/M (165 lb/in)
RIB BUCKLING	SKINNED	1.96×10^5 N/M (1120 lb/in)	1.70×10^5 N/M (971 lb/in)
	UNSKINNED	5.11×10^3 N/M (29.2 lb/in)	1.48×10^3 N/M (8.45 lb/in)

All values are based upon the following:
(a) Formulae of Table 8.2-1
(b) Geometry of Figures 8.2-1 and 8.2-2
(c) An assumed value of γ of 1 and a measured value of E of 2120 MPa (307,000 lb/in^2)

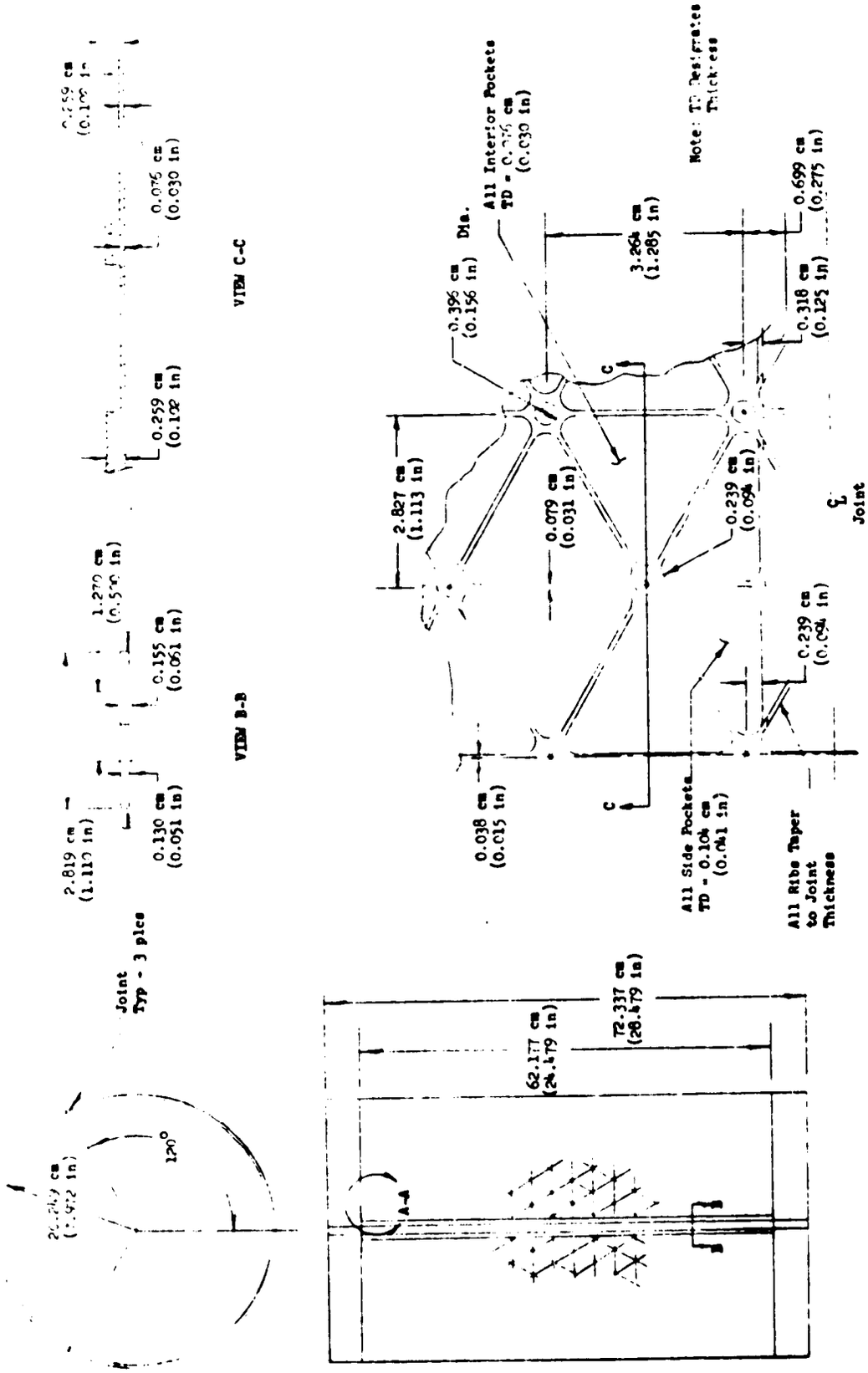

Figure 8.2-1 Configuration and Dimensions of Skinned Isogrid Cylinder

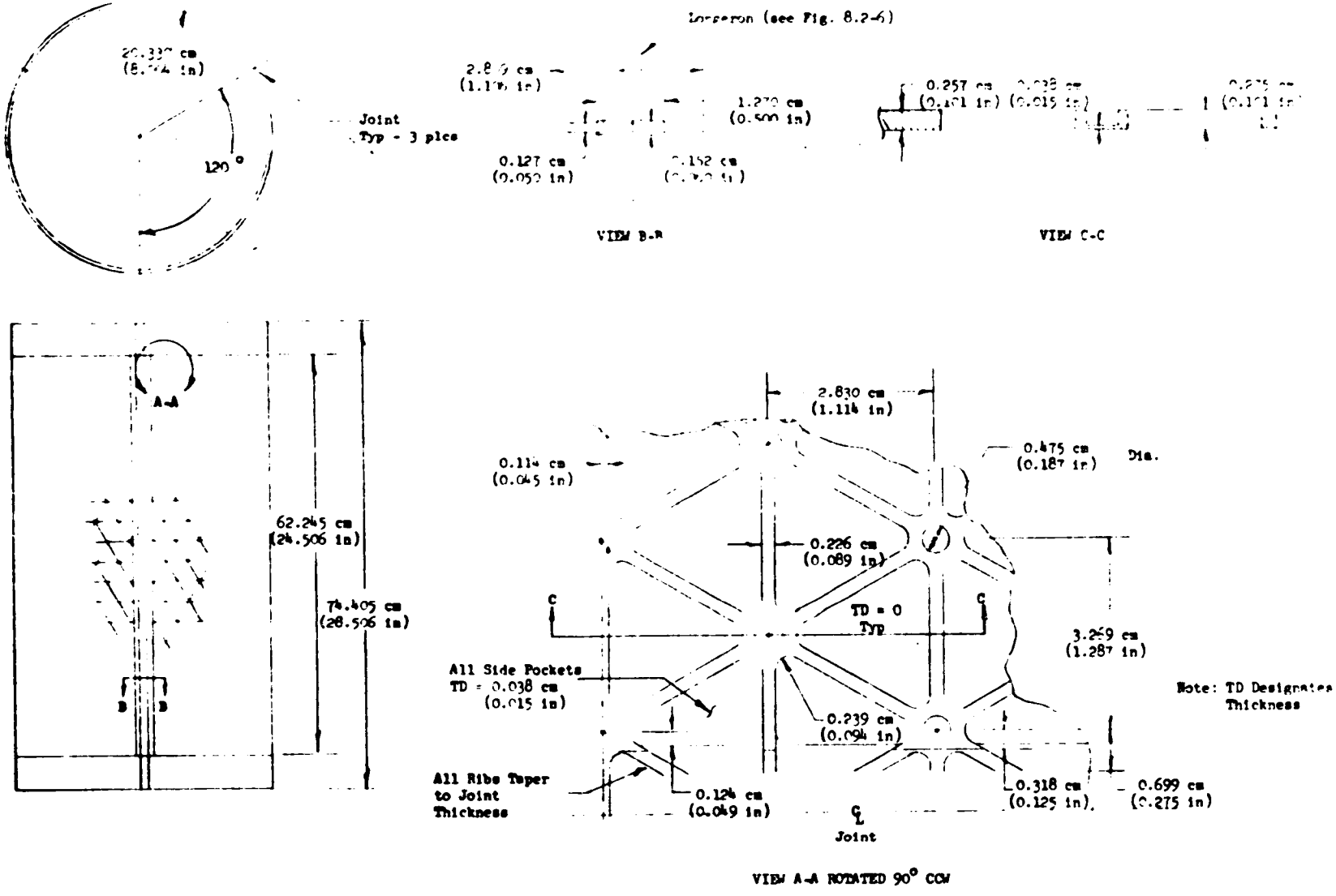

Figure 8.2-2 Configuration and Dimensions of Unskinned Isogrid Cylinder

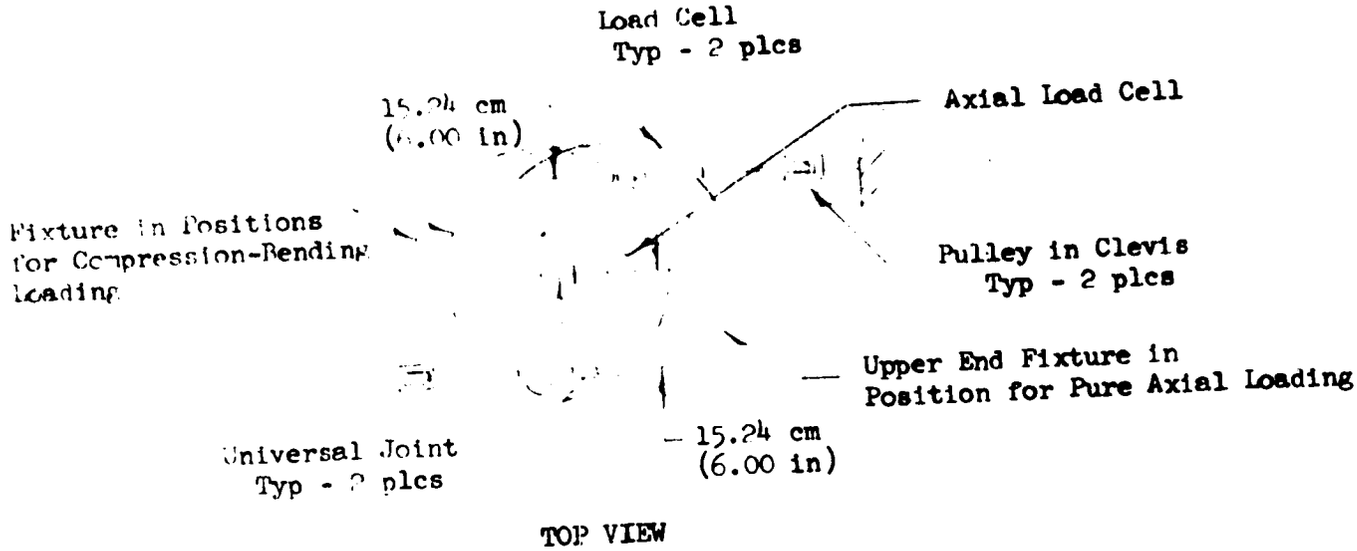

TOP VIEW

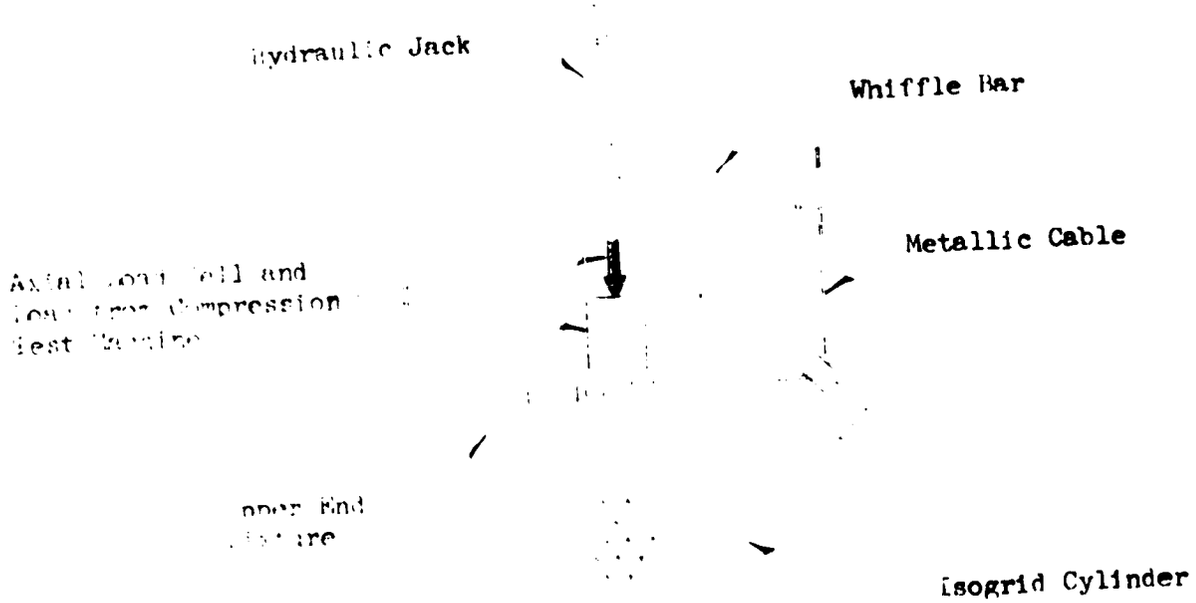

SIDE VIEW

Figure 8.2-3 Schematic of Test Set-Up

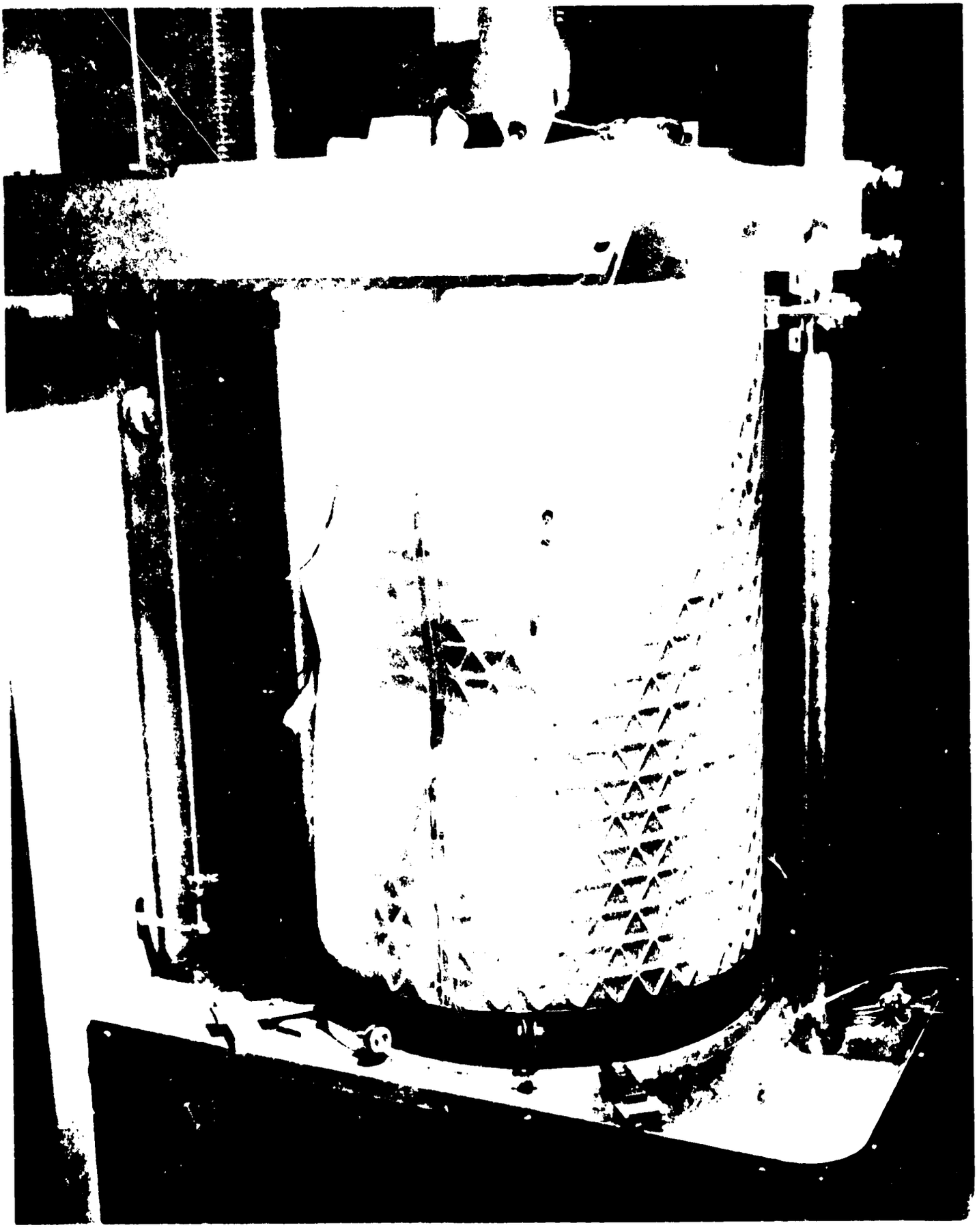

Figure 4.2-4 Buckling Pattern of Skinned Cylinder Subjected to Pure Axial Load

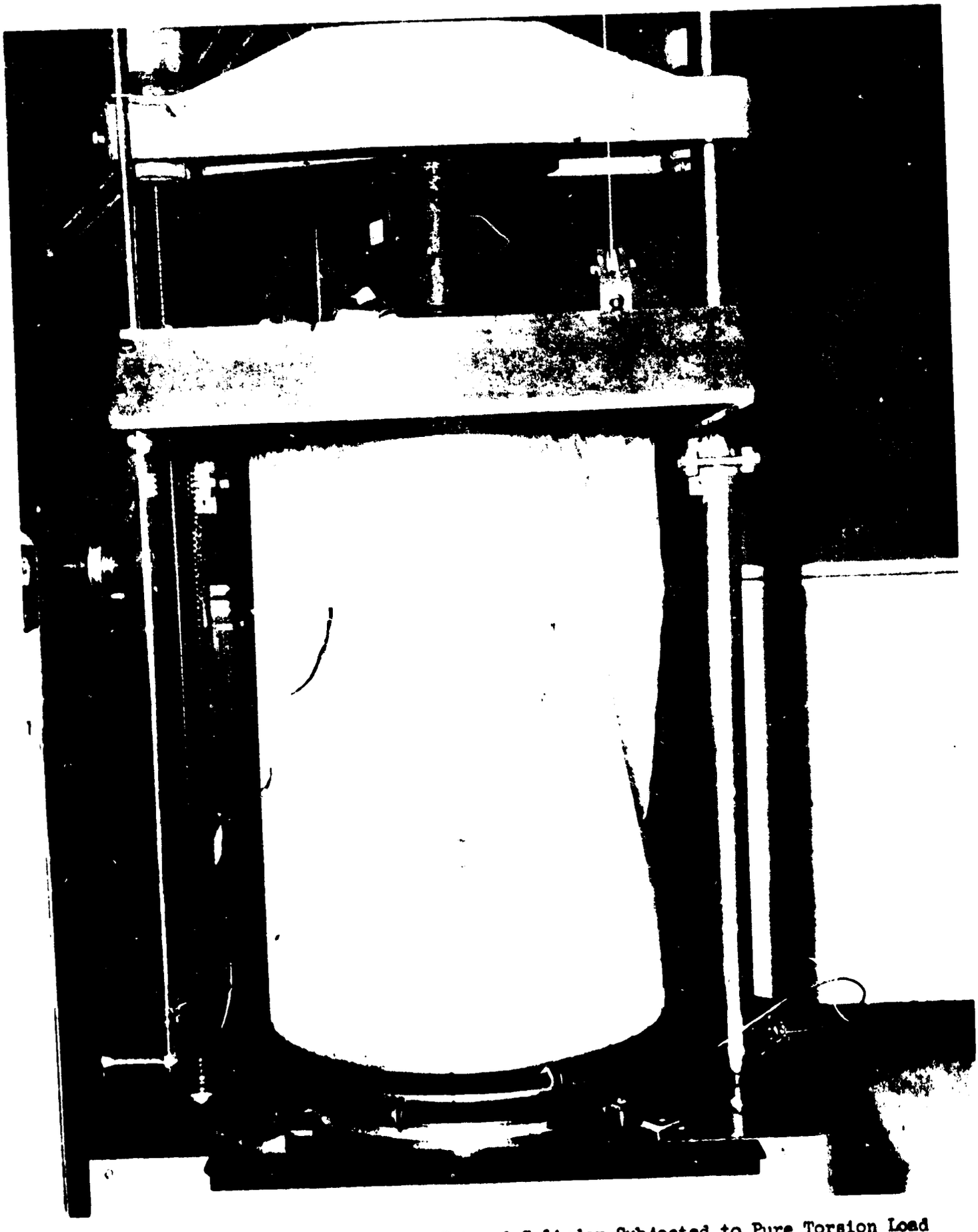

Figure 8.2-5 Buckling Pattern of Skinned Cylinder Subjected to Pure Torsion Load

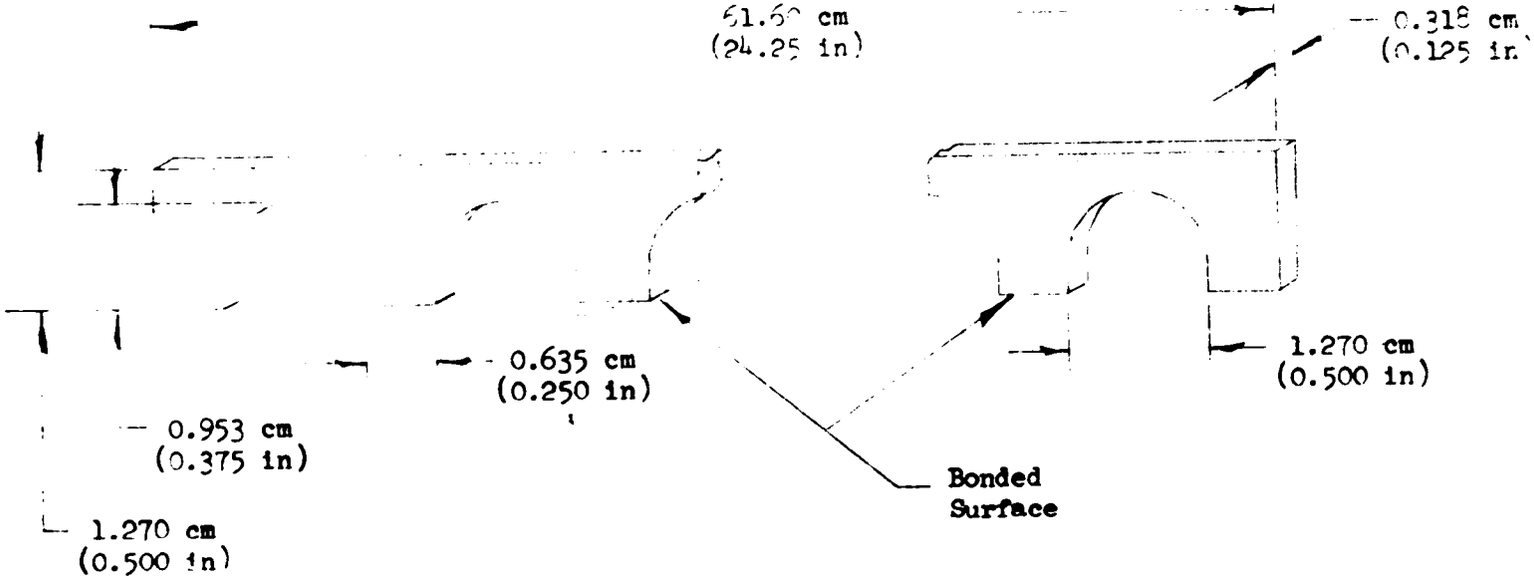

Figure 8.2-6 Configuration and Dimensions of Longerons of Unskinned Cylinder

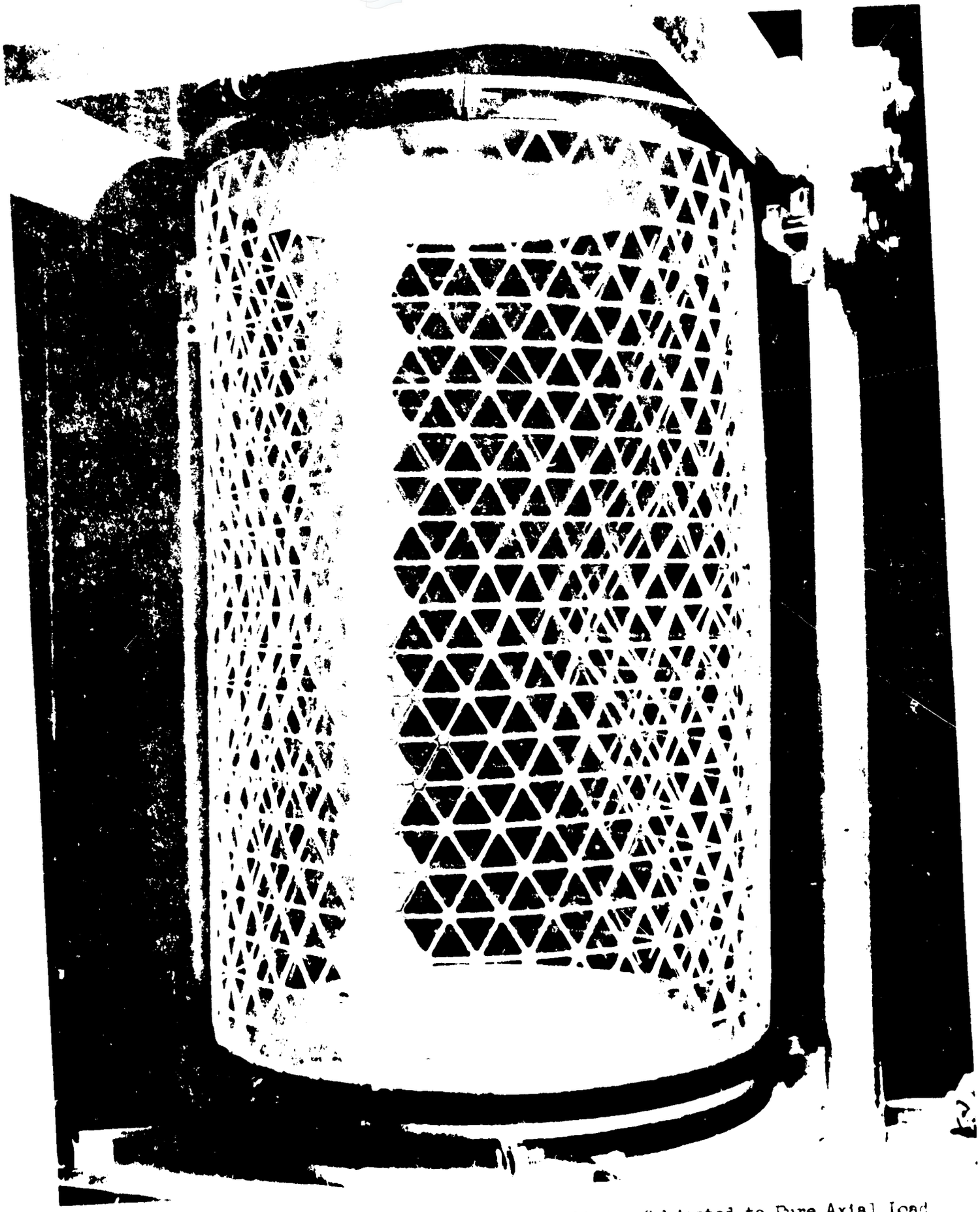

Figure [illegible] Buckling Pattern of Unskinned Cylinder Subjected to Pure Axial Load

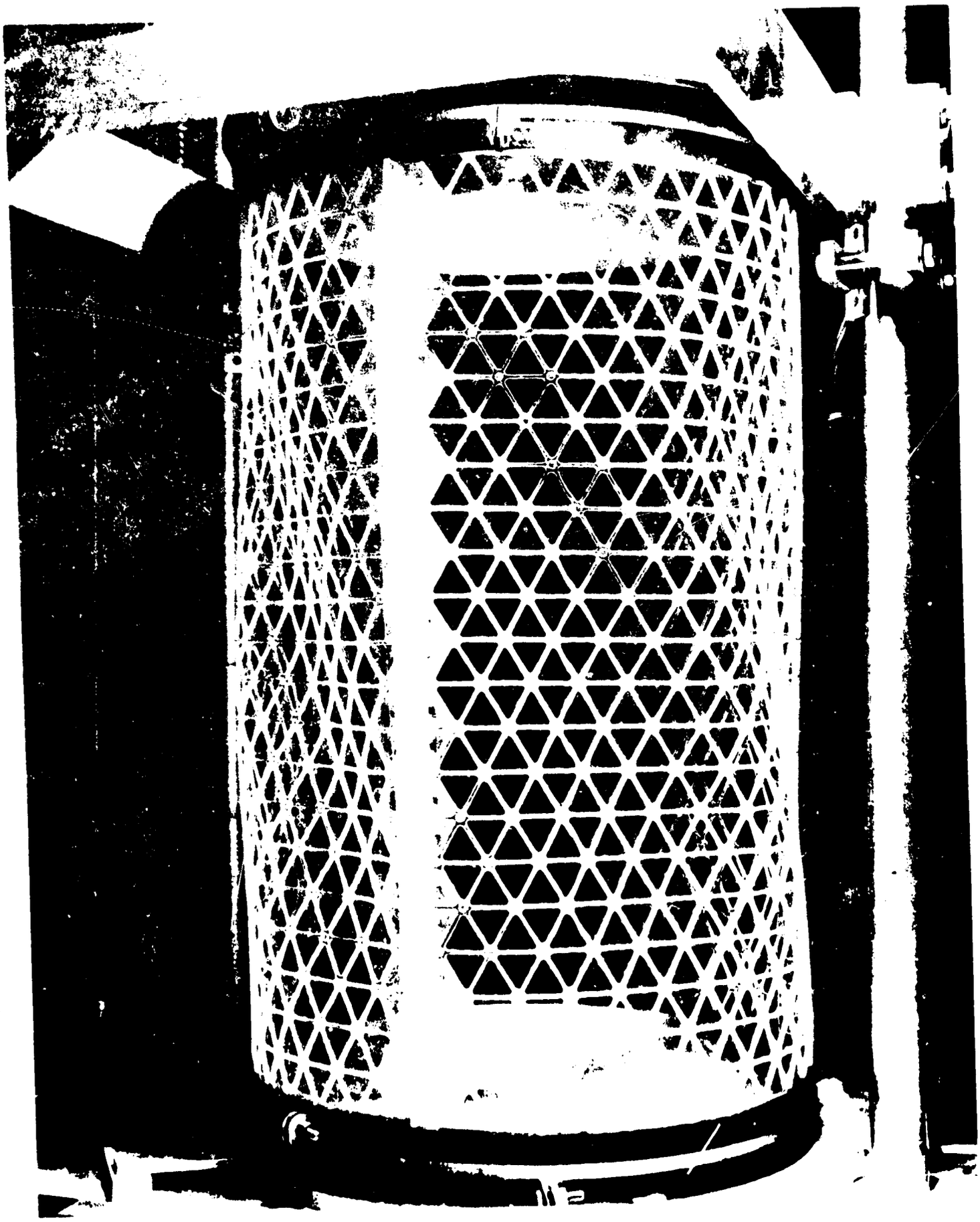

Buckling Pattern of Unskinned Cylinder Subjected to Pure Torsion Load

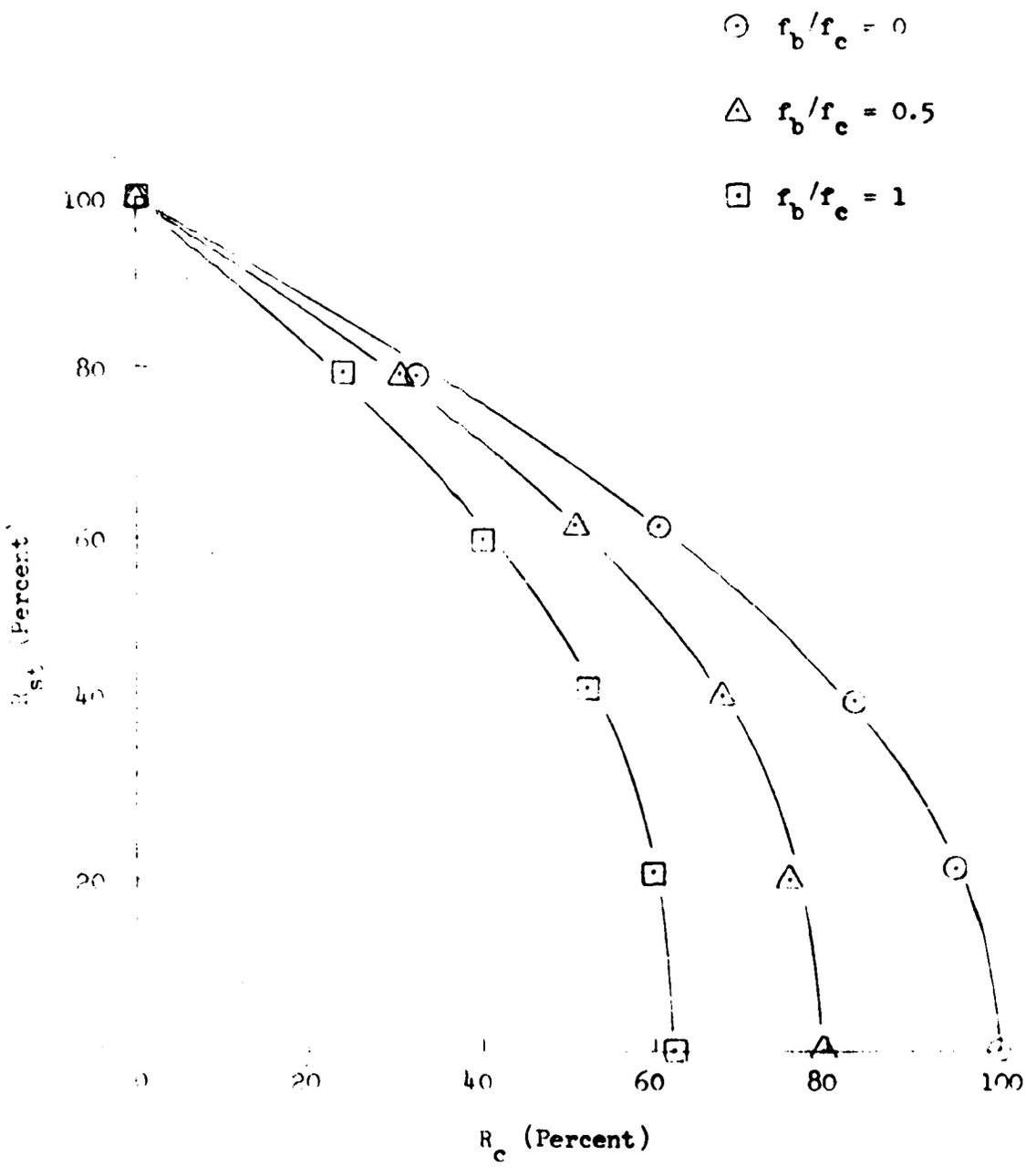

Figure 8.2-9 Experimental Interaction Curves from Skinned Cylinder

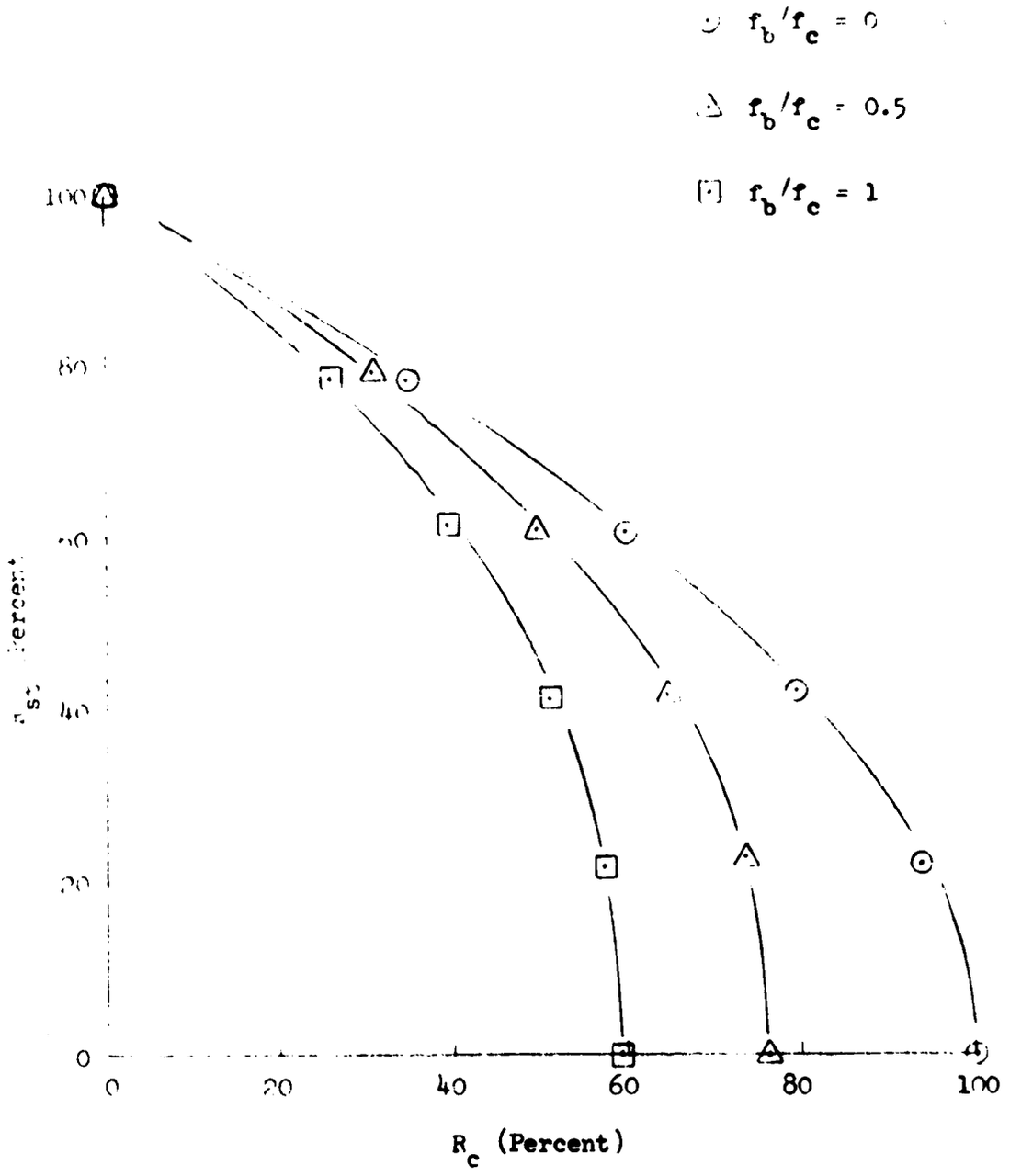

Figure 8.2-10 Experimental Interaction Curves from Unskinned Cylinder

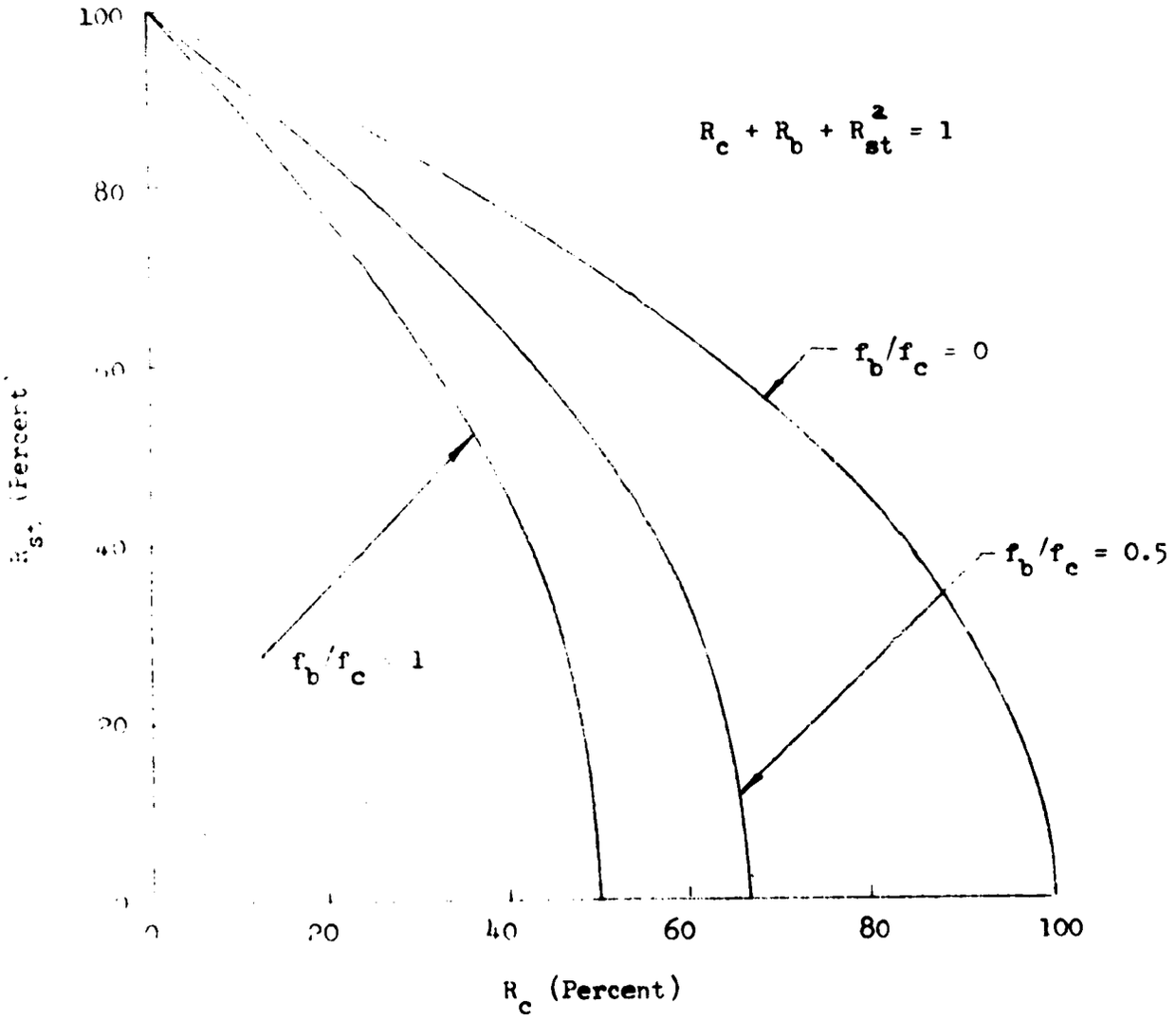

Figure 8.2-11 Theoretical Interaction Curves for Compression, Bending, and Torsion

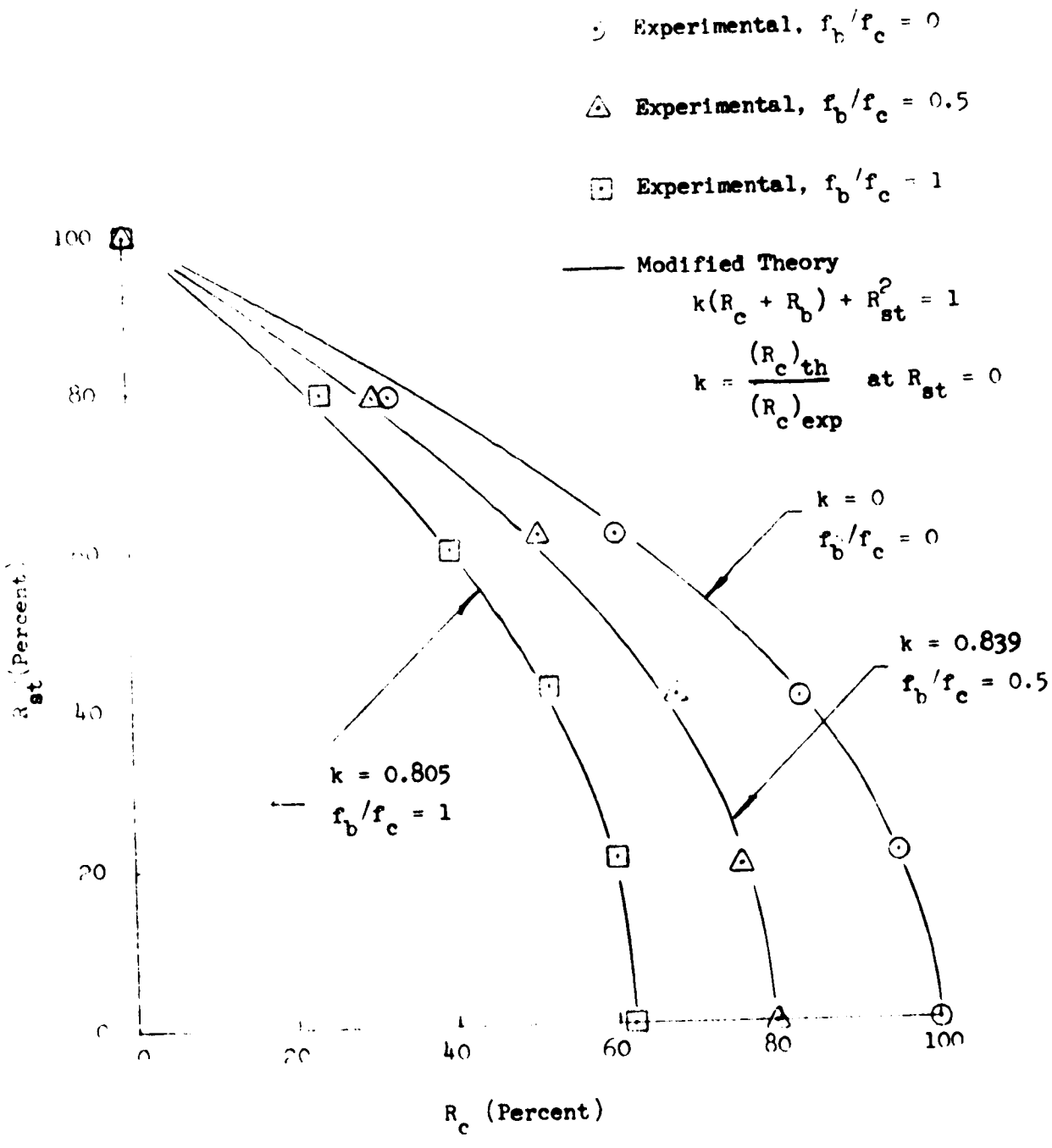

Figure 8.2-12 Comparison of Experimental Data from Skinned Cylinder with Modified Theoretical Equation (Equation (8.2.2))

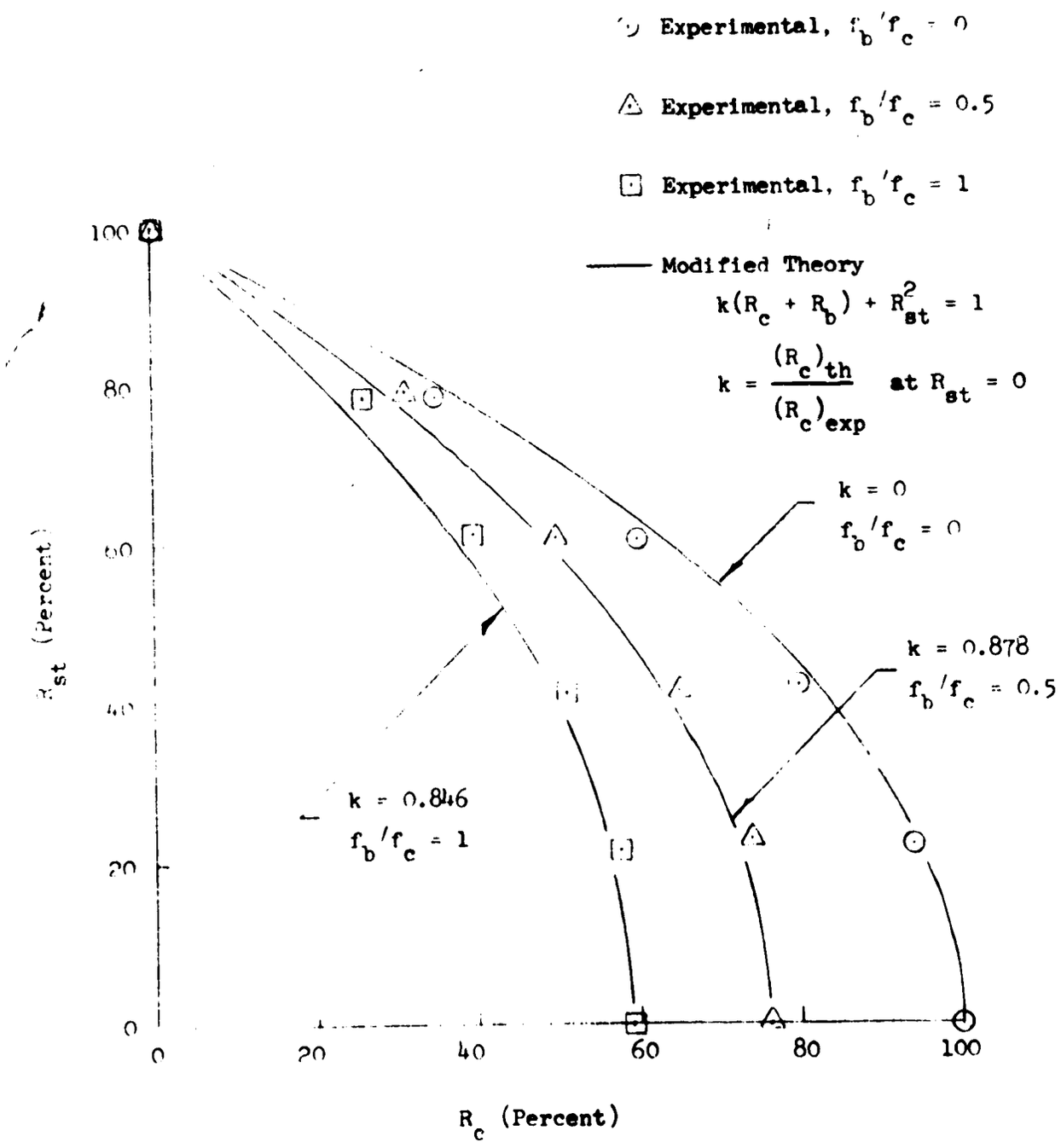

Figure 8.2-13 Comparison of Experimental Data from Unskinned Cylinder with Modified Theoretical Equation (Equation (8.2.2))